Fakultät für Medizin

Klinik für Herz- und Gefäßchirurgie des Deutschen Herzzentrums München

Characterization of the non-myocyte cell populations of the heart

Palgit-Sarit Kogan

Vollständiger Abdruck der von der Fakultät für Medizin der Technischen Universität München zur Erlangung des akademischen Grades eines

Doctor of Philosophy (Ph.D.)

genehmigten Dissertation.

Vorsitzende/r: Prof. Dr. Claus Zimmer

Betreuer/in: Prof. Dr. Markus Krane

Prüfer der Dissertation:

1. Priv.-Doz. Dr. Harald Lahm

2. Prof. Dr. Alessandra Moretti

Die Dissertation wurde am 15.06.2020 bei der Fakultät für Medizin der Technischen Universität München eingereicht und durch die Fakultät für Medizin am 13.08.2020 angenommen.

Contents

Abstract

Objective: Non-myocyte cells (NMC) exhibit multiple central functions in the heart such as vascular supply, production of extracellular matrix (ECM) and contribution to cardiomyocyte survival, making them important players in cardiac homeostasis and disease. However, their proportion in the heart and their ability to change their transcriptional phenotype is still a topic of research. In this work, the main NMC types, cardiac fibroblasts (CF), smooth muscle cells (SMC) and endothelial cells (EC), grown in primary tissue culture were characterized and compared to cardiac biopsy derived cells. Besides, cardiosphere-derived cells (CDC), a cardiac tissue derived cell type which has been used previously in clinical trials, was compared to the analyzed NMC. Assessment of age-related differences of primary cells was performed by comparing CDC and CF derived from pediatric and adult patients.

Methods: Marker analysis by gene (qRT-PCR) and protein expression (immunocytochemistry, flow cytometry) of adult patients' derived CF, SMC, EC and CDC was combined with single-cell RNA sequencing (sc-RNAseq) to draw a detailed picture of biological processes typical for each cell type and to elucidate similarities between them. Infant and adult patient derived CDC's (infant/adult CDC) gene expression was compared using qRT-PCR and sc-RNAseq. The potential of infant/adult CDC derived extracellular vesicles (EV) to mediate angiogenic, anti-fibrotic and anti-apoptotic effects *in vitro* was compared to age-matched CF derived EV. In addition, neonatal patients' (≤ 21 days) CDC were compared to those of older infant patients (1 month-6 years) concerning their gene expression and EV mediated functionality. Further, it was examined whether exposure of CF to culture conditions of CDC (CFSPh) increased similarity between both cell types. Finally, a fresh adult cardiac biopsy was analyzed by sc-RNAseq and clusters identified as NMC were compared to corresponding cultured cells.

Results: Marker analysis as well as sc-RNAseq of cultured NMC revealed a distinct expression profile of EC compared to CF and SMC both upregulating genes related to ECM production. CDC were identified as a distinct, highly heterogenic cell type partly sharing features with CF and SMC. Infant CDC were more divergent from age-matched CF than their adult counterparts. Sc-RNAseq showed that neonatal CDC upregulated genes related to angiogenesis. Infant CDC-EV, in contrast to adult CDC-EV, significantly augmented *in vitro* EC tube formation and migration, but no effects of CDC-EV were observed on CF migration or neonatal rat cardiomyocytes (NRCM) apoptosis. These effects were not reproduced by CF-EV or CFSPh-EV derived from patients of corresponding age. Although the analyzed cardiac biopsy contained many blood-derived immune and apoptotic cells, main NMC populations were identified. Unlike cultured cells, biopsy derived NMC did not upregulate pathways related to protein synthesis, but gene expression patterns were associated with processes known to be crucial for cardiac function.

Conclusion: Cultivated NMC (CF, SMC, EC) showed expression patterns known to be typical for these cell types. Thus, a comparison to NMC shed light on the identity of the previously poorly characterized CDC and further elucidated their heterogeneity. Besides, cultured CDC and CF showed age-related gene expression patterns and secretomic features. However, primary cell culture represents a biased model for studying *in vivo* function of cardiac NMC. A better approach is sc-RNAseq analysis of fresh biopsy samples. To achieve more detailed results, the biopsy digestion method should be further optimized for NMC.

1. Introduction

1.1 Cellular composition of the heart

The heart is an essential organ for all humans and animals whose life depends on its uninterrupted function starting from embryogenesis (1). In order to understand the mechanisms of congenital and acquired heart diseases, it is crucial to gain knowledge about the cells comprising the heart. The adult mammalian heart cell composition has been investigated since several decades (2-4). In humans, four major cell types compose the heart: cardiomyocytes, cardiac fibroblasts (CF), endothelial cells (EC) and smooth muscle cells (SMC) (1, 5). Other cell types include lymphocytes, mast cells and macrophages, which appear transiently in the heart and can interact with the permanent cell types, thereby affecting cardiac function (3).

1.1.1 Non-myocyte cell types

Cardiomyocytes, which have the important task to mediate the contraction of the heart, are estimated to represent about 30% of the total cell number in the rat and human heart (2, 4, 6). However, due to their large volume, cardiomyocytes account for about 70% of the total mass (5) and about 70 to 85% of the heart volume (7, 8).

Non-myocytes are equally important cell populations. Their major functions include preservation of heart homeostasis by production of extracellular matrix (ECM), vascular supply and intercellular communication with cardiomyocytes, thereby supporting heart contraction and long-term survival (7). However, the proportion of the non-myocyte cell populations remains controversial (9). Table 1 summarizes the results of cardiac composition analysis found in the literature. These obvious differences are most probably due to different cell isolation techniques, evaluation methods, antibody set-ups and species differences (9).

Table 1: Cardiac cell composition literature

Ref.	CM	CF	EC	SMC	Other cells	Species/ age	Method	Heart location
(4)	30-35%,	65-70%, (EC, CF, pericytes, SMC and macrophages)				Rat/ adult	TEM	Left Ventricle
(10)	56% (α-MHC)	27% (DDR2)	7% (CD31)	10% (α-SMA)	n.d.	Mouse/ adult	FC	Whole heart
(10)	52% (α-MHC)	37% (DDR2)	11% non-CM/ non-CF population			Mouse/ adult	Morpho metry	Left ventricle
(10)	51% (α-MHC)	37% (DDR2)	12% non-CM/ non-CF population			Mouse/ adult	FC	Left ventricle
(11)	31%±4% (WGA)	n.d.	44%±4% (IB4)	n.d.	5%±1.5% leucocytes (Lin1 cocktail)	Mouse/ adult	IHC	Ventricles and interventricular septum
(11)	32%±5%	13%±2.5%	55%±6%	6%±1.1%	8.5%±1.5	Transgen	IHC	Left Ventricle

		(PDGFRα) 13%±3.6% (Col1a1)	(IB4) 52%±4% (DACH1)	(PDGFRβ) SMC and pericytes	% leucocytes (Lin1 cocktail)	ic Mouse (PDGFRβ- or Col1a1-GFP)		
(11)	31.2%±5.6 % (ACTN2)	n.d.	53.8%±6.4 % (CD31) 51.2 ±2.9 (DACH1)		2.8%±1.2 % leucocytes (CD45)	Human/ Adult	IHC	Ventricles and interventricular septum
(6)	18%±3% (PCM-1)	58% (non PCM-1, non UEA-1) Mesenchymal cells	24%±5% (UEA-I)	See CF		Human/ Adult	IHC	Left Ventricle
(6)	33%±15% (PCM-1)	43%±10% (non PCM-1, non UEA-1) Mesenchymal cells	24%±9.5% (UEA-I)	See CF		Human/ Adult	FC	Ventricle

Modified from (9): *Values are displayed as* mean ± standard deviation. *Abbreviations: Ref.: reference; CM: cardiomyocytes; CF: cardiac fibroblasts; EC: endothelial cells; SMC: smooth muscle cells; n.d.: not determined; IHC: immunohistochemistry, FC: flow cytometry, TEM: transmission electron microscopy.*

This summary clearly illustrates species-related differences of the cellular heart composition. Previously, physiological differences between mouse and rat with respect to collagen amount and heart rate have been reported (3, 12, 13). In contrast, in humans and rats, the ratio of cardiomyocytes to the non-myocyte cell number is around 30:70. In mice up to 55% of cardiomyocytes were detected. This species-related difference may be explained by the greater wall tension correlating with the size of the organ which requires the presence of more fibroblasts (9, 10).

Early publications postulated that fibroblasts comprise the largest non-myocyte cell population (3, 14). However, Pinto *et al.* have recently published an analysis using genetic tracer-based techniques and enhanced flow cytometry (FC) methods which revealed that EC represent the most abundant cell-type among the non-myocytes of the heart (11).

Bergmann *et al.* were the first to publish turnover analyses of postmortem human hearts which had no history of cardiac pathology (6). As the turnover of postnatal cardiomyocytes is very low (< 1% per year), their number remains more or less constant during heart growth. In contrast, the number of mesenchymal and EC exponentially increases in growing hearts and gradually declines thereafter (6).

The fact that many published and widespread used markers for certain cell types are nonspecific, particularly for mesenchymal non-myocyte populations like CF, SMC or pericytes,

poses an immense problem to reliably detect and discriminate these cell types (9). Thus, the state-of-the-art method to analyze cellular diversity is single-cell RNA sequencing (sc-RNAseq). This is an approach, unbiased from cell markers, to create a comprehensive atlas of the diverse facets of cell types revealing their complex transcriptome (15).

In cardiac research several sc-RNAseq studies have been published recently (16-21). Skelly *et al.* (16) and Gladka *et al*. (17) investigated the composition of the adult mouse heart. Although these studies used different digestion protocols and investigated different heart regions, both illustrate that many cell types of the heart are heterogeneous, in particular CF. Suryawanshi *et al.* analyzed three healthy fetal human hearts. In their samples, they detected 49% cardiomyocytes, 22% immune cells, 13% EC and fibroblasts, respectively, 2% of SMC and 1% mesothelial cells. Among the non-myocyte cells, in particular EC and fibroblasts appeared to be very heterogeneous (22). This year Wang *et al.* published the first sc-RNAseq analysis of human adult cardiac tissue of healthy and diseased donors which gave insight into the cellular heart composition change during disease. The various disease-related interactions between different NMC subtypes with cardiomyocytes emphasized the functional heterogeneity of CF, EC and SMC (21).

1.1.2 Endothelial cells (EC) and smooth muscle cells (SMC)

EC support the interior lining of the heart and blood vessels, whereas SMC sustain its vascular system (5).

During embryonic development, coronary vascular SMC originate from proepicardial cells (23). The proepicardium is a structure located dorsal to the developing heart tube. Around embryonic day nine in the mouse, proepicardial cells migrate and attach to the looped heart tube at the dorsal part of the atrioventricular junction forming the epicardium (24). At embryonic day 11 in the mouse the epicardium is formed. Subsequently a subset of cells undergoes transformation to the mesenchyme (epithelial-to-mesenchymal transition, EMT) and migrates either to the sub-epicardium or the myocardium. The latter cells are referred to as epicardial-derived cells (EPDC) (9). The sub-epicardial cells are thought to develop into CF, coronary vascular SMC and EC (23, 24). It was also reported that cardiomyocytes derive from the epicardium (25). A subset of EPDC of the neonatal heart undergo EMT to form a vascular plexus (26). Postnatal coronary vessels partially arise from embryonic coronary vessels. However, it has recently been reported that a substantial part of coronary vessels arise *de novo* after birth resulting in different sources of SMC contributing to coronary growth (26, 27).

SMC represent a plastic cell type which is able to undergo a phenotypic switch from a quiescent, differentiated to a proliferating dedifferentiated state (28). Quiescent SMC express typical SMC markers, such as smooth muscle α-actin (ACTA2), transgelin (TAGLN), myocardin (MYOCD) or myosin heavy chain 11 (MYH11) (26, 29). After the phenotypic switch, which occurs for example during vascular injury repair, these contractile proteins are downregulated resulting in increased

production of ECM, proliferation and migration (26, 28). This dedifferentiation process also plays a role in atherosclerotic plaques evolving during the course of cardiovascular disease where repression of promoters of contractile genes was reported in SMC (30). However, the exact mechanisms of SMC transition and their phenotypic diversity is still not fully elucidated (29). The heterogeneity of SMC in the healthy tunica media has recently been investigated in a study combining sc-RNAseq and SMC lineage-tracing, identifying seven distinct clusters of vascular SMC (31). The current hypothesis is that the SMC in the tunica media consist of different clones some of which can undergo a transition to a mesenchymal-stem cell-like state resulting in lesion phenotypes (29). In a healthy state, it is hypothesized that the SMC phenotype changes reversibly and transiently between a more or less differentiated SMC state which is required to maintain the homeostasis of ECM (29, 32).

EC of the heart can be divided in five distinct groups with different phenotypes: endocardial, coronary arterial, venous, capillary and lymphatic EC (33). Endocardial EC as well as cardiomyocytes arise from the cardiac mesoderm during embryogenesis (33). It is known that, compared to the cardiomyocyte lineage, only a minor part of the cardiac mesodermal population differentiates into EC. However, how endocardial EC precursors are specified remains unclear (33, 34). Endocardial cells line the luminal surface of the heart muscle and connect it with the vascular network. In addition, other functions have been reported such as a contribution to the development of valve leaflets and interventricular and atrial septa, to signaling involved in the formation of the conduction system and trabeculae, and to outflow tract remodeling (35). Coronary EC derive from the proepicardium, similar to SMC (24) and their lineage is likely segregated before the proepicardium arrives at the heart tube (33). In contrast, lymphatic vessels including lymphatic EC, do not originate in the proepicardium, but rather from lymphangioblasts that contribute to the cardiac lymphatic system (33). A topic of debate is whether resident cardiac stem or progenitor cells contribute to the EC pool of the heart (33). Apart of these differences in their origins, structural and functional heterogeneity of EC has been observed as recently reviewed (36, 37). In the heart heterogeneity of EC has been attributed to variable exposure to regional forces and paracrine factors (36).

1.1.3 Cardiac fibroblasts (CF)

In general, a fibroblast is defined as a cell of mesenchymal origin with structural function due to the ability to produce main proteins of ECM such as interstitial type I, III and VI collagens or fibronectin (3, 9, 38). As the main connective tissue cells, they are present in numerous parts and organs of the body. Unlike other cells, CF are characterized by a lack of a basement membrane (39).

Cardiac fibroblasts have their origin in different embryonic progenitor cell lineages including the endocardium, the neural crest and above all the epicardium (9, 40). EPDC differentiate in the compact myocardium into interstitial and adventitial CF and coronary SMC (41). Growth and

transcription factors crucial for CF formation from the epicardial lineage include transcription factor 21 (*Tcf21*) (42), fibroblast growth factors (FGFs), *TBX5* and *SOX9* (9, 41). The endocardium is the lineage which lines the inner lumen of the heart during its development (43). Subsets of endocardial cells undergo endothelial-to-mesenchymal transition which results in a mesenchymal cell type developing to form cardiac valves (44) or in fibroblasts which contribute to the formation of the intraventricular septum (45). The neural crest originates from the dorsal part of the neural tube and one of its subpopulations, the cardiac neural crest, is important for the formation of the cardiac outflow region (40). In addition, some cardiac neural crest-derived cells contribute to the valve mesenchyme and to the myocardium of the right atrium (9, 40).

In the healthy mammalian heart, CF play a major role in formation and maintenance of connective tissue (46). The cardiac connective tissue consists of cells and acellular components (the ECM) which together build a collagen-rich flexible scaffold enabling force transmission and a control of tissue deformation (46). The ECM allows the fibroblasts to modulate their environment through paracrine and autocrine signaling (3). Components of ECM include collagens, proteoglycans, glycoproteins, cytokines, growth factors, matrikines and proteases (3). The homeostasis of the ECM is regulated by production of factors involved in ECM synthesis and degradation processes produced by CF such as cytokines, metalloproteases and growth factors (14). Besides, proteins such as integrins and ion channels allow CF to sense mechanical changes, and thus to react by proliferation, expression of growth factors and cytokines or ECM deposition (3, 14). A close interaction of fibroblasts with cardiomyocytes supports the elastic reaction of the heart to stretches, for example induction of CM hypertrophy or endothelin and angiotensin II production (14).

Other functions of the fibrous meshwork include the contribution to the electrical properties of the myocardium by separating electrical activation of atria and ventricles (14, 46). As obstacle of electrical excitation spread, CF passively control the electrophysiology of the heart by insulating bundles of the electrical conduction system (14, 39, 46). As efficient mechano-electrical transducers, CF can respond to changes in the contractility of the myocardium by adjusting their membrane potential (14). Cell junction connexins enable fibroblasts to connect and couple electrically with isolated cardiomyocytes which could indicate a bridge-like function (3). Interactions of myocytes and fibroblasts have also been shown to activate K^+ ion channels (3, 47).

CF have also been reported to tightly associate with EC both *in vitro* and *in vivo* suggesting that they play a role in angiogenesis (3). Secretion of FGF and vascular endothelial growth factor (VEGF) by CF act on vascular EC in a proangiogenic manner and thereby help restoring blood supply of injured myocardium (3, 48, 49). However, anti-angiogenic properties of CF, such as expression of pigment epithelium-derived growth factor, also have been reported (3, 50).

Metalloproteinases and tissue inhibitors of metalloproteinases (TIMPs) are both secreted by CF and can act with pro- or antiangiogenic properties, depending on the context (3, 51-53).

The prominent role of CF in myocardial remodeling has intensively been investigated. In a pathological state, such as heart failure or after myocardial infarction, the heart must adapt to immense changes in mechanical, chemical and electrical signals (3). These adaptive or maladaptive changes which can include mass, shape and dimensions of the heart, are termed cardiac remodeling and can affect its proper function (39). As described above, CF can react by modulating ECM production and degradation. Chemical signals induced by cardiac injury influence CF to migrate to the injured region and to promote wound healing and scar formation (3). During this process, the gene expression pattern of CF changes, turning them into so-called myofibroblasts, a proliferating, contractile cell-type expressing features of smooth muscle cells (3, 54, 55). Myofibroblasts are key players in wound healing and reparative fibrosis (3, 56, 57). When the scar matures, apoptosis of myofibroblasts was observed (58). Typical markers of myofibroblasts include alpha smooth muscle actin (α-SMA), periostin (POSTN) and tenascin C (TNC) (39). The transformation of CF into myofibroblasts demonstrates the plasticity of this cell-type (59). Cultured fibroblasts have been described to have transient properties of active CF or myofibroblasts (60).

As observed in sc-RNAseq studies (16, 17), CF are a heterogeneous cell population. Therefore, identification of all CF by a single marker is challenging. Common markers to identify fibroblasts include discoidin receptor1 (DDR2), thymocyte 1 (THY1 or CD90), fibroblast-specific protein 1 (FSP-1 or S100A4) or transcription-factor 21 (TCF21) (39). However, none of these markers has been shown to be specific for CF or to comprise all types of CF (9, 39). For this reason, studies about CF have been difficult to conduct and as a result this cell-type is still not fully characterized despite of its clear clinical relevance (39).

1.2 Cardiosphere-derived cells (CDC)

1.2.1 Characterization and clinical trials

CDC are a cell population isolated from fresh human heart biopsies which have been used in several clinical trials. In the CADUCEUS trial adult patients with post-myocardial infarction (MI) left ventricular dysfunction were treated with autologous intracoronary infusion of CDC, however, no significant change in left ventricular ejection fraction was observed between treated and control group (61). Yet, the administration of CDC appeared to be safe. Further, an increase in viable heart mass, regional contractility and a reduction of scar mass were observed in a one-year follow-up assessment (62). Subsequently, the ALLSTAR trial was conducted by the same research group where allogenic intracoronary transplantation of CDC in patients with MI and ischemic left ventricular dysfunction was investigated. Upon termination no significant difference between patients and control group with respect to infarct size or left ventricular volumes were evident and no major adverse cardiac effects occurred (63, 64). In the HOPE-

Duchenne trial, intracoronary allogenic transplantation of CDC was assessed in patients with Duchenne muscular dystrophy (65). In the course of this inherited disease of the skeletal musculature, 95% of patients develop cardiac complications such as sinus tachycardia at an early age and later spreading fibrosis in the ventricular walls (66). When treating Duchenne muscular dystrophy patients with CDC, significant cardiac scar reduction, but no difference in ejection fraction was observed (65). On the contrary, pediatric patients with single-ventricle (SV) physiology undergoing stage 2 and 3 palliations who received autologous CDC transplantation showed beneficial changes in ventricular function compared to controls (TICAP Trial) (67). The phase II trial (PERSEUS) revealed that CDC treatment was associated with improved ventricular volumes, somatic growth, increased trophic factor production and a better quality of life in SV patients (68). The favorable effects of CDC administration to SV patients were also confirmed in a 2-year follow-up (69). Despite this repeated use, cell characteristics of CDC have not been defined in detail and their mechanism of action is still not fully elucidated.

The cultivation protocol of so-called "cardiospheres" was developed relying on the controversial theory that resident cardiac progenitor cells exist in the postnatal heart (70). "Cardiospheres" were termed as "undifferentiated cells that grow as self-adherent clusters […] from subcultures of postnatal atrial or ventricular human biopsy specimens and from murine hearts" by Messina *et al*. (70). Since three-dimensional spheroid culture was known to be beneficial for stimulating proliferation in embryonic cardiomyocytes (71), the idea was to generate a cardiac tissue-derived stem/progenitor cell-type suitable for heart regeneration, in analogy to neurospheres (72). Messina *et al*. postulated that the bright cells growing on a dense cell layer of cardiac biopsy outgrowth, which supposedly were the spheres' main cell type, had cardiac stem cell and partially or fully differentiated cardiomyocyte characteristics, even though the presence of vascular cells was also observed (70). In order to generate a cell-type which can be expanded and transplanted for regenerative purposes, Smith *et al.* modified the protocol by replating the spheres to a monolayer culture, termed cardiosphere-derived cells (CDC) (73). The conclusion that cardiospheres represent stem/progenitor-like cells was mainly based on the detection of the markers C-KIT and CD34 (70, 73). However, the claim that the presence of C-KIT is an indicator for cardiac stem or progenitor cells has recently been severely criticized (74), based on lineage-tracing experiments showing very low contribution of C-KIT positive cells to cardiomyocytes (75). This also correlated with the finding of low cardiomyocyte turnover rates in the human postnatal heart (76). As a result, over 30 falsified studies on C-KIT as a stem cell marker mainly by the group of Piero Anversa were retracted and the clinical CONCERT-HF trial which used C-KIT positive cells was halted (74).

Nowadays, the theory that CDC might have a paracrine effect on ischemic hearts is rather supported than the hypothesis that CDC are a type of heart resident progenitor cells (77). There is increasing evidence which indicates that the function of CDC can be associated with a

paracrine mechanism, mediated by extracellular vesicles (EV) secreted by these cells (78-80). Particularly exosomes, which are endocytic membrane-bound vesicles in the size range of 30-100 nm, have recently drawn attention of the scientific community. Being released by fusion of multivesicular bodies with the cell membrane and taken up by neibouring cells, exosomes can mediate intercellular communication by shutteling proteins, mRNAs and microRNAs (miRs) (81). Cardiovascular effects of exosomes released by different cell types, including cells used for therapeutic cardiac regeneration, have been recently reviewed (82).

Several studies revealed that CDC derived extracellular vesicles (CDC-EV) have pro-angiogenic effects *in vitro* (77, 78, 80, 83-85). Moreover, CDC derived vesicles or CDC conditioned medium were able to reduce apoptosis of stressed cardiomyocytes (77, 80). Barile *et al.* revealed that the reduction of CM apoptosis by cardiac outgrowth cells could be attributed to miRs enriched in the secreted vesicles of these cells, in particular miR-210 and miR-132 (86). Lang *et al.* reported that CDC-EV had no effect on collagen expression and viability of CF, but a significant reduction of CF proliferation was observed (85). A study by Tseliou *et al.* investigated the effect of priming of fibroblasts with CDC-EV and revealed that fibroblasts gain angiogenic and cardioprotective characteristics in *in vivo* and *in vitro* models and change their miR secretome (80). Gallet *et al.* performed an *in vivo* study injecting CDC-EV in pigs which suffered from myocardial infarction, but only in the acute study with intramyocardial delivery of CDC-EV an effect on infarct size area reduction and left ventricular ejection preservation was observed. The authors discuss that EV were not retained in the myocardium upon intracoronary administration because of their small size (79).

A general problem of cell-therapy based clinical trials is the definition of quality parameters of the applied cells (74). In particular, the molecular function of CDC was not well characterized before proceeding to clinical applications (86). Some quality parameters mentioned in the CDC trial publications are the absence of the hematological marker CD45 and a uniform expression of the mesenchymal marker CD105 (61). However, the heterogeneity of the cells was shown by the highly varying expression of the fibroblast or mesenchymal marker CD90 ranging from 25% (61) to over 60% (87). In addition, these cells showed highly variable expression of the endothelial marker CD31 and C-KIT (73).

1.2.2 Age-dependent effects of CDC

Outcomes of clinical trials revealed beneficial effects of CDC treatment for pediatric patients but no or only moderate effects for adult patients (62, 69).

Several groups tried to elucidate the molecular mechanisms which contribute to these differences. Simpson *et al.* found that CDC derived from neonatal patients expressed the angiogenic factors angiogenin (*ANG*) and vascular endothelial growth factor A (*VEGFA*) significantly higher than CDC derived from adult patients. This also correlated with preservation

and formation of blood vessels in infarcted hearts which was significantly higher in neonatal patients. Besides, they reported an increased regenerative potential of CDC derived from neonatal patients, proven by improved ejection fraction in a rat model of myocardial infarction (88).

However, Nakamura *et al.* stated that no significant differences of the angiogenic potential of CDC derived from patients of different age were measured in a matrigel-based tube formation assay (89). On the contrary, Walravens *et al.* reported an increased angiogenic and proliferative potential of CDC derived from adult patients compared to CDC derived from children based on the results from a matrigel tube formation assay and RNA-sequencing, respectively. The authors suggest that differences to previous studies might be the result of the inclusion of pediatric patients of different ages and may particularly be due to the different number of neonates in different studies (90). Sharma *et al.* performed a study comparing the CDC characteristics of pediatric cardiac patients with different diagnoses, particularly distinguishing patients with end-stage heart failure (83). Interestingly, CDC derived from children with end-stage heart failure showed higher restoration capability after myocardial infarction and higher angiogenesis potential compared to CDC derived from patients with ventricular septum defects. This difference could mechanistically be attributed to their heat shock response-directed secretome (83).

The pediatric patients group which was treated in the TICAP and PERSEUS trial and which benefited from CDC transplantation had end-stage heart failure with SV diagnosis such as hypoplastic left heart syndrome (HLHS) (68, 87). HLHS is a severe congenital heart disease which is characterized by the underdevelopment of structures of the left heart side including the aortic and/ or mitral valve, left ventricle, aortic valve, and aortic arch (91, 92). Whereas in the 1980's children could only be provided with supportive care and died shortly after birth, nowadays an established three-stage surgical procedure exists which allows them to live until adulthood (91). The prevalence of HLHS in Germany was reported to be 0.15 per 1,000 live births (92, 93). Although the molecular mechanism leading to the HLHS pathology is still not fully understood, there is growing evidence that the phenotype is accompanied by a complex genotype with alterations such as single base-pair variants, duplication or deletions of larger sequences and aberrant methylation patterns (92, 94).

Even after the three-stage surgical procedure HLHS patients mostly suffer from severe long-term complications, such as high systemic venous pressures, abnormal ventricular morphology, thromboembolic events, and recurrent arrhythmias. The quality of life of HLHS patients is further impaired by specific pathologies such as protein-losing enteropathy and plastic bronchitis (95, 96). For this reason, the goal of research nowadays is to address this long-term challenges in order to enable HLHS patients a better quality of life (91).

2. Aim of the work

The aim of this work was to investigate the main human cardiac non-myocyte cell types (NMC): cardiac fibroblasts (CF), smooth muscle cells (SMC) and endothelial cells (EC). Particularly their heterogenic transcriptomic phenotypes are still not fully understood, but are essential to have a more detailed view into the different molecular processes ongoing in the heart. Additionally, the clinically used, but poorly characterized, cardiosphere-derived cells (CDC) were examined concerning similarities to NMC and donor age-related differences.

Cultivated CF, SMC and EC were characterized by known markers and further analyzed by single-cell RNA sequencing (sc-RNAseq) to reveal their identity and transcriptional heterogeneity. Furthermore, using the same methods, CDC were compared to the NMC in order to elucidate common features. Analysis of gene expression of CDC and CF derived from pediatric and adult patients was performed with the goal to assess whether there is age-related difference in heart-tissue-derived primary cells. To gain in-depth understanding of the transcriptomic differences of CDC derived from different aged donors, an infant and adult CDC sample were comped by sc-RNAseq. Functional *in vitro* tests with CDC- and CF- derived extracellular vesicles (EV) were performed to assess their effects on main cardiac cells, therby again considering the aspect of the donor's age from which the tissue for cell cultivation was derived. To address the patient group which mostly benefitted from clinical trials with CDC, the majority of pediatric patients included in these analyses had a single-ventricle (SV) diagnosis. Further, both gene expression and EV-mediated functional *in vitro* effects were compared between two pediatric age groups (≤ 21 days or 1 month-6 years) which were chosen according to the age at which SV patients undergo surgical palliation procedures. Additionally, it was examined whether sphere-formation of CF derived from neonatal patients (≤ 21 days) alters the analyzed aspects. Finally, a fresh cardiac biopsy was analyzed by sc-RNAseq to gain insight into NMC present *in vivo* and corresponding biopsy clusters were compared to cultured cells.

3. Materials

In the following paragraphs all materials used in this work are listed. Order numbers are marked with "#". Manufacturers' headquarters are indicated. If the headquarter is in USA, only the according state abbreviation is given.

3.1 General laboratory material

Table 2: General laboratory material

Equipment	Manufacturer
30 µm pre-separation filter, #130-041-407	Miltenyi Biotech, Bergisch Gladbach, Germany
30 µm Syringe Filcons Non- sterile, #340599	BD Biosciences, Franklin Lakes, NJ
96-well ImageLock™ tissue culture plate, #4379	EssenBiosciences, Hertfordshire, UK
Cell Culture Dishes, 60/15 mm (6 cm), #628160	Greiner Bio-One International GmbH, Frickenhausen,Germany
Cell Culture Flask T25, #G200FF-25	Kisker Biotech GmbH & Co. KG, Steinfurt, Germany
Cell Culture Flask T75, #G200FF-75	Kisker Biotech GmbH & Co. KG, Steinfurt, Germany
Cell Culture Multiwell Plate, 12 Well, PS, Clear, Cellstar®, sterile, #665180	Greiner Bio-One International GmbH, Frickenhausen, Germany
Cell Culture Multi-well Plate, 24 well, PS, Clear, Cellstar®, sterile, #662160	Greiner Bio-One International GmbH, Frickenhausen, Germany
Cell Culture Multi-well Plate, 6 well, PS, Transp., Cellstar®, sterile, #657160	Greiner Bio-One International GmbH, Frickenhausen, Germany
Cell Culture Multiwell Plate, 96 well, PS, Clear, Cellstar®, sterile, #655180	Greiner Bio-One International GmbH, Frickenhausen,Germany
Cryogenic vials Nunc 1.0 mL, #479-6842P	VWR International, Radnor, PA
EASYSTRAINER 70 µM, FOR 50 ML TUBES, #542070	Greiner Bio-One International GmbH, Frickenhausen, Germany
Eppendorf Safe-Lock Tubes, 1.5 mL, Eppendorf Quality™, #30120086	Eppendorf AG, Hamburg, Germany
Eppendorf Safe-Lock Tubes, 2.0 mL, Eppendorf Quality™, #30120094	Eppendorf AG, Hamburg, Germany
Falcon® 14mL Round Bottom Polystyrene Test Tube, with Snap Cap, sterile, #734-0444	VWR International, Radnor, PA
Falcon® 15mL High Clarity PP Centrifuge Tube, Conical Bottom, sterile, #734-0451	VWR International, Radnor, PA
Falcon® 50mL High Clarity PP Centrifuge Tube, Conical Bottom, sterile, #734-0448	VWR International, Radnor, PA
Injection syringes, 10 mL #4606108V, 20 mL #4606205V	B. Braun Melsungen AG, Melsungen, Germany
Menzel™ Microscope Coverslips 24x60 mm, #11778691	Thermo Fisher Scientific, Waltram, MA
MicroAmp™ Optical 96-Well Reaction Plate, #N8010560	Thermo Fisher Scientific, Waltram, MA
MicroAmp™ Optical Adhesive Film, #4311971	Applied Biosystems™, Thermo Fisher Scientific, Waltram, MA
Nunc™ Multidish, 4 well Multi well, 66x66 mm, #734-2176	VWR International, Radnor, PA
Parafilm® M, #P7793-1EA	Sigma-Aldrich, Merck Millipore, Merck KGaA, Darmstadt, Germany
PCR sealing film, #G040-TS-N	Kisker Biotech GmbH & Co.KG, Steinfurt, Germany
PCR SingleCap 8er Soft strips 0,2 mL, colorless, #710970	Biozym Scientific GmbH, Hessisch Oldendorf, Germany
PURPLE NITRIL examination gloves, #52002M	Halyard Health, Alpharetta, GA
PVDF-Filter 0,22 µm, #P666.1	Carl Roth GmbH + Co. KG, Karlsruhe, Germany

SafeSeal SurPhob Filter Tips, 10 µL, extra long, sterile, #VT0200	Biozym Scientific GmbH, Hessisch Oldendorf, Germany
SafeSeal SurPhob Filter Tips, 100 µL, sterile, #VT0230	Biozym Scientific GmbH, Hessisch Oldendorf, Germany
SafeSeal SurPhob Filter Tips, 1250 µL, sterile, #VT0270	Biozym Scientific GmbH, Hessisch Oldendorf, Germany
Sempercare® one-way gloves, Latex, Premium, #0321	Sempercare, Semperit AG, Wien, Austria
Serological Pipettes 10 mL, sterile, scale: 0.1 mL, color: orange, #GPS-10.0	Kisker Biotech GmbH & Co. KG, Steinfurt, Germany
Serological Pipettes 5 mL, sterile, scale: 0.1 mL, color: blue, #GPS-5.0	Kisker Biotech GmbH & Co. KG, Steinfurt, Germany
Surgical Disposable Scalpels, #BA220	B. Braun Melsungen AG, Melsungen,Germany
SurPhob Tips, without filter, low binding, DNA-, DNase-, RNase- free, 1250µL, #VT0173	Biozym Scientific GmbH, Hessisch Oldendorf, Germany
Syringe Filter, sterile, 0,22µm, #P666.1	Carl Roth GmbH + Co. KG, Karlsruhe, Germany
Tissue Culture Cell Scraper 25 cm, #831830	Sarstedt AG & Co, Nümbrecht,Germany

Table 3: Surgical Material

Name/ Catalogue Number	Producer
ETHIBOND EXCEL™ Polyester Suture, #EH7556H	Ethicon Inc., Somerville, NJ
Ligating Appliers, #137111	Teleflex Inc., Wayne, Pennsylvania
STANDARD FORCEPS SERR 145MM, #BD047R	B. Braun Melsungen AG, Melsungen, Germany
Surgical gloves, #82265	Manchester BIOGEL, Alderley Edge, Cheshire,
Surgical Scissors, #BC313R	B. Braun Melsungen AG, Melsungen, Germany
Titanium Ligating Clips, #001204	Teleflex Inc., Wayne, Pennsylvania

3.2 Instruments

Table 4: Instruments

Instrument	Manufacturer
10x Chromium Controller	10xGenomics, Pleasanton, CA
Agilent 2100 Bioanalyzer	Agilent, Santa Clara, CA
Analytical balance e Kern ABT 220-5 DNM	Kern & Sohn GmbH, Bahlingen, Germany
Autoclave, HICLAVE HI-50	HMC Europe GmbH, Tüßling, Germany
Biological Safety Cabinets Safe 2020	Thermo Fisher Scientific, Waltram, MA
C1000™ Thermal Cycler	Bio-Rad Laboratories GmbH, Munich, Germany
ChemDoc XR System	Bio-Rad Laboratories GmbH, Munich, Germany
Countess II FL	Life Technologies™, Thermo Fisher Scientific, Waltram, MA
Cryo 1°C Freezing Container, Nalgene™	Thermo Fisher Scientific, Waltram, MA
DNA/RNA UV-Cleaner Box	Kisker Biotech GmbH & Co. KG, Steinfurt, Germany
Drying Chamber, Modell ED 56	Binder GmbH, Tuttlingen, Germany
Eppendorf Thermomixer comfort	Eppendorf, Hamburg, Germany
Eppendorf® Research® plus Pipettes (10 µL, 20 µL, 100 µL, 1000 µL)	Eppendorf, Hamburg, Germany
FACS (BD LSR Fortessa)	Becton, Dickinson and Company, BD Bioscience, San Jose, CA
Fluorescence microscope Axiovert 200M	Zeiss, Oberkochen, Germany

Gel chamber Sub-Cell Modell 96	Bio-Rad Laboratories GmbH, München, Germany
GFL 7601 Hybridization Incubator	GENEO BioTechProducts GmbH, Hamburg, Germany
HERA Freezer Basic (-80°C)	Thermo Fisher Scientific, Waltram, MA
HERACell 240i CO_2 Incubator	Thermo Fisher Scientific, Waltram, MA
Heraeus Megafuge 40R	Thermo Fisher Scientific, Waltram, MA
HiSeq 1500	Illumina, San Diego, CA
HiSeq 3000/4000	Illumina, San Diego, CA
ImageQuant LAS 4000	GE Healthcare, Life Sciences, General Electric Company, Boston, MA
IncuCyte ZOOM® 96-Well Migration Assay system, including IncuCyte® Cell Migration Kit #4493	EssenBiosciences, Hertfordshire, UK
Infinite® 200 PRO	Tecan Trading AG, Männedorf, Switzerland
Lauda Aqualine AL 12, water bath	LAUDA-Brinkmann, LP, Delran, NJ
Liquid Nitrogen System	Messer Griesheim, Bad Soden, Germany
Microwave MW 7849 900W	Severin, Sundern, Germany
MIKRO 220 Table Centrifuge	Kirchlengern, Germany
MilliQ	Merck Millipore, Merck KGaA, Darmstadt, Germany
Mini Plate Spinner mps 1000	Labnet International, Cary, NC
NanoDrop 2000c Spectrophotometer	Thermo Fisher Scientific, Waltham, MA
Neubauer counting chamber	Thomas Scientific, Svedesboro, NJ
Nikon Eclipse Ts2	Nikon, Minato, Japan
pH Meter Multical pH540 GLP	Xylem Analytics Germany Sales GmbH & Co. KG, WTW, Weilheim, Germany
pipetus® 100-240 Volt	Hirschmann Laborgeräte GmbH & Co. KG, Eberstadt, Germany
PowerPac Basic	Bio-Rad Laboratories GmbH, Munich, Germany
Quant Studio 3 Real-Time PCR System	Applied Biosystems by Thermo Fisher Scientific, Waltram, MA
Refrigerator Liebherr Medline (4°C)	Liebherr, Bulle, Germany
Refrigerator Liebherr Premium No Frost (-20°C)	Liebherr, Bulle, Germany
Table Centrifuge 5417R	Eppendorf, Hamburg, Germany
Veriti™ Dx 96-well Fast Thermal Cycler	Applied Biosystems by Thermo Fisher Scientific, Waltram, MA
Vortex Genie 2	Scientific Industries Inc., Bohemia, NY
ZetaView PMX110 instrument	Particle Metrix, Inning, Germany

3.3 Antibodies

Table 5: Primary antibodies

Protein Target	Dilution used	Fluorescent Dye if directly labeled	Application	Producer	Catalogue Number (Cat. No.)
CD90	1 to 11	PE-Cy5	FC	eBioscience, Inc., San Diego, CA	15-0909
CD105	1 to 11	APC	FC	eBioscience, Inc., San Diego, CA	17-1057
CD31	1 to 11	PE-Cy7	FC	eBioscience, Inc., San Diego, CA	25-0319-42
CD45	1 to 11	FITC	FC	eBioscience, Inc., San Diego, CA	11-94-59
DDR2	1 to 20	-	FC/ ICC (AF/CDC/CF/SMC/ EC)	LSBio, Seattle, WA	LS-C99151/64099
SIRPA	1 to 25	-	FC	BioLegend, San Diego, CA	323802

Vimentin	1 to 1000	-	ICC (AF/CDC/CF/SMC/ EC)	Abcam, Cambridge, UK	45939
CD90	1 to 50	-	ICC (AF/CDC/CF/SMC/ EC)	antibodies-online GmbH, Aachen, Germany	ABIN1724884
CD31	1 to 100	-	ICC (AF/CDC/CF/SMC/ EC)	Abcam, Cambridge, UK	ab28364
α-SMA	1 to 100	-	ICC (AF/CDC/CF/SMC/ EC)	Abcam, Cambridge, UK	ab5694
Tnnt2	1 to 50	-	ICC (NRCM)	Abcam, Cambridge, UK	ab125266
α-Actinin	1 to 200	-	ICC (NRCM)	Abcam, Cambridge, UK	ab9465
Anti-αMHC	1 to 100	-	ICC (NRCM)	Novus Biologicals, R&D Systems, Minneapolis, MN	MAB4470
Tnni3	1 to 100	-	ICC (NRCM)	Abcam, Cambridge, UK	ab200080
Cx43	1 to 100	-	ICC (NRCM)	Sigma-Aldrich, Merck Millipore, Merck KGaA, Darmstadt, Germany	MAB3068

Abbreviations FC: Flow cytometry, ICC: immunocytochemistry, cell type for which the antibody was used is indicated in brakets, NRCM: neonatal rat cardiomyocytes.

Table 6: Secondary antibodies

Antibody	Fluorescent Dye	Producer	Catalogue Number (Cat. No.)	Dilution/ Application
Goat Anti-Mouse IgG H&L	(Alexa Fluor® 555)	Abcam, Cambridge, UK	ab150114	1:500 (ICC)
Goat Anti-Mouse IgG H&L	(Alexa Fluor® 488)	Abcam, Cambridge, UK	ab150113	1:500 (ICC), 1:2,000 (FC)
Goat Anti-Rabbit IgG H&L	(Alexa Fluor® 555)	Abcam, Cambridge, UK	ab150078	1:500 (ICC)
Goat Anti-Rabbit IgG H&L	(Alexa Fluor® 488)	Abcam, Cambridge, UK	ab150077	1:500 (ICC), 1:2,000 (FC)

Abbreviations: FC: Flow cytometry, ICC: immunocytochemistry, cell type for which the antibody was used is indicated in brackets.

3.4 Kits

Table 7: Kits

Kit	Manufacturer
Agilent High Sensitivity DNA Kit, #5067-4626	Agilent, Santa Clara, CA
Chromium Next GEM Single Cell 3' GEM, Library & Gel Bead Kit v3.1, # 1000128	10xGenomics, Pleasanton, CA
Chromium™ Single Cell 3' Library & Gel Bead Kit v2, # 120267	10xGenomics, Pleasanton, CA
Chromium i7 Multiplex Kit, #120262	10xGenomics, Pleasanton, CA
Dead cell removal Kit, #130-090-101	Miltenyi Biotech, Bergisch Gladbach, Germany
Exo-Flow Exosome Capture Kit, #EXOFLOW15A-1	System Biosciences, Palo Alto, CA

ExoQuick-TC, #EXOTC50A-1	System Biosciences, Palo Alto, CA
microRNA PCR ExiLENT SYBR® Green master mix, # 203421	Exiquon, now Qiagen, Hilden, Germany
miRCURY LNA™ microRNA PCR, # 20342	Exiquon, now Qiagen, Hilden, Germany
miRCURY LNA™ RT Kit, #339340	Exiquon, now Qiagen, Hilden, Germany
M-MLV Reverse Transkriptase Kit, #28025013	Invitrogen™, Thermo Fisher Scientific, Waltram, MA
peqGOLD DNase I Digest Kit, #732-2982	Peqlab Biotechnologie GmbH, Erlangen, Germany
peqGOLD Total RNA Kit (S-Line), #732-2871	VWR International, Radnor, PA
Power SYBR® Green PCR Master Mix, #4367659	Applied Biosystems by Life Technologies™, Thermo Fisher Scientific, Waltram, MA
Ready Probe Viablity Imaging Kit Blue/Green, #R37609	Thermo Fisher Scientific, Life Technologies™, Waltram, MA
SeraMir Exosome RNA Purification Column Kit, #RA808A-1	System Biosciences, Palo Alto, CA

3.5 Primer sequences

Table 8: Primer Sets qRT-PCR (messenger RNA, mRNA)

Official gene symbol	official name	Gene bank identification (ID)	5´→ 3´ (forward)	5´→ 3´ (reverse)
GATA4	GATA Binding Protein 4	NM_001308093., NM_001374274.1, NM_001374273.1, NM_002052.5, NM_001308094.2	GGA AGC CCA AGA ACC TGA AT	GCT GGA GTT GCT GGA AGC
ACTB	Homo sapiens Actin Beta	NM_001101.3	CCA AAC GCG AGA AGA TGA	CCA GAG GCG TAC AGG GAT AG
ACTA2	Homo sapiens actin, alpha 2, smooth muscle, aorta	NM_001141945.2	GTG ATC ACC ATC GGA AAT GAA	TCA TGA TGC TGT TGT AGG TGG T
ALDH1A2	Homo sapiens aldehyde dehydrogenase 1 family member A2	NM_170697.3, NM_170696.3	ATC AAC AAG GCC CTC ACA GT	TCT GGG CAT TTA AGG CAT TG
CDH5	Homo sapiens cadherin 5	NM_001795.4	AAG CCT CTG ATT GGC ACA GT	CTG GCC CTT GTC ACT GGT
COL1A1	Homo Sapiens Collagen Type I Alpha 1 Chain	NM_000088.3	CAA GAG TGG TGA TCG TGG TG	GCC TGT CTC ACC CTT GTC A
COL3A1	Homo sapiens collagen type III alpha 1 chain	NM_000090.3	ACA TCG AGG ATT CCC TGG TA	GCT GGA GTT GCT GGA AGC
COL6A2	Homo sapiens collagen type VI alpha 2 chain	NM_001849.3, NM_058174.2, NM_058175.2	AGA ACG GGA CCG ATG GAC	CCT GGA CTC CCT GCT TCC
CXCL3	Homo sapiens C-X-C motif chemokine ligand 3	NM_002090.2	AAA TCA TCG AAA AGA TAC TGA ACA AG	GGT AAG GGC AGG GAC CAC
CXCL6	Homo sapiens C-X-C motif chemokine ligand 6	NM_002993.3	GTC CTT CGG GCT CCT TGT	CAG CAC AGC AGA GAC AGG AC
DDR2	Homo sapiens discoidin domain receptor tyrosine kinase 2	NM_001014796.3, NM_001014796.3, NM_001354983.2	TAT GGC ACC CAC AAC CTA TG	TGG CCA GGA GGA TAA AGA TG

ENG (CD105)	Homo sapiens endoglin (ENG)	NM_001114753.2, NM_000118.3, NM_001278138.1	AAT GCC ATC CTT GAA GTC CA	GTG CCA TTT TGC TTG GAT G
FLBN2	Homo sapiens fibulin 2	NM_001998.3, NM_001165035.2, NM_001004019.2	CCC CAG AAG TAG CCC TAG A	CAG GCA CTC GTC ATT GTC A
IL1B	Homo sapiens interleukin 1 beta	NM_000576.2	TAC CTG TCC TGC GTG TTG AA	TCT TTG GGT AAT TTT TGG GAT CT
NKX2-5	Homo sapiens NK2 homeobox 5	NM_004387.3	TTC TAT CCA CGT GCC TAC AGC	CTG TCT TCT CCA GCT CCA CC
PECAM1 (CD31)	Homo sapiens platelet and endothelial cell adhesion molecule 1 (PECAM1)	NM_000442.4	ATG CCG TGG AAA GCA GAT AC	CTG TTC TTC TCG GAA CAT GGA
PDGFRA	Homo sapiens platelet derived growth factor receptor alpha	NM_006206.6	CCA CCT GAG TGA GAT TGT GG	TCT TCA GGAAGT CCA GGT GAA
PDGFRB	Homo sapiens platelet derived growth factor receptor beta	NM_002609.3	GTG CTG GGA AGA GAA GTT TGA	TCA TCC ACC TGC TGG TAC TTC
S100A4	Homo sapiens S100 calcium binding protein A4	NM_002961.2, NM_019554.2	GCT CAA CAA GTC AGA ACT AAA GGA G	GCA GCT TCA TCT GTC CTT TTC
TBX5	Homo sapiens T-box 5	NM_000192.3	TGA TCA TAA CCA AGG CTG GA	GAT TAA GGC CCG TCA CCT TC
TIMP3	Homo sapiens TIMP metallopeptidase inhibitor 3	NM_000362.4	GCT GGA GGT CAA CAA GTA CCA	CAC AGC CCC GTG TAC ATC T
TAGLN	Homo sapiens transgelin	NM_001001522.1, NM_003186.3	CAG ACT GTT GAC CTC TTT GAA GG	GCC CAT CAT TCT TGG TCA CT
THY1 (CD90)	Thy-1 Cell Surface Antigen	NM_006288.5, NM_001372050.1, NM_001311162.2, NM_001311160.2	CAG AAC GTC ACA GTG CTC AGA	GAG GAG GGA GAG GGA GAG C
Actb	Rattus norvegicus Actin Beta	NM_031144	CCA ACC GTG AAA AGA TGA CC	ACC AGA GGC ATA CAG GGA CA
Aldh1a2	Rattus norvegicus aldehyde dehydrogenase	NM_053896.2	ACA AGG CTC TCA TGG TGT CC	TCT GAG CAT TTA AGG CGT TG
Fas	Rattus norvegicus Fas cell surface death receptor	NM_139194.2	TGC GCC TTC TGT GAT GAA	CTT TGC ACC TGC ACT TGG T
Tnnt2	Rattus norvegicus troponin T2, cardiac type (Tnnt2)	XM_006249842.3, XM_017598673.1, XM_006249840.3	TTC GAC CTG CAG GAA AAG TT	CTT CCC ACG AGT TTT GGA GA

Table 9: Primer Sets (miR qRT-PCR)

MiR name	Manufacturer	Catalogue Number
Hsa-miR-132-3p	Exiquon, now Qiagen, Hilden, Germany	YP00206035
Hsa-miR-146-5p	Exiquon, now Qiagen, Hilden, Germany	YP00204688

Hsa-miR-21	Exiquon, now Qiagen, Hilden, Germany	YP00204230
Hsa-miR-423-3p	Exiquon, now Qiagen, Hilden, Germany	YP00204488

3.6 Chemicals and reagents

Table 10: Chemicals and Reagents

Chemicals and reagents	Manufacturer
100 nm NanoStandards	Applied Microspheres, Leusden, The Netherlands
4',6-Diamidino-2-Phenylindole (DAPI), #422801	Biolegend, San Diego, CA
Accutase, #7920	StemCell™ Technologies, Köln, Germany
Agarose (PeqGOLD Universal), #35-1020	PEQLAB GmbH, VWR Life Science Competence, Erlangen, Germany
β-Mercaptoethanol (55 mM), #21985-023	Gibco® by Life Technologies™, Thermo Fisher Scientific, Waltram, MA
Boric acid, #6943.1	Carl Roth GmbH + Co. KG, Karlsruhe, Germany
BSA (bovine serum albumin), #A7906	Sigma-Aldrich, Merck Millipore, Merck KGaA, Darmstadt, Germany
CHIR99021, #C-6556	LC Laboratories, Woburn, MA
Cobalt (II) chloride hexahydrate, #C2644	Sigma-Aldrich, Merck Millipore, Merck KGaA, Darmstadt, Germany
Collagenase Type II, #17101-015	Life Technologies™, Thermo Fisher Scientific, Waltram, MA
Collagenase, Type IV, #17104019	Life Technologies™, Thermo Fisher Scientific, Waltram, MA
Corning® Matrigel® hESC-Qualified Matrix, #354277	Corning, Tewksbury, MA
D (+)-Trehalose Dihydrate, #5151.1	Carl Roth GmbH + Co. KG, Karlsruhe, Germany
Dimethylsulfoxid (DMSO), #A994.1	Carl Roth GmbH + Co. KG, Karlsruhe, Germany
DNA Away® Decontamination Solution, #732-2353	VWR, Radnor, PA
DNA Gel Loading Dye (6x), # R0611	Thermo Scientific™, Thermo Fisher Scientific, Waltram, MA
DNA/RNA-Dye, peqGREEN, 2x1mL, #732-2960	VWR, Radnor, PA
DNAse I recombinant, RNase-free, #04716728001	Roche Molecular Systems, Inc., Rotkreuz, Switzerland
dNTP-Set 1 (100 mM dATP, dTTP, dGTP, dCTP), #K039.1	Carl Roth GmbH + Co. KG, Karlsruhe, Germany
D-PBS, w: Ca^{2+} and Mg^{2+}, #P04-36500	PAN-Biotech GmbH, Aidenbach, Germany
DTT, 1 mM, #28025013	Invitrogen™, Thermo Fisher Scientific, Waltram, MA
Dry ice	TKD TrockenEis und Kohlensäure Distribution GmbH, Fraunberg-Tittenkofen, Germany
EDTA, #CN06.1	Carl Roth GmbH + Co. KG, Karlsruhe, Germany
Ethanol 96% denatured, #T171.3	Carl Roth GmbH + Co. KG, Karlsruhe, Germany
Ethanol absolute 95%, #64-17-5	Sigma-Aldrich, Merck Millipore, Merck KGaA,
Ethanol, Pure (200 Proof, anhydrous), #E7023-500ML	Sigma-Aldrich, Merck Millipore, Merck KGaA, Darmstadt, Germany
Ethidiumbromide, #MKBV9660V	Sigma Life Science, Sigma Aldrich, Merck Millipore, Merck KGaA, Darmstadt, Germany
Fetal Bovine Serum, EU Approved origin, South America, #10270-106	Gibco® by Life Technologies™, Thermo Fisher Scientific, Waltram, MA
Fibronectin bovine plasma, #F4759	Sigma-Aldrich, Merck Millipore, Merck KGaA, Darmstadt, Germany
Gelatine, #G9391	Sigma-Aldrich, Merck Millipore, Merck KGaA, Darmstadt,

	Germany
GeneRuler™ DNA Ladder, 50 bp, #SM0371	Thermo Scientific™, Thermo Fisher Scientific, Waltram, MA
Glycerin solution, 50% (v/v), #3290-32	Ricca Chemical Company, Arlington, TX
H_2O VE	water purification system Research Center DHM
H_2O, nuclease-free, #R0581	Thermo Fisher Scientific™, Thermo Fisher Scientific, Waltram, MA
Hank's Balanced Salt solution (HBSS), #H9394	Sigma-Aldrich, Merck Millipore, Merck KGaA, Darmstadt, Germany
Horse serum, #16050112	Life Technologies™, Thermo Fisher Scientific, Waltram, MA
Hydrochloric acide, c(HCl) = 0,1 mol/l (0,1 N) Titripur® Reag. Ph Eur, Reag. USP, #109060	Merck Millipore, Merck KGaA, Darmstadt, Germany
Immersion oil, #56822	Sigma-Aldrich, Merck Millipore, Merck KGaA, Darmstadt, Germany
INCIDIN™ OXYFOAM S, #3087450	Ecolab, Saint Paul, MN
Isofluran (2-chloro-2-(difluoromethoxy)-1,1,1-trifluoro-ethane Baxter vet 100mg/g, #HDG9623V	Baxter, Deerfield, IL
L-Ascorbic acid-2-phosphate, #A8960	Sigma-Aldrich, Merck Millipore, Merck KGaA, Darmstadt, Germany
Methanol, #34860	Sigma-Aldrich, Merck Millipore, Merck KGaA, Darmstadt, Germany
Mitomycin C, #M4287	Sigma-Aldrich, Merck Millipore, Merck KGaA, Darmstadt, Germany
Mounting Medium with DAPI, #ab104138	Abcam, Cambridge, UK
Normal goat serum, #ab7841	Abcam, Cambridge, UK
Nuclease Free H_2O, #10977-035	Invitrogen™, Thermo Fisher Scientific, Waltram, MA
Paraformaldehyde, #0964.1	Carl Roth GmbH + Co. KG, Karlsruhe, Germany
PBS powder without Ca2+, Mg2+, #L-182-50	Biochrom, Merck Millipore, Merck KGaA, Darmstadt, Germany
Penicillin – Streptomycin (100x) for cell culture BC, #A8943	PanReac AppliChem, AppliChem GmbH, Darmstadt, Germany
peqGREEN 20 000X DNA/RNA binding dye, #732-2960	VWR, Radnor, PA
Poly-D-lysine solution, 1.0 mg/mL, #A-003-E	Sigma-Aldrich, Merck Millipore, Merck KGaA, Darmstadt, Germany
Potassium chloride KCl, ≥ 99,0%, #P9541	Sigma-Aldrich, Merck Millipore, Merck KGaA, Darmstadt, Germany
Quantitas DNA Marker 25 – 500 bp, #250216	Biozym Scientific GmbH, Hessisch Oldendorf, Germany
Random Hexamer Oligonucleotide, #48190011	Invitrogen™, Thermo Fisher Scientific, Waltram, MA
Recombinant human cardiotrophin-1, #300-32	Peprotech, Rocky Hill, NJ
Recombinant human FGF-basic, #AF-100-18B	Peprotech, Rocky Hill, NJ
Recombinant humane serum albumin, #A0237	Sigma-Aldrich, Merck Millipore, Merck KGaA, Darmstadt, Germany
Red Blood Cell Lysis Buffer, #130-094-183	Miltenyi Biotech, Bergisch Gladbach, Germany
ReLeSR™, #05872	StemCell™ Technologies, Köln, Germany
Rock Inhibitor Y-27632, #72304	StemCell™ Technologies, Köln, Germany
Sodium hydroxide solution, c(NaOH) = 0,1 mol/l (0,1 N) Titripur® Reag. Ph Eur, Reag. USP, #1.09141	Sigma-Aldrich, Merck Millipore, Merck KGaA, Darmstadt, Germany
Sodium pyruvate, #11360-070	Gibco® by Life Technologies™, Thermo Fisher Scientific, Waltram, MA
SPRIselect Reagent, #B23317	Beckman Coulter GmbH, Krefeld, Germany
Sucrose, for molecular biology, ≥99.5%, #S0389	Sigma-Aldrich, Merck Millipore, Merck KGaA, Darmstadt,

	Germany
Thiazolyl Blue Tetrazolium Bromide, #M5655	Sigma-Aldrich, Merck Millipore, Merck KGaA, Darmstadt, Germany
TrisBase, #5429.3	Carl Roth GmbH + Co. KG, Karlsruhe, Germany
Triton-X-100, #3051.3	Carl Roth GmbH + Co. KG, Karlsruhe, Germany
Trypan blue 0.5% (w/v), #L6323	Biochrom, Merck Millipore, Merck KGaA, Darmstadt, Germany
Trypsin-EDTA (0.25%, phenol red), #25200-056	Life Technologies™, Thermo Fisher Scientific, Waltram, MA
UltraPure™ 0.5M EDTA, pH 8.0, #15575-038	Gibco® by Life Technologies™, Thermo Fisher Scientific, Waltram, MA
Universal-Agarose, peqGOLD, #732-2789	VWR, Radnor, PA
Water, RNase-free, DEPC treated, Molecular Biology Grade, Ultrapure, # J70783	Thermo Fisher Scientific™, Thermo Fisher Scientific, Waltram, MA
Wnt-C59, #S7037	Sellekchem, Houston, TX

3.7 Buffers and solutions

Production, storage and stability of solutions used for this work is listed in the following paragraph. All sterile filtrations were performed using 0.22 µm PVDF-filters (#P666.1, Carl Roth GmbH + Co. KG, Karlsruhe, Germany). Demineralized water was provided by the water purification system at the Research Center of the German Heart Center (German name: "Forschungsneubau, DHM"). Millipore water refers to bi-distilled water which was filtered through Milli-Q® Type 1 Ultrapure Water System filters (Merck Millipore, Merck KGaA, Darmstadt, Germany). Autoclaving of solutions was performed using the Autoclave, HICLAVE HI-50 (HMC Europe GmbH, Tüßling, Germany) applying the appropriate program. Freeze-thaw cycles of aliquots were either avoided or omitted according to manufacturer's instructions.

Dulbecco´s Phosphat buffered saline (1x D-PBS)

PBS powder without Ca^{2+}, Mg^{2+} (#L-182-50, Biochrom, Merck Millipore, Merck KGaA) was dissolved in Millipore water to a 10x stock solution according to manufacturer's instructions. 10x Dulbecco's Phosphat buffered saline (10x D-PBS) was diluted with Millipore water (v/v). 1x D-PBS was autoclaved for sterilization and stored at room temperature (15-25°C).

Trypan blue solution (0.2%)

Trypan blue solution (0.2%) was used for counting the viable cell fraction in cell culture. Trypan blue (0.5% (w/v), #L6323 Biochrom, Merck Millipore, Merck KGaA) was diluted with sterile 1x D-PBS to a concentration of 0.2% (w/v). Aliquots were stored at 4°C for up to 36 months.

Trypsin EDTA solution (0.05%)

Trypsin EDTA solution (0.05%) was used for the harvest protocol of cardiac outgrowth cells. Trypsin-EDTA (0.25%, #25200-056, Life Technologies™, Thermo Fisher Scientific, Waltram, MA) was diluted with sterile 1x D-PBS. This working solution was stable for 2 weeks at 4°C.

Ethanol (70%)

Ethanol (70%) was used for sterilization of plastic materials and equipment used under the safety cabinet. This solution was prepared by dilution of 96% denatured ethanol (#T171.3, Carl Roth GmbH + Co. KG) with demineralized water (v/v) and stored at room temperature.

Collagenase II solution (0.2%)

Collagenase II solution (0.2%) was used for digestion of adipose and cardiac tissue during isolation of adipose or cardiac fibroblasts. Collagenase type II (#17101-015, Life Technologies™, Thermo Fisher Scientific) was dissolved in sterile 1x D-PBS at a concentration of 0.2% (w/v). The solution was supplemented with penicillin and streptomycin (#A8943, PanReac AppliChem, AppliChem GmbH, Darmstadt, Germany) to a final concentration of 100 U/mL penicillin und 100 µg/mL streptomycine. The solution was filter-sterilized and stored for up to one week at 4°C in the dark.

Collagenase IV solution (1%)

Collagenase IV solution (1%) was used as a component of COG digestion solution (see below). Collagenase IV (#17104019, Life Technologies™, Thermo Fisher Scientific) was dissolved in 1x D-PBS at a concentration of 1.0% (w/v) and filter-sterilized. The solution was stored for up to one week at 4°C in the dark.

Albumin from bovine serum (BSA) solution

BSA solutions were used either for stabilization of cytokines after reconstitution or as a component of serum-free medium. A 10 mg/mL BSA working solution was prepared by dissolving BSA (#A7906, Sigma-Aldrich, Merck Millipore, Merck KGaA) in sterile 1x D-PBS followed by filter-sterilization. This solution was further diluted according to manufacturer's instructions for cytokine reconstitution. For serum-free medium production, a working solution of 100 mg/mL was prepared using the same procedure. BSA working solutions were stored at 4°C for up to one week.

Cardiac outgrowth (COG) digestion solution

COG digestion solution was used to pre-digest the atrial tissue biopsy for cardiac outgrowth generation as the first step in the CDC generation protocol. It was freshly prepared on the day when a fresh biopsy was processed. COG digestion solution consisted of 80% (v/v) 0.25% trypsin-EDTA (#25200-056, Life Technologies™, Thermo Fisher Scientific), 10% collagenase-IV-solution (v/v) and 10% 1x D-PBS (v/v).

Poly-D-lysine solution

Poly-D-lysine solution was used to coat 4-well plates (Nunc™ Multidish, 4 well Multi well, 66x66 mm, #734-2176), for the second step of the CDC generation protocol. Purchased poly-D-lysine solution (1.0 mg/mL, #A-003-E, Sigma-Aldrich, Merck Millipore, Merck KGaA) was aliquoted upon arrival and stored at -20°C until use for up to 18 months. For coating of plates, an aliquot was thawed at 4°C, diluted with sterile 1x D-PBS to a 50 µg/mL working solution and filter-sterilized. 200 µL of the poly-D-lysine were pipetted per well and incubated at 4°C overnight. On the next day, the coated plates were directly used according to the cell culture protocol described in paragraph 4.4.1.

Fibronectin solution

Fibronectin solution was used for coating 12-well plates (Cell Culture Multiwell Plate, 12 Well, PS, Clear, Cellstar®, sterile, #665180, Greiner Bio-One International GmbH, Frickenhausen, Germany) on which cardiospheres were replated (third step of the CDC generation protocol). Purchased fibronectin (#F4759, Sigma-Aldrich, Merck Millipore, Merck KGaA) was dissolved in Millipore water at a concentration of 1 mg/mL (w/v), aliquoted and stored at -20°C. For coating of plates, an aliquot was thawed at 4°C and diluted to a concentration of 20 µg/mL in 1x D-PBS (Working fibronectin solution). Working fibronectin solution was pipetted into each well to ensure full coverage of the well surface and immediately aspirated, leaving a thin layer of liquid on top of each well. The plates were then left open under the Safety Cabinet, to allow the evaporation of the remaining liquid. The coated plates were directly used according to the cell culture protocol described in paragraph 4.4.1.

bFGF solution (20 µg/mL)

Recombinant human FGF-basic (#AF-100-18B, Peprotech, Rocky Hill, NJ) was reconstituted in sterile Millipore water with 0.1% BSA (#A7906, Sigma-Aldrich, Merck Millipore, Merck KGaA) at a concentration of 20 µg/mL (w/v). Aliquots of the reconstituted solution were stored at -20°C for up to one year. bFGF solution was used for preparation of cardiosphere-growing medium (CGM, see Table 12). On the day of medium preparation, an aliquot of the reconstituted bFGF solution was thawed at 4°C. Final concentration of bFGF soluti in the medium was 20 ng/mL. CGM which was supplemented with bFGF solution was used directly after it was prepared and was not stored.

Cardiotrophin-1 solution

Recombinant human cardiotrophin-1 (#300-32, Peprotech, Rocky Hill, NJ) was reconstituted in sterile 1x D-PBS containing 20 mM Tris (pH = 8.0, #5429.3, Carl Roth GmbH + Co. KG) and 0.1% BSA (#A7906, Sigma-Aldrich, Merck Millipore, Merck KGaA) at a concentration of 2 µg/mL (w/v). Aliquots were stored at -80°C for up to one year. Cardiotrophin-1 solution was used for preparation of CGM (see Table 12). On the day of medium preparation, an aliquot of the

reconstituted cardiotrophin-1 solution was thawed at 4°C. The final concentration in CGM was 40 ng/mL. CGM which was supplemented with cardiotrophin-1 solution was used directly after it was prepared and was not stored.

Epidermal growth factor (EGF) solution

Recombinant human epidermal growth factor (#236-EG, R&D Systems, Minneapolis, MN) was reconstituted at 500 µg/mL (w/v) in sterile 1x D-PBS. Aliquots were stored at -80°C for up to three months. EGF-solution was used for preparation of CGM (see Table 12). On the day of medium preparation, an aliquot of the reconstituted cardiotrophin-1 solution was thawed at 4°C. The final concentration in CGM was 250 ng/mL. CGM which was supplemented with EGF-solution was used directly after it was prepared and was not stored.

Thrombin solution

Thrombin (#T4648, Sigma-Aldrich, Merck Millipore, Merck KGaA) was reconstituted with a solution of 0.1% BSA (#A7906, Sigma-Aldrich, Merck Millipore, Merck KGaA) in sterile 1x D-PBS to a stock solution of 100 units/mL and pH was adjusted to 6.5, according to manufacturer's instructions. The stock solution was aliquoted and stored at -20°C according to manufacturer's instructions. Thrombin was used in the CGM at a final concentration of 1 unit/mL. CGM which was supplemented with thrombin-solution was used directly after it was prepared and was not stored.

β-Mercaptoethanol solution

β-Mercaptoethanol is a reducing agent which is used in cell culture media in order to reduce toxic concentrations of oxygen radicals. β-Mercaptoethanol solution (#21985-023, Gibco® by Life Technologies™, Thermo Fisher Scientific) is a 55 mM stock solution in *Dulbecco's Modified Eagle* medium (#FG0435, DMEM, Biochrom, Merck Millipore, Merck KGaA). This solution was stored at 4°C for up to 36 months. It was used in self-made culture media at the concentration 0.1 mmol/L (see Table 12).

EDTA/PBS solution (0.5 mM)

EDTA/PBS solution (0.5 mM) was used for dissociation of human iPSC which were used for direct cardiac differentiation. 0.5 M EDTA (#15575-038, UltraPure™ 0.5 M EDTA, pH 8.0, Gibco® by Life Technologies™, Thermo Fisher Scientific) was diluted with sterile 1x D-PBS, filter-sterilized and stored for up to six months at room temperature.

Recombinant human serum albumin solution

O. sativa-derived recombinant human serum albumin (#A0237, Sigma-Aldrich, Merck Millipore, Merck KGaA) was a component of direct cardiac differentiation medium for iPSC (CDM3). The

powder is stored at -20°C. A stock solution of 75 mg/mL (w/v) was made in Millipore water and aliquots were stored at -20°C for up to six months.

L-Ascorbic acid-2-phosphate solution

L-Ascorbic acid-2-phosphate (#A8960, Sigma-Aldrich, Merck Millipore, Merck KGaA) was a component of direct cardiac differentiation medium for iPSC (CDM3). A stock solution of 64 mg/mL (w/v) in Millipore water was filter-sterilized and aliquots were stored for a maximum of six months at -20°C in the dark. L-Ascorbic acid-2-phosphate was freshly added to CDM3 medium at each medium change.

CHIR99021 solution

CHIR99021 (#C-6556, LC Laboratories, Woburn, MA) was stored at -20°C. A 6 mM stock solution in DMSO (Carl Roth GmbH + Co. KG) was aliquoted and stored at -80°C. According to manufacturer's instructions this solution is stable at -80°C for a maximum of six months.

Wnt-C59 solution

Unreconstituted Wnt-C59 (#S7037, Sellekchem, Houston, TX) is stable for three years at -20°C (manufacturer's instructions). A 2 mM stock solution in DMSO was aliquoted and stored at -80°C. Maximal storage time was limited to six months to ensure compound stability (manufacturer's instructions).

Rock inhibitor Y-27632 solution

A 10 mM stock solution was prepared by dissolving 1 mg Rock Inhibitor Y-27632 (#72304, StemCell™ Technologies) in 312 µL 1x D-PBS, aliquoted and stored at -20°C in the dark. The stability of reconstituted Rock inhibitor Y-27632 is six months according to manufacturer's instructions. Prior to use, an aliquot was thawed and a dilution in cell culture medium resulting in a final concentration of 10 µM was prepared. The thawed aliquot was kept at 4°C for up to two weeks.

PBS-T (0.1% / 0.25%)

The dilution of Triton-X-100 solution (#3051.3, Carl Roth GmbH + Co. KG) in 1x D-PBS was named PBS-T. Dilutions of 0.1% (v/v) or 0.25% (v/v) were produced for different steps of ICC. The solutions were stored at room temperature for up to three years.

FACS buffer 2mM EDTA (PBS/0.5% BSA/ 2 mM EDTA)

FACS buffer 2mM was used during cell preparation for flow cytometric analysis. Due to BSA and EDTA cells are stabilized and prevented from clumping. One g BSA (#A7906, Sigma-Aldrich, Merck Millipore, Merck KGaA) and 0.11 g EDTA (#CN06.1, EDTA, Carl Roth GmbH + Co. KG) were

dissolved in 200 mL of 1x D-PBS (w/v) and filter-sterilized. FACS buffer 2mM was stored at 4°C for up to four weeks.

FACS buffer 4mM EDTA (PBS/0.5% BSA/ 4 mM EDTA)

FACS buffer 4mM was used for cell suspension during flow cytometric measurement. One g BSA (#A7906, Sigma-Aldrich, Merck Millipore, Merck KGaA) and 0.22 g EDTA (#CN06.1, EDTA, Carl Roth GmbH + Co. KG) were dissolved in 200 mL of 1x D-PBS (w/v) and filter-sterilized. FACS buffer 4mM was stored at 4°C for up four weeks.

DAPI-solution

DAPI (4',6-Diamidino-2-Phenylindole, Dilactate, #422801, Biolegend, San Diego, CA) was dissolved in Millipore water at a concentration of 5 mg/mL, aliquoted and stored at -20°C, according to manufacturer's instructions (stock solution). Working solution was prepared by dilution of the stock solution to 0.1 mg/mL and stored protected from light at 4°C for up to 3 months. When performing flow cytometric analysis working solution was added to cell suspension at a ratio of 1:100, resulting in an end concentration of 1 µg/mL (see paragraph 4.5.3)

TRIS Borate EDTA buffer

TRIS borate EDTA buffer (1x TBE) was used for agarose gel electrophoresis. A 10x TBE buffer, consisting of 55.03 g boric acid (#6943.1, Carl Roth GmbH + Co. KG), 107.81 g Tris Base (#5429.3, Carl Roth GmbH + Co. KG) and 5.85 g EDTA (#CN06.1, Carl Roth GmbH + Co. KG) in 750 mL Millipore water was adjusted to a pH of 8.3. 10x TBE was stored for up to six months at room temperature. 1x TBE was prepared by dilution of 10x TBE with Millipore water (v/v) directly before use.

25mM Trehalose solution

D-(+)-Trehalose Dihydrate (#5151.1, Carl Roth GmbH + Co. KG) was dissolved in 1x D-PBS (D-PBS, without Ca^{2+} and Mg^{2+}, #P04-36500, PAN Biotech GmbH, Aienbach, Germany) resulting in a 25 mM solution, filter-sterilized and stored at 4°C for up to one week before use. This solution was used to resuspend and store isolated EV (see passage "EV isolation").

Mitomycin C solution

In this work mitomycin C was used to inhibit cell proliferation prior to performing migration assays with either EC or CF. Mitomycin C (#M4287, Sigma-Aldrich, Merck Millipore, Merck KGaA) was dissolved in Millipore water to a concentration 0.5 mg/mL (w/v), filter-sterilized and aliquots were stored at -20°C in the dark. For usage, an aliquot was thawed and stored at 4°C for up to one week. Final concentration used in the according medium was 20 µg/µL.

Gelatine solution

Gelatine 0.1% (w/v) was used for coating cell culture plates utilized for cultivation of neonatal rat cardiomyocytes. First, a 1% (w/v) stock solution was produced by dissolving gelatine (#G9391, Sigma-Aldrich, Merck Millipore, Merck KgaA) in Millipore water. The stock solution was autoclaved and stored at -20°C for up to one year.

The 0.1% (w/v) solution was produced out of the 1% (w/v) gelatine stock solution by dilution with Millipore water. Then it was pre-warmed to 55°C and filter sterilized. The 0.1% (w/v) gelatine solution was stored at 4°C for up to six weeks. When culture plates were coated, gelatine (0.1%, (w/v)) was pipetted to the according well using a volume that completely covers the surface. The plates were then placed into the HERACell 240i CO_2 incubators (Thermo Fisher Scientific) at 37°C overnight. On the next day, remaining liquid was aspirated and plates were dried under the Safety Cabinet (Safe 2020 Class II Biological Safety Cabinets, Thermo Fisher Scientific) and then closed with Parafilm® M (#P7793-1EA, Sigma-Aldrich, Merck Millipore, Merck KGaA) for storage for up to 4 weeks at room temperature.

3 mM cobalt chloride solution

A 3 mM Cobalt Chloride ($CoCl_2$) solution was prepared freshly on the day of the apoptosis test with neonatal rat cardiomyocytes (NRCM, see: 4.7.3.3). First a 10 mM $CoCl_2$ solution was prepared by dissolving 11.8 mg $CoCl_2$ hexahydrate (Cobalt-(II) chloride hexahydrate, #C2644, Sigma-Aldrich, Merck Millipore, Merck KGaA) in 5 mL DMEM/Ham´s F12 (#FG-4815, Biochrom, Merck Millipore, Merck KGaA). Thereafter, the solution was filter-sterilized and diluted with DMEM/Ham´s F12 (#FG-4815, Biochrom, Merck Millipore, Merck KGaA) to a 3 mM solution. Both 10 mM and 3 mM $CoCl_2$ solutions were directly used and not stored.

NRCM fixation solution

In order to fix NRCM for ICC, a solution of 4% (v/v) para-formaldehyde (#0964.1, Carl Roth GmbH + Co. KG), and 4% (w/v) sucrose (#S0389, Sigma-Aldrich, Merck Millipore, Merck KGaA) was prepared in 1x D-PBS. The solution was stored at 4°C for up to six months.

MTT-solution

MTT powder (Thiazolyl Blue Tetrazolium Bromide, #M5655, Sigma-Aldrich, Merck Millipore, Merck KGaA) was diluted in 1x D-PBS at a concentration of 5 mg/mL and stored protected from light at -20°C (stock solution). The working solution was generated by diluting the stock solution 1:10 with serum-free IMDM medium on the day of the experiment (see paragraph 4.7.3.2.2).

Tissue digestion solution for single-cell RNA sequencing

Tissue digestion solution for single-cell sequencing was used to digest the atrial appendage biopsy for single-cell RNA sequencing. The final solution consisted of 0.017% trypsin-EDTA

solution (1:15 dilution of commercial 0.25% solution, #25200-056, Life Technologies™, Thermo Fisher Scientific), 9.3 mg/mL collagenase type II (#17101-015, Life Technologies™, Thermo Fisher Scientific), and 19% FBS (#10270-106, Gibco® by Life Technologies™, Thermo Fisher Scientific) in 1x D-PBS. The solution was freshly prepared on the day of tissue digestion and stored on ice in the dark until use. As mentioned in the paragraph 4.5.4.1.2, the tissue was first incubated in undiluted 0.25% trypsin-EDTA (#25200-056, Life Technologies™, Thermo Fisher Scientific) before the rest of the solution was added.

3.8 Service providers

Primers for qRT-PCR were ordered from EllaBiotech GmbH (Martinsried, Germany). Dry ice was ordered from "TKD TrockenEis und Kohlensäure Distribution GmbH" (Fraunberg-Tittenkofen, Germany). Sequencing of sc-RNAseq samples was performed by the Research Group of PD Dr. Tim-Matthias Strom (Helmholtz Zentrum München, German Research Center for Environmental Health, Institute of Human Genetics, Ingolstaedter Landstr. 1, D-85764 Neuherberg) and by the Research Group of Prof. Eckhard Wolf and Dr. Helmut Blum at the Laboratory for Functional Genome Analysis (LAFUGA) (Gene Center Munich, Ludwigs-Maximilians Universität München, Feodor-Lynen-Straße 25, 81377 München).

3.9 Cooperation partners

Research groups cooperating in this project were the groups of Dr. Raffaele Teperino (Helmholtz Zentrum München, German Research Center for Environmental Health, Environmental Epigenetics, Ingolstaedter Landstr. 1, D-85764 Neuherberg), Dr. Reinhard Zeidler (Helmholtz Zentrum München, German Research Center for Environmental Health, Haematologikum, Research Unit Gene Vectors, Marchioninistraße 25, 81377 München), Prof. Dr. Lesca Holdt (Institut für Laboratoriumsmedizin, Ludwig-Maximilians-Universität München, Marchioninistr. 15, 81377 München) and Prof. Stefan Engelhardt (Institut für Pharmakologie und Toxikologie, Technische Universität München (TUM), Biedersteiner Str. 29, 80802 München).

3.10 Software

Figures were arranged in Microsoft PowerPoint 2010. Some illustrations within the figures were taken from BioRender.com. If the entire figure was created with BioRender.com, this is stated in the figure legend. Standard Academic License for BioRender.com is provided by a paid account (created on 11th May 2020).

Software	Application	Manufacturer
BD FACSDiva™, (version 8.0.1)	FC	BD Biosciences, Becton, Dickinson and Company, Franklin Lakes, NJ
Carl Zeiss™ Axio Vision Rel., (version 4.8.2)	Fluoresence microscopy	Zeiss, Oberkochen, Germany
Cell Ranger (version 3.1.0)	Sc-RNAseq raw data	10xGenomics, Pleasanton, CA

	analysis	
FlowJo (version 7.6.5)	FC	FlowJow LLC, Ashland, OR
i-control™ Microplate Reader Software, (version 2.0.)	MTT assay	Tecan, Tecan Group AG, Männedorf, Switzerland
Inkscape (version 0.92.4) https://inkscape.org/, (05.03.20)	Sc-RNAseq data analysis and visualization	Inkscape Community
Image Lab™ (version 4.0)	Gel documentation	Bio-Rad Laboratories GmbH, München, Germany
ImageJ (97, 98) via Fiji (99) (Windwos version, 64-bit Java 1.8.0_112)	Image analysis of matrigel assay and scratch assays	See citations
Quant Studio Design & Analysis Software, (version 1.4)	qRT-PCR	Applied Biosystems by Thermo Fisher Scientific, Waltram, MA
Quantity One Chemidox XRS, (version 4.6.9)	Gel documentation	Bio-Rad Laboratories GmbH, Munich, Germany
R (version 3.5.3), RStudio. (100) and R package Seurat, (version 3.1), https://satijalab.org/seurat/, (27.12.19)	Sc-RNAseq data analysis and visualization	RStudio Inc.
SPSS Statistics, (version 25.0)	Statistics and visualization	IBM, Armonk NY
TCapture, (version 4.3.0.602)	Microscopy	Tucsen Photonics, Gaishan Town, Cangshan Area, Fuzhou, Fujian, P. R. CHINA

Abbreviations: FC: flow cytometry; MTT assay: Proliferation assay with cardiac fibroblasts; sc-RNAseq: single-cell RNA sequencing

3.11 Websites and databases

- **N**ational **C**enter for **B**iotechnology **I**nformation, U.S. National Library of Medicine, Bethesda, MD (NCBI), https://www.ncbi.nlm.nih.gov/ (27.12.19)
- **B**asic **l**ocal **a**lignment **s**earch **t**ool (BLAST), (101), https://blast.ncbi.nlm.nih.gov/ (27.12.19)
- **Universal Probe Library System Assay Design** (Roche Molecular Systems, Inc., Rotkreuz, Switzerland), https://lifescience.roche.com/en_de/brands/universal-probe-library.html#assay-design-center/ (27.12.19)
- **Technical Manual Maintenance of Human Pluripotent Stem Cells in mTeSR™1,** https://cdn.stemcell.com/media/files/manual/MA29106 Maintenance_Human_Pluripotent_Stem_Cells_mTeSR1.pdf (27.12.19)
- NanoDrop 2000/2000c Spectrophotometers User Manual, ThermoFischer, https://assets.thermofisher.com/TFS-Assets/CAD/manuals/NanoDrop-2000-User-Manual-EN.pdf (27.12.19)
- **Biorender,** https://app.biorender.com/gallery/illustrations (09.01.20)
- **Gene Set Enrichment Analysis (GSEA):** http://software.broadinstitute.org/gsea/msigdb/annotate.jsp (27.12.19)
- **Manual Heatmap generation** http://heatmapper.ca/expression/, (27.12.19)
- **Venn Diagram Generation** http://bioinformatics.psb.ugent.be/webtools/Venn/ (27.12.19)

- **Manual 10xGenomics, sc-RNAseq Library Preparation**: https://support.10xgenomics.com/single-cell-gene-expression/library-prep/doc/user-guide-chromium-single-cell-3-reagent-kits-user-guide-v31-chemistry (06.12.2019)

- **Image J: https://imagej.nih.gov/ij/** (27.12.19)
- **ImageJ Angiogenesis Analyzer Tool** (by Gilles Carpentier, (102)): https://imagej.nih.gov/ij/macros/toolsets/Angiogenesis%20Analyzer.txt, (15.11.19) and http://image.bio.methods.free.fr/ImageJ/?Angiogenesis-Analyzer-for-ImageJ&artpage=4-6&lang=en#outil_sommaire_4, (15.11.19)

3.12 Cell culture media

Table 11: Commercially available media

Medium	Description	Manufacturer
Iscove's Modified Dulbecco's Medium (IMDM) with stable glutamine, #FG-0465	This medium is a modification of Dulbecco's Modified Eagle's Medium (DMEM) containing selenium, additional amino acids and vitamins, sodium pyruvate, HEPES buffer, and potassium nitrate. L-alanyl-L-glutamine dipeptide guarantees stable glutamine concentrations for cell culture.	Biochrom, Merck Millipore, Merck KGaA, Darmstadt, Germany
Ham's F-12 with L-Glutamine, #FG-0815	F-12 Nutrient Medium	Biochrom, Merck Millipore, Merck KGaA, Darmstadt, Germany
DMEM/Ham´s F12, #FG-4815	DMEM/Ham´s F-12 (Dulbecco's Modified Eagle Medium: Nutrient Mixture F-12): Liquid medium with stable glutamine	Biochrom, Merck Millipore, Merck KGaA, Darmstadt, Germany
Dulbecco´s MEM Medium (DMEM) high Glucose, #FG0435	DMEM liquid medium, without sodium-pyruvate, with 3,7 g/l $NaHCO_3$, 4,5 g/l D-glucose and stable glutamine (2 mM)	Biochrom, Merck Millipore, Merck KGaA, Darmstadt, Germany
mFreSR™, #05854	Defined, serumfree cryopresevation medium for human induced pluripotent stem cells (iPSC)	StemCell™ Technologies, Köln, Germany
TeSR™-E8™, #05990	Feeder-free animal component-free culture medium for iPSC. Consists of two components: TeSR™-E8™ Basal Medium and TeSR™-E8™ 25X Supplement	StemCell™ Technologies, Köln, Germany
Smooth Muscle Cell Growth Medium 2 (Ready-to -use), #c-22062	Low-serum medium developed to establish and maintain smooth muscle cell cultures from blood vessels and hollow organs.	Promocell GmbH, Heidelberg, Germany
RPMI 1460, #FG-1215	*Roswell Park Memorial Institute* (RPMI) 1640: Liquid basel medium with stable glutamine and 2.0 g/L $NaHCO_3$	Biochrom, Merck Millipore, Merck KGaA, Darmstadt, Germany
Endothelial Cell Growth Medium 2 Kit, #c-22111	Low-serum medium which has been developed for the *in vitro* cultivation of endothelial cells from large blood vessels. The Kit version consists of basal medium and supplemental pack containing fetal calf serum, epidermal growth factor, basic fibroblast growth factor, insulin-like growth factor, vascular endothelial	Promocell GmbH, Heidelberg, Germany

	growth factor 165, ascorbic acid, heparin, hydrocortisone				

Table 12: Self-made media mixtures

Medium name	Cell type for which used	Explanation	Stability and Storage	Composition (end concentration in medium is indicated)	Catalogue-Nr. /Producer
MEF medium	Adipose and cardiac fibroblasts		4°C, 4 weeks	10% FBS	#10270106 / Thermo Fisher Scientific, Waltram, MA
				100 Units/mL penicillin G, 100 µg/mL streptomycin	#A8943 / PanReac AppliChem, AppliChem GmbH, Darmstadt, Germany
				1% sodium pyruvate	#11360039 / Thermo Fisher Scientific, Waltram, MA
				DMEM high glucose with glutamine	#FG 0435 / Biochrom, Merck Millipore, Merck KGaA, Darmstadt, Germany
Complete explant medium (CEM)	COG, CDC	Based on the publication of Messina et al., 2004 (70)	4°C, 4 weeks	20% FBS	#10270106 / Thermo Fisher Scientific, Waltram, MA
				100 Units/mL penicillin g, 100 µg/mL streptomycin	#A8943 / PanReac AppliChem, AppliChem GmbH, Darmstadt, Germany
				0.1 mmol/L 2-Mercaptoethanol	#21985-023/ Gibco® by Life TechnologiesTM, Thermo Fisher Scientific, Waltram, MA
				IMDM with stable glutamine	#FG-0465/ Biochrom, Merck Millipore, Merck KGaA, Darmstadt, Germany
Cardiosphere-growing medium (CGM)	Cardiosphere-forming cells	Based on the publication of Messina et al., 2004 (70)	4°C, 7 days	100 Units/mL penicillin g, 100 µg/mL streptomycin	#A8943/ PanReac AppliChem, AppliChem GmbH, Darmstadt, Germany
				3,5% FBS	#10270106 / Thermo Fisher Scientific, Waltram, MA
				0.1 mmol/L 2-Mercaptoethanol	#21985-023/ Gibco® by Life TechnologiesTM, Thermo Fisher Scientific, Waltram, MA

				20 ng/mL Recombinant human FGF basic	#100-18B**,** Peprotech, Rocky Hill, NJ
				40 ng/mL Cardiotrophin-1	#300-32, Peprotech Rocky Hill, NJ
				2% B-27	#17504-001, Invitrogen™ by Thermo Fisher Scientific, Waltram, MA
				40 nmol/L Thrombin	#T4648, Sigma-Aldrich, Merck Millipore, Merck KGaA, Darmstadt, Germany
				250 ng/mL Recombinant human EGF	#236-EG, R&D System, Minneapolis, MN
				65% DMEM/Ham's F12, with +L-Glutamin	#FG-4815/ Biochrom, Merck Millipore, Merck KGaA, Darmstadt, Germany
				35% IMDM with stable glutamine	#FG-0465/ Biochrom, Merck Millipore, Merck KGaA, Darmstadt, Germany
Serumfree IMDM medium	EV production / Negative Control in functional assays	As FBS contains bovine serum derived EV, bovine serum albumin was used instead to ensure cell growth without FBS during EV production and *in-vitro* assays.	4°C, 4 weeks	10 mg/mL BSA	B4287 / Sigma-Aldrich
				100 Units/mL penicillin g, 100 µg/mL streptomycin	A8943/ PanReac AppliChem, AppliChem GmbH, Darmstadt, Germany
				0.1 mmol/L 2-Mercaptoethanol	#21985-023/ Gibco® by Life TechnologiesTM, Thermo Fisher Scientific, Waltram, MA
				IMDM with stable glutamine	#FG-0465/ Biochrom, Merck Millipore, Merck KGaA, Darmstadt, Germany
NRCM medium	Cultivation of NRCM and positive control at apoptosis assay		Was prepared freshly at the day of experiment	5% Horse serum,	#16050112/Life Technologies™, Thermo Fisher Scientific, Waltram, MA
				100 Units/mL penicillin g, 100 µg/mL streptomycin	#A8943/ PanReac AppliChem, AppliChem GmbH, Darmstadt, Germany

				DMEM/Ham´s F12	#FG-4815/ Biochrom, Merck Millipore, Merck KGaA, Darmstadt, Germany
Serumfree EC-medium	Starvation of endothelial cells before Tube Formation Assay		4°C, 6 weeks	10.7 mg/mL BSA	#B4287 / Sigma-Aldrich
				100 Units/mL penicillin g, 100 µg/mL streptomycin	#A8943/ PanReac AppliChem, AppliChem GmbH, Darmstadt, Germany
				Endothelial Cell Growth Medium 2 without supplements	#c-22111/ Promocell GmbH, Heidelberg, Germany
CDM3 medium	Direct differentiation of iPSC	Based on the publication of Burridge et al., 2015(103)	4°C, 4 weeks	500 µg/mL Recombinant human serum albumine	#A0237, Sigma-Aldrich, Merck Millipore, Merck KGaA, Darmstadt, Germany
				213 µg/mL L-ascorbic acide-2-phosphate (added freshly at each medium change)	#A8960, Sigma-Aldrich, Merck Millipore, Merck KGaA, Darmstadt, Germany
				Roswell Park Memorial Institute (RPMI) 1460	Biochrom, Merck Millipore, Merck KGaA

Table 13: Self-made cryopreservation media

Medium name	Cell type(s) for which used	Composition	Cat. -Nr. /Producer
Cryopreservation medium CF/AF	AF, CF	80% MEF medium	s. Table 12
		10% FBS	#10270106 / Thermo Fisher Scientific, Waltram, MA
		10 % DMSO	#A994.1/ Carl Roth GmbH + Co. KG, Karlsruhe, Germany
Cryopreservation medium CDC	CDC	80% CEM medium	s. Table 12
		10 % FBS	#10270106/ Thermo Fisher Scientific, Waltram, MA
		10% DMSO	#A994.1/ Carl Roth GmbH + Co. KG, Karlsruhe, Germany
Cryopreservation medium EC	EC	80% Endothelial Cell Growth Medium 2 with all supplements	s. Table 11
		10% FBS	#10270106/Thermo Fisher Scientific, Waltram, MA
		10% DMSO	#A994.1/Carl Roth GmbH + Co. KG,

			Karlsruhe, Germany
Cryopreservation medium SMC	SMC	80% Smooth Muscle Cell Growth Medium 2 with all supplements	s. Table 11
		10% FBS	#10270106/Thermo Fisher Scientific, Waltram, MA
		10% DMSO	#A994.1/Carl Roth GmbH + Co. KG, Karlsruhe, Germany

All cryopreservation media were prepared freshly shortly before freezing the cells and kept at 4°C.

3.13 Patient data

Table 14: Adult patients

Nr.	Lab-ID	Sex	Age (years)	Surgery	Diagnosis	Cell types	Experiment
1	A3964	male	61	CABG + MVR	atherosclerotic heart disease	AF, CDC	qRT-PCR (cells)
2	A4331	male	58	CABG	atherosclerotic heart disease	AF, CDC	qRT-PCR (cells)
3	A4401	male	55	CABG	atherosclerotic heart disease	AF, CDC, CF	qRT-PCR (cells), ICC
4	A4712	male	58	CABG	atherosclerotic heart disease	AF	FC
5	A4762	male	62	AVR + Aorta + MAZE	combined aortic vitium	AF, CDC	FC
6	A4834	female	76	AVR	aortic stenosis	AF	FC
7	A5394	male	68	CABG	atherosclerotic heart disease	CF	EC Scratch, CF Scratch
8	A5409	female	59	AVR + MVR + MAZE	combined aortic vitium	CDC, CF	qRT-PCR (EV)
9	A5451	male	72	AVR + MAZE	aortic stenosis	CDC	qRT-PCR (cells), Matrigel
10	A6163	female	73	AVR	aortic stenosis	CDC, CF	qRT-PCR (cells)
11	A6761	male	67	CABG	atherosclerotic heart disease	CF, SMC	qRT-PCR (cells), ICC
12	A6772	male	66	CABG	atherosclerotic heart disease	EC, SMC	qRT-PCR (cells), sc-RNAseq (SMC), FC
13	A6828	male	63	CABG	atherosclerotic heart disease	CF, EC, SMC	qRT-PCR (cells), sc-RNAseq (CF, EC)
14	A6842	male	56	CABG	atherosclerotic heart disease	SMC	qRT-PCR (cells), FC
15	A6993	male	70	CABG + Aorta	atherosclerotic heart disease	AF, CDC, CF	qRT-PCR (cells), qRT-PCR (EV), Matrigel, EC Scratch, CF Scratch,NRCM assay, ICC

16	A7065	female	64	CABG	atherosclerotic heart disease	CDC, CF	qRT-PCR (cells), FC, Matrigel, EC Scratch, CF Scratch,NRCM assay, ICC
17	A7185	male	66	CABG	atherosclerotic heart disease	CDC, CF	qRT-PCR (cells), qRT-PCR (EV), FC, Matrigel, EC Scratch, CF Scratch,NRCM assay
18	A7399	male	54	MVR+TVR + MAZE	mitral valve insufficiency	CDC, CF	qRT-PCR (cells), qRT-PCR (EV), Matrigel, EC Scratch, CF Scratch,NRCM assay
19	A7437	male	67	CABG	atherosclerotic heart disease	CDC, CF	qRT-PCR (cells), EC Scratch, CF Scratch,NRCM assay
20	A8578	male	76	CABG	atherosclerotic heart disease	CDC	qRT-PCR (cells), FC
21	A8597	male	61	CABG	atherosclerotic heart disease	CDC	qRT-PCR (cells), FC, sc-RNAseq (CDC), ICC
22	A8828	female	75	MVR + TVR + Tumor	biatrial tumor and mitral valve insufficiency	Biopsy	sc-RNAseq (Biopsy)

Abbreviations: ***CABG****: Coronary artery bypass surgery,* ***MVR****: Mitral valve replacement,* ***AVR****: aortic valve Replacement,* ***MAZE****: MAZE Procedure for Atrial Fibrillation,* ***TVR****: Tricuspid valve replacement,* ***Cell types****: which cell types were generated from this patinet's tissue samples,* ***Experiment:*** *for which experiment the cells generated from this patients' tissue were used,* ***qRT-PCR (cells):*** *semiquantitative real-time polymerase chain reaction with RNA isolated from cell lysates, ICC: immunocytochemistry,* ***FC:*** *Flow cytometry,****Matrigel:*** *Tube formation assay on matrigel,* ***EC Scratch:*** *endothelial cell migration assay,* ***CF Scratch:*** *cardiac fibroblast migration assay,* ***qRT-PCR (EV):*** *semiquantitative real-time polymerase chain reaction with RNA isolated from extracellular vesicles, Matrigel: Tube formation assay on matrigel,* ***sc-RNAseq****: single-cell RNA sequencing, sample indicated in brackets,* ***NRCM assay:*** *apoptosis test with neonatal rat cardiomyocytes.*

Table 15: Pediatric patients

Nr.	Lab-ID	Sex	Age_ years	Age_ months	Age_ days	STS-code	Main diagnosis	Age group	Cell types	Experiment
1	4360	male			21	69	HLHS	1	CDC	qRT-PCR (cells)
2	4482	male			9	69	HLHS	1	AF, CDC	qRT-PCR (cells)
3	4581	female				96	hypoplastic aortic arch	1	AF, CDC	qRT-PCR (cells), FC
4	4639	male			6	85	TGA, VSD	1	AF, CDC, CF	qRT-PCR (cells), FC, ICC
5	4659	male			7	90	DORV, TGA-type	1	AF, CDC, CF	qRT-PCR (cells), FC

6	4681	male			10	69	HLHS	1	AF, CDC, CF	qRT-PCR (cells), FC
7	4722	male			11	69	HLHS	1	AF, CDC, CF	qRT-PCR (cells), qRT-PCR (EV), FC
8	4747	male			6	69	HLHS	1	AF, CDC, CF	qRT-PCR (cells), FC
9	4890	male			6	83	TGA, IVS	1	CDC	qRT-PCR (cells)
10	4932	female			10	69	HLHS	1	AF, CDC, CF, CFSPh	qRT-PCR (cells), qRT-PCR (EV)
11	4953	female			10	69	HLHS	1	CDC, CF, CFSPh	qRT-PCR (cells), qRT-PCR (EV), Matrigel, EC Scratch, CF Scratch, NRCM assay
12	4961	male			8	69	HLHS	1	AF, CDC, CF, CFSPh	qRT-PCR (cells), qRT-PCR (EV)
13	5027	male			9	69	HLHS	1	AF, CDC, CF, CFSPh	qRT-PCR (cells)
14	5093	female			13	69	HLHS	1	CDC, CF	qRT-PCR (cells), Matrigel, MTT assay
15	5211	male			19	69	HLHS	1	AF, CDC, CF	qRT-PCR (cells)
16	5252	female			9	69	HLHS	1	AF, CDC, CF, CFSPh	qRT-PCR (cells), Matrigel, EC Scratch, CF Scratch, NRCM assay
17	5290	male			12	2	ASD, secudum	1	AF, CDC, CF, CFSPh	qRT-PCR (cells)
18	5311	female			12	115	Atrial Isomerism right	1	CDC, CF	qRT-PCR (cells)
19	5347	female			6	69	HLHS	1	AF, CDC, CF, CFSPh	qRT-PCR (cells), Matrigel, EC Scratch, CF Scratch, MTT assay
20	5413	male			19	69	HLHS	1	AF, CDC, CF	qRT-PCR (cells), Matrigel, EC Scratch
21	5463	female			6	69	HLHS	1	CDC, CF	qRT-PCR (cells), Matrigel, EC Scratch, CF Scratch, MTT assay

22	5543	male			17	83	TGA, IVS	1	CF	MTT assay
23	5627	male			14	69	HLHS	1	CDC, CF	qRT-PCR (cells), EC Scratch, CF Scratch
24	5689	male			5	69	HLHS	1	CDC, CF	qRT-PCR (cells), CF Scratch, NRCM assay
25	5845	male			10	69	HLHS	1	CDC, CF	qRT-PCR (cells), Matrigel, EC Scratch, CF Scratch, NRCM assay
26	5967	male			12	69	HLHS	1	CDC, CF, CFSPh	qRT-PCR (cells), EC Scratch, CF Scratch, NRCM assay
27	5990	male			7	69	HLHS	1	CDC, CF, CFSPh	qRT-PCR (cells), qRT-PCR (EV), Matrigel, CF Scratch, NRCM assay, ICC
28	6045	female			7	69	HLHS	1	CDC, CF, CFSPh	qRT-PCR (cells), Matrigel, EC Scratch, CF Scratch, NRCM assay
29	6153	male			6	2	ASD, secundum	1	CF, CFSph	CF Scratch, NRCM assay, ICC
30	6440	male			8	69	HLHS	1	CFSph	FC
31	6588	female			11	69	HLHS	1	CDC, CF	qRT-PCR (cells), FC
32	6589	female			7	69	HLHS	1	CDC, CF	qRT-PCR (cells), sc-RNAseq (CDC)
33	5148	female		1		121	Hypoplastic LV	2	AF, CDC, CF	qRT-PCR (cells), EC Scratch, CF Scratch, NRCM assay
34	5885	male		3		69	HLHS	2	CDC, CF	qRT-PCR (cells), qRT-PCR (EV), Matrigel, EC Scratch, CF Scratch, NRCM assay
35	5659	male		22		69	HLHS	2	CDC, CF	qRT-PCR (cells), Matrigel, EC Scratch, CF Scratch, NRCM assay
36	5398	female	1			69	HLHS	2	CDC, CF	qRT-PCR (cells), Matrigel, MTT

										assay
37	5501	male	1			10	AVC (AVSD), Complete CAVSD	2	CDC, CF	qRT-PCR (cells), Matrigel, CF Scratch, NRCM assay
38	5508	male	2			77	Single ventricle, Tricuspid atresia	2	CDC, CF	qRT-PCR (cells), EC Scratch, CF Scratch, NRCM assay
39	4732	male	2			69	HLHS	2	AF, CDC, CF	qRT-PCR (cells), qRT-PCR (EV)
40	4854	male	2			69	HLHS	2	AF, CDC, CF	qRT-PCR (cells)
41	5202	female	2			69	HLHS	2	AF, CDC, CF	qRT-PCR (cells), Matrigel
42	4725	female	3			99	Patent ductus arteriosus	2	CDC, CF	qRT-PCR (cells), Matrigel, EC Scratch, CF Scratch, NRCM assay, MTT assay
43	5432	male	3			69	HLHS	2	AF, CDC, CF	qRT-PCR (cells)
44	4885	female	3			78	Single ventricle, Unbalanced AVC	2	AF, CDC, CF	qRT-PCR (cells), qRT-PCR (EV)
45	5787	male	3			77	Single ventricle, Tricuspid atresia	2	CDC, CF	qRT-PCR (cells),EC Scratch, CF Scratch, NRCM assay
46	4884	female	3			10	AVC (AVSD), Complete CAVSD	2	AF, CDC, CF	qRT-PCR (cells)
47	4650	female	4			16	Truncus arteriosus	2	CDC, CF	qRT-PCR (cells)
48	5049	male	4			74	Single ventricle, DILV	2	AF, CDC, CF	qRT-PCR (cells), Matrigel
49	5624	female	6			69	HLHS	2	CDC, CF	qRT-PCR (cells), Matrigel, EC Scratch, CF Scratch, NRCM assay, MTT assay

*Abbreviations: **STS-code**: diagnostic code of the Society of Thoracic Surgeons. **HLHS**: Hypoplastic left heart syndrome, **TGA**: Transposition of the great arteries, **VSD**: Ventricular septal defect, **DORV**: Double-outlet left ventricle, **IVS:** intact ventricular septum, **ASD secundum**: atrial septal defect type 2, **LV**: left ventricle, **AVC**: atrioventricular canal, **(C)AVSD:** (Complete) atrioventricular spetal defect, **DILV:** Double-inlet left ventricle, **Cell types**: which cell types were generated from this patinet's tissue samples, Age groups: **1**-HLH1, **2**-HLH2/3,*

***Experiment**: for which experiment the cells generated from this patients' tissue were used, **qRT-PCR (cells)**: semiquantitative real-time polymerase chain reaction with RNA isolated from cell lysates, **ICC**: immunocytochemistry, **FC**: Flow cytometry, **EC Scratch**: endothelial cell migration assay, **CF Scratch**: cardiac fibroblast migration assay, **qRT-PCR (EV)**: semiquantitative real-time polymerase chain reaction with RNA isolated from extracellular vesicles, **Matrigel**: Tube formation assay on matrigel, **sc-RNAseq**: single-cell RNA sequencing, **NRCM assay:** apoptosis test with neonatal rat cardiomyocytes.*

4. Methods

4.1 Patient tissue samples

Human biopsies derived from adipose, atrial or vessel tissue from patients (aged from 5 days to 76 years) undergoing heart surgery (see Table 14 and Table 15). All patients have signed an informed consent. In the case of children consent was signed by their parents or legal guardians. The local ethical committee of the medical faculty of the Technical University of Munich controlled and approved the study with the title "Analysis of transciptome and proteome of different heart regions and different cardial cell lineages" (German title: "Untersuchung des Transkriptoms und Proteoms verschiedener Regionen des Herzens und verschiedener kardialer Zelltypen", Project number 570/16S). The tissue sampling and the establishment of the cardiovascular biobank (German title: Kardiovaskuläre Biobank innerhalb des Deutschen Herzzentrums München (KaBi-DHM)) was approved by the local ethical committee of the Medical Faculty of the Technical University of Munich (Project number 5943/13). All experimental procedures were performed in accordance with the principles outlined in the Declaration of Helsinki.

4.2 Animals

Murine cardiac fibroblasts were generated from adult mouse hearts. Transgenic mice were housed in an accredited facility in compliance with the European Community Directive related to laboratory animal protection (2010/63/EU). For extraction of adult murine ventricles, mice were anesthetized with isoflurane (2-chloro-2-(difluoromethoxy)-1,1,1-trifluoro-ethane, #HDG9623V, Baxter, Deerfield, IL) and then euthanized by cervical dislocation. For this experiment Nkx2-5 cardiac enhancer eGFP (NkxCE GFP) reporter mice, characterized previously by Wu *et al.* (104), were used.

Neonatal rat cardiomyocytes (NRCM) were isolated from 0-1 day old Sprague Dawley rats (non transgenic) after decapitation. NRCM were kindly provided by the TUM Institute of Pharmacology and Toxicology (IPT) (Director: Prof. Dr. med Dr. rer. nat. Stefan Engelhardt). Rats were housed in an accredited facility in compliance with the European Community Directive related to laboratory animal protection (2010/63/EU).

All animal sacrifices for harvesting organs were approved by the relevant authority "Regierung von Oberbayern" [Regional Government of Upper Bavaria] and accorded German TierSchG (Animal protection law). All animal experiments (organ extractions) were performed in accordance with the European guidelines and regulations for animal care and handling (Directive 2010/63/EU).

4.3 General cell culture methods

Cell culture was carried out in Safe 2020 Class II Biological Safety Cabinets (Thermo Fisher Scientific, Waltram, MA). Cells were cultured in HERACell 240i CO_2 incubators (Thermo Fisher

Scientific) at 37°C, 100% humidity and 5% CO_2. If not stated otherwise, centrifugations were performed in a Heraeus Megafuge (Thermo Fisher Scientific). The microscope used for general cell culture was a Nikon Eclipse Ts2 (Nikon, Minato, Japan) with visualization software TCapture v. 4.3.0.602 (Tucsen Photonics, Gaishan Town, Cangshan Area, Fuzhou, Fujian, P. R. CHINA). Sterilization of the safety cabinet surface was done with INCIDIN™ OXYFOAM S (#3087450 Ecolab, Saint Paul, MN). All equipment used under the safety cabinet was wiped with 70% ethanol solution (see paragraph 3.7) to assure aseptic conditions. Eppendorf Safe-Lock Tubes, 1.5 mL and 2.0 mL (#30120086 and #30120094, Eppendorf AG, Hamburg, Germany), SurPhob Tips , without filter (#VT0173, Biozym Scientific GmbH, Hessisch Oldendorf, Germany) and surgical material (see Table 3) were sterilized using the autoclave HICLAVE HI-50 (HMC Europe GmbH, Tüßling, Germany) and dried with a Drying Chamber (Binder GmbH, Tuttlingen, Germany). Pipetting under the Biological Safety Cabinet was done with sterile 10 µL/100 µL/1250 µL SafeSeal SurPhob Filter Tips (#VT0200/#VT0230/#VT0270 Biozym Scientific GmbH) or using a pipetus® 100-240 Volt (Hirschmann Laborgeräte GmbH & Co. KG, Eberstadt, Germany) with 5 mL/10 mL serological pipettes (#GPS-5.0/#GPS-10.0 Kisker Biotech GmbH & Co. KG, Steinfurt, Germany).
When incubations of sterile vessels were performed outside the Biological Safety Cabinet, vessel were sealed with Parafilm® M (#P7793-1EA, Sigma-Aldrich, Merck Millipore, Merck KGaA, Darmstadt, Germany). 1x D-PBS refers to Dulbecco´s Phosphat buffered saline (see paragraph 3.7)

4.3.1 Cell count determination using a Neubauer chamber and trypan blue

Trypan blue (0.2% (w/v), diluted from 0.5% (w/v) #L6323, Biochrom, Merck Millipore, Merck KGaA, Darmstadt, Germany, see paragraph 3.7) is a staining dye which passes through the perforated cell membrane of dead cells (105). In order to count cells, cells were first detached applying the suitable method for the respective cells. As high cell concentrations are favorable for cell counting, cells were usually centrifuged prior to counting (300 x *g* for 5 min at room temperature). The cell pellet was then resuspended in a suitable volume of the cell-specific cell culture medium. For counting, an aliquot was taken and diluted with 0.2% trypan-blue solution. This mixture was carefully pipetted into a Neubauer counting chamber slide (chamber depth: 0.1 mm, Thomas Scientific, Svedesboro, NJ) and manual counting of living and dead cells was carried out. Cells were distinguished from debris and other particles by their typical size. Living cells are not stained by the blue dye and appear white, and dead cells were completely blue. Cell count was performed in all four quadrants of the Neubauer chamber. Only cells which were located on the inner lines of the quadrants were counted. To calculate total cell count, the following formula was used:

Cell concentration (10^4 cells/mL) = cell number in 4 Quadrants/4 * dilution factor (ratio: trypan blue solution/cells suspension)

4.3.2 Detaching cells with Trypsin-EDTA (Trypsinization)

Except for iPSC, all other cell types used in this work were detached using 0.25% trypsin-EDTA (#25200056, Thermo Fisher Scientific) or a dilution of it in 1x D-PBS according to manufacturer's recommendations. This purchasable trypsin is a mixture of proteases derived from the porcine pancreas. It has a strong digesting activity and thus, is suitable for detachment of strongly adhering cells. Standardized detachment procedure consisted of the following steps: 1) Cell medium was removed; 2) Cells were washed with 1x D-PBS; 3) Cells were incubated with 0.25% trypsin-EDTA at a volume which just covers the cell layer for 2-5 min at 37°C; 4) If cells detached when tapping on the side of the culture plate, trypsin was stopped with the triple amount of the according culture medium; 5) Cell suspension was then collected in a 14 mL round bottom tube (#734-0444, VWR International, Radnor, PA) or a 15 ml tube (#734-0451, VWR International) and centrifuged (300 x *g*, 5 min, room temperature); 6) Cell pellet was resuspended in the according medium or another buffer depending on the further experimental workflow.

4.3.3 Cryopreservation of cells

For long-term storage cells were cryopreserved in a liquid nitrogen system (Messer Griesheim, Bad Soden, Germany). Except for iPSC (see paragraph 4.4.5), standardized freezing procedure consisted of the following steps: 1) Cells were detached with 0.25% trypsin-EDTA as described in paragraph 4.3.2; 2) After centrifugation, the cell pellet was resuspended in 800 µL of the according culture medium and transferred into 1 mL cryogenic vials Nunc 1.0 mL (#479-6842P, VWR International) ; 3) and 200 µL pre-cooled freezing solution consisting of 100 µL FBS (#10270-106, Thermo Fisher Scientific) and 100 µL DMSO (#A994.1, Carl Roth GmbH + Co. KG, Karlsruhe, Germany) were added. This procedure resulted in a specific cryopreservation medium for each cell type listed in Table 13. Cryogenic vials were rapidly transferred to a -80°C freezer (HERA Freezer Basic, Thermo Fisher Scientific) for at least 24h before transferring them to the liquid nitrogen system (Messer Griesheim, Bad Soden, Germany). Transport of cells from the -80°C freezer to the liquid nitrogen tank was carried out on dry ice (TKD TrockenEis und Kohlensäure Distribution GmbH, Fraunberg-Tittenkofen, Germany).

4.4 Specific cell culture protocols

In the following chapter the isolation and cultivation procedures of the primary cells used in this work are described. Cardiosphere-derived cells (CDC), adipose and cardiac fibroblasts (AF and CF), endothelial cells (EC) and smooth muscle cells (SMC) were isolated from fresh tissue samples recruited during heart surgeries perfomed at the German Heart Center. The tissue samples were transported to the laboratory in sterile 1x D-PBS on ice within 30 min. If not otherwise stated, tissue was cut into small pieces with surgical disposable scalpels (#BA220, B. Braun Melsungen AG, Melsungen, Germany).

4.4.1 Cultivation of CDC

CDC were isolated from human fresh atrial appendage tissue according to a published protocol (70) with some modifications. Residual blood was removed by washing fresh myocardial tissue several times with 1x D-PBS. Then, tissue was cut into 1-2 mm^3 sized pieces, and digested thrice for 5 min at 37°C with the COG digestion solution (see paragraph 3.7). Each digestion step consisted of a short vortex of the tissue pieces in the COG digesting solution using Vortex Genie 2 (Scientific Industries Inc., Bohemia, NY), rotation of the tube inside a pre-warmed GFL 7601 Hybridization Incubator (GENEO BioTechProducts GmbH, Hamburg, Germany) at 37°C for 5 min, followed by a short centrifugation step (pulse-mode at the table centrifuge 5417R, Eppendorf, Hambung, Germany) of the tissue pieces and replacement of the COG digestion solution. After the last digestion step, the digestion solution was discarded, and the tissue fragments were plated into a 24-well plate (Cell Culture Multi-well Plate, 24 well, PS, Clear, Cellstar®, sterile, #662160, Greiner Bio-One International GmbH, Frickenhausen, Germany) in complete explant medium (CEM) (see Table 12). On the first day of culture a small amount of medium (about 600 µL) was put in each well so that the pieces were covered but could easier attach to the plate. On the second day of culture, wells were filled to 1 mL CEM per well. Over the course of the next days, cells grew out of the tissue pieces. When the outgrowth cell layer reached confluence (approximately after two weekes), the sample was considered to be ready for harvest. The phase-bright cells were then harvested by pooling the conditioned medium, one wash 1x D-PBS, one wash with 0.05% trypsin-EDTA Solution (see paragraph 3.7) after 1 min incubation at room temperature and one wash with cardiosphere-growing medium (CGM) (see Table 12), cells were plated on poly-D-lysine (#A-003-E , Sigma-Aldrich, Merck Millipore, Merck KGaA) coated 4-well Multi well (#734-2176, VWR International) at a concentration of 8×10^4/mL (see coating procedure described in paragraph 3.7) in CGM. Harvesting of cardiosphere-forming cells from each cardiac outgrowth sample was performed thrice with one week intervals. The incubation with CGM containing bFGF, cardiotrophin, EGF, thrombin and B27 supplement (see Table 12) led to formation of three dimensional spheres out of the majority of harvested cells.
After about 5 days the newly built cardiospheres were replated on fibronectin (#F4759, Sigma-Aldrich, Merck Millipore, Merck KGaA) coated 12-well plates (see paragraph 3.7 for coating procedure) yielding in one-dimensional culture of CDC. CDC were cultured in CEM, changing the medium every other day. CDC were passaged by tryptic digestion (see paragraph 4.3.2).

4.4.2 Cultivation of primary adipose tissue derived fibroblasts and cardiac fibroblasts (AF and CF)

AF and CF were isolated from human fresh adipose or atrial appendage tissue, according to a previously published protocol by Doll *et al*. (5). The tissue samples were minced manually and incubated with collagenase II solution (0.2%) (see paragraph 3.7) while rotating inside a pre-warmed GFL 7601 hybridization incubator at 37°C for 2.5h. For adult tissue samples, the incubation time was adjusted to the size of the tissue sample, to obtain optimal digest. If tissue

pieces remained in the digestion solution after the incubation period, the solution was filtered through an EASYSTRAINER 70 µM (#542070, Greiner Bio-One International GmbH, Frickenhausen, Germany) and centrifuged at 300 x *g* for 5 min at room temperature. Pelleted cells were plated in MEF medium (see Table 12) on 12-well plates (#665180, Greiner Bio-One International GmbH, Frickenhausen, Germany). Medium was changed twice a week and cells were passaged as described in the paragraph 4.3.2.

Murine cardiac fibroblasts (mCF) for qRT-PCR were isolated with the same protocol from ventricles of adult transgenic NkxCE-GFP mice. The digestion time for murine tissue was set to 1h.

4.4.3 Cultivation of endothelial cells and smooth muscle cells (EC and SMC)

EC were isolated from a fresh human vessel (vein or internal mammary artery) by digesting the inner part of the vessel with collagenase II solution (0.2%, see paragraph 3.7) for 30 min at 37°C. For this procedure surgical material (see Table 3) was used. Firstly, residual blood was washed off the inner part of the vessel with sterile 1x D-PBS using a 10 mL sterile injection syringe (#4606108V, B. Braun Melsungen AG). Secondly, after the vessel was closed on one side using titanium ligating clips (#001204, Teleflex Inc., Wayne, Pennsylvania), collagenase II solution (0.2%) was injected into the interior of the vessel followed by closure of the vessel on the other side. The vessel was placed into a 50 ml falcon tube (#734-0448, VWR International) filled with 1x D-PBS which was incubated in a water bath (Lauda Aqualine AL 12, LAUDA-Brinkmann, LP, Delran, NJ) for 30 min at 37°C. After the incubation, EC were flushed off the inner part of the vessel with 1x D-PBS. Cell suspension was centrifuged at 300 x *g* for 5 min at room temperature and pelleted cells were plated on a 12-well culture plate in EC medium (#c-22111, Promocell GmbH, Heidelberg, Germany) supplemented with all provided supplements and 100 Units/mL penicillin G, 100 µg/mL streptomycin (#A8943, PanReac AppliChem, AppliChem GmbH, Darmstadt, Germany).
The remaining vessel was cut into pieces of 1-2 mm^2. They were put on a 6-well culture plate (#657160, Greiner Bio-One International GmbH, Frickenhausen, Germany) with the inner side of the vessel facing to the bottom of the culture plate to allow SMC outgrowth. After 2-3h of drying without medium, pieces attached to the culture plate and SMC medium (#c-22062, Promocell GmbH, Heidelberg, Germany) with all provided supplements was added.
These protocols were previously published by Doll *et al*. (5). For both, EC and SMC, medium was changed every other day and cells were passaged with 0.125% trypsin-EDTA (1:2 dilution of the commercial 0.25% trypsin-EDTA with 1x D-PBS).

4.4.4 Cultivation of sphere-derived cells from cardiac fibroblasts (CFSPh)

CF at passage 0 were passaged by trypsin (as described in paragraph 4.3.2) to a 12 well plate (#665180, Greiner Bio-One International GmbH, Frickenhausen, Germany) at a 1:3 ratio. When grown to confluence, cells were trypsinized (see paragraph 4.3.2) and further processing was

according to the CDC cultivation protocol (see paragraph 4.4.1). Cells were replated on 4-well plates pre-coated with poly-D-lysine at a concentration of 8×10^4 cells/mL in CGM. After about 5 days arising three-dimensional cardiospheres were replated on fibronectin coated 12-well plates in CEM, taking care that every well contains at least one sphere. In most cases, the spheres did not attach to the cell culture plate and could be easily collected by taking off the supernatant. Otherwise, they detached from the culture plate after gently rinsing the cell layer with a small volume of medium. Analogically to CDC, cells grew out of the spheres after several days. These cells were named cardiac-fibroblast-sphere-derived cells (CFSPh). Analogically to CDC, medium was changed every other day and cells were passaged with 0.25% trypsin-EDTA (#25200-056, Life Technologies™, Thermo Fisher Scientific)

This protocol was performed to check whether incubation with growth factors containing CGM might change CF in a way to develop similar characteristics to CDC.

4.4.5 Cultivation of human induced pluripotent stem cells (iPSC)

Human iPSC were cultured in TeSR™-E8™ medium (#05990, StemCell™ Technologies, Köln, Germany) on 6 well culture plates coated with Corning® Matrigel® hESC-Qualified Matrix (#354277, Corning, Tewksbury, MA). This purchasable matrix is extracted from the basement membrane of the Engelbreth-Holm-Swarm (EHS) mouse sarcoma. It has particularly suitable properties for human iPS-cell culture because it is enriched with ECM proteins such as laminin (a major component), collagen IV, heparin sulfate proteoglycans, entactin/nidogen, and in addition it contains a number of growth factors (106-109). Besides, it has the capacity to polymerize at room temperature.
Corning® Matrigel® hESC-Qualified Matrix was thawed on ice according to manufacturer's instructions and aliquots were made depending on the protein content indicated in the datasheet. Aliquots were then stored at -20°C until further use. In order to coat matrigel plates, an aliquot was thawed on ice and diluted to the desired concentration with precooled (4°C) DMEM/Ham´s F-12 Medium (Biochrom, Merck Millipore, Merck KGaA, see Table 11). The dilution and the volume to coat 6 well plates was calculated in order to achieve a defined matrix concentration of 8.7 µg protein/cm^2, as indicated in the publications of Lian *et al.* and Burridge *et al.* (110, 111). Matrix polymerization was performed for at least 30 min at 37°C as indicated in the manual of StemCell™ Technologies (*Technical Manual Maintenance of Human Pluripotent Stem Cells in mTeSR™1:* https://cdn.stemcell.com/media/files/manual/MA29106-Maintenance_Human_Pluripotent_Stem_Cells_mTeSR1.pdf). After the incubation residual liquid was removed and 1 mL of TeSR™-E8™ medium was added to each 6-well.

Human iPSC need daily medium change which was performed by removing the previous day's medium, washing cells with DMEM/Ham´s F12 and adding 2 mL of fresh TeSR™-E8™ medium to each well of the 6 well culture plate.

Passaging of iPSC was carried out using ReLeSR™ (#05872, StemCell™ Technologies) according to manufacturer's instructions. ReLeSR™ is an enzyme-free reagent which selectively dissociates undifferentiated iPSC as aggregates. Passaging procedure consisted of the following steps: 1) TeSR™-E8™ medium was removed and cells were washed with 1x D-PBS; 2) 1mL ReLeSR™ was added to each well of a 6 well culture plate and incubated for 1 min at room temperature; 3) ReLeSR™ was removed and the culture plate was incubated for another 3-5 min at 37°C (HERAcell 240i CO2 Incubator, Thermo Scientific); 4) After the incubation, 2 mL TeSR™-E8™ medium per well were added and cells were detached by carefully taping the side of the plate for approximately 30-60 seconds; 5) cell aggregates were collected and centrifuged at 300 x *g* for 5 min at room temperature: 6) the cell pellet was replated at a 1:12 ratio on pre-coated matrigel 6 well culture plates. This ratio was optimized for the iPSC-line used in this work and confluence of the cells was achieved approximately 5-7 days after passaging.

For all iPSC-lines stocks at a low passage (p10 to p20) were kept for long-time storage in liquid nitrogen. Cryopreservation was carried out with mFreSR™ (#05854, StemCell™ Technologies) according to manufacturer's instructions. Unlike described in the paragraph 4.3.3, iPSC were frozen gradually using a Nalgene ® 5100-0001 Cryo 1°C "Mr. Frosty" Freezing Container Rack (Thermo Fisher Scientific) which ensured a temperature decrease of -1°C/min. Cryovials were placed at -20°C for 2h in this container rack and then transferred to -80°C for overnight storage. On the next day, cells were transported on dry ice for long-time storage in liquid nitrogen.

The iPSC-line used in this study was kindly provided to the Division of Experimental Surgery (German Heart Center Munich, DHM) by the laboratory of Prof. Joseph Wu (*Standford Cardiovascular Institute, Stanford University School of Medicine*, Stanford, CA) within a cooperation project. Generation by fibroblast reprogramming and characterization of this iPSC-line were published previously (112).

4.4.6 Directed cardiac differentiation of induced pluripotent stem cells

Human iPSC underwent cardiac differentiation by a protocol developed by Burridge *et al.* (103). The procedure is illustrated in Figure 4B. Using small molecules, which influence the Wnt-signaling pathway, a yield of over 80% of cardiomyocytes can be achieved by this differentiation protocol (110, 111). As previously described, Rock Inhibitor Y-27632 was used in human iPSC culture to improve survival of iPSC during splitting and thawing before differentiation (113). Y-27632 is a selective inhibitor of two isoforms of rho-dependent protein kinase ROCK, ROCK I and ROCK II (114). It competes with ATP for binding to the catalytic site of the enzyme (115). In this work a concentration of 10 µM was used, because it was described to be the optimal concentration to maintain the stem cell character of human stem cells (116-119). Besides, supplementation with Rock inhibitor Y-27632 was described to increase cell survival rates of iPSC plated as monolayer before initiation of differentiation (120). This was also recommended in the direct cardiac differentiation protocol by Burridge *et al.* used in this work (111).

The differentiation was performed on a complete 24-well culture plate. In order to achieve sufficient cell number for differentiation, iPSC were first expanded in TeSR™-E8™ medium to confluence on two complete 6-well culture plates. Two days before starting differentiation, iPSC were passaged by 0.5 mM EDTA/PBS (see paragraph 3.7) to a matrigel-coated 24-well plate.
The passaging procedure included the following steps: 1) TeSR™-E8™ culture medium was removed and cells were washed once with 1x D-PBS; 2) each well was incubated with 1 mL 0.5 mM EDTA/PBS for 5-8 min at 37°C; 3) 0.5 mM EDTA/PBS solution was removed and 1 mL of TeSR™-E8™ with 10 µM Y27632 ROCK inhibitor (#72304, StemCell™ Technologies, see paragraph 3.7) was added; 4) cells were dissociated from the plate by carefully rinsing and the single cell suspension was centrifuged (300 × *g*, 8 min at room temperature). Resuspended cells were seeded on a matrigel-coated 24-well plate in 1 mL TeSR™-E8™ per well. Change of TeSR™-E8™ medium was performed every day until the start of the cardiac differentiation. Before medium was changed, cells were washed with DMEM/Ham´s F12.
After two days, iPSC grew to a dense monolayer and directed cardiac differentiation was started. At the starting day of differentitation, day 0 (D0), CHIR99021 (#C-6556, LC Laboratories, Woburn, MA, see paragraph 3.7) was added at a concentration of 3.5 µM in CDM3 medium (see Table 12). CHIR99021 is a small molecule which is used to initiate direct differentiation of iPSC into cardiomyocytes. CHIR99021 activates the Wnt signaling pathway by specific inhibition of glycogen synthase kinase 3 and stabilization of free cytosolic β-cathenin (121). On D2, the medium was changed to CDM3 containing 2 µM Wnt-C59 (#S7037, Sellekchem, Houston, TX, see paragraph 3.7). Wnt-C59 is a small molecule which is used as an inhibitor of the Wnt-signaling pathway in the second step of the direct cardiac differentiation protocol of iPSC (110, 111). From D4, medium change with CDM3 was performed every second day. Usually, beating cells were observed by D8 and by D14 large parts of the wells contained beating cells. To measure gene expression by qRT-PCR, RNA was isolated at D8 of differentiation, considering most human iPSC to be in a cardiac progenitor state (see paragraph 4.5.1 for RNA quantification procedure).

4.4.7 Isolation of neonatal rat cardiomyocytes (NRCM)

Neonatal rat cardiomyocytes were kindly provided by the TUM Institute of Pharmacology and Toxicology (IPT) (Director: Prof. Dr. med. Dr. rer. nat. Stefan Engelhardt).
Isolation procedure was performed according to previously published standard procedures (122) by Prof. Engelhardt's research group. Therefore, materials indicated in the following brief description are not listed in the material section of this work. In brief, the NRCM isolation procedure was performed as follows: 0–1-day old Sprague Dawley rats were decapitated after disinfection of their neck area. Whole hearts were then explanted and digested with collagenase type II (Worthington) and pancreatin (Sigma Aldrich) in CBFHH buffer (120 mM NaCl, 5 mM KCl, 0.8 mM $MgSO_4$, 0.5 mM KH_2PO_4, 0.3 mM Na_2HPO_4, 20 mM HEPES, 5.6 mM glucose, pH 7.3 including penicillin/streptomycin) at 37°C for 1h. In intervals of 10 min, digestion

solution containing dissociated tissue cells was collected in FCS (Sigma Aldrich) and fresh enzymatic solution was added to the undigested heart tissue pieces (5 times). Thereafter, collected cells were centrifuged at 50 × g for 5 min and the pellet was resuspended in MEM medium containing 5% FCS. After undigested tissue was filtered out with a 40 µm strainer (BD), cells were pre-plated at 37°C and 1% CO_2 for 75 min on 10 cm cell culture dishes (Nunc) to adhere cardiac fibroblasts. Cell culture supernatant containing NRCM was then collected and kept at 37°C/1% CO_2 until transportation to the German Heart Center.
After transportation to German Heart Center, NRCM were centrifuged at 100 x *g* for 2 min at room temperature and replated on a 96-well plate coated with 0.1% gelatine (for coating procedure see paragraph 3.7) in NRCM medium (see Table 12) at a concentration of 4×10^4 cells/well.

4.5 Characterization of primary cells

4.5.1 Gene expression analysis

4.5.1.1 RNA isolation and purification

Total cellular RNA was isolated from primary cells (CDC, CF, AF, EC, SMC, CFSPh) at passage 0 and from iPSC on D8 (DIFF D8) of cardiac differentiation using the peqGOLD Total RNA Kit (S-Line), (#732-2871, Peqlab, VWR International, Erlangen, Germany) according to manufacturer's instructions.
Cells were lysed by denaturation with the provided RNA Lysis Buffer and lysates were stored at -20°C until further use. The peqGold Total RNA Kit contains DNA Removing columns which selectively remove DNA from the lysate. In a second step, the flow through is pipetted on a PerfectBind RNA column with silica membranes which bind RNA molecules. DNA digestion with the peqGOLD DNase I Digest Kit (#732-2982, Peqlab Biotechnologie GmbH, Erlangen, Germany) was carried out according to manufacturer's instructions directly on the column. By washing with specific buffers provided in the kit, cellular debris, digested DNA and other contaminants were removed. Finally, purified RNA was eluted with nuclease-free water from the column and stored at -80°C (long term).

4.5.1.2 Quality control and quantification of RNA

In order to assess the quality of purified RNA samples and to measure their concentrations, NanoDrop 2000c Spectrophotometer (Thermo Fisher Scientific, Waltham, MA) was used. This instrument utilizes a modified Beer-Lambert equation to calculate nucleic acid concentration after measurement of the absorbance of each sample. The extinction coefficient for RNA is 40 ng-cm/µL (information from ThermoFischer Scientific).

Beer-Lambert equation: **$c = (A * \varepsilon)/b$**

c = the nucleic acid concentration in ng/microliter; A = the absorbance in AU; ε = the wavelength-dependent extinction coefficient in ng-cm/microliter; b= the pathlength in cm

For quality control absorbance at 230 nm, 260 nm and 280 nm were measured. The ratios of A260/280 and A230/260 were calculated to assess RNA purity. For pure high quality RNA samples A260/280 should be around 2 and A230/260 should be in the range of 1.8-2.2. A260/280 ratio which is significantly lower indicates contaminations with phenols or proteins that absorb near 280 nm. Lower A230/260 ratio indicates the presence of other contaminants.

For measurement 1 µL of the sample was used. To enable measurement of concentrated samples, short pathlengths between 1.0 mm to 0.05 mm were applied. The nucleic acid application absorbance values were normalized to a 1.0 cm (10.0 mm) path for all measurements. All measurements were performed according to manufacturer's instructions (NanoDrop 2000/2000c Spectrophotometers User Manual, ThermoFischer; https://assets.thermofisher.com/TFS-Assets/CAD/manuals/NanoDrop-2000-User-Manual-EN.pdf, 05.03.2020).

4.5.1.3 Analysis of gene expression

4.5.1.3.1 Reverse transcription and cDNA production

For qRT-PCR of messenger RNA (mRNA), 100 ng of isolated total RNA were reverse transcribed with the M-MLV Reverse Transcriptase Kit (#28025013, Invitrogen™, Thermo Fisher Scientific) according to manufacturer's instructions. The enzyme M-MLV (Moloney Murine Leukemia Virus) reverse transcriptase is a recombinant DNA-polymerase, which is able to synthetize a complementary DNA strand from the single-stranded RNA template (manufacturer's information). Random hexamer oligonucleotides (#48190011, Invitrogen™, Thermo Fisher Scientific) are short oligodesoxyribonecleotides which bind randomly to complementary RNA-sites and thus served as primers for reverse transcription. Before usage, the purchasable 100 µL of random hexamers (3 µg/µL) were diluted with 1100 µL H_2O (# J70783, Water, RNase-free, DEPC treated, Molecular Biology Grade, Ultrapure, Thermo Fisher Scientific) to a final concentration of 250 ng/µL and aliquots were stored at -20°C.
In the first step of complementary DNA (cDNA) synthesis, 100 ng RNA were mixed with random hexamer oligonucleotides and dNTPs (#K039.1, Carl Roth GmbH + Co. KG) and incubated in the C1000 Thermal Cycler (Bio-Rad Laboratories GmbH) at 65°C for 5 min. In Table 16 the components used for this first reaction are indicated (Mastermix 1).

Table 16: Reverse Transcription Mastermix 1

Component	Volume
Random Hexamers (250 ng/µL)	1.5 µL
dNTPs (100 mM dATP, dGTP, dCTP, dTTP)	1.5 µL
RNA (100 ng) diluted in nuclease-free water	16.25 µL

In a second step Mastermix 2 was added to Mastermix 1. Components per reaction are listed in Table 17. An incubation of 2 min at 37°C in the C1000 Thermal Cycler (Bio-Rad Laboratories GmbH) followed.

Table 17: Reverse Transcription Mastermix 2

Component	Volume
5x First Strand Buffer	6 µL
0.1 M DTT	3 µL
RNase free water	1 µL

In the third step 0.75 µL M-MLV were added to the reaction mix (Mastermix 1 and Mastermix 2), resulting in an end volume of 30 µL. Subsequently, the incubation steps listed in Table 18 which were carried out in a C1000 Thermal Cycler (Bio-Rad Laboratories GmbH). After this step, cDNA was stored at -20°C until further use.

Table 18: Reverse Transcription Incubation steps

Reaction	Temperature	Incubation period
Incubation	25°C	10 min
cDNA synthesis	37°C	50 min
Enzyme inactivation	75°C	15 min
	4°C	∞

4.5.1.3.2 Semiquantitative real-time polymerase chain reaction (qRT-PCR)

During a polymerase chain reaction (PCR), cDNA is amplified using sequence-specific oligonucleotides, heat-stable DNA polymerase and thermal cycling. Initially, thermostable DNA polymerase is activated at 95°C. Thereafter, a three-step PCR reaction, termed cycle, is set to amplify the desired cDNA region. By default, the number of cycles was set to 40. One PCR cycle consists of denaturation, an annealing and an extension phase. In the denaturation phase, a high temperature is applied to break up double-stranded DNA into single strands, whereas during the annealing phase a lower temperature is used to enable hybridization of complementary sequences. During the following extension phase the temperature is set to the optimum of the DNA polymerase to recognize annealed primers and to synthesize the oligonucleotides in 5'→3' direction. In this work the annealing and extension phases were performed at one step, resulting in a two-step cycle.

Semiquantitative real-time PCR allows the measurement of the amount of synthesized PCR product after each cycle. In this work, the fluorescent dye SYBR Green I is used for detection and quantification of the PCR product. SYBR Green I binds to the minor groove of double-stranded DNA (dsDNA) (123). As the excitation of dsDNA-bound SYBR Green I produces a much stronger signal than the unbound dye, the fluorescence signal is proportional to the amount of the PCR product during the exponential phase.

During the initial cycles (usually 3-15) there is little change of the fluorescent signal. This low signal level can be referred to as noise or background. The qRT-PCR software calculates this baseline level automatically and determines a threshold value which reflects a statistically significant increase over the calculated baseline signal. The threshold value is calculated as ten-fold standard deviation of the fluorescence value of the baseline. At a certain cycle, the fluorescence signal of the PCR product increases exponentially. The cycle number of the threshold value is called cycle threshold (C_t)-value and is used for quantification of the PCR product. After the exponential phase, the amplification curve reaches a plateau because of lack of reagents and inefficiency of the DNA polymerase.

At the end, the quality of the product is analyzed by applying a melting protocol. During this protocol, the temperature is gradually augmented and the change in fluorescence is permanently recorded. At a certain temperature which is specific for the synthesized PCR product, dsDNA melts to single strands and thus the fluorescence signal decreases drastically due to the release of bound SYBR Green I. The melting curve helps the user to assess the quality of the PCR product and to exclude the presence of primer dimers or other unspecific products. (https://www.thermofisher.com/content/dam/LifeTech/Documents/PDFs/PG1503-PJ9169-CO019861-Update-qPCR-Handbook-branding-Americas-FLR.pdf, 26.11.19)

In this work, the instrument Quant Studio 3 (Applied Biosystems by Thermo Fisher Scientific) was used for qRT-PCR. The Kit Power SYBR® Green PCR Master Mix (#4367659, Applied Biosystems by Life Technologies™, Thermo Fisher Scientific) provided all needed reagents excluding the primers. The primers were designed at the website *Universal ProbeLibrary System Assay Design* (Roche Molecular Systems, Inc., Rotkreuz, Switzerland, https://lifescience.roche.com/en_de/brands/universal-probe-library.html#assay-design-center, 27.12.19). Synthesis of primer sets was performed by Ella Biotech GmbH (Martinsried, Germany). Primer sequences are provided in Table 8. The components of mRNA qRT-PCR Master Mix (for Quant Studio 3) which were pipetted into each well of the MicroAmp™ Optical 96-Well Reaction Plate (#N8010560, Thermo Fisher Scientific) are listed in Table 19. The reaction plate was sealed with MicroAmp™ Optical Adhesive Film (#4311971, Thermo Fisher Scientific). The PCR reaction conditions which were applied in the Quant Studio 3 instrument are listed in Table 20.

Table 19: qRT-PCR Mastermix

Components of mRNA PCR Master Mix (for Quant Studio 3)	Volume/Reaction	Final concentration
Power SYBR® Green PCR MasterMix 2x	10 µL	1x
Primer (forward), 5 µM	2 µL	0.5 µM
Primer (reverse), 5 µM	2 µL	0.5 µM
cDNA	1 µL	~3 ng/reaction
RNase-free water	5 µL	
Total reaction volume	20 µL	

Table 20: qRT-PCR Amplification Conditions

		Cycles	Time	Temperature	Rate
		1	2 min	50°C	1.6°C/s
Initial activation step		1	10 min	95°C	1.6°C/s
Amplification		40			
	Denaturation		15 s	95°C	1.6°C/s
	Annealing/ Elongation		1 min	60°C	1.6°C/s
Melting curve analysis		1			
	1. Segment		15 s	95°C	1.6°C/s
	2. Segment		1 min	60°C	1.6°C/s
	3. Segment		1 s	95°C	0.15°C/s
Cooling		1	∞	4°C	

4.5.1.3.3 Relative quantification of mRNA expression with arbitrary units method

To perform quantification of gene expression, experimental results, including C_t values, were exported using Quant Studio Design & Analysis Software (version 1.4, Applied Biosystems by Thermo Fisher Scientific).

For each primer set, dilution series of six $\log_{10}$ or $\log_5$ dilutions of known template concentrations were measured in duplicates by qRT-PCR. Standard curves were then calculated using the the C_t values (y-axis) and relative DNA concentration (x-axis). Linear regression curve was calculated according to the following formula:

y = - m ln(x) + zp, m: slope, zp: y-axis intercept

Amplification efficiancy E was caluculated as $\mathbf{E = 10^{(-1/m)}}$

Efficiency values E in the range of 1.8 and 2.0 refer to amplification efficiencies of 90% to 100%. In order to determine the quality of the standard curve correlation the coefficient R^2 was calculated which should ideally have the value of 1.

For relative quantification of gene expression, C_t values were converted into arbitrary units (AU) using the slope and y-axis intercept of the according primer sets as follows:

$$\mathbf{AU\ (arbitary\ units) = e^{(Ct\ value - zp)/m)}}$$

For relative quantification the reference gene *Actin Beta* (*ACTB,* NM_001101.3) was used for normalization of human samples. For rat and mouse samples *Actb* (NM_031144) was used. Relative gene expression for each sample was calculated as follows:

Relative gene expression = AU (Gene of interest)/AU (*ACTB*)

Table 8 shows the utilized primer sets. Statistical analysis was performed according to paragraph 4.8.

4.5.1.3.4 Agarose gel electrophoresis for quality control of qRT-PCR products

In order to assess the quality of qRT-PCR primers upon first use, the amplification products were checked for their estimated size on an agarose gel. As shown in Suppl. (Supplementary) Figure S1, all amplified PCR products had a unique length (range between 50 to 100 bp). Several different sized bands would be a sign for primer dimers or unspecific amplification (124).

As the size of amplification products was in the range between 100-200 bp, a 2% agarose gel was used. It was prepared by dissolving 1 g agarose in 50 mL of 1x TBE-Buffer. The solution was heated in a Microwave MW 7849 900W (Severin, Sundern, Germany) until the agarose was completely dissolved. After the solution has cooled to about 52°C, 10 µL of 50 µg/mL ethidium bromide solution (#MKBV9660V, Sigma Life Science, Sigma-Aldrich, Merck Millipore, Merck KGaA) or peqGREEN 20 000X DNA/RNA binding dye (#732-2960, VWR, Radnor, PA) was added according to manufacturer's instructions. Ethidium bromide is a phenathridin-dye which is used to stain nucleic acids in gel electrophoresis. It intercalates into DNA in a concentration dependent manner. Due to its aromatic structure, ultraviolet light activates the electrons of ethidium bromide which emit light while returning to their ground state (125). PeqGreen is reported by its manufacturer to be equally sensitive as ethidium bromide in terms of binding to DNA.

The agarose solution was poured into a gel chamber (Gel chamber Sub-Cell Modell 96, Bio-Rad Laboratories GmbH, Munich, Germany). When the solution has hardened to a gel, the qRT-PCR reaction (20 µL) mixed with 1 µL 6x DNA Gel Loading Dye (#R0611, Thermo Scientific™, Thermo Fisher Scientific) was pipetted to the gel pockets. The markers used to assess the DNA fragment sizes were either Quantitas DNA Marker 25-500 bp (#250216, Biozym Scientific GmbH) or GeneRuler™ DNA Ladder (#SM0371, 50 bp, Thermo Scientific™, Thermo Fisher Scientific) according to manufacturer's instructions. The electrophoresis was performed with a PowerPac Basic device (Bio-Rad Laboratories GmbH, München, Germany) at 120 V for 40 min in a gel chamber filled with 1X-TBE Buffer. Visualization was performed with a ChemDoc XR System (Bio-Rad Laboratories GmbH, Bio-Rad Laboratories GmbH) using the software Quantity One Chemidox XRS (version 4.6.9, Bio-Rad Laboratories GmbH) or Software Image Lab™ (version 4.0, Bio-Rad Laboratories GmbH).

4.5.1.4 Analysis of cellular miR expression

MiRs are non-coding RNAs of about 22 nt length which play a role in post-transcriptional regulation, such as mRNA cleavage or translational repression (126). Quantification of mature miRNAs is technically challenging because of their low-abundance, short length and similarity to their precursor transcripts (127). Therefore, special kits were developed for miR specific qRT-PCR.

For miR analysis, total RNA was isolated from CDC, CF and CFSPh cell lysates according to paragraph 4.5.1.1. Reverse transcription and qRT-PCR followed specialized protocols optimized for miR detection.

4.5.1.4.1 Reverse transcription (RT) for miR analysis

For miR analysis, isolated RNA was reverse transcribed with the miRCURY LNA™ RT Kit (#339340, Qiagen, Hilden, Germany) according to manufacturer's instructions. The reagents of the kit enable tailing of miRNAs with a poly(A)-sequence at their 3'-end followed by a reverse transcription using a universal poly(T) primer with a 3' end degenerate anchor and a 5' end universal tag (127). This construct allows binding of locked nucleic acid (LNA) enhanced primers for qRT-PCR of specific miRs. LNAs are nucleic acid analogues containing LNA nucleotide monomers with a bicyclic furanose unit locked in an RNA mimicking sugar conformation. Their uniquely high affinity to bind complementary nucleic acids and thermal stability makes them a good tool for determination of rare sample targets (128).

100 ng of isolated RNA was mixed with 5 x reaction buffer, enzyme, nuclease-free water and UniSp6 RNA spike-in as listed in Table 21. The incubation procedure was carried out on a C1000 Thermal Cycler (Bio-Rad Laboratories GmbH) as indicated in Table 22.

Table 21: miR RT-Mastermix

Component	Volume
5 x reaction buffer	2 µL
enzyme	1 µL
UniSp6 RNA spike-in	1 µL
RNA (100 ng) diluted in nuclease-free water	6 µL
Total reaction volume	10 µL

Table 22: miR RT temperature conditions

Reaction	Temperature	Incubation period
cDNA synthesis	60°C	42 min
Enzyme inactivation	95°C	5 min
Storage	4°C	∞

4.5.1.4.2 qRT-PCR for miR quantification

qRT-PCR was performed on a QuantStudio3 (Applied Biosystems, Foster City, CA) using the miRCURY LNA™ microRNA PCR ExiLENT SYBR® Green master mix (# 203421, Exiquon, now Qiagen, Hilden, Germany). As mentioned above, LNA primer technology allowed sensitive and specific amplification of miRs. Components of miR qRT-PCR Master Mix are listed in Table 23. ExiLENT SYBR® Green master mix contains DNA-polymerase. Prior to measurement cDNA-samples were diluted with nuclease-free water (#R0581, Thermo Fisher Scientific™, Thermo Fisher Scientific) at a 1:80 dilution. Used PCR primer mixes are provided in Table 9. Settings applied on QuantStudio3 are listed in Table 24.

Table 23: micro qRT-PCR Master Mix

Components of microrRNA qRT-PCR Master Mix (for Quant Studio 3)	Volume/Reaction
ExiLENT SYBR® Green master mix	5 µL
PCR primer mix	1 µL
cDNA (diluted 1:80)	4 µL
Total reaction volume	10 µL

Quantification was performed using the $\Delta\Delta C_t$ method. Data were normalized to housekeeping miR-423-3p. First, a difference between the C_t-values is calculated using following equation:

ΔC_t (Gene of interest) = C_t (Gene of interest) - C_t (miR-423-3p)

A reference value (Rf) is calculated as the mean of all ΔC_t (Gene of interest).

The value which is compared between samples is: $\mathbf{2^{-\Delta\Delta Ct}}$

$\Delta\Delta C_t = \Delta C_t$ (Gene of interest) - Rf

C_t values of not amplified samples were set to 40 (maximal number of cycles) for calculation of the reference value, but were excluded from the statistical analysis between groups.

Table 24: miR qRT-PCR amplification settings

		Cycles	Time	Temperature	Rate
Initial activation step		1	2 min	95°C	Fast mode
Amplification		40			
	Denaturation		10 s	95°C	Fast mode
	Annealing/ Extension		1 min	56°C	Fast mode
Melting curve analysis		1			
	1. Segment		15 s	95°C	1.6°C/s
	2. Segment		1 min	60°C	1.6°C/s
	3. Segment		1 sec	95°C	0.15°C/s
Cooling		1	∞	4°C	

4.5.2 Immunocytochemistry (ICC)

ICC is a method by which proteins or macromolecules can be visually identified in cells using chemical reactions (129). In this work, antigen specific primary antibodies were used to mark proteins of interest. In a second step, a secondary antibody labeled with a fluorescent dye was bound to the primary antibody and enabled to visualize the protein of interest. It is crucial to know whether the protein of interest has an extra- or intracellular distribution, because intracellular staining requires permeabilization of the cells.

Cells (AF, CDC, CF, SMC, EC) were fixed with ice-cold methanol (#34860, Sigma-Aldrich, Merck Millipore, Merck KGaA) at -20°C for 15 min. For the detection of intracellular markers (Vimentin, α-SMA), cells were permeabilized with 0.25% Triton-X-100 in 1x D-PBS (0.25% PBS-T, see paragraph 3.7) for 15 min and all subsequent washes of these wells were performed with 0.1% Triton-X-100 in 1x D-PBS (0.1% PBS-T, see paragraph 3.7). Unspecific binding was blocked with 5% normal goat serum (#ab7841, abcam, Cambridge, UK) for 30 min at room temperature. Primary antibodies were diluted according to the concentrations shown in Table 5. Cells were incubated with primary antibodies overnight at 4°C. After washing off the primary antibodies, cells were incubated with secondary antibodies according to dilutions specified in Table 6 for 1h at room temperature in the dark. After the last wash slides were air-dried, mounted in Abcam Mounting Medium with DAPI (#ab104139, abcam, Cambridge, UK), sealed with cover slips (Menzel™ Microscope Coverslips 24x60 mm, #11778691, Thermo Fisher Scientific) and evaluated under a fluorescence microscope (Axiovert 200M, Zeiss, Oberkochen, Germany) equipped with a camera (AxioCam MRm, Zeiss) using the software Carl Zeiss™ Axio Vision Rel. (version 4.8.2, Zeiss). The ICC protocol for NRCM is described in paragraph 4.6.2.

4.5.3 Flow Cytometry (FC)

For characterization of CDC in comparison to AF, CF, SMC and EC, flow cytometry (FC) analysis of cell surface markers was performed. The technique of FC permits the identification of specific cell subpopulations based on labeling expressed proteins with fluorescent dye-conjugated antibodies. Flow cytometers consist of a fluidics system that allows to measure one cell at a time after its excitation with multiple lasers. The emission signals are then captured by complex optics and detectors systems. The forward scatter (FSC) detector captures the scattered light at the an angle of +/- 5° to the cell, so that the detected signal is proportional to the cell diameter. The side scatter (SSC) signal is captured at an angle of 90° to the cell and is proportional to the granular structures within the cell or the cell surface complexity (130). Forward and side scatter signals allow distinguishing cells from other particles in the solution. Lasers with excitation wavelengths optimized for the fluorophores are then used to detect cells labeled with the conjugated antibodies.

For FC analysis, cells were grown on a T75 flask (#G200FF-75, Kisker Biotech GmbH & Co. KG) or a 6 cm culture dish (#628160, Greiner Bio-One International GmbH, Frickenhausen, Germany) at passage 2-3. At the day of FC analysis cells grown in the T75 flask were detached using trypsin-EDTA 0.25% (see paragraph 4.3.2) and analyzed for expression of CD90, CD45, CD105 and CD31. Detached cells were centrifuged (300 × *g,* 5 min, room temperature), resuspended in FACS buffer 2mM EDTA (1x D-PBS/0.5% BSA/2 mM EDTA, see paragraph 3.7) and kept on ice during the staining procedure unless otherwise stated. Primary and secondary antibodies used for flow cytometric analyses are listed in Table 5 and Table 6, respectively.

Cells to be co-stained against CD90/CD45 or against CD105/CD31 were centrifuged and incubated with fluorophore-labeled antibodies at a 1:11 dilution for 30 min on ice in the dark (**CD90:** anti-CD90 PE-Cy5, eBioscience, #15-0909, Thermo Fisher Scientific; **CD45:** anti-CD45 FITC, #11-9459e, Bioscience, Thermo Fisher Scientific; CD105: anti-CD105 APC, eBioscience, #17-1057, Thermo Fisher Scientific, **CD31:** anti-CD31 PE-Cy7, #25-0319-42, eBioscience, Thermo Fisher Scientific). After two additional washes with FACS buffer 2 mM EDTA, cells were kept in FACS buffer 4 mM EDTA for FC analysis. All samples were filtered through a 30 µm filter (30 µm Syringe Filcons, #340599, BD Biosciences, Franklin Lakes, NJ) before FC. Unstained cells undergoing the same centrifugation procedures were used as negative controls for CD90/CD45 and CD105/CD31 staining. Shortly before measurement cells were incubated with DAPI-solution (4',6-Diamidino-2-Phenylindole, #422801, Biolegend, San Diego, CA) at a ratio 1:100 (1 µg/mL) to stain dead cells (see paragraph 3.7). DAPI is a DNA labeling fluorescence dye which associates with the minor groove of double-stranded DNA (131).
The FC analysis was performed on a FACS BD LSR Fortessa (Becton, Dickinson and Company, BD Bioscience, San Jose, CA) with the software BD FACSDiva™ (version 8.0.1, Becton, Dickinson and Company, BD Bioscience). The following gating strategy was used: After filtering out small particles (e.g. cell debris) by setting the gates on the majority of bigger particles in the FSC versus SSC window, DAPI negative cells (living cells) were chosen for analysis. Gates for the according channels (PE-Cy5/FITC or PE-Cy7/APC) were set depending on the respective negative controls. FCS files were exported and finally analyzed with the FlowJo software (version 7.6.5, FlowJow LLC, Ashland, OR).

4.5.4 Single-cell RNA sequencing

4.5.4.1 Preparation of samples for single-cell RNA sequencing (scRNA-seq)

In order to achieve a high-quality single cell cDNA-library, the viability of used cells is crucial. A high percentage of dead cells or non-cellular particles, such as cell debris, can lead to a reduced cell recovery. Therefore, the sample preparation procedure must be fast and experimental steps which may lead to enhanced cell death should be avoided. Cells derived from fresh tissue biopsies are particularly vulnerable, because they are not used to *in vitro* conditions.
Except for cell cultivation and biopsy recruitment, all preparation steps for scRNA-seq were performed at the laboratory of Dr. R. Teperino, Helmholtz-Zentrum München, HMGU.

4.5.4.1.1 Cultured cells

Cells to be analyzed (Table 25) were grown in T25 flasks (#G200FF-25, Kisker Biotech GmbH & Co. KG) or T75 flasks to about 70% confluence. After washing off residual medium with 1x D-PBS, cells were trypsinized with 0.125% trypsin-EDTA (1:2 dilution of 0.25% trypsin-EDTA with 1x D-PBS) as described in paragraph 4.3.2. Trypsin was stopped with the triple amount of the respective cell culture medium and cells were centrifuged at 100-300 x *g* for 5 min at 4°C. Supernatant was discarded and pellets were resuspended in medium and filtered through

30 µm pre-separation filters (#130-041-407, Miltenyi Biotech, Bergisch Gladbach, Germany). Cells were counted with a Countess II FL (Life Technologies™, Thermo Fisher Scientific) using the Ready Probe Viablity Imaging Kit Blue/Green (#R37609, Life Technologies™, Thermo Fisher Scientific) according to manufacturer's instructions to label all cells with the blue dye (detection with DAPI channel) and dead cells only with the green dye (detection in GFP channel). Dyes were applied to the cell suspension at a dilution of 1:10, mixed carefully by pipetting without introducing bubbles and incubated for 15 min before the measurement. Cell preparations with > 95% positive cells in the DAPI-channel and < 10% positive cells in the GFP channel were used for library preparation. Sample 4 is a mixture of samples 1-3 according to the percentages indicated in Table 25.

Table 25: Samples for single-cell sequencing

Sample No.	Cell type	Age group	Passage
1	EC	Adult	P1
2	CF	Adult	P2
3	SMC	Adult	P2
4	Mixture of 20% EC, 30%SMC, 50% CF	Adult	P1/P2
5	CDC	Adult	P0
6	CDC	Infant	P0

4.5.4.1.2 Biopsy

A left atrial appendage biopsy was obtained during heart surgery (for patient details see patient 22, in Table 14). Transportation from operating room to the laboratory was performed on ice. Tissue was washed twice with ice-cold 1x D-PBS in order to remove most of residual blood. Before mincing the biopsy, adipose tissue and white fibers were removed. The remaining tissue was minced with a surgical disposable scalpel to small pieces of approximately 1 mm^3 and incubated in 1 ml 0.25% trypsin-EDTA at 37°C for 10 min. Thereafter, 14 mL of digestion solution containing 10 mg /mL collagenase II (#17101-015, Life Technologies™, Thermo Fisher Scientific) and 20% FBS in 1x D-PBS were added (see Tissue digestion solution for single-cell RNA sequencing in paragraph 3.7), and the tissue was digested at 37°C for another 80 min. To remove undigested tissue the digest was filtered through an EASYSTRAINER 70 µM and the strainer was washed with 5 mL ice-cold Hank's balanced salt solution (HBSS, #H9394, Sigma-Aldrich, Merck Millipore, Merck KGaA). Cell suspension was centrifuged (300 x *g*, 10 min, 4°C) and the supernatant was discarded. The pellet was resuspended in 600 µL ice-cold HBSS. Then, 6 mL of 1:10 dilution of 10x red blood lysis solution (#130-094-183, Miltenyi Biotech) in Millipore water were added and cells were incubated at room temperature for 3 min with continuous inversion. After centrifugation (300 x *g*, 10 min, room temperature), the pellet was resuspended in 1,000 µL ice-cold HBSS and filtered through a 30 µm pre-separation filter which

was pre-equilibrated with 500 µL ice-cold HBSS. The filter was washed with 3 mL ice-cold HBSS. Cell suspension was centrifuged (300 x *g*, 10 min at 4°C) and the supernatant was discarded. The cell pellet was then incubated with 100 µL magnetic beads of the Dead Cell removal Kit (#130-090-101, Miltenyi Biotech). Magnetic separation was performed twice according to manufacturer's instructions. In brief, the living cell fraction (flow through from the magnetic column) after the first separation was collected and centrifuged at 300 x *g* for 5 min at 4°C. The pellet was incubated a second time with 100 µL of magnetic beads. The second living cell fraction was centrifuged (300 x *g* for 5 min at 4°C) and resuspended in 1x D-PBS. Analysis of cell viability was performed using Ready Probe Viability Kit as described in paragraph 4.5.4.1.1. The total digestion procedure took about 3h.

4.5.4.2 Library Preparation

Single-cell libraries were prepared using the technology from 10xGenomics (Pleasanton, CA). This technology is based on nanoliter-scale Gel Bead-In-EMulsions (GEMs). The 10x GEM pool contains ~ 750,000 barcodes to individually index each cell's transcriptome. Cells are partitioned into GEMs in a microfluidic platform which is provided through a 10x Chip placed into a 10x Controller instrument. As a highly diluted cell suspension is used, single-cell resolution can be achieved. All figures illustrated in the following paragraphs are modified from the Chromium Single Cell 3' Reagent Kits User Guide (version 3.1). https://support.10xgenomics.com/single-cell-gene-expression/library-prep/doc/user-guide-chromium-single-cell-3-reagent-kits-user-guide-v31-chemistry, (06.12.2019)

4.5.4.2.1 *Step 1: GEM Generation & Barcoding*

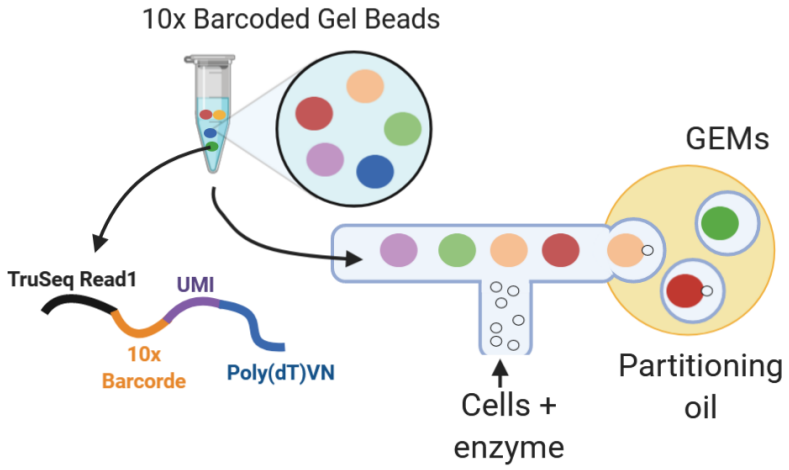

Figure 1: GEM generation

Created with BioRender.com

Figure 1 illustrates the first step of library preparation: GEM generation. GelBeads barcoded with TruSeq Read 1, 10xBarcode, Unique Molecular Identifier (UMI) and Poly(dT)-primer are combined with a master mix containing cell suspension and partitioning oil, generating an emulsion containing GelBead droplets with or without single cells. The 10x Barcode is used to allocate individual reads to a single partition, which ideally represents a single cell. UMI is a sequence tag which enables the detection and quantification of unique mRNA transcripts, without consideration of the copies made during library preparation (132). TruSeq Read 1 is used for the paired-end sequencing technology (see paragraph 4.5.4.2.4) and Poly(dT)-primers are used for reverse transcription.

Cell samples 1-4 were processed according to the library preparation protocol of Chromium™ Single Cell 3' Library & Gel Bead Kit v2 (#120267, 10xGenomics, Pleasanton, CA), whereas cell samples 5, 6 and the biopsy were processed at a later time point with according to the protocol of Chromium Next GEM Single Cell 3' GEM, Library & Gel Bead Kit v3.1 (#1000128, 10x genomics, Pleasanton, CA). In Table 26 shows the cell stock concentrations and the targeted cell recovery which were chosen for the samples. Prior to loading the cells on the chip, cells at the stock concentration from Table 26 were mixed with nuclease-free water and a master mix according to the corresponding protocols' instructions.

Table 26: Cell stock concentrations and targeted cell recovery

Sample No.	Cell stock concentration (cells/µL)	Targeted cell recovery
1	100	1,000
2	100	1,000

3	100	1,000
4	100	1,000
5	700	2,000
6	800	2,000
Biopsy	1200	2,000

As indicated in the corresponding protocols, for samples 1-4 Chip A Single Cell (#2000019, 10x genomics, Pleasanton, CA) and for samples 5, 6 and the biopsy the Chromium Next GEM Chip G (#2000177, 10x genomics, Pleasanton, CA) was used. Empty wells of the chip were filled with 50% glycerol solution (#3290-32, Ricca Chemical Company, Arlington, TX). Both chips were run on the Chromium Controller with the firmware version fitting to the chip (version 3.16 and version 4.00). Immediately thereafter, GEMs were transferred to a tube strip and GEM-RT was performed on a Veriti™ Dx 96-well Fast Thermal Cycler (Applied Biosystems by Thermo Fisher Scientific). Thermal cycle protocol is shown in Table 27.

Table 27: Thermal Cycle Protocol Step 1

Lid Temperature	**Reaction Volume**	**Run Time**
53°C	125 µL	~55 min
Step	**Temperature**	**Time**
1	53°C	45 min
2	85°C	5 min
3	4°C	Hold

During the incubation in the thermal cycler Gel Beads were dissolved, releasing bound primers, and co-partitioned cells were lysed. The master mix which contains reverse transcription reagents enabled the production of full-length cDNA from poly-adenylated mRNA which is captured by the poly(dT) primers

4.5.4.2.2 Step 2: Post GEM-RT Cleanup & cDNA Amplification

The second step, post GEM-RT cleanup and cDNA amplification was performed according to the corresponding protocols. During this step a recovery reagent breaks up the emulsion and thus the GEMs, resulting in a biphasic separation. The oily part was discarded, and the aqueous phase was cleaned up with Dynabeads MyOne SILANE (#2000048, 10xGenomics) to remove residual biochemical reagents and primers from the post GEM reaction mixture. The first strand cDNAs were bound to the magnetic beads and retained with a magnet in the tube. The supernatant was removed, and the beads were washed twice with fresh solution of 80% ethanol in Millipore water (v/v, #E7023-500ML, Sigma-Aldrich, Merck Millipore, Merck KGaA). Finally, barcoded cDNA was eluted from the beads and amplified in the thermal cycler Veriti™ Dx 96-well Fast Thermal Cycler according to corresponding protocols. The aim of this PCR was to amplify cDNA to generate enough starting material for library construction. As the targeted cell

recovery was 1,000-2,000 cells, total cycle number of 14 (samples 1-4) or 12 (samples 5, 6 and biopsy) cycles was chosen, as recommended. These conditions were chosen for all samples.

Thereafter, one sided size selection was performed as cDNA was cleaned up with 0.6 x SPRIselect reagent (#B23317, Beckman Coulter GmbH, Krefeld, Germany).

SPRI beads selectively bind DNA according to the volume ratio of SPRIselect reagent's magnetic beads to total volume. The lower this ratio, the higher is the selectivity of the beads to bind larger DNA fragments. Figure 2 illustrates an example in which first a low ratio of SPRIselect reagent is used, so only large DNA fragments are bound to the beads. The supernatant was collected and underwent another cleanup procedure with a highly concentrated SPRIselect reagent which resulted in very small fragments in supernatant and medium sized fragments bound to the beads, which can be eluted.

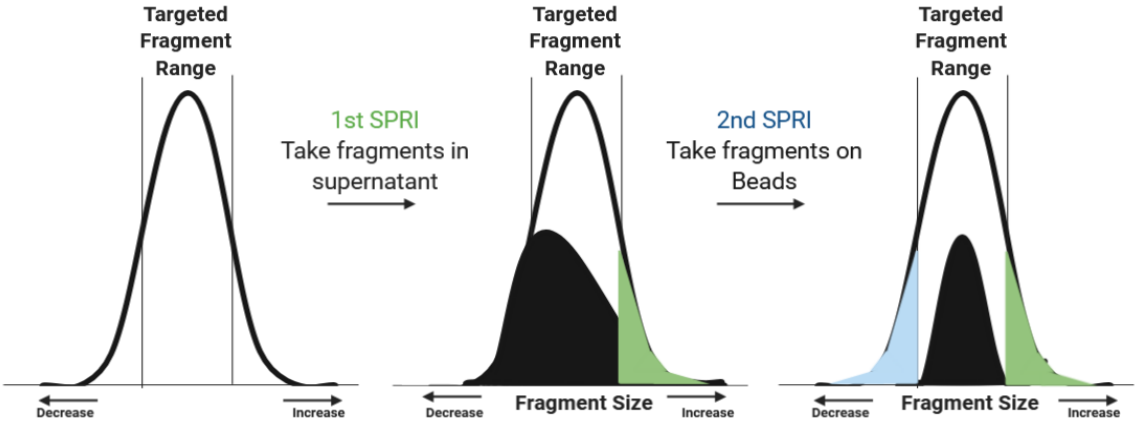

Figure 2: Scheme of double-sided size selection

Created with BioRender.com

Quality check was performed with an Agilent Bioanalyzer 2100 (Agilent, Santa Clara, CA) using the Agilent High Sensitivity DNA Kit (#5067-4626, Agilent).

4.5.4.2.3 Step 3: Gene Expression library construction

At this step cDNA amplicon size was optimized by fragmentation and size selection. Amplified bulk cDNA was preprocessed in several steps. Read 2 for paired-end sequencing, sample index and P5/P7 illumina adaptors were added to the fragments and after each step a magnetic purification was performed. As recommended in the protocol, 25% of the generated cDNA was used to achieve optimal complexity. First, enzymatic fragmentation was performed in the thermal cycler. Afterwards, double-sided size selection was performed as explained above (see paragraph 4.5.4.2.2). Afterwards, adaptors were ligated to the fragments and another clean-up with 0.8 x SPRI-selection followed.

In order to distinguish individual samples in the pool during sequencing, sample indices were annealed to each DNA fragment by PCR. To that end, a Chromium i7 Sample Index plate (PN220103) of the Chromium i7 Multiplex Kit 96 rxns (#120262, 10xGenomics) was used. Table 28 summarizes which sample index wells were used for which sample and the number of cycles performed during SI-PCR.

Table 28: Sample indices

Sample No.	Sample index plate well	Number of cycles in SI PCR
1	A9	14
2	A10	14
3	A11	14
4	A12	12
5	D1	12
6	D3	12
Biopsy	D4	13

Following SI-PCR, another double-sided clean-up procedure with SPRI reagent (0.6 x and 0.8 x) was performed. Quality control of cDNA library was performed with an Agilent Bioanalyzer 2100 using the Agilent High Sensitivity DNA Kit. Figure 3 illustrates the final sequence after the library preparation protocol.

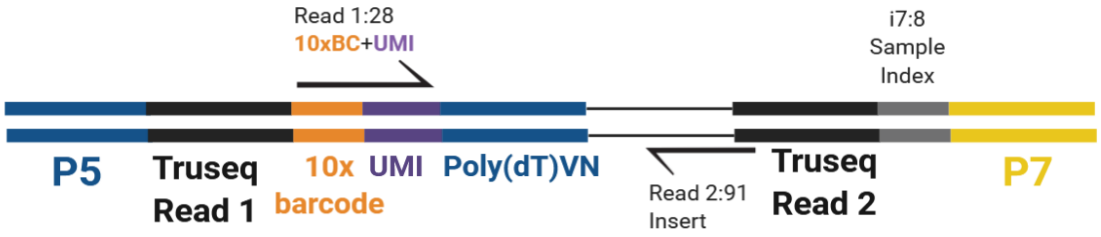

Figure 3: Final sequence of tagged cDNA fragments
Created with BioRender.com

The Read1 and Read2 tags are used for the paired-end sequencing method. P5 and P7 are adapter constructs which provide two dimensions for sample labeling and allow detection of PCR duplicates (133).

4.5.4.2.4 Step 4: Sequencing

Sequencing of samples 1-4 was performed at the laboratory of PD Dr. Tim-Matthias Strom (Helmholtz Zentrum München, Germany) on a HiSeq 3000/4000 (Illumina, San Diego, CA). Sequence length was set to 151 bp with a total count of 250 million reads. Sequencing of samples 5, 6 and the biopsy was performed with at the Laboratory for Functional Genome Analysis (LAFUGA) at the Gene Center, Ludwig-Maximilians-Universität, Munich, Germany. Two technical replicates were performed. The instrument used was a HiSeq 1500 (Illumina). A 100 bp

flow cell was used in a paired-end mode with a total count of 250 million reads. In both experiments, the samples were pooled and measured on 1.5 lanes.

4.5.4.3 Analysis of sequenced data

Raw data were analyzed with the Cell Ranger Single-Cell Software Suite (version 3.1.0, 10X Genomics Inc., for samples 1-4: 3' Gene Expression V2 Libraries, Samples 5, 6 and biopsy: 3' Gene Expression V3 Libraries). The demultiplexed FASTQ files were generated using the Cell Ranger mkfastq command. Then, the FASTQ files were aligned to the human genome reference sequence GRCh38. Subsequently, the preliminary data analysis including alignment, filtering, barcode counting and UMI quantification for determining gene transcript counts per cell, quality control, clustering and statistical analysis were performed using CellRanger count command and generated files for each sample that contained a barcode table, a feature table and an expression matrix. The files were further processed with the package Seurat v3.1 (134-136) implemented in R (v 3.5.3.)(100). The individual samples were first cleaned and normalized. Only data from cells with a minimum of 300 detected genes, and from genes expressed in at least 5 cells were retained. As described in the tutorials (https://satijalab.org/seurat/, 14.11.19), low quality cells such as doublets and cells containing high numbers of mitochondrial genes were filtered. Table 29 reports the filtering parameters used for individual samples. Parameters were chosen in a way to exclude most of the outliers shown in the violin plots (see: Figure 7E-G and Figure 17D-F).

Table 29: Filtering parameters Seurat

Sample Nr. / Name	**Genes/cell** (nFeature_RNA)	**UMI count/cell** (nCount_RNA)	**% MT Genes** (percent.mt)
1/ EC	> 200	< 55,000	< 20
2/ CF	No filtering	No filtering	No filtering
3/ SMC	> 200	No filtering	< 20
5/ CDC Adult	> 200	< 150,000	< 20
6/ CDC Infant	> 200	< 120,000	< 20
Biopsy	> 200	< 55,000	< 75

Abbreviations: Genes/cell (named in Seurat: nFeature_RNA): number of genes detected per cell; UMI count/cell (named in Seurat: nCount_RNA): number of UMIs per cell; % MT Genes (named in Seurat: percent.mt): percentage of mitochondrial genes per cell.

For each sample a SeuratObject was created with "CreateSeuratObject" using the formulas "NormalizeData", "FindVariableFeatures" and "ScaleData" which present the standard workflow for sample pre-processing prior to a principle component analysis (PCA). When several samples were compared, the "merge" formula was utilized prior to the PCA pre-processing workflow.

When comparing samples 1, 2 and 3 to sample 5 and/or the biopsy, the samples were merged separately into two objects based on which kit version was used for GEM preparation (see paragraph 4.5.4.2.1). Since the data came from two different batches of sequencing, to avoid

batch effects affecting downstream analysis and to correct for technical variation due to different kit versions, canonical correlation analysis (CCA) was performed with the formula "RunCCA" (134). Gene read counts were normalized with the Seurat NormalizeData function (normalization.method = LogNormalize, scale.factor = 10,000). The "FindVariableGenes" function was used to identify genes showing significant variation across cells and were selected based on 'LogVMR' dispersion. These highly variable genes were analyzed using "RunPCA" function to identify principle components (PCs). Uniform manifold approximation and projection (UMAP) (137) dimensionality reduction was utilized to project sample populations into two dimensions ("RunUMAP" formula). Table 30 indicates the total number of PCs and dimensions (dims) which were used in PCA and UMAP reduction, respectively. These settings were chosen after testing of different parameter combinations based on the biological interests this work is focused on.

Table 30: Parameters used for RunPCA and RunUMAP functions

Seurat objects	Total Number of PCs to be computed and stored by RunPCA function (npcs)	Which dimensions to be used as input features by RunUMAP function (dims)
Merged CCA-corrected object of CDC_adult, CF, SMC, EC	25	20
CDC_adult (for subclustering analysis)	25	20
CF (for subclustering analysis)	25	20
EC (for subclustering analysis)	50	25
SMC (for subclustering analysis)	50	25
Merged object of CDC_adult and CDC_Infant	50	25
Biopsy (for subclustering analysis)	50	25
Merged CCA corrected object of Biopsy, CDC_adult, CF, SMC, EC	100	50

Abbreviations: PC: principle components; PCA: principle component analysis; UMAP: uniform manifold approximation and projection; CCA: canonical correlation analysis; CDC: cardiosphere-derived cells; CF: cardiac fibroblasts; SMC: smooth muscle cells; EC: endothelial cells.

Graph-based, semi-unsupervised clustering was performed using "FindNeighbors" and "FindClusters" formulas applying default settings, following UMAP projection for visualization. In order to identify marker genes samples as well as clusters were compared for differential gene expression using the "FindAllMarkers" formula with Wilcoxon rank-sum test (Default settings). All analyses of output data were performed only with genes with an adjusted *p*-value < 0.05 (indicated in table provided from Seurat as "p_val_adj"). Enriched genes for a sample or clusters were considered if the average natural logarithm of the gene's fold change (avg_logFC) was ≥ 0.25.

Identification of gene ontology terms enriched in a group of genes was performed by gene set enrichment analysis (GSEA, http://software.broadinstitute.org/gsea/msigdb/annotate.jsp, 27.12.19) which uses gene set collections from the MSigDB26 (138). Overlaps were calculated

for the three gene ontology (GO) gene sets (biological process, cellular component and molecular function) and top 50 terms were selected to display. The GO project is a bioinformatics resource (http://www.geneontology.org, 27.12.19) which provides evidence-supported annotations describing the biological roles of individual genomic products such as genes and proteins and considering their associated processes, functions and cellular locations (ontologies). An annotation is an association between a GO-term and a gene supported by references (139, 140). GO-terms were considered as significantly enriched, if their *p*-value's negative decadic logarithm was higher or equal to 6 (–LOG (*p*-value) ≥ 6).

Data was visualized in Seurat using violin plots ("VlnPlot" function), FeaturePlot ("FeaturePlot"), Clustertrees ("BuildClusterTree and "PlotClusterTree") and Heatmaps ("DoHeatmap") of individual genes. Manual heatmaps were generated using the website http://heatmapper.ca/expression/ (27.12.19) in order to illustrate gene expression of genes which are not expressed in all samples. In case an avg_logFC-value is not displayed for a sample in the FindAllMarkers-table (avg_logFC < 0.25 or > -0.25) the value was manually set to 0 in the manual heatmap. Venn Diagrams were generated using http://bioinformatics.psb.ugent.be/webtools/Venn/ (27.12.19) and formatted with the software Inkscape (version 0.92.4, https://inkscape.org/, 5.3.2020).

Sample similarity calculation (Figure 14B) was performed according to the method published by Wang *et al.* (21). The "FindVariableFeatures" function of Seurat was used to first identify variable genes in the CCA-corrected merged object (including CDC, CF, SMC and EC) which were then selected based on their average expression level. Dispersion was restricted to between 0.01 and 3. Dispersion cutoff was set as greater than 1. Next, genes were divided into 10 equally sized bins based on mean expression, and 10% of genes with the lowest variance from each bin were selected, excluding the high and low extremes. The average gene expression profile of a sample was calculated using selected genes as the centre. The Pearson correlation was calculated for each sample to the centre and shown as a density line graph.

Determination of similarly expressed genes in CDC and CF (Figure 15E) was performed as following: First, separate comparison of CDC to CF, SMCs and EC, respectively, was performed. Similarly expressed genes, which were defined by avg_logFC values lying between -1 and +1, were retrieved for the groups CDC-CF; CDC-EC; CDC-SMC and were analyzed in a Venn-diagram. Genes found exclusively in the CDC-CF group were then analyzed with GSEA. Genes attributed to selected highly significant enriched GO-terms of this GSEA analysis were illustrated in a heatmap.
Comparison of sc-RNAseq data to proteomics data by Doll *et al.* (5) was performed by filtering out the overexpressed proteins (FC = 2) for CF, SMC and EC, respectively, compared to all analyzed cell types (AF included, see Suppl. Figure S 4). The list of the according gene names was compared to the list of overexpressed genes in sc-RNAseq experiment for CF, SMC and EC,

respectively (avg_logFC = 0.7, CDC included). Since the proteomic experiment was generally more sensitive and thus a higher number of gene names was present in its list, the percentage of overlapping gene names was built to the total amount of gene names detected by sc-RNAseq.

4.6 NRCM characterization

4.6.1 qRT-PCR

Expression analysis of myocyte marker *Tnnt2* of NRCM was performed according to the procedure described in paragraph 4.5.1. Information on used primer sets is provided in Table 8. In order to compare the gene expression of NRCM to cardiac fibroblasts, murine CF were cultivated as described in paragraph 4.4.2 and RNA was isolated at passage 2.

4.6.2 ICC of NRCM

NRCM were fixed with NRCM fixation solution (see paragraph 3.7) containing 4% (v/v) para-formaldehyde and 4% (w/v) sucrose in 1x D-PBS. For the detection of intracellular markers (αActinin, TropT, αMHC, Tnni), cells were permeabilized with 0.25% Triton-X-100 in PBS (0.25% PBS-T, see paragraph 3.7) for 15 min and subsequently washed with 0.1% Triton-X-100 in PBS (0.1% PBS-T, see paragraph 3.7). The permeabilization step was left out during staining with Cx43 which is a surface marker. Unspecific binding was blocked with 5% normal goat serum (#ab7841, abcam, Cambridge, UK) for 30 min. Primary antibodies were diluted according to the concentrations shown in Table 5. Cells were incubated with primary antibodies overnight at 4°C. After washing, cells were incubated with secondary antibodies according to the dilutions specified in Table 6 for 1h at room temperature in the dark. Antibody dilutions were prepared in 0.1% PBS-T (intracellular markers) or 1x D-PBS (Cx43) containing 1.5% normal goat serum to minimize unspecific binding. After the last wash, slides were air-dried, mounted in Abcam Mounting Medium with DAPI, sealed with cover slips and evaluated under a fluorescence microscope (Axiovert 200M, Zeiss) equipped with camera (AxioCam MRm, Zeiss).

4.7 Analysis of extracellular vesicles (EV)-mediated paracrine effects of CDC and CF

4.7.1 EV isolation

CDC and CF were each expanded in five T75 flasks. When cells had reached 80-90% confluence, they were washed thrice with 1x D-PBS to remove all traces of FBS containing medium. Then cells were conditioned with serum-free IMDM medium (see Table 12) for 7 days to allow sufficient EV release into the medium. After conditioned medium was collected, cells were detached by trypsinization (see paragraph 4.3.2) to assess cell count of viable and dead cells by trypan blue staining (4.3.1). EV were isolated from conditioned medium with ExoQuick-TC (#EXOTC50A-1, System Biosciences, Palo Alto, CA) according to manufacturer's protocol. In brief, conditioned medium was centrifuged at 3000 x *g* for 15 min to pellet cells and debris. The supernatants were incubated with ExoQuick-TC in a volume ratio of 5:1 overnight at 4°C. The next day medium-Exoquick-TC mixtures were centrifuged at 1,500 x *g* for 30 min and the

supernatant was removed as far as possible. After a second centrifugation at 1,500 x *g* for 5 min, any remaining supernatant was removed and the pellet was resuspended in 50 µL 25 mM Trehalose solution in 1x D-PBS (see paragraph 3.7) which was reported to be beneficial for the cryopreservation of EV (141). Exosome preparations were stored at -80°C until further use.

4.7.2 EV characterization

4.7.2.1 Nanoparticle tracking

In order to assure that experiments with EV are accurate and reproducible, the knowledge of the exact EV concentration is crucial. A commonly used method is nanoparticle tracking. In solution, nanoparticles move according to the Brownian motion. Nanoparticle tracking instruments illuminate particles in a defined volume by a laser and capture their scatter light with a camera. Thus, their trajectory is measured. As the measurement is performed at a defined temperature, Stokes-Einstein equation can be applied in order to calculate particle radius for each tracked particle. Additionally, particle count is determined and thus the concentration in a defined volume can be calculated (142).

For measurement of EV concentration and mean size, a ZetaView PMX110 instrument (Particle Metrix, Inning, Germany) was kindly provided by the group of Prof. Dr. Reinhard Zeidler (Helmholtz Zentrum München). Calibration was performed with polystyrene beads of known size and concentration (100 nm NanoStandards; Applied Microspheres, Leusden, The Netherlands) as previously reported (143). EV were diluted with1x D-PBS to a concentration of 100- 200 particles per video frame, according to manufacturer's instructions. Each sample was measured at eleven positions with one reading cycle at each position. Camera control settings were set to a sensitivity of 75, a shutter of 50 and a frame rate of 50. Post acquisition parameters were set to minimal brightness of 20, maximal size of 200 and minimal size of 5, and tracelength of 15.

4.7.2.2 miR expression in EV

To measure the miR content in the isolated EV-preparations, total RNA was isolated using the SeraMir Exosome RNA Purification Column Kit (#RA808A-1, System Biosciences) according to manufacturer's instructions. In brief, the EV pellet after the isolation procedure (see paragraph4.7.1) was directly resuspended in 350 µL lysis buffer provided in the kit. Exosomal RNA was purified with RNA-binding spin-columns. Other components of EV (such as proteins and lipids) were washed off using the wash buffer provided in the kit. Finally, exosomal RNA was eluted from the column with 30 µL elution buffer. Quality of isolated RNA was controlled as described in paragraph 4.5.1.2. MiR optimized reverse transcription and qRT-PCR was performed as described in paragraphs 4.5.1.4.1 and 4.5.1.4.2.

4.7.2.3 Flow cytometric analysis of EV

Isolated EV were analyzed for the presence of exosomal markers CD63 and CD81 with the Exo-Flow Exosome Capture Kit (#EXOFLOW15A-1, SystemBiosciences, Palo Alto, CA) according to

manufacturer's instructions. In brief, magnetic beads were prepared by washing them twice with the Bead Wash Buffer provided in the kit. Biotinylated antibodies (either CD81 or CD63) were bound to the magnetic beads, which are coated with a streptavidin layer for 2h on ice. Residual antibodies were washed off by three washes with Bead Wash Buffer. Isolated EV from one T75 cell culture flask were diluted to a total volume of 100 µL in 1x D-PBS (#P04-36500, PAN-Biotech GmbH, Aidenbach, Germany) and incubated with the stained beads overnight at 4°C. The negative control was incubated with serum-free IMDM medium (see Table 12). During this incubation the bead-coupled antibodies should bind to the EV. In order to to detect the EV-bead fraction by FC, the bead preparation was incubated with Exo-FITC- exosome stain for 2h on ice. This dye binds to exosome modifications such as glycosylations and carbohydrate additions. Residual dye solution was washed off three times with Bead Wash Buffer. During FC analysis, the first gate was set on the majority of the bead singlets which could be distinguished from bead multimers in the FSC versus SSC window. The secondary gate was set according to the FITC signal of the negative control. FC analysis was performed on a FACS BD LSR Fortessa with the software BD FACSDiva™ (version 8.0.1). FCS files were exported and analyzed with FlowJo (version 7.6.5).

4.7.3 Functional in vitro assays with EV

4.7.3.1 Effects of CDC/CF EV on endothelial cells

4.7.3.1.1 Tube formation assay on matrigel (matrigel assay)

Tube formation assays on matrigel were performed according to previously published protocols with certain modifications (78, 80). Primary EC (see paragraph 4.4.3) were cultured up to passage 6 in T75 flasks. One day prior to the experiment, the complete EC medium was removed and cells were cultivated with serum-free EC-medium (see paragraph 3.12) overnight. Wells of a 96 well plate were coated with matrigel (Corning® Matrigel® hESC-Qualified Matrix, #354277, Corning, Tewksbury, MA) using 50 µL undiluted gel per well according to manufacturer's instructions. The plate was incubated at 37°C for 30 min to allow polymerization of the gel. EC were detached from a T75 cell culture flask using a 1:1 dilution of accutase (#7920, StemCell™ Technologies) with 1x D-PBS at 37°C for 5 min. Detached cells were washed with 1x D-PBS and centrifuged at 300 x *g* for 10 min at room temperature. Supernatant containing accutase was removed and the pellet was resuspended in 200 µL 1x D-PBS. Cells were counted using the Neubauer Chamber (see paragraph 4.3.1) and plated at 2×10^4 cells per well with either complete EC-medium (PosCtr) or serum-free IMDM medium (NegCtr) or CDC- or CF-EV preparations derived from different patients (see Table 14 and Table 15) in serum-free IMDM medium (1×10^9 particles per well). After 16h, pictures of the cells were taken on an Axiovert 200M microscope, using the software Carl Zeiss™ Axio Vision Rel. (version 4.8.2). To improve image quality, wells were filled with 1x D-PBS prior to photography. Images were taken using the BrightPhase mode and a 4 x objective. Image scales are indicated in the images. Parameters of tube formation were analyzed using the ImageJ angiogenis analyzer tool written by Gilles

Carpentier, 2012, with default settings (97-99, 102). The macro is available here: https://imagej.nih.gov/ij/macros/toolsets/Angiogenesis%20Analyzer.txt, (15.11.19) and more information can be found at http://image.bio.methods.free.fr/ImageJ/?Angiogenesis-Analyzer-for-ImageJ&artpage=4-6&lang=en#outil_sommaire_4, (15.11.19). This software marks different parts of the the tubuli with different colors and calculates the number and length of these elements. Parameters chosen for mean comparisons were tube length, number of pieces, number of master junctions and total master segments length, because these parameters reflected visual assessment of the image. Several (at least three) pictures were taken per well. The means of the output data for each parameter were calculated and divided by the mean of the negative control (fold change, FC, over negative control).

4.7.3.1.2 Migration assay of endothelial cells (EC scratch assay)

Scratch assays were performed according to published protocol with modifications (144). Primary EC (see paragraph 4.4.3) were cultured up to passage six in T75 flasks. On the day of the experiment EC were trypsinized (see paragraph 4.3.2) and seeded at 7.5×10^4 cells per well on 96-well ImageLock™ microplates. On the next day, EC were incubated with mitomycin C solution (see paragraph 3.7) at a final concentration of 20 µg/mL in serumfree EC-medium (see paragraph 3.12) for 2h at 37 °C and 5% CO_2. Mitomycin C covalently binds to DNA and by cross-linking complementary strands it inhibits DNA replication which results in an anti-proliferative effect on the cells (145). In this assay, mitomycin C was used to inhibit cell proliferation, so only migration was assessed. After treatment with mitomycin, cells were washed twice with 1x D-PBS to remove mitomycin C and the EC layer was scratched using the WoundMaker™ (IncuCyte® Cell Migration Kit, #4493, EssenBiosciences). Subsequently, cells were incubated with either EC medium (PosCtr), serum-free IMDM medium (NegCtr) or EV preparations isolated from conditioned medium of CDC or CF derived from different patients in serum-free IMDM medium (see Table 14 and Table 15) for 48h. The EV were diluted to a concentration of 1×10^9 particles per 96 well. Pictures of the scratch area were taken every hour using the IncuCyte ZOOM® system camera (EssenBiosciences, Hertfordshire, UK).
Images were then manually evaluated using ImageJ (97-99). Cell-free area was measured using the function “freehand selections” at 0h, 8h, 12h, 24h and 48h after the scratch. The difference of the area at a certain timepoint to the area at timepoint 0 (Diff (x)) was calculated as:

Diff (x) = Area (x)- Area (0), x = 8h; 12h; 24h; 48h;

For each assay the mean of the according timepoint difference for the wells with NegCtr was calculated as: (Mean (Diff $(x)_{Negctr}$)). Fold change value over the NegCtr was calculated as follows:

FC over NegCtr (x) = Diff $(x)_{sample}$ / Mean (Diff $(x)_{Negctr}$)

The later value was statistically compared between samples for each timepoint.

4.7.3.2 Effects of CDC/ CF-EV on cardiac fibroblasts (CF)

4.7.3.2.1 Migration assay of CF (CF scratch assay)

Scratch assays were performed according to published protocol with modifications (144). Migation assays with CF were performed by either scratching the cell layer manually and taking pictures with the Axiovert 200M microscope or with the automated IncuCyte ZOOM® 96-Well Migration Assay system (EssenBiosciences). As all measurements were normalized to the negative control of the corresponding assay, it was possible to analyze and evaluate the results of both assays together.

For manual migration assay, CF were seeded at a concentration of 5×10^4 cells per well of a 96 well plate (#655180, Greiner Bio-One International GmbH, Frickenhausen, Germany). On the next day, cells were incubated with mitomycin C solution (see paragraph 3.7) at a concentration of 20 µg/mL in serum-free IMDM medium (see paragraph 3.12) for 2h at 37 °C and 5% CO_2, to avoid faulty measurement of cell proliferation. Afterwards, cells were washed twice with 1x D-PBS to remove mitomycin C and the cell layer was scratched manually using a 10 µL pipette tip. Subsequently, cells were incubated with either MEF medium (positive control, PosCtr), serum-free IMDM medium (negative control, NegCtr) or EV preparation from conditioned medium of CDC derived from different patients (see Table 14 and Table 15) for 48h. The EV were diluted in serum-free IMDM medium to a concentration of 2.5×10^9 particles per well. Phase-contrast pictures of the scratch area were taken at 0h, 12h, 24h and 48h after the scratch (Axiovert 200M, Zeiss), using the software Carl Zeiss™ Axio Vision Rel. (version 4.8.2). Images were taken using bright phase mode and a 4x objective. To improve image quality, wells were filled with 1x D-PBS prior to photography. Several (at least three) images were taken per well and timepoint. Image scales are indicated in the images.

In the automated migration assay, cardiac fibroblasts were seeded on a 96-well ImageLock™ tissue culture plate (#4379, EssenBiosciences) at a concentration of 1.5×10^4 cells per 96 well. This cell concentration is ideal for pictures taken by the IncuCyte ZOOM® system camera. Incubation with mitomycin C solution, washing and incubation with EV preparations were performed as described above. Scratch was performed automatically by WoundMaker™. Images were taken every hour with IncuCyte ZOOM® system camera (EssenBiosciences).

Finally, images were manually evaluated using ImageJ (97-99). Cell-free area was measured using the function “freehand selections” at timepoint 0h, 8h, 12h, 24h and 48h after the scratch. The difference of the area at a certain timepoint to the area at timepoint 0 (Diff (x)) was calculated as:

Diff (x) = Area (x)- Area (0), x = 8h; 12h; 24h; 48h

For each assay the mean of the according timepoint difference was calculated for the wells with the NegCtr as: Mean (Diff (x)Negctr)).

Fold change value over the NegCtr was calculated as follows:

FC over NegCtr (x) = Diff (x)sample / Mean (Diff (x)NegCtr)

The later value was statistically compared between samples for each timepoint. After 48h, cells were lysed for RNA isolation followed by reverse transcription and qRT-PCR (see paragraph 4.5.1). CF were analyzed for expression of *COL1A1* and *COL3A1* (see Table 8).

4.7.3.2.2 Proliferation assay of CF (MTT assay)

CF were seeded at a concentration of 5×10^3 cells per well of a 96 well plate in MEF medium (see paragraph 3.12). On the next morning, cells were washed twice with 1x D-PBS to remove all traces of FBS and medium was changed to serum-free IMDM medium (see paragraph 3.12). After 24h of serum-free treatment (starvation period), cells were incubated for 48h with either MEF medium (positive control, PosCtr), serum-free IMDM medium (negative control, NegCtr) or CDC- derived EV CF from pediatric patients (see Table 15) diluted in serum-free IMDM medium to a concentration of 3×10^9 particles per well. Then these media preparations were removed and CF were incubated with MTT-solution which was diluted in serum-free IMDM medium to 0.5 mg/mL (see paragraph 3.7) for 3h. MTT is a dye which is used to detect living, proliferative and metabolically active cells in a colorometric assay. MTT is cleaved by living cells to a violet-colored formazan which can be detected by a spectrometer. The generated amount of formazan is directly proportional to the number of cells which were incubated with MTT (146).
The MTT solution was then removed and cells were lysed with 100 µL DMSO. The extent of MTT metabolization was measured by the absorbance of the violet formazan on the spectrometer Infinite® 200 PRO (Tecan Trading AG, Männedorf, Switzerland) at a wavelength of 570 nm. The reference wavelength was set to 690 nm. The software i-control™ Microplate Reader (version 2.0., Tecan Trading AG) was used for measurement. This previously described method (146) was adjusted to the settings of this work.

4.7.3.3 Effects of CDC/CF EV on NRCM (NRCM assay)

To test whether CDC/CF-derived EV reduce apoptosis of stressed cardiomyocytes, neonatal rat cardiomyocytes (NRCM) were plated at 4×10^4 cells per well of a 96 well plate in NRCM medium (see paragraph 3.7). After two days, beating cells were visible in the cell layer. To mimic hypoxic conditions in the heart, cells were incubated with 3 mM cobalt chloride solution (see paragraph 3.7) for 1h in the cell incubator (Safe 2020 Class II Biological Safety Cabinets, Thermo Fisher Scientific). $CoCl_2$ was washed off the cells twice with 1x D-PBS. Subsequently, NRCM were incubated with either EV isolated from CDC and CF from different patients (see Table 14 and Table 15) at a concentration of 3×10^9 particles per well in serum-free IMDM medium (see

paragraph 3.7), serum-free IMDM medium (NegCtr) or NRCM medium (PosCtr). Some wells were not incubated with $CoCl_2$ solution to function as NegCtr for apoptosis induction. Finally, 48h after EV incubation, cells were lysed for gene expression analysis. RNA isolation, reverse transcription and qRT-PCR of the apoptosis marker *rFas* was performed as mentioned in paragraph 4.5.1. This protocol was developed relying on previously published protocols with some modifications (80, 85).

4.8 Statistics

To statistically evaluate the data, comparison of means between groups was performed. Although different tests must be used depending on data characteristics, the principle of the tests always relies on whether a null hypothesis can be rejected in favor of an alternative hypothesis. The null hypothesis states that the means of two or more groups do not differ, whereas the alternative hypothesis states that they do. The *p*-value is the probability for the observed result or a more extreme result under the null hypothesis. A priori a significance level α is specified under which *p* must fall in order that the null hypothesis can be rejected. (Course "Statistics for PhD Students, Part II: Point and Interval Estimation Statistical Tests", July 2017, Institute of Medical Statistics and Epidemiology, Technische Universität München, Prof. Dr. Kurt Ulm)

Statistical analyses and graphs of each experiment were performed with the software SPSS Statistics 25 (IBM, Armonk NY). Data distribution was evaluated using Box-Whisker-Plots for each group. Values of three-fold interquartile range were considered as extreme outliers and were removed. Descriptive data analysis was performed, and Shapiro-Wilk test was used to check for normal distribution. Comparison of means was carried out using One-way ANOVA (Analysis of Variance) which has been described to be robust against violations of normal distribution assumption (147). A prerequisite to use ANOVA as a test is homengeneity of variances. Therefore, groups were examined for variance homogeneity with the Levene-Test. Significance level α was set to $p < 0.05$. In case the Levene-Test was not significant for a parameter, ANOVA was used to compare means of two groups. Comparison of more than two groups was performed with post-hoc tests (a posteriori tests) Tukey-HSD (HSD = honestly significant difference) or Bonferroni correction. If Levene-Test was significant, robust tests for inhomogenous variances such as Welch-test and Brown-Forsythe-test were used to compare two groups. For multiple group comparison, Games-Howell-test and Dunnett-T3-test were used as robust post-hoc tests in this case. Comparison of two groups in Microsoft Excel 2010 was performed using the two-sided heteroscedastic student's t-test. Bar diagrams show mean ± standard error of the mean (SEM). Significance levels are shown as: * for $p < 0.05$; ** for $p < 0.01$ and *** for $p < 0.001$.

5. Results

All results presented in this work except of those listed in paragraphs 5.2.3 and 5.3 are part of the following manuscript:
Palgit-S. Kogan, Archana Tomar, Jonathan Darr, Raffaele Teperino, Harald Lahm, Martina Dreßen, Nazan Puluca, Zhong Zhang, Kathrin Gärtner, Corinna Hüls, Reinhard Zeidler, Deepak Ramanujam, Stefan Engelhardt, Catharina Wenk, Lesca M. Holdt, Rüdiger Lange, Markus Krane, Stefanie A. Doppler. *Single Cell RNA Sequencing of Cardiosphere Derived Cells (CDCs) Revealed Their Heterogeneity and Similarities to Cardiac Non-Myocyte Cell Types.* Manuscript submitted for publication (2020).
In the following paragraphs this manuscript is reffered to as (148).

5.1 Characterization of primary cardiac non-myocyte cultivated cell types

The three main NMC types, CF, EC and SMC were cultivated from fresh tissue by well-established cell culture procedures (see paragraph 4.4). CF were isolated by full enzymatic digestion of fresh atrial appendage tissue derived from adult patients (age: 55-76 years) undergoing cardiovascular operations such as coronary artery bypass graft (CABG), MAZE procedure for atrial fibrillation or aortic, mitral or tricuspid valve replacement (see also Table 14). EC and SMC were isolated from fresh vessels of male patients (age range: 56-67 years) undergoing CABG surgery by first digesting and flushing the inner part of a thoracic vessel (EC isolation) and then generating a vessel tissue outgrowth culture (SMC isolation) followed by culture in specialized media, respectively (Figure 4A and Table 14).
To elucidate the molecular characteristics of CDC compared to NMC, CDC were cultivated from atrial apprendage tissue from the same patients group as CF according to a three-step-protocol (Figure 4A) first published by Messina *et al.* and also used in the TICAP trial (70, 87). In this protocol first cardiac tissue outgrowth is generated. Then “cardiospheres” are formed by stimulation of cells which were carefully harvested from the cardiac outgrowth layer, with several growth factors. In the last step cardiospheres are replated on fibronectin coated dishes which results in two-dimensional cell layers (see detailed description in paragraph 4.4.1).
As a non-cardiac cell lineage, adipose-tissue-derived fibroblasts (AF) generated by full enzymatic digestion of subcutaneous adipose tissue were utilized (Figure 4A and Table 14). Besides, human induced pluripotent stem cells (iPSC) at day 8 of cardiac differentiation (directed cardiac differentiation protocol) (103) (Figure 4B and paragraph 4.4.6) were used as a positive control for human cardiac progenitor cells (DIFF D8). The utilized iPSC line was generated by reprogramming fibroblasts derived from a healthy individual and its characterization was described previously (112). (Kogan *et al.*, submitted manuscript 2020 (148))

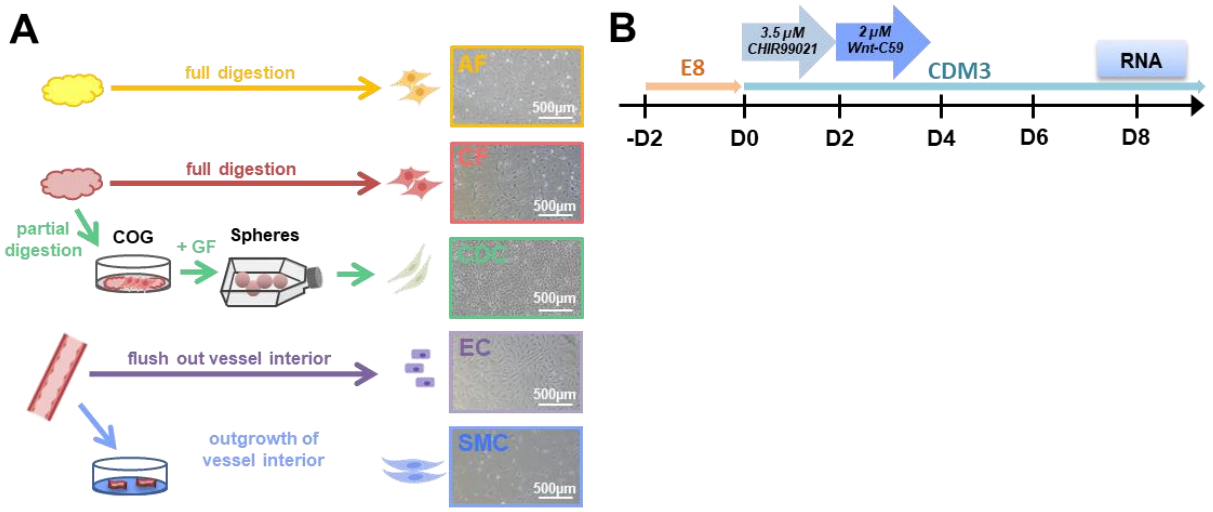

Figure 4: Generation of adult cell types - protocol schemes.
A) Isolation of primary cell types. Illustrated from top to bottom are the isolation procedures of adipose-tissue-derived fibroblasts (AF), cardiac-tissue derived fibroblasts (CF), cardiosphere-derived cells (CDC), endothelial cells (EC) and smooth muscle cells (SMC). COG: cardiac outgrowth; GF: growth factors. B) Induced pluripotent stem cells (iPSC) cardiac differentiation protocol. Arrows indicate the time periods when iPSC were cultivated with TeSR™-E8™ (E8) medium or CDM3 medium supplemented with the small molecules CHIR99021 and Wnt-C59 as described in paragraph 4.4.6. Cell lysates for RNA isolation were taken on day 8 of cardiac differentiation (DIFF D8). Adapted from Figure 1 and Suppl. Figure S1 from (148).

5.1.1 Molecular characterization of adult primary non-myocyte cultivated cell types

Gene and protein expression profiles of markers used previously to identify cardiac cell types were compared between AF, CF, SMC, EC and CDC (Figure 5 and Figure 6). Significances displayed in Figure 5 and Figure 6 correspond to differences between CDC and the other cell types, however all significances between all cell types are summarized in Table 31 and Table 32, respectively.

First, gene expression profiles of several markers from above mentioned cell samples were assessed by qRT-PCR (Figure 5A-F). The cardiac transcription factor (TF) *GATA4*, reported to be expressed both in cardiac progenitor cells and CF (149), did not show significant differences between CDC and DIFF D8 or CF, but was upregulated both in CDC and CF compared to EC and SMC (Figure 5A, right panel, Table 31). Although not statistically significant, *GATA4* was 13-fold higher expressed in DIFF D8 than in CDC. Both *TBX5* and *NKX2-5*, crucial transcription factors in cardiac development (150, 151), were significantly upregulated in DIFF D8 compared to CDC. Additionally, *TBX5* was downregulated in AF and EC compared to CDC (Figure 5A, left panels, Table 31). The mesenchymal marker *ENG* (CD105), previously used as a quality marker for CDC (61), was expressed in all NMC and CDC, but was downregulated in DIFF D8 compared to AF, CDC, CF and SMC (Figure 5B, Table 31). Previously described CF markers such as *DDR2*, *PDGFRA* (9) or the cardiac fibrosis associated microRNA (miR)-21 (152, 153) were not significantly

upregulated in CF compared to CDC. However, unlike *PDGFRA*, *DDR2* was significantly upregulated in AF, CDC, CF and SMC compared to DIFF D8 and downregulated in EC compared to AF (Figure 5C, left upper panel, Table 31). The CF marker *ALDH1A2* (5) was significantly upregulated in CF compared to all other cell types analyzed. Similarly, *THY1* (known as *CD90*) (9) was significantly increased in CF compared to CDC, EC and DIFF D8 (Figure 5C, Table 31).

Well-known SMC markers such as *TAGLN* (154) or *PDGFRB* (155) were not specifically up-regulated in SMC compared to the other cell types (Figure 5D, Table 31). On the contrary, EC were obviously distinguishable from all other cell types by high expression levels of *PECAM1* (*CD31*) (Figure 5E, left panel, Table 31) (5). *CDH5* was significantly upregulated in CDC compared to CF, SMC and DIFF D8. However, although 24-fold higher expressed in EC compared to CDC, *CDH5* expression did not significantly differ between these cell types (Figure 5E, right panel). MiR-146a was described to be a marker for CDC and to be partially responsible for their beneficial effects (78, 80). Compared to CF, miR-146a-5p was not significantly enriched in CDC, even though its expression was 3-fold higher in CDC (Figure 5F, left panel). MiR-132, previously shown to be enriched in EV derived from cardiac outgrowth cells (86), was not upregulated in CDC versus CF (Figure 5F, right panel). (Kogan *et al.*, submitted manuscript 2020, (148))

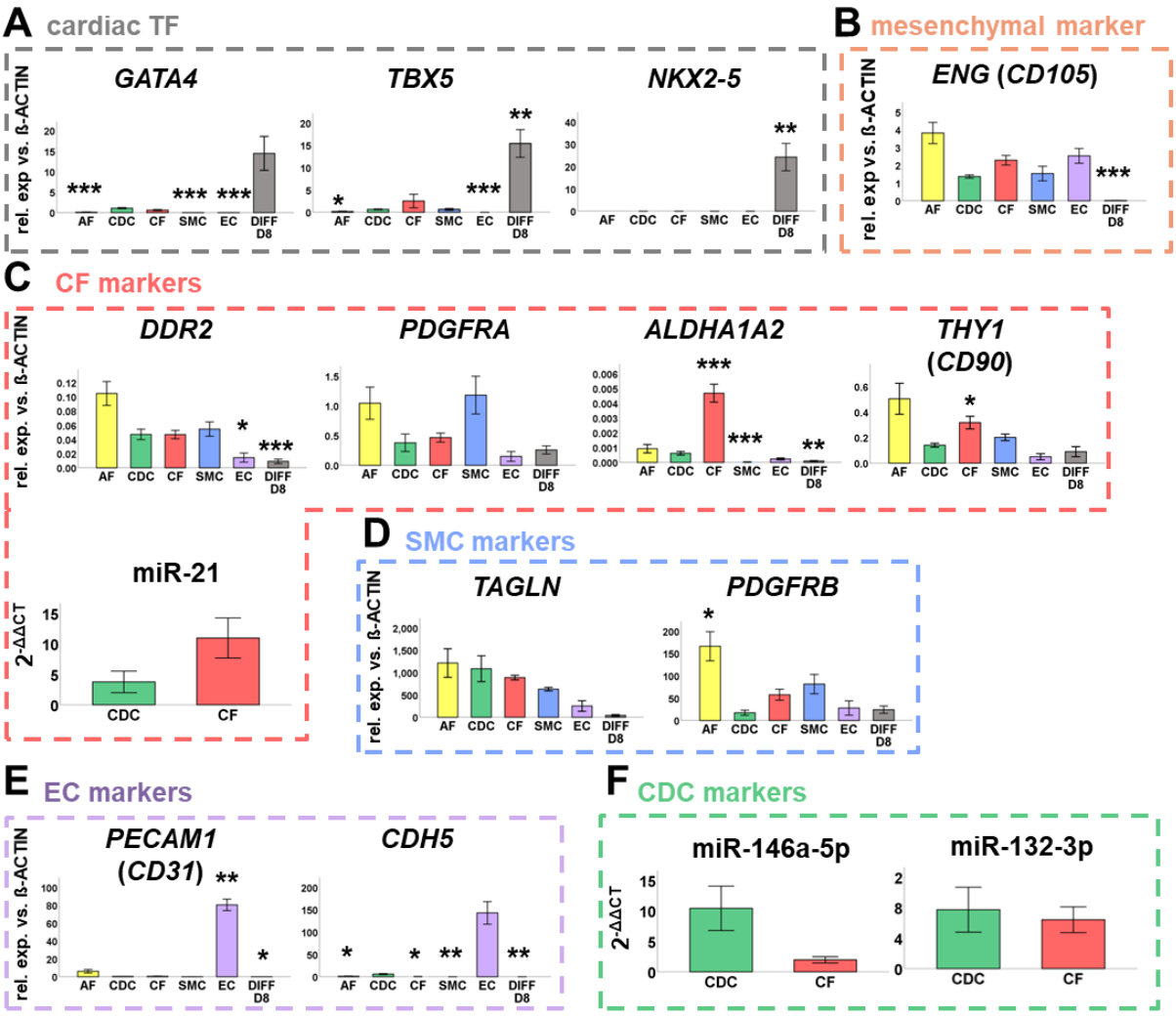

Figure 5: Characterization of adult CDC compared to other primary non-myocyte cell types by gene expression level (qRT-PCR).

*Analyzed cell types are abbreviated as follows: AF: adipose-tissue derived fibroblasts; CDC: cardiosphere-derived cells; CF: cardiac fibroblasts; SMC: smooth muscle cells; EC: endothelial cells; DIFF D8: Human induced pluripotent cells on day 8 of cardiac differentiation protocol. Relative RNA expression versus ß-ACTIN (gene symbol: ACTB) is illustrated for A) cardiac transcription factors (TFs) GATA4, TBX5 and NKX2-5, B) mesenchymal marker ENG (CD105), C) CF markers DDR2, PDGFRA, ALDH1A2, THY1 (CD90) and miR-21, D) SMC markers TAGLN and PDGFRB, E) EC markers PECAM1 (CD31) and CDH5, F) CDC typical microRNAs miR-146a-5p and miR-132-3p. Data are represented as mean ± standard error of the mean (SEM), each gene was evaluated in at least 4 independent samples (n ≥ 4), significance to CDC is shown as *: p < 0.05, **: p < 0.01, ***: p < 0.001. Post-hoc tests: Tukey-HSD/Bonferroni for homogeneous variances or Games-Howell-test/Dunnett-T3-test for inhomogeneous variances. For complete overview of p-values and statistical tests see Table 31. Adapted from Figure 1 and Suppl. Figure S1 from* (148)

Table 31: Significant differences in marker expression (qRT-PCR, Figure 5)

Marker	Cell type 1	Cell type 2	Significance Test	*p*-value
GATA4	CDC	SMC	Dunnett-T3	0.000
GATA4	CDC	EC	Dunnett-T3	0.000
GATA4	CF	SMC	Dunnett-T3	0.042
GATA4	CF	EC	Dunnett-T3	0.042
TBX5	AF	CDC	Dunnett-T3	0.036
TBX5	AF	DIFF D8	Dunnett-T3	0.003
TBX5	CDC	EC	Dunnett-T3	0.000
TBX5	CDC	DIFF D8	Dunnett-T3	0.004
TBX5	CF	DIFF D8	Dunnett-T3	0.021
TBX5	SMC	DIFF D8	Dunnett-T3	0.004
TBX5	EC	DIFF D8	Dunnett-T3	0.003
NKX2-5	CDC	DIFF D8	Dunnett-T3	0.013
NKX2-5	CF	DIFF D8	Dunnett-T3	0.013
NKX2-5	EC	DIFF D8	Dunnett-T3	0.013
CD105	DIFF D8	AF	Dunnett-T3	0.013
CD105	DIFF D8	CDC	Dunnett-T3	0.000
CD105	DIFF D8	CF	Dunnett-T3	0.000
CD105	DIFF D8	SMC	Dunnett-T3	0.043
CD105	DIFF D8	SMC	Dunnett-T3	0.043
DDR2	AF	EC	Dunnett-T3	0.035
DDR2	AF	DIFF D8	Dunnett-T3	0.033
DDR2	CDC	DIFF D8	Dunnett-T3	0.000
DDR2	CF	DIFF D8	Dunnett-T3	0.001
DDR2	SMC	DIFF D8	Dunnett-T3	0.012
ALDH1A2	CDC	CF	Dunnett-T3	0.000
ALDH1A2	CDC	SMC	Dunnett-T3	0.001
ALDH1A2	CDC	DIFF D8	Dunnett-T3	0.004
ALDH1A2	CF	AF	Dunnett-T3	0.000
ALDH1A2	CF	CDC	Dunnett-T3	0.000
ALDH1A2	CF	SMC	Dunnett-T3	0.000
ALDH1A2	CF	EC	Dunnett-T3	0.000
ALDH1A2	CF	DIFF D8	Dunnett-T3	0.000
CD90	CDC	CF	Dunnett-T3	0.038
CD90	CF	EC	Dunnett-T3	0.002
CD90	CF	DIFF D8	Dunnett-T3	0.027
CD90	SMC	EC	Dunnett-T3	0.018
TAGLN	DIFF D8	CF	Dunnett-T3	0.001
TAGLN	DIFF D8	SMC	Dunnett-T3	0.000
TAGLN	CF	SMC	Games-Howell	0.041
TAGLN	CF	EC	Games-Howell	0.040
PDGFRB	AF	CDC	Games-Howell	0.037
PDGFRB	AF	EC	Games-Howell	0.049
PDGFRB	AF	DIFF D8	Games-Howell	0.043
CD31	EC	AF	Dunnett-T3	0.005
CD31	EC	CDC	Dunnett-T3	0.007
CD31	EC	CF	Dunnett-T3	0.007
CD31	EC	SMC	Dunnett-T3	0.007
CD31	EC	DIFF D8	Dunnett-T3	0.007
CD31	DIFF D8	CDC	Dunnett-T3	0.016
CD31	DIFF D8	EC	Dunnett-T3	0.007

CDH5	CDC	AF	Dunnett-T3	0.028
CDH5	CDC	CF	Dunnett-T3	0.014
CDH5	CDC	SMC	Dunnett-T3	0.009
CDH5	CDC	DIFF D8	Dunnett-T3	0.009

Abbreviations: AF: adipose-tissue derived fibroblasts; CDC: cardiosphere-derived cells; CF: cardiac fibroblasts; SMC: smooth muscle cells; EC: endothelial cells; DIFF D8: Human induced pluripotent cells on day 8 of cardiac differentiation protocol.

Next, protein expression was evaluated for selected markers by immunocytochemical stainings or flow cytometry (FC, Figure 6). While DDR2 was ubiquitously abundant in all analyzed cell types (Figure 6A), immunocytochemical staining showed the absence of CD90 in EC (Figure 6B) which was confirmed by FC (Figure 6C, Table 32). Besides, CDC demonstrated heterogenic abundance of CD90 validated by flow cytometric analysis, ranging between 40 to 60% of CD90-positive cells (Figure 6D, Table 32). Smooth muscle actin (α-SMA), reported to be a smooth muscle cell marker (156), was expressed to a comparable level in SMC, AF, CF and CDC (high level) and was also detected in EC (low level) by immunocytochemistry (ICC, Figure 6E). High and specific abundance of CD31 in EC was detected by ICC and FC (Figure 6F-H) confirming gene expression (Figure 5E). Mesenchymal markers CD105 and VIMENTIN (VIM) (157) were found to be expressed ubiquitously in all analyzed cell types (Figure 6I-J). The described absence of the hematopoietic marker CD45 in CDC (61) was confirmed for all adult non-myocyte cell types by FC (Figure 6C,K). (Kogan *et al.*, submitted manuscript 2020, (148))

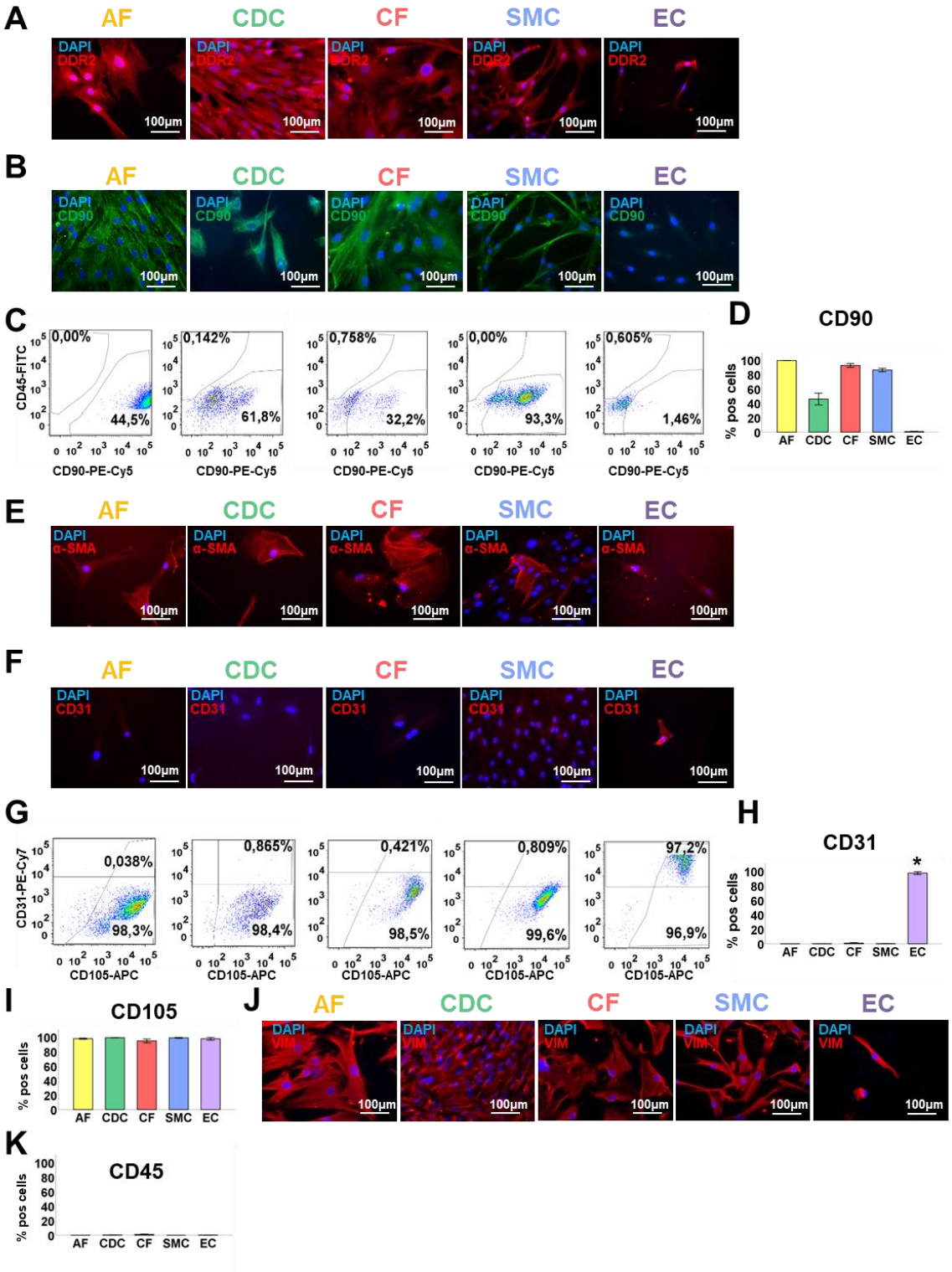

Figure 6: Protein characterization of adult CDC compared to other primary non-myocyte cell types.
Abbreviations: AF: adipose-tissue derived fibroblasts; CDC: cardiosphere-derived cells; CF: cardiac fibroblasts; SMC: smooth muscle cells; EC: endothelial cells; FC: flow cytometry; ICC: immunocytochemistry. A-B) ICC staining for CF marker DDR2 (A) and CD90 (B). C) Exemplary dot plots for FC analysis of CD90 (antibody is conjugated with PE-Cy5) and CD45 (antibody is conjugated with FITC). D)

*Frequency of CD90 positive cells in FC analysis. E) ICC staining for SMC marker α-SMA. (F) ICC staining for EC marker CD31. G) Exemplary dot plots for FC analysis of CD31 (antibody is conjugated with PE-Cy7) and CD105 (antibody is conjugated with APC). Frequency of CD31 (H) and CD105 (I) positive cells in FC analysis. J) ICC staining for mesenchymal marker vimentin (VIM). K) Frequency of CD45 positive cells in FC analysis. FC data are represented as mean of positive cells of the according marker, n ≥ 2. Data are represented as mean ± SEM, significance of difference to CDC is shown as *: p < 0.05. Post-hoc tests: Tukey-HSD/Bonferroni for homogeny variances or Games-Howell-test/Dunnett-T3-test for inhomogeneous variances. For complete overview of p-values and statistical tests see Table 32. Adapted from Figure 1 and Suppl. Figure S1 from* (148)

Table 32: Significant differences in marker expression (FC, Figure 6)

Marker	Cell type 1	Cell type 2	Significance Test	*p*-value
CD90	EC	AF	Dunnett-T3	0.004
CD90	EC	CF	Dunnett-T3	0.002
CD90	EC	SMC	Dunnett-T3	0.035
CD31	EC	CDC	Dunnett-T3	0.030
CD31	EC	AF	Dunnett-T3	0.030
CD31	EC	CF	Dunnett-T3	0.015
CD31	EC	SMC	Dunnett-T3	0.029

Abbreviations: FC: flow cytometry; AF: adipose-tissue derived fibroblasts; CDC: cardiosphere-derived cells; CF: cardiac fibroblasts; SMC: smooth muscle cells; EC: endothelial cells.

In summary, the preliminary marker analysis by gene and protein expression revealed many similarities between CF, SMC and CDC. Particularly for CDC, no specific markers were identified. In contrast, EC stood out by their distinct marker profile.

5.1.2 *Single cell RNA sequencing of CDC in comparison to other cardiac non-myocyte cell types*

The next aim was to gain a more detailed picture of gene expression patterns of CF, SMC, EC and CDC using single-cell RNA sequencing (sc-RNAseq) as state-of-the-art technology. For this purpose, the same cell isolation and cultivation techniques were used as described in paragraph 4.4 and illustrated in Figure 4A. By selecting only patients with coronary heart disease who underwent CABG surgery and were in the small age range between 61 and 66 years (samples 1, 2, 3, 5 in Table 33), a potential influence of patient diagnosis and age was minimalized. Analysis of the infant CDC sample (sample 6 in Table 33-35) is described in paragraph 5.2.1. (Kogan *et al.*, submitted manuscript 2020, (148))

Table 33: Cell samples for sc-RNAseq

Sample No.	Cell type	Age group	Cell passage	Patients' sex	Patients' age	surgery	diagnosis
1	EC	Adult	P1	male	63 years	CABG	atherosclerotic heart disease
2	CF	Adult	P2	male	63 years	CABG	atherosclerotic heart disease
3	SMC	Adult	P2	male	66 years	CABG	atherosclerotic heart disease

5	CDC	Adult	P0	male	61 years	CABG	atherosclerotic heart disease
6	CDC	Infant	P0	female	7 days	Norwood	HLHS

Abbreviations: CDC: cardiosphere-derived cells; CF: cardiac fibroblasts; SMC: smooth muscle cells; EC: endothelial cells, sc-RNAseq: single-cell RNA sequencing, P0/1/2: cell culture passage 0/1/2, CABG: coronary artery bypass graft, Norwood: Norwood I procedure for single-ventricle patients, HLHS: .

To ensure cell quality prior to the experiment, cell morphology was carefully checked by microscopy (Figure 7A) and qRT-PCR for some selected markers was performed (Figure 7B-D). High expression of miR-146-5p (Figure 7B) and low expression of *ALDH1A2* and *THY1* (Figure 7C) in CDC compared to CF ensured that the CDC sample used was not highly contaminated with CF. CF identity was confirmed by high expression of *ALDH1A2* and *THY1* (Figure 7C). As no specific marker for SMC was available, the quality of SMC was mainly assessed by the typical cell morphology and elevated expression of *THY1* (Figure 7A,C). *PECAM*1 and *CDH5* assured the EC-specific gene regulation patterns of the EC sample compared to the other samples analyzed (Figure 7D).

The 10x Chromium platform was used for cDNA library preparation and raw data analysis, whereas subsequent data analysis was performed with the Seurat (v3.1.2) software suite (134-136) (see paragraphs 4.5.4.2 and 4.5.4.3). Quality controls performed by bioanalyzer after steps 2 and 3 of cDNA library preparation are shown in Suppl. Figure S 2 (CF, SMC and EC) and Suppl. Figure S 3 (Adult CDC). Batch effects which might result from the usage of different 10x Chromium kit versions were removed by CCA (134). Further, low quality cells, doublets and cells with high percentage of mitochondrial genes were filtered out of the analyzed sample data (158) (Figure 7E-G, filtering criteria and cell numbers before and after filtering in Table 34). The resulting cell numbers after filtration are summarized in the right column of Table 34 for each sample. In total, the filtered merged CCA-corrected object of CDC, CF, SMC and EC comprised 2,815 cells and exhibited median values of 3,428 genes per cell and 17,078 UMI counts per cell (Figure 7H-I). Median values of quality control parameters for each filtered sample are shown in Table 35. On top of these parameters, quality of sc-RNAseq was controlled by generating a mixed sample, consisting of 20% EC, 30% SMC, and 50% CF (see paragraph 4.5.4.1.1 and sample 4 in Table 25). All steps of library preparation and sequencing of this mixed sample were conducted in parallel to the according primary cell samples (EC, SMC and CF). UMAP plot illustrated in Figure 7J shows that the clusters of the mixed sample overlaped with all clusters of according primary cells. Besides, the mixed sample clusters were distributed among the primary cell clusters approximately to the percentages in which they were mixed (CF: 44%, SMC: 28%, EC: 28%). (Kogan *et al.*, submitted manuscript 2020, (148))

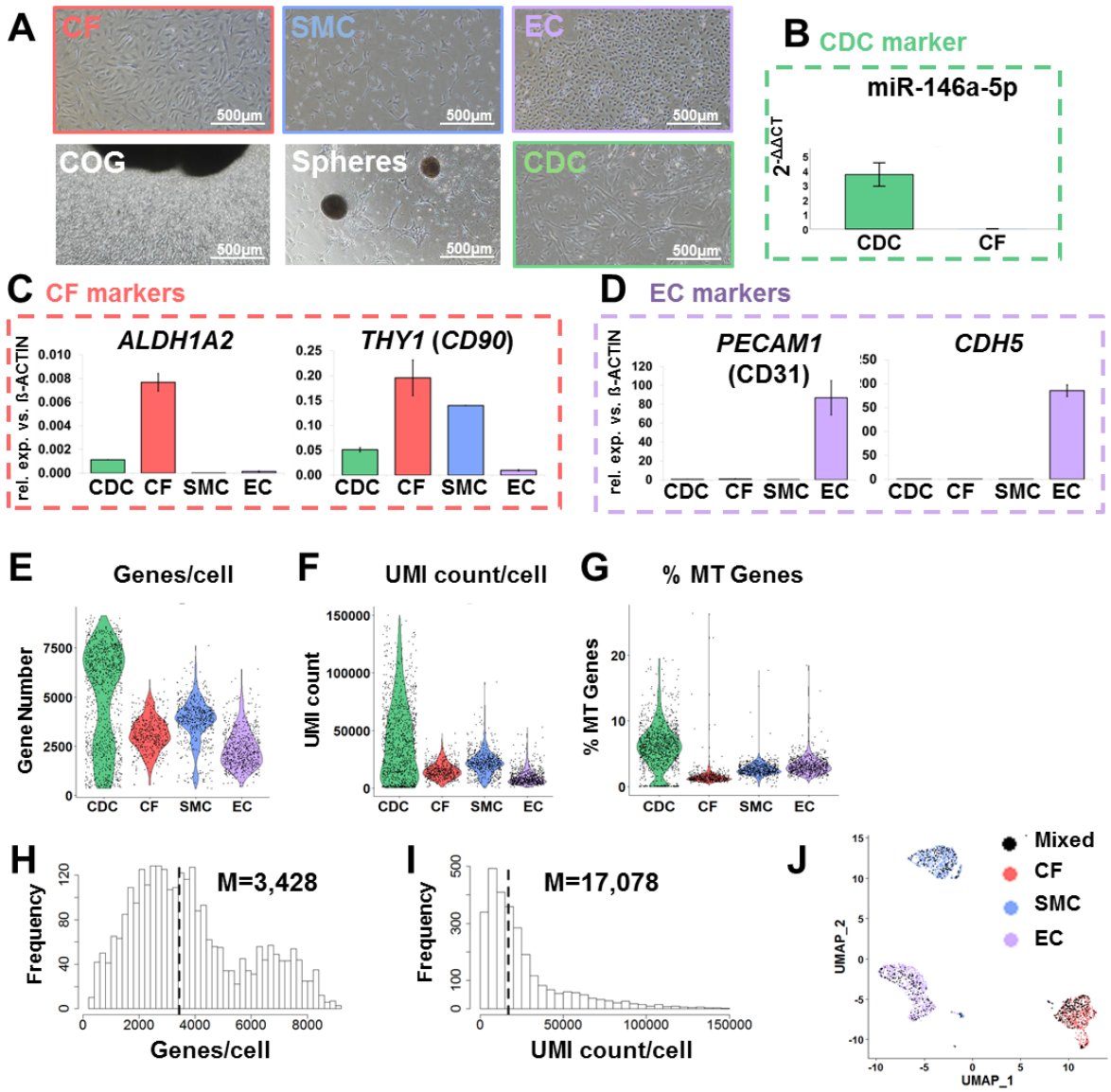

Figure 7: Quality control of samples used for single-cell RNA sequencing (sc-RNAseq).

Analyzed cell types are abbreviated as follows: CF: cardiac fibroblasts; SMC: smooth muscle cells; EC: endothelial cells, COG: cardiac outgrowth, CDC: cardiosphere-derived cells. A) Morphological assessment of the utilized cell samples (adult CDC, CF, SMC, EC) by microscopy at the day of the experiment. B-D) Expression profiles of CDC- (B), CF- (C), and EC- (D) markers of the samples used for the sc-RNAseq experiment (adult CDC, CF, SMC, EC, see samples 1, 2, 3, 5 in Table 33). MiR-146a-5p expression of the CDC sample is illustrated next to CF generated from the same patient's cardiac biopsy (not the CF used for sc-RNAseq). For each sample two culture wells were used for RNA isolation (n = 2). Bar diagrams show mean ± SEM. E-G) Violin plots of detected E) gene number per cell (genes/cell), F) unique molecular identifier (UMI) count per cell (UMI counts/cell) and G) percentage of mitochondrial genes per cell (% MT Genes), illustrated for each sample analyzed after filtering procedure. See Table 35 for median values. H-I) Histograms illustrating H) genes/cell or I) UMI count/cell of the filtered merged CCA-corrected Seurat object containing CDC, CF, EC and SMC. J) UMAP plot of the sc-RNAseq CF, SMC, EC and the mixed sample. Adapted from Suppl. Figure S2 from (148)

Table 34: Filtering parameters in Seurat

Sample Nr. / Name	Genes/cell	UMI count/cell	% MT_Genes	Cells before filtering	Cells after filtering
1/ EC	> 200	< 55,000	< 20	672	668
2/ CF	No filtering	No filtering	No filtering	457	457
3/ SMC	> 200	No filtering	< 20	585	581
5/ CDCAdult	> 200	< 150,000	< 20	1,196	1,109
6/ CDC Infant	> 200	< 120,000	< 20	1,060	960

Abbreviations: Genes/cell: number of genes detected per cell; UMI count/cell: number of UMIs per cell; % MT_Genes: percentage of mitochondrial genes per cell

Table 35: Median of quality control parameters after filtering

Sample Nr. / Name	Genes/cell (median)	UMI count/cell (median)	% MT_Genes (median)	Reads per cell (mean)
1/EC	2,179	7,762.5	3.0	58,268
2/CF	3,043	14,373	1.3	122,176
3/SMC	3,924	21,437	2.5	117,533
5/CDC (adult)	5,803	36,171	6.0	99,694
6/CDC (infant)	5,549	32,482	6.9	100,206

Abbreviations: Genes/cell: number of genes detected per cell; UMI count/cell: number of UMIs per cell; % MT_Genes: percentage of mitochondrial genes per cell

To identify upregulated differentially expressed genes (uDEG) in each cell type compared to all other cell types in the Seurat object the "FindAllMarkers" formula with Wilcoxon rank-sum test was used. Figure 8A illustrates unsupervised cell clustering with coloring according to cell sample identity. Next, the top ten genes upregulated in each cell type compared to all other cell types (CDC, CF, SMC and EC) were identified (Figure 8B).

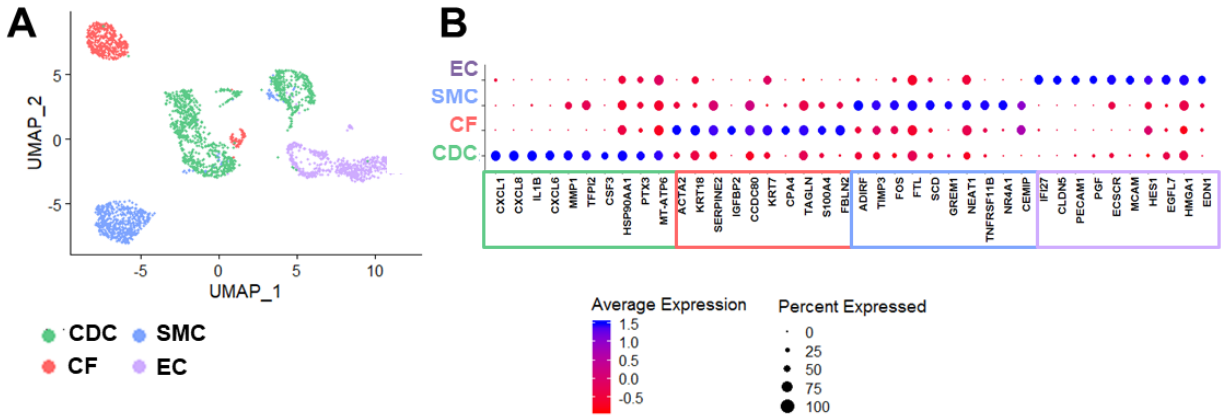

Figure 8: Comparison of primary cell types by sc-RNAseq.
Analyzed cell types are abbreviated as follows: CDC: cardiosphere-derived cells; CF: cardiac fibroblasts; SMC: smooth muscle cells; EC: endothelial cells. A) Uniform manifold approximation and projection (UMAP) plot of analyzed samples in sc-RNAseq (samples per cell type, n = 1) colored by sample identifier. B) Top ten upregulated differentially expressed genes (uDEG) in each sample compared to all other samples sorted by average natural logarithm of the gene's fold change (avg_logFC). Significant uDEG were defined by p < 0.05 (Wilcoxon rank-sum test) and avg_logFC ≥ 0.25. Adapted from Figure 2 from (148)

Compared to the non-myocyte cell types, top ten uDEG in CDC encoded for chemokine ligands (such as *CXCL1/8/6*), cytokines (*IL1B1* and *CSF3*) or the cytokine-inducible protein *PTX3* (159) (Figure 8B). Figure 9A illustrates the specific expression of *IL1B* and *CXCL6* in CDC. In CF, genes such as fibroblast specific protein 1 (*FSP1 = S100A4*) and fibulin 2 (*FBLN2*), coding for an ECM protein (160), were highly upregulated (Figure 8B and Figure 9B). Besides, among the uDEG in CF, cardiac fibrosis associated *SERPINE2* (161) and keratins (*KRT18* and *KRT7*) were found (Figure 8B). The only gene exclusively expressed and highly upregulated in CF was *IGFBP2* (avg_logFC = 1.94) (Figure 8B). Top ten uDEG in the SMC sample included genes associated with immunomodulatory processes such as *GREM1* involved in TGFβ-signaling (162) and TNF receptor superfamily member 11b (*TNFRSF11B*). *NR4A1,* a nuclear receptor involved in angiogenesis (163), was identified as the only gene selectively expressed in SMC (Figure 9C, left panel). Nevertheless, many genes upregulated in SMC were also expressed in the CF and CDC samples (Figure 8B), as previously recognized (Figure 5). For example, TIMP metallopeptidase inhibitor 3 (*TIMP3*) belonged to the top ten uDEG in SMC, but was also expressed in CF- and

CDC-samples, respectively (Figure 9C, right panel). The top three uDEG in EC were *IFI27* (Interferon alpha inducible protein 27), *CLDN5* (Claudin 5) and *PECAM1* (*CD31*) (Figure 8B and Figure 9D). (Kogan *et al.*, submitted manuscript 2020, (148))

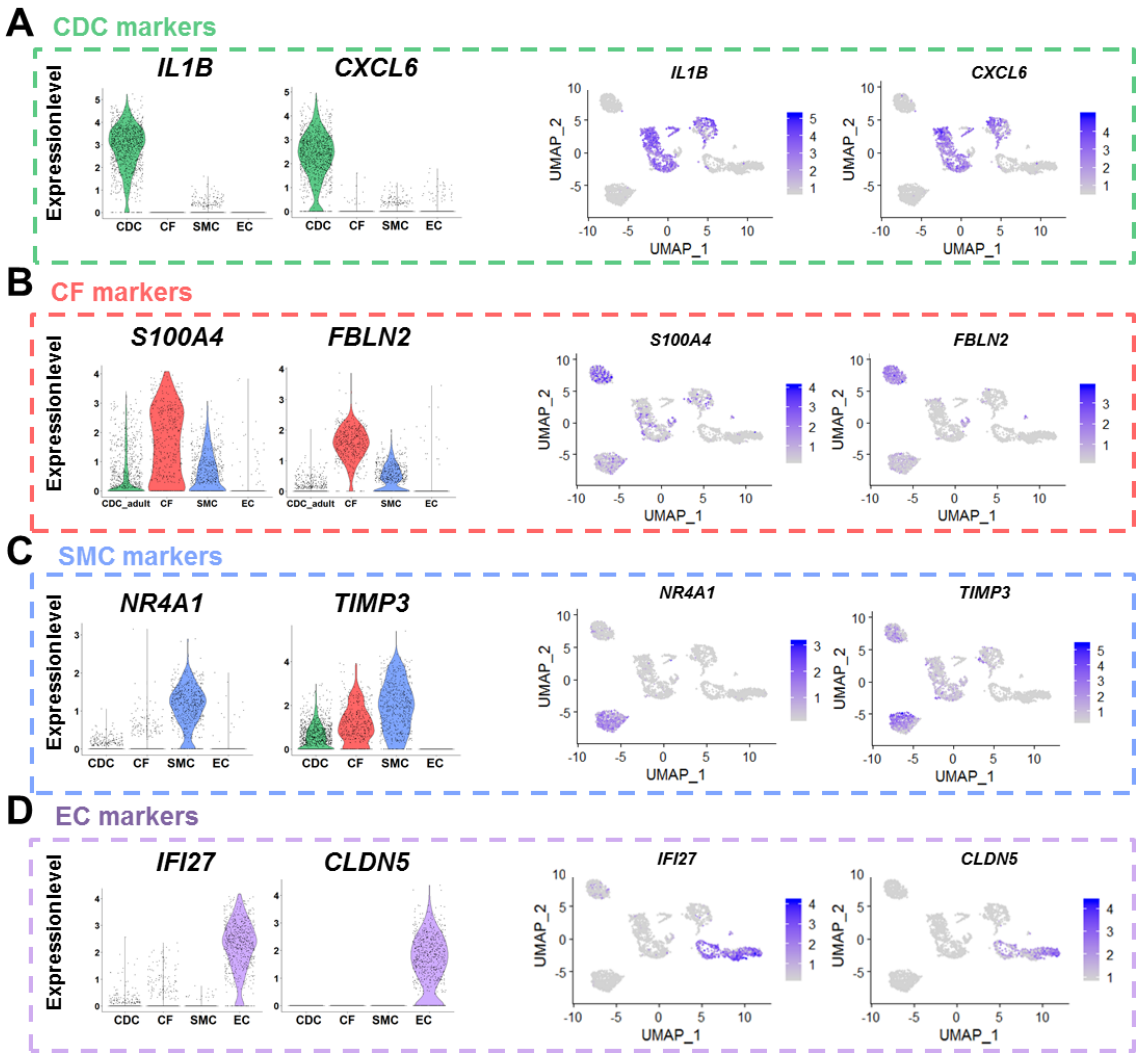

Figure 9: Expression profiles of selected top ten markers.
Analyzed cell types are abbreviated as follows: CDC: cardiosphere-derived cells; CF: cardiac fibroblasts; SMC: smooth muscle cells; EC: endothelial cells. Violin and feature plots generated from sc-RNAseq data (samples per cell type, n = 1) for selected top ten markers, as illustrated in Figure 8B, of the A) CDC sample, B) CF sample, C) SMC sample and D) EC sample. Adapted from Suppl. Figure S3 from (148).

To validate gene expression patterns, markers previously used for cell characterization by qRT-PCR and protein analysis were analyzed in the sc-RNAseq data. Corresponding to previous qRT-PCR results (Figure 5C), *THY1* (*CD90*) was among the top 25 upregulated genes in CF, however the marker *DDR2* was upregulated in SMC compared to all other cells by avg_logFC = 0.25

(Figure 10A). Notably, α-SMA (*ACTA2*) *and TAGLN* which have been described as SMC markers (154, 156), were interestingly part of the top ten uDEG in CF (Figure 8B). However, violin and feature plots of *ACTA2* and *TAGLN* showed that these markers were not specific either for CF or SMC (Figure 10B). *PECAM1* and *CDH5* showed a selective expression profile in EC (Figure 10C). However, unlike *PECAM1*, *CDH5*, was not among the top ten uDEG in EC and was also expressed in CDC (Figure 10C), confirming qRT-PCR results (Figure 5E). Expression of cardiac transcription factors already analyzed by qRT-PCR, was also examined in the sc-RNAseq data (Figure 10D). As far as can be judged despite their low expression levels, sc-RNAseq profiles of *TBX5* and *GATA4* revealed a higher expression in CDC and CF compared to SMC and EC, which corresponded to qRT-PCR results (Figure 5A). However, *NKX2-5* expression could not be detected in the sc-RAseq dataset. (Kogan *et al.*, submitted manuscript 2020, (148))

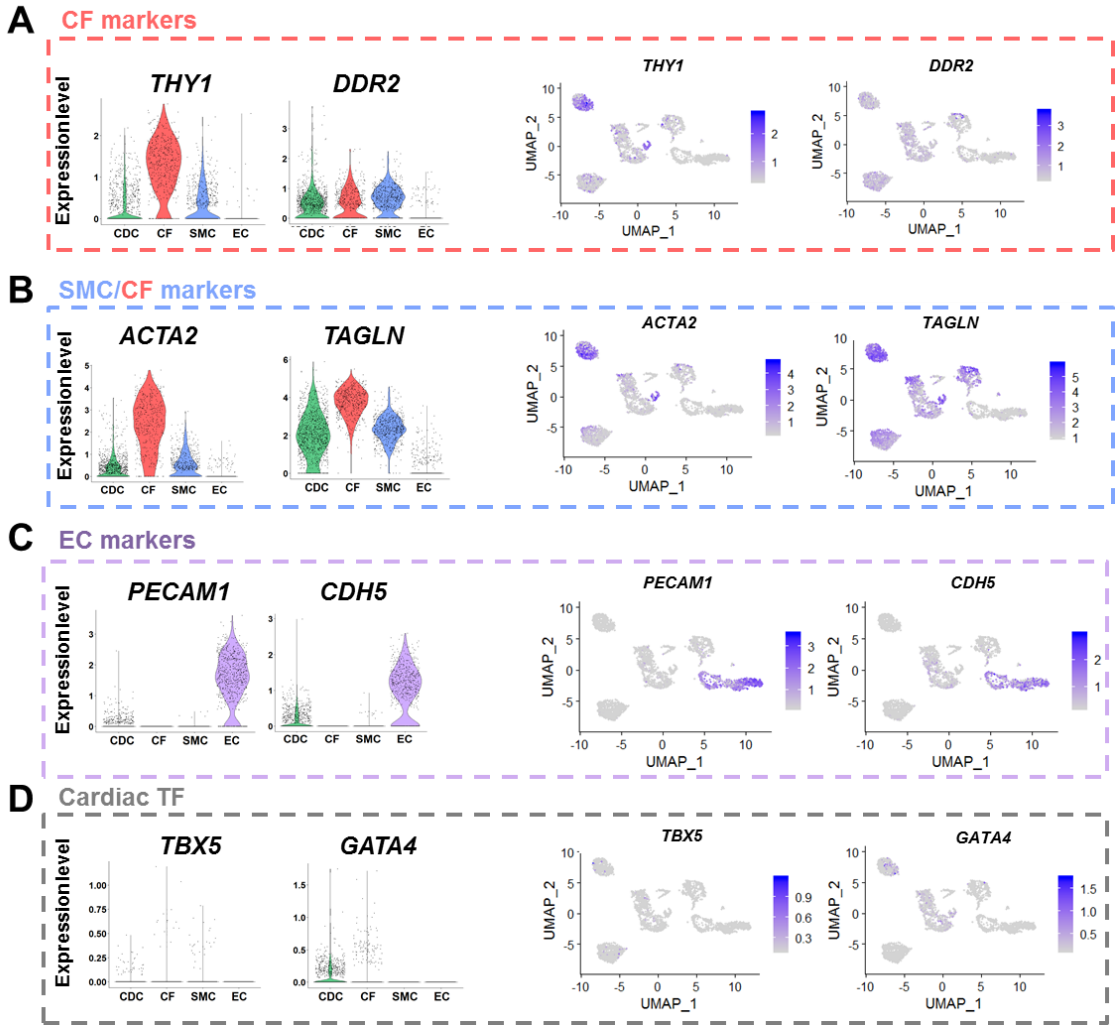

Figure 10: Validation of marker by sc-RNAseq.

Analyzed cell types are abbreviated as follows: CDC: cardiosphere-derived cells; CF: cardiac fibroblasts; SMC: smooth muscle cells; EC: endothelial cells. Violin and feature plots generated from sc-RNAseq data (samples per cell type, n = 1) for markers previously used in qRT-PCR or protein analysis (Figure 5 and 6)

as A) CF marker, B) SMC marker, C) EC marker and D) cardiac developmental transcription factors (TFs). Adapted from Suppl. Figures S3 and S4 from (148).

Expression of selected uDEG in CDC, CF and SMC was further validated by qRT-PCR analysis of independent samples and confirmed reliability of sc-RNAseq data (Figure 11).

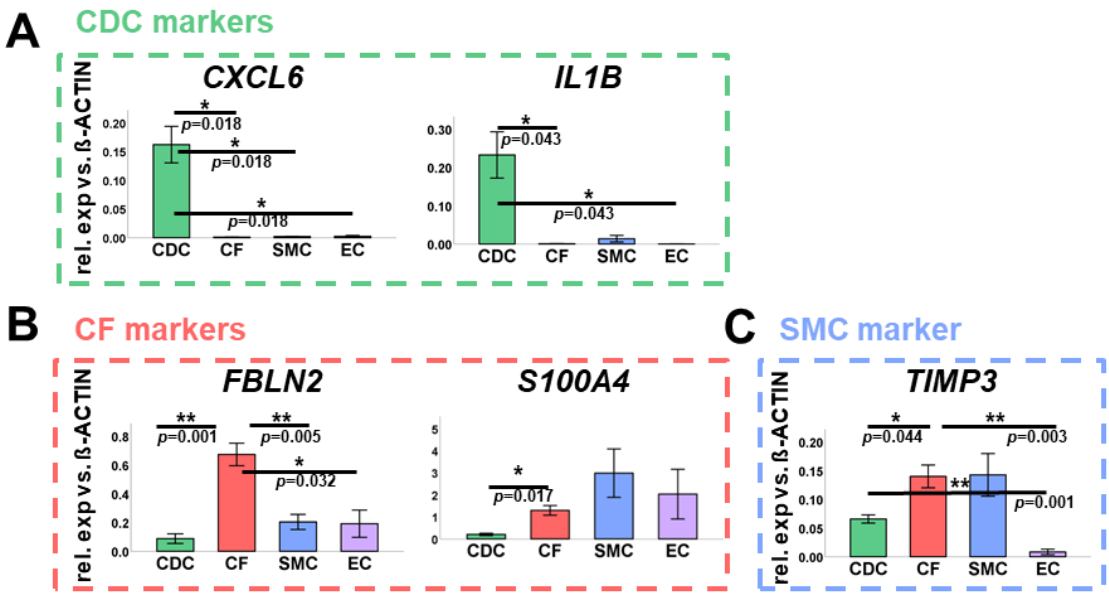

Figure 11: Validation of gene expression by qRT-PCR.
*Analyzed cell types are abbreviated as follows: CDC: cardiosphere-derived cells; CF: cardiac fibroblasts; SMC: smooth muscle cells; EC: endothelial cells. Genes found to be upregulated in sc-RNAseq data in A) CDC sample, B) CF sample and C) SMC sample were measured in independent samples by qRT-PCR. Data are represented as mean ± SEM, each gene was evaluated in at least 4 independent samples (n ≥ 4), significance is shown as *: p < 0.05, **: p < 0.01. Dunnett-T3-test was used as post-hoc test for all comparisons illustrated. Adapted from Suppl. Figure S4 from (148).*

In the next step the merged Seurat object was subclustered in an unsupervised manner which resulted in ten distinct clusters for the four cell types analyzed (Figure 12A, right panel). To better understand which biological processes can be attributed to these clusters, enrichment analysis of gene ontology (GO) terms was performed with significantly uDEG in each cluster using gene set enrichment analysis (GSEA) (138) as described in paragraph 4.5.4.3. UDEG were defined as genes with an average natural logarithm of the gene's fold change (avg_logFC) ≥ 0.25 and $p < 0.05$.

SMC were mainly found in one cluster (cluster 0, 90% of SMC), whereas EC and CF split into three or two clusters, respectively (EC: cluster 1, 6, 10, CF: cluster 2, 9). CDC subdivided into five clusters (clusters 3, 4, 5, 7, 8) and thus represented the most heterogeneic sample (Figure 12A, left panel). Among highly enriched GO-terms in cluster 0 (SMC) were processes such as "response to endogenous stimulus" and "circulatory system development" (Figure 12B-C).

Cluster 1 (61% of EC) revealed processes related to angiogenesis such as “blood vessel morphogenesis” and “tube morphogenesis” (Figure 12B, D). Clusters 10 and 6, including 8% and 28% of EC, represented growing (GO-terms enriched: “RNA binding” and “protein targeting”) and dividing (GO-terms enriched: “cell division”, “cell cycle process”) EC, respectively (Figure 12B). Cluster 2 which included the majority (87%) of CF was enriched for terms such as “structural molecule activity” and “collagen containing extracellular matrix” (Figure 12B, E). Besides, cluster 9 (13% of CF) was separated as a CF population of dividing cells (Figure 12B).

CDC were observed to be the most heterogeneous cell type, subdividing into five different clusters (3, 4, 5, 7, 8). Representative significantly enriched GO-terms for cluster 3 (26% of CDC) were “response to cytokine” and “cytoplasmic vesicle part” (Figure 12B, F), whereas terms associated with cell division dominated in cluster 4 (24% of CDC) (Figure 12B, G). Genes upregulated in cluster 7 (15% of CDC) were additionally enriched for GO-terms of cellular processes such as “adhesion”, “catalytic complexes” and “intracellular transport”. In cluster 8 (14% of CDC) GO-terms such as “mitochondrion”, “cytoskeletal part” and “cell substrate junction” were enriched.

Notably, cluster 5 represented a cluster which comprised cells of several samples, namely CDC (20% of total CDC), SMC (5.5% of total SMC) and EC (0.5% of total EC). GSEA of cluster 5 revealed many terms associated with mitochondrial activity as well as GO-terms indicating “response to cytokines”, “cell activation involved in immune response” and “secretory vesicle”. (Kogan *et al.*, submitted manuscript 2020, (148))

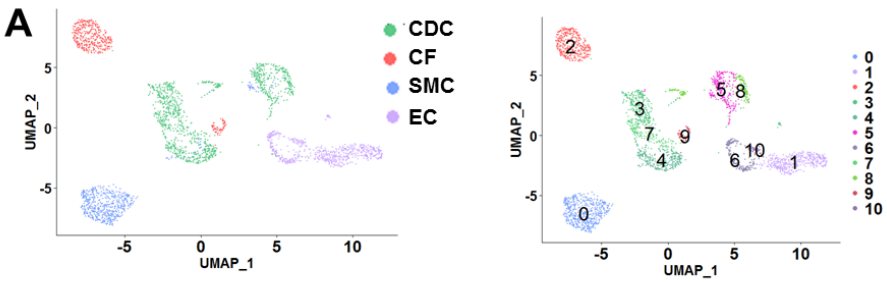

B

Cluster	Sample (% of total sample cells)	Selected enriched GO-Terms (-LOG [*p*-value])
0	SMC (90)	• Response to endogenous stimulus (32) • Circulatory system development (28)
1	EC (61)	• Blood vessel morphogenesis (39)
2	CF (87)	• Structural molecule activity (52) • Collagen containing extracellular matrix (44)
3	CDC (26)/ EC (1.2)	• Response to cytokine (58) • Cytoplasmic vesicle part (53)
4	CDC (24)/ SMC (3)	• Mitotic cell cycle (106)
5	CDC (20)/ SMC (6)	• Cell activation involved in immune response (26) • Secretory vesicle (36)
6	EC (28)	• Cell cycle process (31) • Cell division (27)
7	CDC (15)	• Cell adhesion molecule binding (43) • Catalytic complex (56)
8	CDC (14)	• Mitochondrion (15) • Cytoskeletal part (16)
9	CF (13)	• Mitotic cell cycle (27)
10	EC (8)	• RNA binding (18) • Protein targeting (14)

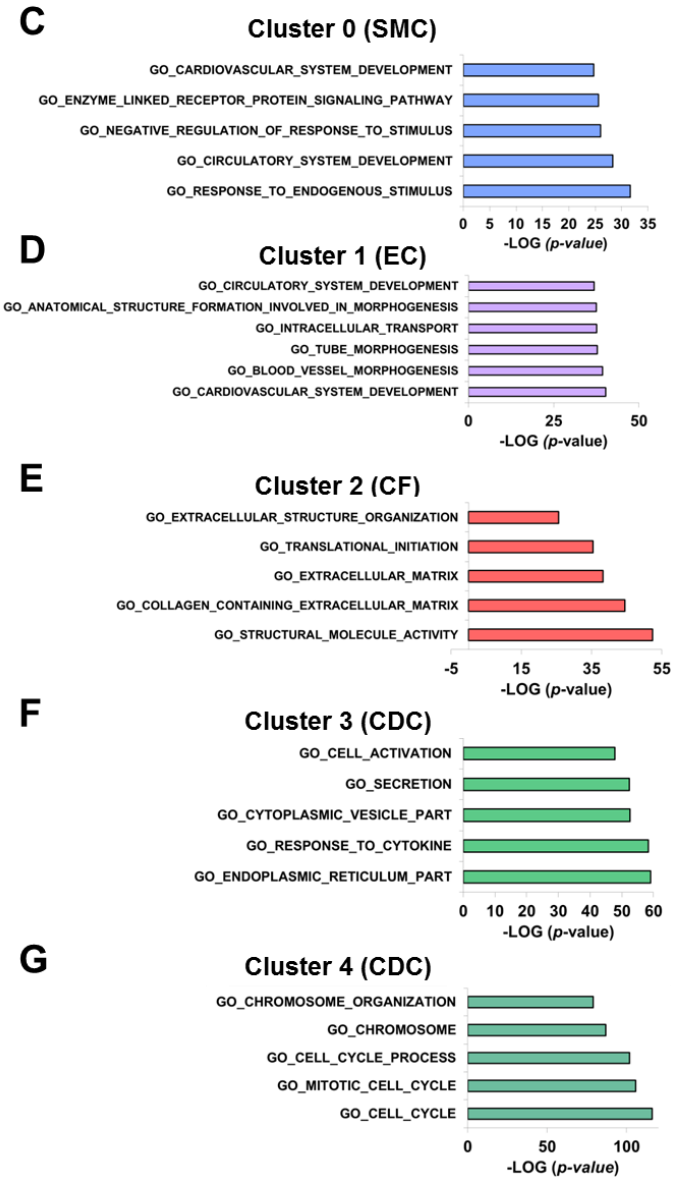

Figure 12: Global clustering of CDC, CF, SMC, and EC.

Analyzed cell types are abbreviated as follows: CDC: cardiosphere-derived cells; CF: cardiac fibroblasts; SMC: smooth muscle cells; EC: endothelial cells. A) Uniform manifold approximation and projection (UMAP) plot of analyzed samples in single cell-RNA sequencing (sc-RNAseq) colored by sample identifier (left) and by cluster (right). B) Gene ontology (GO)-terms significantly enriched for each cluster. Middle

column reports the percentages of cells of each sample included per cluster (percentages < 1% are not displayed. C-G) Highly enriched GO-terms for the main clusters of primary cells: C) SMC (cluster 0), D) EC (cluster 1), E) CF (cluster 2) and F-G) CDC (clusters 3 and 4). Samples per cell type: n = 1. Adapted from Figure 2 from (148).

To reveal, to which extent the process "response to cytokines" is specific for CDC, all uDEG in cluster 3 associated with this term were analyzed in a cluster tree and selected genes were visualized in a heatmap, showing clear overexpression in CDC compared to all other analyzed cell types (Figure 13A). UDEG in cluster 1 associated with the GO-term "tube development" showed EC specificity (Figure 13B). "Collagen containing extracellular matrix" associated uDEG in cluster 2 were mainly expressed in CF as shown in Figure 13C. However, in the SMC specific cluster 0 uDEG enriched for the GO-tem "cardiovascular system development" had similar specifity for SMC and CF, as shown by the clustertree in Figure 13D (left panel). Nevertheless, selected exemplary genes shown in the heatmap were upregulated in SMC (Figure 13D, right panel). (Kogan *et al.*, submitted manuscript 2020, (148))

CF, SMC, EC and AF were previously compared on the proteomic level by Doll *et al*. (5). Hence, I addressed the question whether abundant proteins identified in CF, SMC and EC were also present among uDEG in CF, SMC, EC of sc-RNAseq data. Therefore, I performed a comparison of these two datasets, as described in paragraph 4.5.4.3. Genes detected by proteomic and sc-RNAseq accounted for 24% percent of total uDEG (sc-RNAseq) for CF and SMC, respectively, whereas for EC 47% of uDEG overlapped (Suppl. Figure S 4).

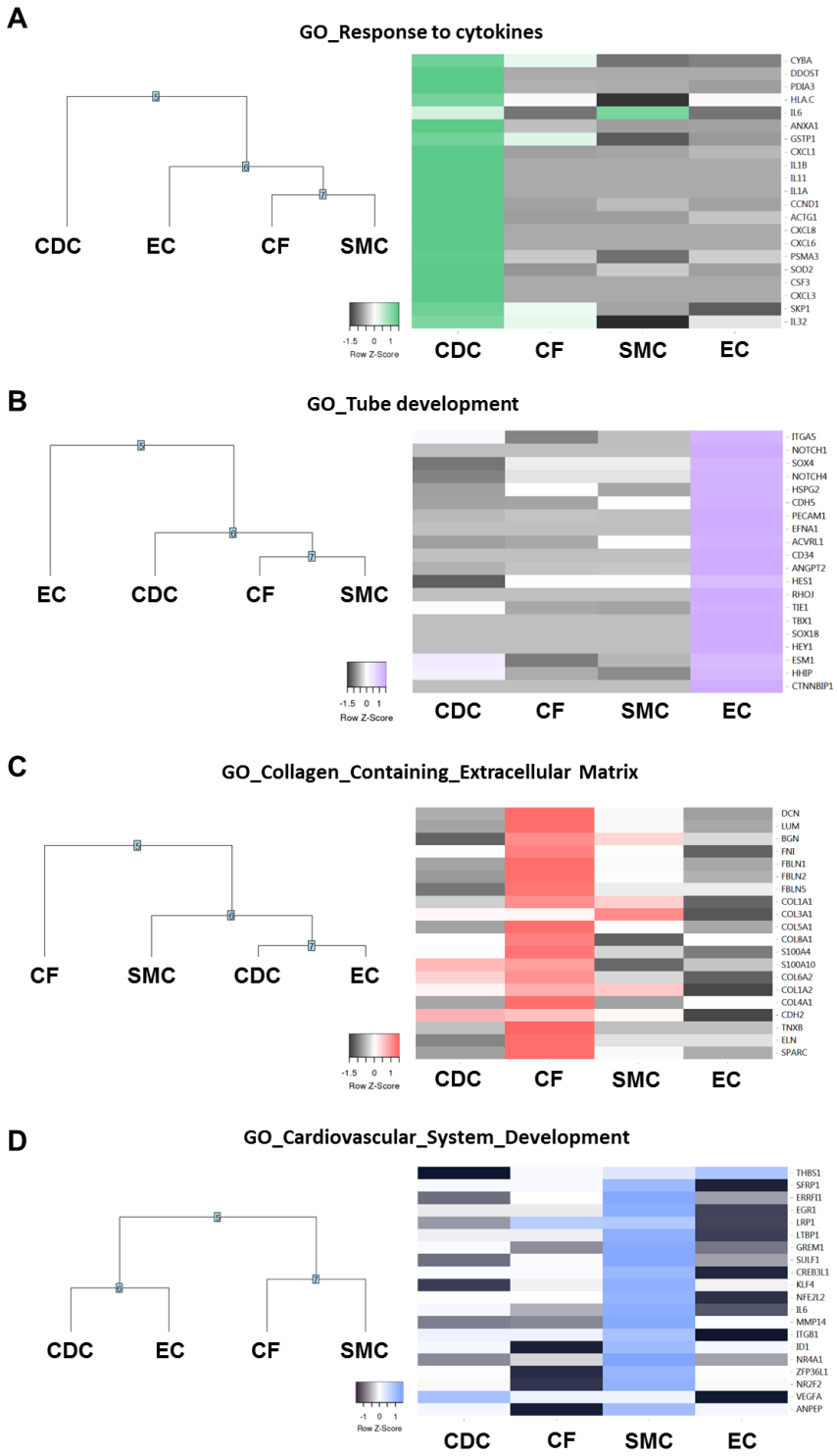

Figure 13: Cluster trees and heatmaps.

Analyzed cell types are abbreviated as follows: CDC: cardiosphere-derived cells; CF: cardiac fibroblasts; SMC: smooth muscle cells; EC: endothelial cells. Genes associated with the gene ontology (GO)-term "Response to cytokines" in cluster 3 were analyzed in a cluster tree (left) and exemplary genes are shown in a heatmap (right) (A). Analogical analysis was performed for genes associated with the GO-term "tube formation" in cluster 1 (B), genes associated with the GO-term "collagen containing extracellular matrix"

in cluster 2 (C) and genes associated with the GO-term "cardiovascular System Development" in cluster 0. Samples per cell type: n = 1. Adapted from Suppl. Figure S5 from (148).

Taken together, the results of sc-RNAseq confirmed molecular characteristics which are known to be typical for cultured CF, SMC and EC. Again, EC exhibited a clearly distinguishable expression profile from CF and SMC. The heterogeneous cell type CDC was discriminated from all other cell types by its highly proliferative, secretory and metabolic molecular fingerprint.

5.1.3 Heterogeneity of CDC

Since the result of global clustering of all cultured cell types (Figure 12A) revealed the heterogeneity of CDC, unsupervised subclustering analysis of the adult CDC sample alone was performed to further elucidate the characteristics of this cell type. This analysis yielded seven distinct clusters (Table 36, Figure 14A).

Cluster 0 and 5 (30% of CDC) represented cell populations mainly involved in protein synthesis processes, whereas cluster 2 and 6 (24% of cells) represent dividing cells. Cells in cluster 7 were associated with GO-terms such as "intracellular transport" as well as "cytoplasmic vesicle part". UDEG of cluster 1 could be attributed to GO-terms associated with angiogenesis such as "circulatory system development" and "tube development". In cluster 3 and 4, an enrichement for the GO-term "response to cytokine" was highly significant. UDEG in cluster 4 were linked to GO-terms related to "extracellular matrix".

As GO-terms highly enriched in clusters 1, 3 and 4 were also enriched in CF-, SMC- and EC-samples (see Table 36, Figure 12 and paragraph 5.1.2), I further examined to which extent CDC are similar to these non-myocyte cell types. Therefore, calculation of cell similarity of CDC, CF, SMC and EC was performed according to Wang *et al.* (21). Corresponding to marker analysis (see paragraphs 5.1.1 and 5.1.2), similarity score maxima of the CF and the SMC sample were closest to each other, whereas the maximum of the EC sample was different (Figure 14B). In the CDC-sample, three peaks showed up. The highst peak (similarity score around 0.7) clearly stood out from all cell types analyzed. In contrast, the second highest peak (similarity score around 0.4) was in the range of the CF maximum and the smallest peak (similarity score around 0.18) resembled the smaller peak of the SMC curve (Figure 14B). To further reveal, which processes were similar between CDC and the according non-myocyte cell types, CDC clusters 1, 3 and 4 were compared to their counterpart clusters in CF and SMC regarding GO-terms associated with their uDEG. CDC-cluster 4 and CF-cluster 1 both yielded GO-terms associated with "extracellular matrix". The top 50 enriched GO-terms for these two clusters overlapped to 46%. Examples for common GO-terms were "extracellular matrix", "biological adhesion" and "tube development" (Figure 14C). As both CDC and SMC upregulated processes associated with angiogenesis and response to cytokines, several clusters of each sample were used for the comparative analysis. CDC cluster 1 and 3 overlapped with SMC cluster 1, 2, and 3 to 46% of enriched GO-terms which were related to angiogenesis (exemplary GO-terms: "tube development", "circulatory system

development", "blood vessel morphogenesis") and "response to cytokine". In a second comparison, clusters related to ECM in CDC (cluster 4) and SMC (clusters 1, 2, 3) revealed an overlap of 54% showing common terms such as "cell adhesion molecule binding", "extracellular matrix" and "response to cytokine" (Figure 14D).

The heterogeneic features of CDC were further visualized in a two-dimensional principal component analysis (PCA) plot of the merged CCA-corrected Seurat object of all adult cell types. While CF, SMC and a major part of CDC accumulated in PC_2, EC and a smaller part of the CDC-sample segregated in the direction of PC_1 (Figure 14E). However, PC_1 and PC_2 constituted only 6.2% and 4.3% of total variance, respectively. (Kogan *et al.*, submitted manuscript 2020, (148))

Table 36: GO-term enrichment in CDC Clusters (Figure 14A)

Cluster	% cells	GO-Terms (-LOG [*p*-value])
0	18.4	Protein targeting (76), Peptide biosynthetic process (65)
1	15.1	Circulatory system development (11), Blood vessel morphogenesis (8)
2	14.2	DNA replication (47), Mitotic cell cycle (37)
3	13.0	Response to oxygen containing compound (31), response to lipid (26), response to cytokine (24)
4	12.3	Extracellular structure organization (48), Response to cytokine (35)
5	11.3	RNA binding (19), Cytosolic ribosome (13)
6	10.2	Mitotic cell cycle (92), Cell division (84)
7	5.6	Intracellular transport (32), Cytoplasmic vesicle part (18)

Abbreviation: GO: gene ontology

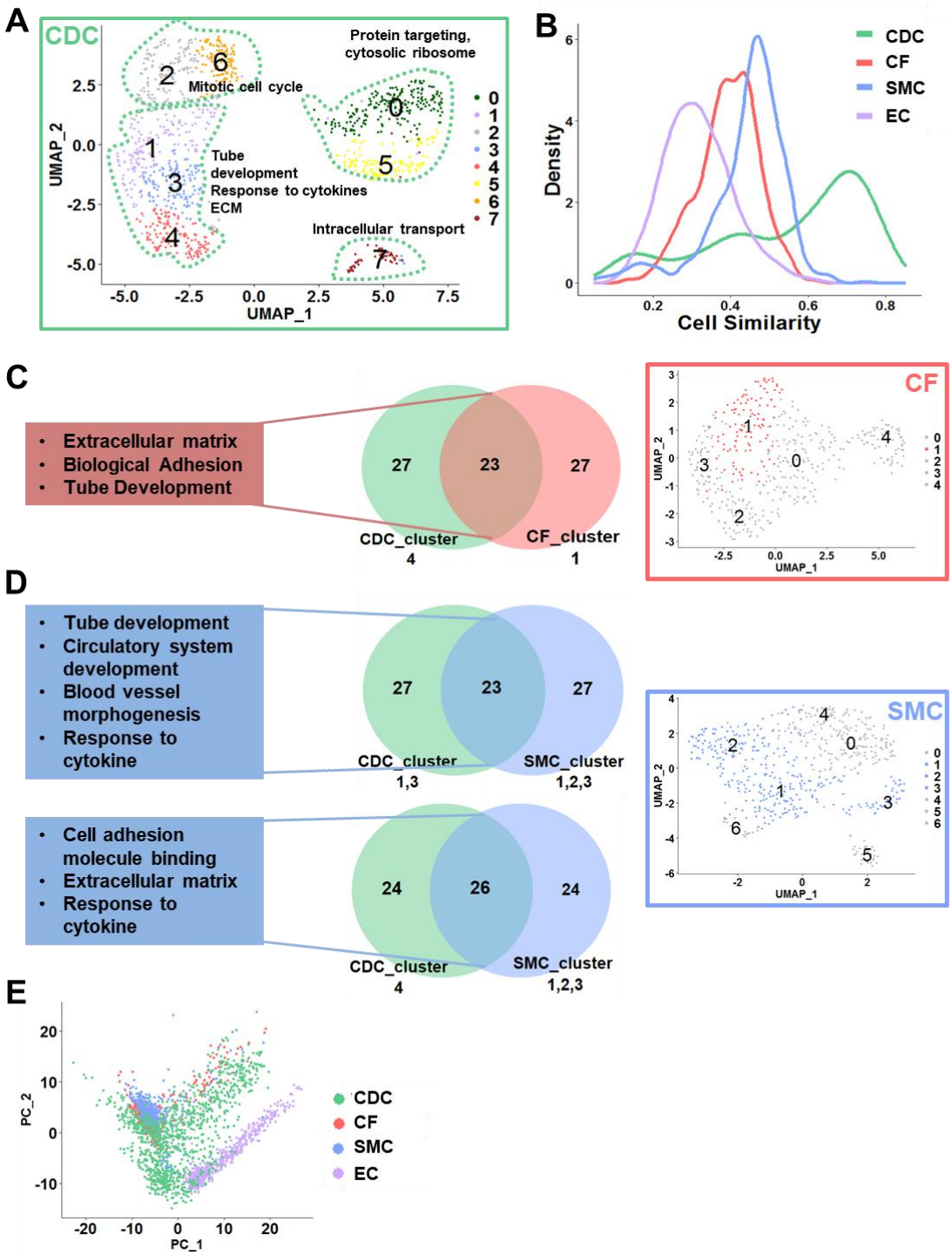

Figure 14: Heterogeneity of CDC.

Analyzed cell types are abbreviated as follows: CDC: cardiosphere-derived cells; CF: cardiac fibroblasts; SMC: smooth muscle cells; EC: endothelial cells. A) Uniform manifold approximation and projection (UMAP) plot of subclustered adult CDC sample (see also Table 36). B) Transcriptional similarity plots of CDC, CF, SMC and EC. C-D) Comparison of common gene ontology (GO)-terms in selected clusters of CDC and CF (C) or SMC (D) are associated. E) Principal component analysis (PCA) plot of adult primary

samples. Percent of total variance was for PC_1: 6.2% and for PC_2: 4.3%. Samples per cell type: n = 1. Adapted from Figure 3 from (148).

COL6A2 and *COL3A1* (annotated for the GO-term: "extracellular matrix structural constituent conferring tensile strength") are examples of genes in the sc-RNAseq dataset which are expressed in CDC, CF and SMC, but hardly in EC (Figure 15A-B). Independent samples were analyzed for the expression of *COL6A2* and *COL3A1* by qRT-PCR and confirmed sc-RNAseq expression patterns (Figure 15C-D). Analysis of similarly expressed genes in CDC and CF (avg_logFC between -1 and +1) uncovered that these genes were mainly associated with GO-terms such as "extracellular matrix" and "biological adhesion". Many of these genes were also upregulated in the SMC-sample (Figure 15E). (Kogan *et al.*, submitted manuscript 2020, (148))

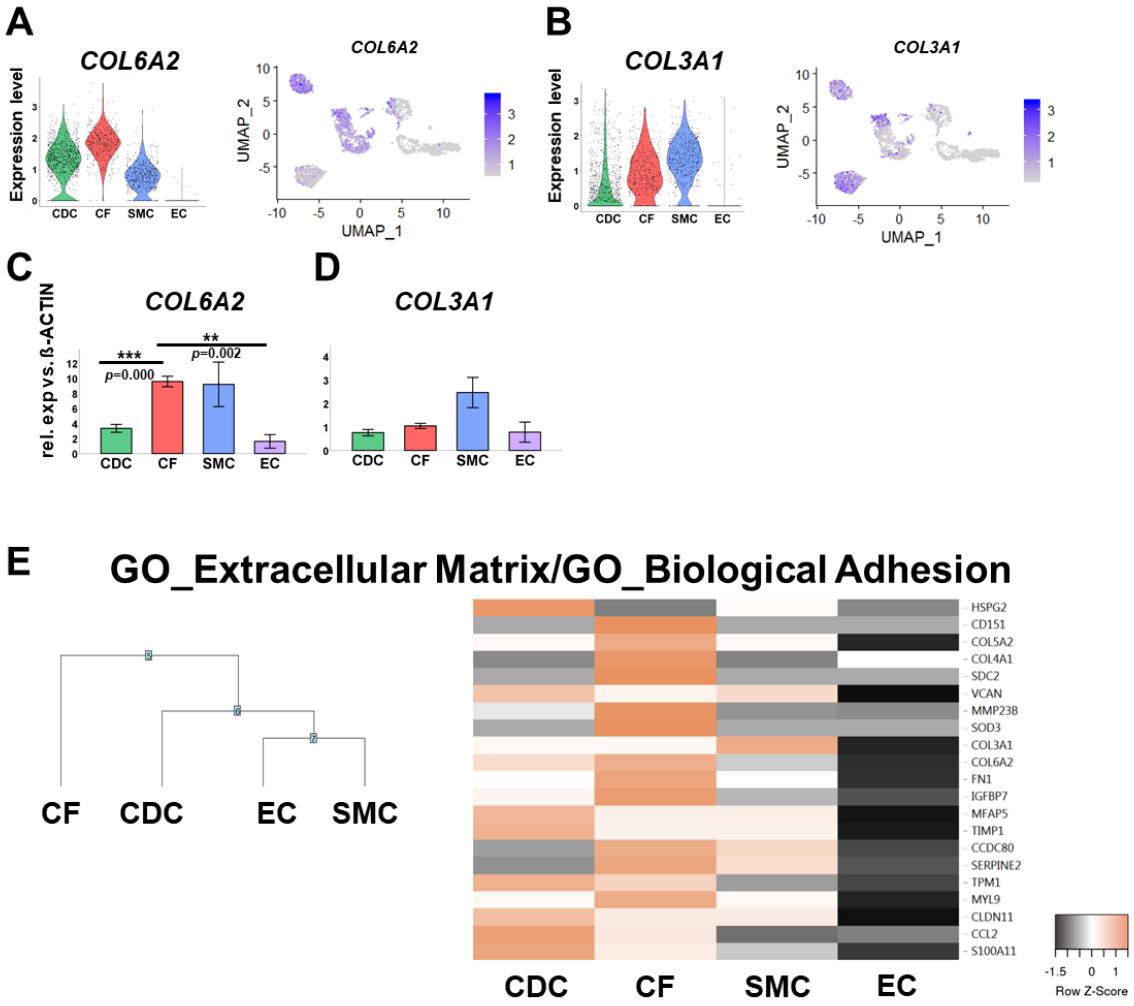

Figure 15: Similarity between CDC, CF and SMC.

Analyzed cell types are abbreviated as follows: CDC: cardiosphere-derived cells; CF: cardiac fibroblasts; SMC: smooth muscle cells; EC: endothelial cells. A-B) Expression levels of COL6A2 (A) and COL3A1 (B) in CDC, CF, SMC and EC as measured by single cell-RNA sequencing (sc-RNAseq) are illustrated by violin plot (left panel) and feature plot (right panel). C-D) qRT-PCR of COL6A2 (siginifance tested with Games-

*Howell-test for inhomogeneous variances) (C) and COL3A1 (D) in CDC, CF, SMC and EC (Data are represented as mean ± SEM, n ≥ 4, significance is shown as **: p < 0.01, ***: p < 0.001. E) Similarly upregulated genes in the CDC and the CF sample (sc-RNAseq data) were associated with the terms "extracellular matrix" and "biological adhesion", as shown in a cluster tree (left) and as illustrated in a heatmap of a selected gene subset (right). Adapted from Suppl. Figure S6 from (148).*

In conclusion, sc-RNAseq analysis of CDC demonstrated its high heterogeneity. Although a major part of CDC showed molecular signatures of either highly mitotic or synthetizing cultured cells, certain similarities with CF and SMC such as response to cytokines, ECM production and tube development were evident.

5.2 Age-depedent comparison of non-myocyte primary cell cultures

Clinical trials suggested that CDC derived from pediatric patients might have more beneficial therapeutic effects than CDC derived from adult patients (68, 87). This poses the question whether the characteristics of infant derived cardiac primary cells might have intrinsic features which discriminate them from their adult counterparts. To tackle this issue, molecular characteristics of cells obtained from infant (age: 5 days - 6 years, see Table 15) and adult (age: 55-76 years, see Table 14) patients were compared. Most of the pediatric patients had a single-ventricle (SV) diagnosis and adult patients with various diagnosis were undergoing cardiovascular operations such as coronary artery bypass graft (CABG), MAZE procedure for atrial fibrillation or aortic, mitral or tricuspid valve replacement.

5.2.1 Molecular comparison of infant and adult CDC and CF

Gene expression analysis by qRT-PCR of CDC and CF derived from these two patient groups showed a downregulation of the cardiac TFs *GATA4* and *TBX5* in infant CDC compared to adult CDC (Figure 16A, left panels). However, a significantly higher expression of these TFs in infant CF compared to infant CDC was observed (Figure 16A, left panels). In contrast, the cardiac TF *NKX2-5* was significantly higher expressed in CDC and CF of the infant group compared to the adult group in both cell types, respectively (Figure 16A, right panel). CF marker *ALDH1A2* was upregulated in adult cells compared to infant cells, and in CF compared to CDC in both age groups, respectively (Figure 16B, upper left panel). *THY1* (*CD90*) was upregulated in CDC and CF in the infant group compared to the adult group, and its expression was consistenly higher in CF in both age groups (Figure 16B, upper middle panel). Other CF markers such as *DDR2* and miR-21 did not show significant differences between the infant and the adult group. However, when comparing cell types, *DDR2* showed upregulation in infant CF compared to infant CDC (Figure 16B, upper right and bottom panel). MiR-146a-5p demonstrated specific expression in CDC compared to CF only in the infant group, whereas miR-132-3p did not significantly differ between age groups and cell types (Figure 16C). An overview of age- and cell type-dependent significant differences is provided in Table 39. (Kogan *et al.*, submitted manuscript 2020, (148))

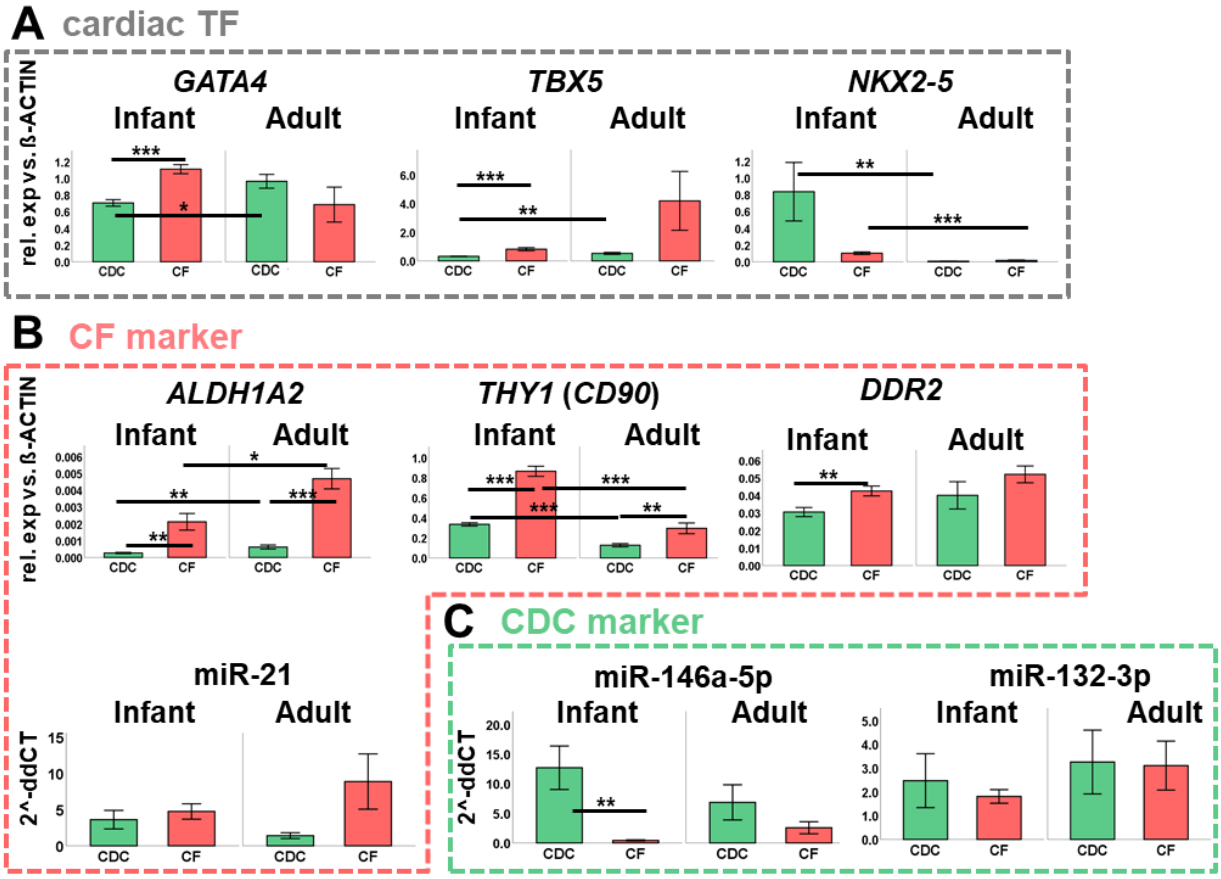

Figure 16: Gene expression analysis by qRT-PCR of CDC and CF derived from infant (age: 5 days- 6 years) and adult (age: 55-76 years) patients.

*Analyzed cell types are abbreviated as follows: CDC: cardiosphere-derived cells; CF: cardiac fibroblasts. Relative gene expression levels versus ß-ACTIN (gene symbol: ACTB) are shown for A) Cardiac transcription factors (TFs), B) CF- and C) CDC markers. Data are represented as mean ± SEM, n ≥ 5, significance tests performed: One-way ANOVA for homogeneous variances or Welch-test and Brown-Forsythe-test for inhomogeneous variances, significance is shown as *: p < 0.05, **: p < 0.01, ***: p < 0.001; for complete overview of p-values and statistical tests see Table 39. Adapted from Figure 4 from (148)*

A more detailed analysis of age-related gene expression patterns was performed by comparing a neonatal CDC sample (patient age: 7 days, diagnosis: HLHS) to an adult CDC sample (patient age: 61 years, diagnosis: coronary heart disease) using sc-RNAseq (see samples 5 and 6 in Table 33).

In analogy to the adult CDC sample (see paragraph 5.1.2 and Figure 7), quality of the infant CDC sample was controlled by morphological evaluation (Figure 17A) and qRT-PCR of selected CDC- and CF-markers in comparison to the CF generated from the same patient (Figure 17B-C). Single-

cell cDNA library was prepared using the 10x Chromium platform. Quality controls performed by bioanalyzer after steps 2 and 3 of cDNA library preparation are shown in Suppl. Figure S 3. After filtration procedures to exclude low quality cells, doublets and cells with high percentage of mitochondrial genes (Figure 17D-F, Table 34-35), 960 cells of the infant CDC sample and 1109 cells of the adult CDC sample were analyzed. In total the filtered merged object depicted median values of 5,649 genes/cell and 33,731 UMI count/cell (Figure 17G-H). (Kogan *et al.*, submitted manuscript 2020, (148))

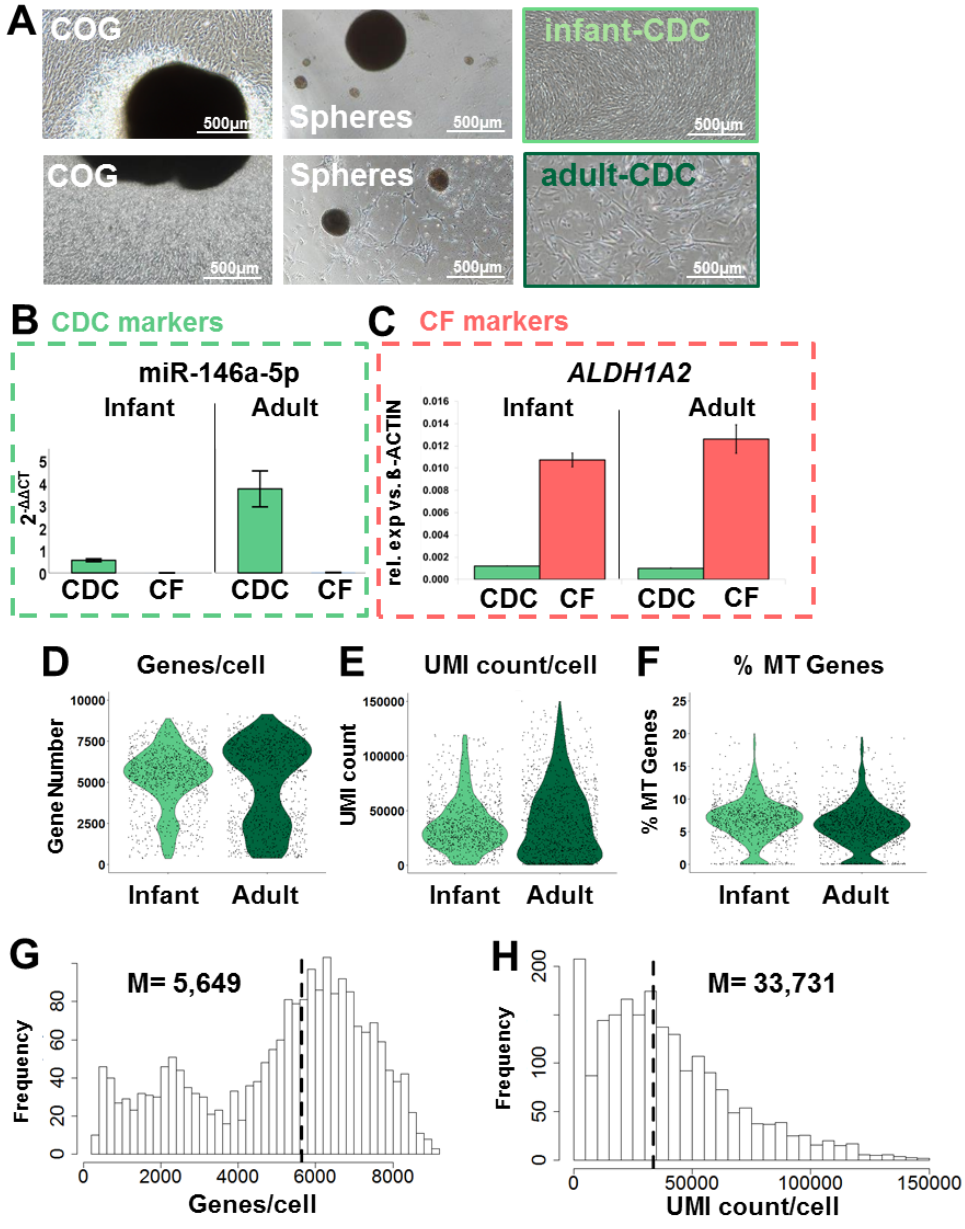

Figure 17: Quality control of infant and adult CDC samples used for sc-RNAseq.
Abbreviations: COG: cardiac outgrowth; CDC: cardiosphere-derived cells; CF: cardiac fibroblasts; sc-RNAseq: single cell RNA sequencing, UMI: unique molecular identifier. A) Morphological assessment of

the utilized cell samples (infant and adult CDC) on the day of the experiment by microscopy. B-C) Expression profiles of CDC (B), and CF (C) markers of infant and adult CDC samples used for sc-RNAseq compared to CF generated from the same cardiac biopsy. For each sample two culture wells were used for RNA isolation (n = 2). Bar diagrams show mean ± SEM. D-F) Violin plots of detected (D) gene number per cell (Genes/cell), (E) UMI counts per cell (UMI count/cell) and (F) percentage of mitochondrial genes per cell (% MT Genes), illustrated for each sample analyzed (n = 1) after filtering procedure, see Table 35 for median values. G-H) Histogram illustrating G) genes/cell or H) UMI count/cell of the filtered merged Seurat object containing infant and adult CDC. Adapted from Suppl. Figure S7 from (148)

Unsupervised subclustering analysis of the two CDC sc-RNAseq samples (infant and adult) partitioned them into six clusters (Table 37, Figure 18A-B). The samples shared four common clusters (cluster 0, 3, 4, 5) with which protein synthesis, growth and cell division processes were associated (Table 37).

However, exclusively infant CDC sample derived cells were found in cluster 1, whereas cluster 2 was specific for adult CDC derived cells (Figure 18A-D, Table 37). GO analysis of uDEG in cluster 1 by GSEA pointed out that infant CDC upregulated processes such as "circulatory system development", or "blood vessel morphogenesis". On the contrary, uDEG in cluster 2 (adult CDC only) were mainly attributed to GO-terms such as "biological adhesion" and "cytoplasmic vesicle part" (Figure 18C-D). GO-term "extracellular matrix" was enriched in both cluster 1 and cluster 2.

When exploring uDEG in the infant sample compared to uDEG from the adult sample, GO-terms "blood vessel morphogenesis" and "embryo development" were enriched. On the contrary, uDEG in the adult CDC sample compared to the infant sample were attributed to terms such as "extracellular matrix" and "response to stress" (selected genes shown in Figure 18E-F). (Kogan *et al.*, submitted manuscript 2020, (148))

Table 37: Cluster analysis of infant and adult CDC samples (Figure 18B)

Cluster	Sample	Enriched GO-terms (*p*-value)
0	Infant/Adult	RNA binding (37) Cytosolic ribosome (34)
1	Infant	Circulatory system development (32) Blood vessel morphogenesis (25)
2	Adult	Biological adhesion (39) Cytoplasmic vesicle part (34)
3	Infant/Adult	Cell cycle (80)
4	Infant/Adult	Cotranslational protein targeting to membrane (85)
5	Infant/Adult	Catalytic complex (11) RNA binding (8) Intracellular transport (8)

Abbreviations: GO: gene ontolog, Infant: infant CDC sample used for single cell RNA sequencing; Adult: adult CDC sample used for single cell RNA sequencing.

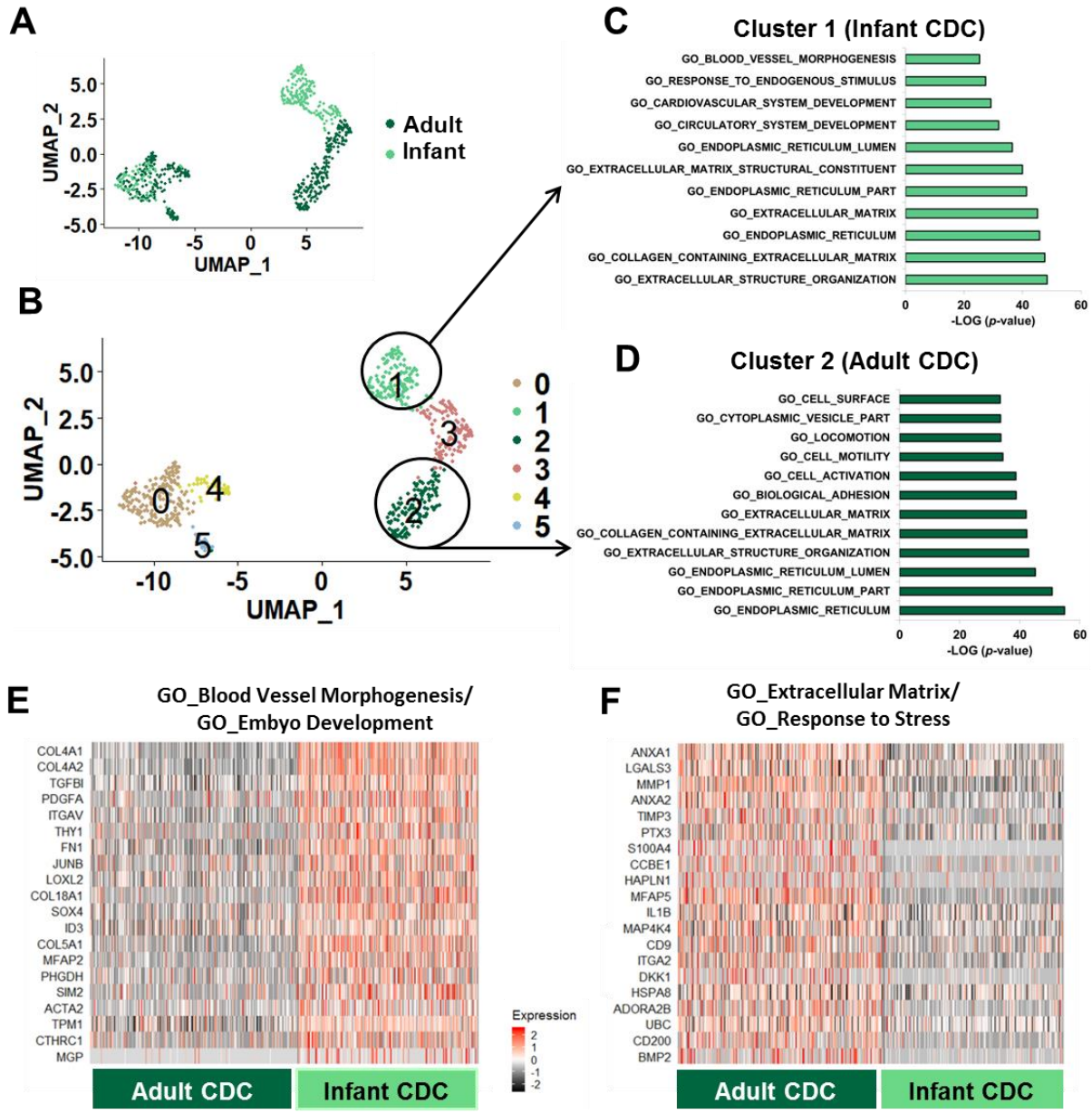

Figure 18: Comparison of infant and adult CDC samples by sc-RNAseq.

Analyzed cell types are abbreviated as follows: CDC: cardiosphere-derived cells; CF: cardiac fibroblasts. Results of sc-RNAseq of infant (age: 7 days) and adult (age: 61 years) CDC samples (each sample, n = 1) illustrated uniform manifold approximation and projection (UMAP) plots A) colored by sample identifier or B) colored by clusters. (C) Gene ontology (GO)-terms highly enriched for genes of cluster 1 containing cells of infant CDC only and (D) cluster 2 containing cells of adult CDC only. Additional information of enriched terms in particular clusters can be found in Table 37. E-F) Heatmaps of selected uDEG in the infant CDC sample and (E) in adult CDC sample (F). GO-terms associated with the selected uDEG are indicated above the according heatmap. Adapted from Figure 4 and Suppl. Figure S7 from (148)

In summary, as assessed by qRT-PCR data, infant CDC were more distinct from age-matched CF than their adult counterparts. Developmental and angiogenic processes were upregulated in neonatal CDC when compared to adult CDC according to sc-RNAseq data.

5.2.2 *Functional effects of CDC derived extracellular vesicles (EV) compared to CF derived EV and age-dependent differences*

Many studies showed paracrine effects of CDC such as a positive angiogenic potential, anti-fibrotic effects or inhibition of cardiomyocyte apoptosis (78, 80, 85) suggesting that they constitute a mechanism of the biological activity of CDC when used for regenerative cell therapy. One central cellular paracrine mechanism is the secretion of extracellular vesicles (EV). Particularly small EV of endocytic origin, termed exosomes, are involved in intercellular communication by shutteling proteins, lipids, miRs and mRNAs (81). For this reason, *in vitro* assays were developed to analyze the impact of CDC derived EV (CDC-EV) on different cardiac cell types. To elucidate whether comparable paracrine effects could be reproduced by CF-EV and to check for age dependency, EV preparations of infant and adult derived CDC and CF were compared to adequate positive and negative controls in each assay.

EV were precipitated from serum-free medium conditioned for seven days by CDC or CF grown on a T75 flask (Figure 19A, paragraph 4.7.1). To ensure high viability of cells conditioned with serum-free medium, percentage of dead cells was assessed by trypan blue staining and unveiled fewer than 5% dead cells per flask (Figure 19B). Although no significant difference in cell numbers per T75 cell culture flask was detected between CDC and CF (Figure 19C), the number of secreted particles per T75 cell culture flask was significantly higher in CDC-EV compared to CF-EV samples, measured by nanoparticle tracking analysis (Figure 19D). Both in CDC- and CF-EV preparations the size of the majority of included particles ranged between 40 nm and 200 nm indicating that exosomes and not apoptotic bodies are included in the EV preparations (164, 165) (Figure 19E-G). Flow cytometric analysis confirmed the presence of typical exosomal markers CD63 and CD81 (166) in selected CDC-EV preparations (Figure 19H). MiR-146a-5p was significantly more abundant in CDC-EV compared to CF-EV both in infant and adult patients (Figure 19I). Yet, no significant differences between cell types or age groups were detected for miR-132-3p or miR-21 EV content (Figure 19J-K). (Kogan *et al.*, submitted manuscript 2020, (148))

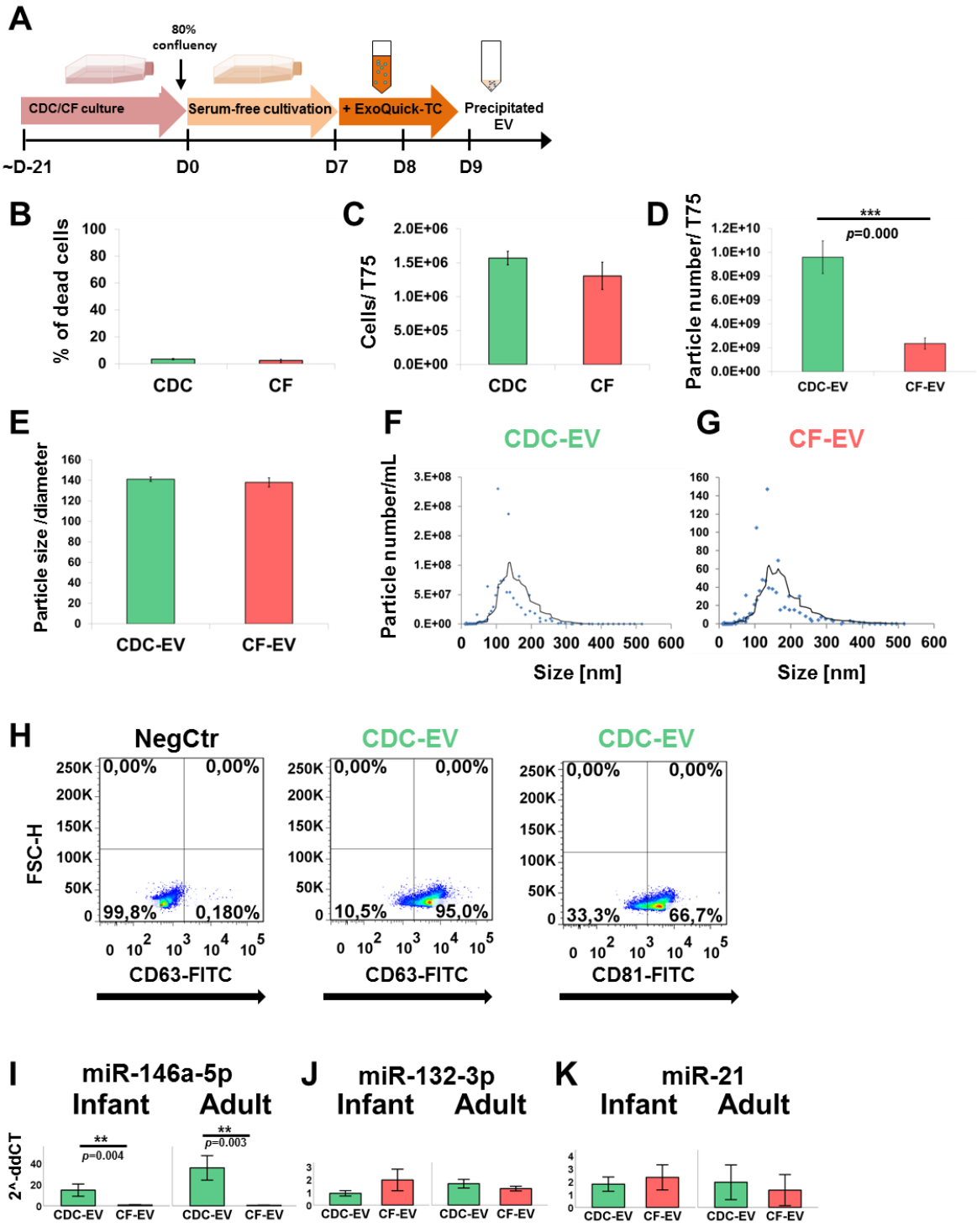

Figure 19: Quality control of CDC/CF-EV.

Abbreviations: CDC: cardiosphere-derived cells; CF: cardiac fibroblasts; EV: extracellular vesicles; FC: flow cytometry. A) Isolation procedure of EV from conditioned medium of CDC or CF cultured in serum-free medium for seven days. B-C) Percentage of dead cells (n ≥ 3) (B) and cell number per T75 cell culture flask (n ≥ 19) (C) after conditioning CDC/CF with serum-free medium for seven days, measured by trypan blue

staining. D) EV yield measured by particle number per T75 cell culture flask (n ≥ 37, significance test: One-way ANOVA). E) Statistical analysis of particle size in CDC-EV and CF-EV. F-G) Exemplary size distribution of particles in a CDC- and a CF-EV preparation. H) FC analysis of the exosome markers CD63 and CD81 in selected CDC-EV preparations. I-K) MicroRNA (miR) expression analysis in infant /adult CDC-/CF-EVs (n ≥ 5, significance tests performed: One-way ANOVA for homogeneous variances or Welch for inhomogeneous variances.
*Data are represented as mean ± SEM, significance is shown as **: p < 0.01, ***: p < 0.001. Adapted from Suppl. Figure S8 from (148)*

Following EV isolation, *in vitro* functional effects of CDC- and CF-EV on various cardiac cell types were evaluated.

Analysis of *in vitro* angiogenesis was performed with EC tube formation assay on matrigel (matrigel assay) and EC scratch assay (Figure 20 and Figure 21, see paragraphs 4.7.3.1.1 and 4.7.3.1.2 for detailed methods). When grown on ECM such as matrigel, EC are able to differentiate to tube like structures (167), an important prerequisite for vessel formation (168). At the beginning of the experiment, the surface of the cell culture wells was coated with a thin layer of matrigel. In a second step, EC are replated on these wells in different medium preparations. As positive control (PosCtr), EC medium with all provided supplements, which create the optimal conditions for tube formation, was used. Since EV were isolated from cell conditioned serum-free medium, unconditioned serum-free medium was used as negative control (NegCtr) for all assays. Isolated EV samples were diluted with unconditioned medium to achieve consistant concentrations across all samples (experimental scheme in Figure 20A). After overnight incubation with these medium preparations, photographs of the wells were taken and evaluated with ImageJ angiogenesis analyzer tool (97-99, 102) to assess the extent of tube formation. Four selected parameters were normalized to the NegCtr and compared between samples: Number of master junctions, Total master segments length, Total length and Number of pieces. As a proof of principle, I first tested the effect of different concentrations of neonatal CDC-EV. Increasing concentration of neonatal CDC-EV clearly tended to augment EC ability for tube formation (Figure 20B-E). The experiments with adult CDC-and CF-EV, as well as infant CDC- and CF-EV were performed. Compared to the NegCtr, EC tube formation was significantly promoted by infant CDC-EV only, but not by CF-EV or adult CDC-EV, documented by parameters such as Total length or Number of pieces (sum of length or number of segments, isolated elements and branches detected in the analyzed area, respectively) (Figure 20F-J). (Kogan *et al*., submitted manuscript 2020, (148))

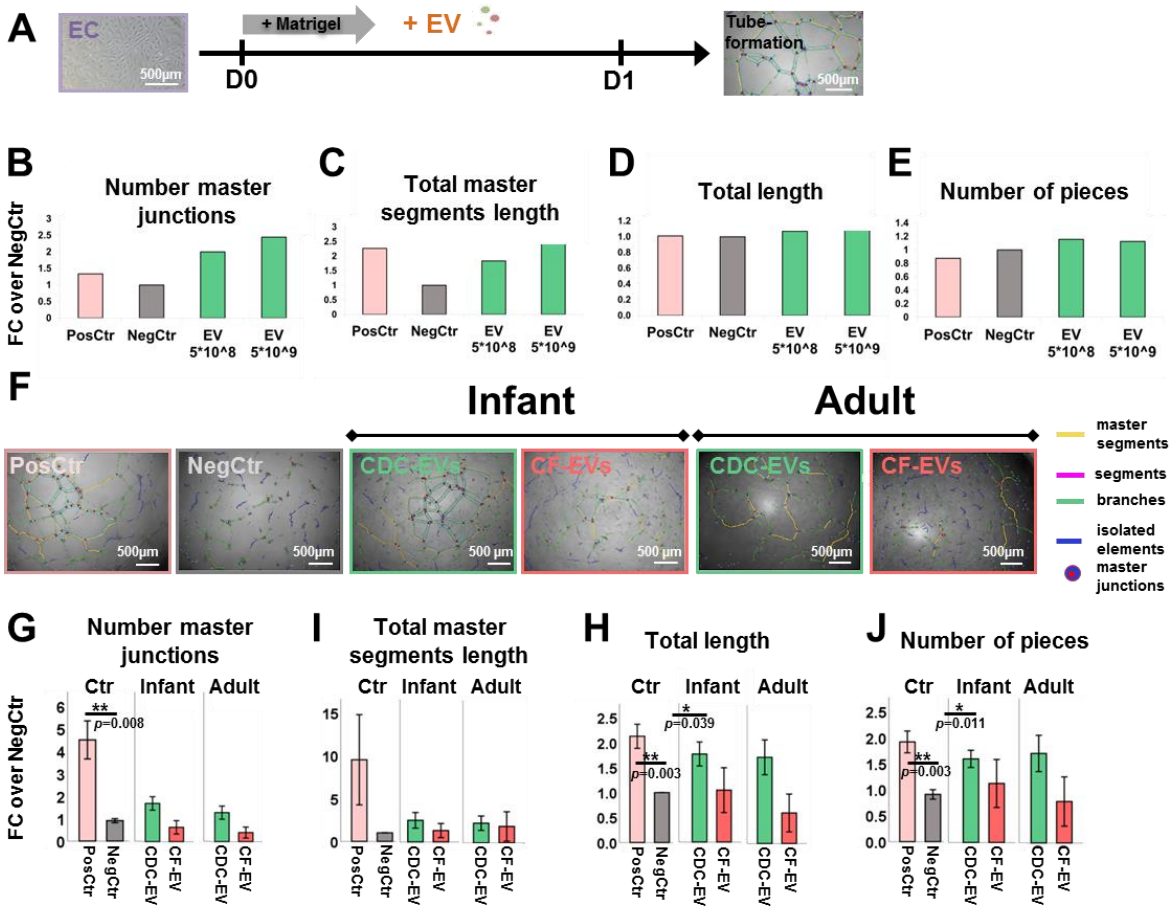

Figure 20: Tube formation assay on matrigel.

*Abbreviations: EC: endothelial cells, CDC: cardiosphere-derived cells; CF: cardiac fibroblasts, EV: extracellular vesicles. A) Experimental outline. B-E) Neonatal patient derived CDC-EV preparations of different concentrations (particle number per 96 well) were evaluated for the different parameters of the matrigel-assay (n = 1). The software Angiogenesis Analyzer (ImageJ (97-99)) highlights structures such as master segments, branches, isolated elements and master junctions (see legend of F) and calculates the number of master junctions in the analyzed area ("number of master junctions"), the sum of length of segments, isolated elements and branches in the analyzed area ("Total length"), the sum of the length of the detected master segments in the analyzed area. ("Total master segments length") and the sum of number of segments, isolated elements and branches detected in the analyzed area ("number of pieces"). F) Exemplary pictures of the positive control (PosCtr, EC medium with supplements), negative control (NegCtr, serum-free medium) and serum-free medium supplemented with infant/adult CDC-/CF-EV at the end of the matrigel assay. G-J) Quantitative analysis of selected parameters which were normalized to the NegCtr (fold change over NegCtr, "FC over NegCtr"), so that different assays could be compared, n ≥ 4, exact sample numbers for each group are indicated in Table 38, data are represented as mean ± SEM, post-hoc tests: Tukey-HSD/Bonferroni for homogeneous variances or Games-Howell-test/Dunnett-T3-test for inhomogeneous variances, significance is shown as *: p < 0.05, **: p < 0.01, complete overview of significance tests is shown in Table 39. Adapted from Figure 5 from (148)*

Another important angiogenic property is the migratory ability of EC. In a so-called scratch assay, a dense EC layer was first treated with mitomycin C for 2h to prevent proliferation allowing the evaluation of cell migration only. Then, a scratch was conducted in the EC-layer. Subsequently, over a time period of 48h, EC were incubated with EC growth medium (PosCtr), serumfree medium (NegCtr) or serumfree medium supplemented with infant /adult CDC-/CF-EV. Using the IncuCyte ZOOM® 96-Well Migration Assay system, the closure of the scratch was recorded in one-hour intervals (Figure 21A). First, as a proof of principle, neonatal CDC-EV concentration series revealed a dose-dependent paracrine influence of CDC on EC migration (Figure 21B-E). For the final experiments, similarly to the matrigel assay, only infant CDC-EV significantly promoted EC migration compared to the NegCtr at 12h and 24h after the scratch was made (Figure 21F-H). Yet, no significant difference between CDC-EV and CF-EV was observed in both assays. (Kogan *et al.*, submitted manuscript 2020, (148))

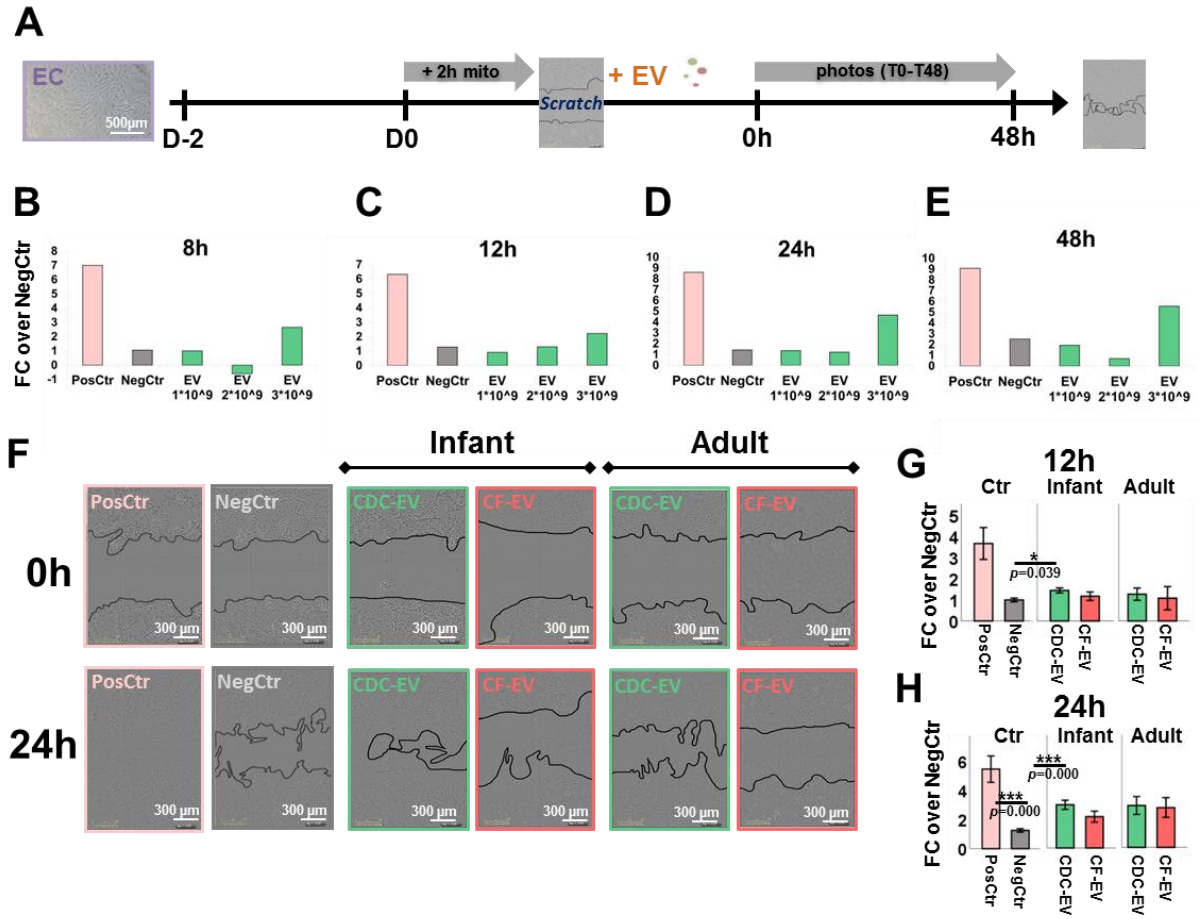

Figure 21: Endothelial Cell Migration assay (EC scratch assay)

Analyzed cell types are abbreviated as follows: EC: endothelial cells, CDC: cardiosphere-derived cells; CF: cardiac fibroblasts. A) Experimental outline, B-E) Concentration series performed with neonatal patient derived CDC-extracellular vesicles (EV) preparations of different concentrations (particle number per 96 well) at 8h, 12h, 24h and 48h after the scratch (n = 1). F) Exemplary pictures of the positive control

*(PosCtr, EC medium with supplements), negative control (NegCtr, serum-free medium), and Infant /Adult CDC- and CF-EV preparations at 0h and 24h after the scratch. G-H) Comparison of difference of cell-free area between the 12h (G) or 24h (H) and 0h after the scratch normalized to the according NegCtr (fold change to NegCtr, "FC over NegCtr"), n ≥ 4, exact sample numbers for each group are indicated in Table 38, data are represented as mean ± SEM, post-hoc tests: Tukey-HSD/Bonferroni for homogeneous variances or Games-Howell-test/Dunnett-T3-test for inhomogeneous variances, significance is shown as *: p < 0.05, **: p < 0.01, ***: p < 0.001, exact significances including the used test are indicated in Table 39. Adapted from Figure 5 from (148)*

Since the ability of CDC-EV to decrease cardiomyocyte apoptosis was reported in several studies (80, 85), an appropriate *in vitro* assay with neonatal rat cardiomyocytes (NRCM) was developed. As a quality control, NRCM were first checked for the presence of cardiomyocyte markers such as α-Actinin, TropT, Cx43, α-MHC and Tnni by ICC (Figure 22A). Gene expression of *Tnnt2* (TropT) was significantly higher in NRCM compared to murine cardiac fibroblasts (mCF), measured by qRT-PCR (Figure 22B). As a further quality control of NRCM, it was controlled if NRCM were beating before starting an experiment. After induction of apoptosis by incubation with cobalt chloride, NRCM were incubated with either NRCM growth medium (PosCtr), serumfree medium (NegCtr) or serumfree medium supplemented with infant/adult CDC/CF-EV for 2 days. Finally, the extent of the anti-apoptotic effect of CDC- and CF-EV on NRCM was assessed by gene expression of the death surface receptor *Fas* (169) (Figure 22C). Before final experiments, a concentration series revealed that NRCM apoptosis was not decreased by CDC-EV, but a trend for decrease was observed when applying highly concentrated CF-EV (Figure 22D-E). Final experimental results approved that neither infant nor adult CDC-EV significantly reduced apoptosis of NRCM compared to the NegCtr, in contrast to adult CF-EV. Besides, a significant difference between adult CDC- and adult CF-EV was observed (Figure 22F). (Kogan *et al.*, submitted manuscript 2020, (148))

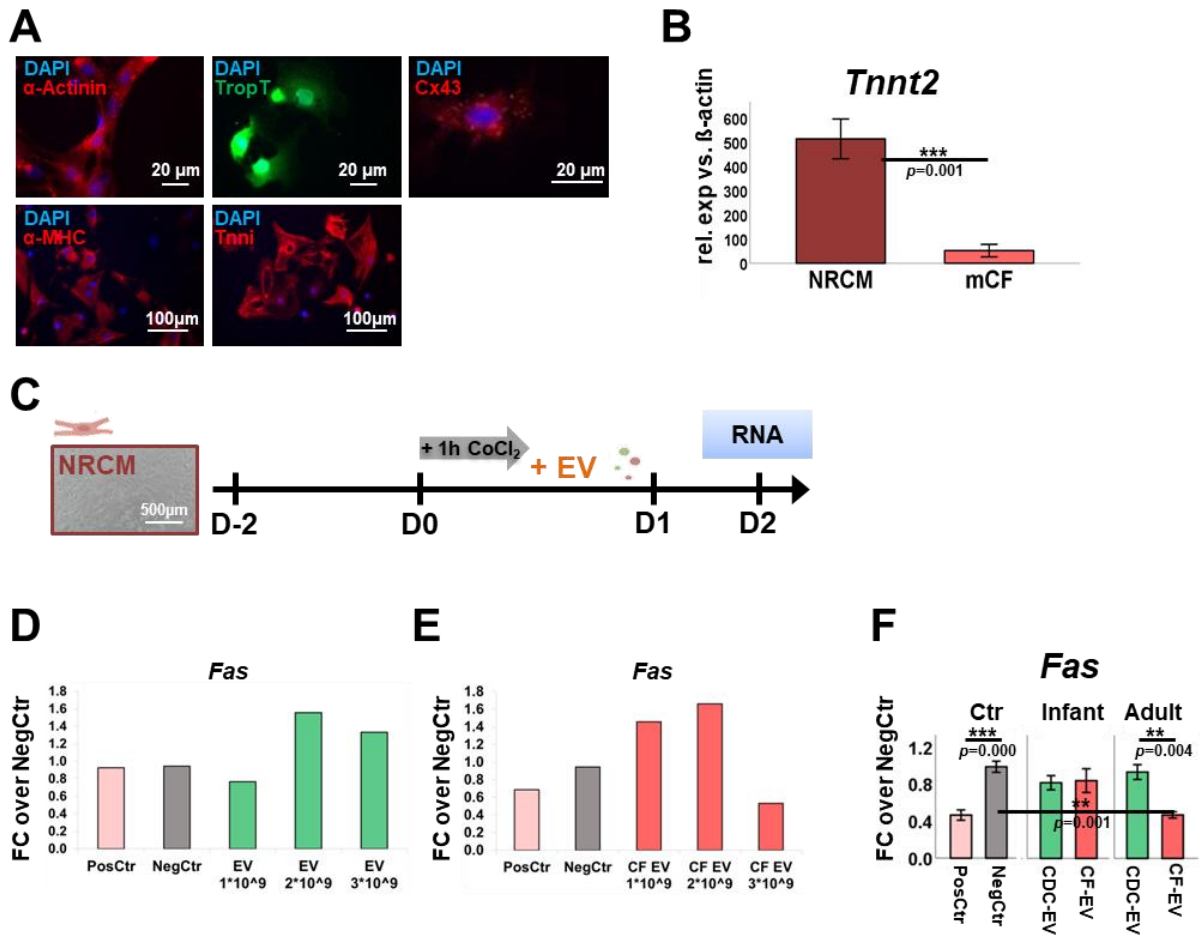

Figure 22: Neonatal rat cardiomyocytes (NRCM) apoptosis assay.

*Abbreviations: NRCM: neonatal rat cardiomyocytes, mCF: murine cardiac fibroblasts, EV: extracellular vesicles, CDC: cardiosphere-derived cells; CF: cardiac fibroblasts. A) Immunocytochemical analysis of the cardiomyocyte markers α-Actinin, TropT, Cx43, α-MHC and Tnni in NRCM, B) Gene expression analysis of the cardiomyocyte marker Tnnt2 in NRCM compared to murine cardiac fibroblasts (mCF) used as negative control (n ≥ 6). C) Experimental outline. D-E) Concentration series for NRCM apoptosis assay performed with adult CDC- (D) and CF- EV (E). F) Expression analysis (measured by qRT-PCR) of the apoptosis marker FAS in NRCM at the end of the test. Relative expression to β-ACTIN (ACTB) was normalized to according NegCtr (fold change to NegCtr, "FC over NegCtr"), n ≥ 6, exact sample numbers for each group are indicated in Table 38, data are represented as mean ± SEM, post-hoc tests: Tukey-HSD/Bonferroni for homogeneous variances or Games-Howell-test/Dunnett-T3-test for inhomogeneous variances, significance is shown as **: p < 0.01, ***: p < 0.001, an overview of significance tests can be found in Table 39. Adapted from Suppl. Figure S9 from (148)*

Anti-fibrotic properties of CDC-EV had been reported in different experimental settings (79, 80, 85). Therefore, we further analyzed the effect of CDC-EV and CF-EV derived from patients with different ages on CF. In analogy to EC described above (see Figure 21) a scratch assay was

performed in confluent CF cell layers. The experimental procedure differed only in the usage of fibroblast medium as PosCtr (Figure 23A). In first tests with different concentrations of EV, CF migration tended to increase when applying high concentration of neonatal CDC-EV (Figure 23B-D). However, no age- or cell type-related significant difference was observed between infant or adult CDC-/CF-EV groups at the analyzed time points (Figure 23E-F). At the end of the assay, further gene expression of the collagens *COL1A1* and *COL3A1* was measured, revealing no significant change upon incubation with CDC-EV derived from the infant or the adult age group (Figure 23G-H). As one previous study reported that CDC-EV decreased proliferation of CF (85), MTT assays (146) were performed with CF incubated either with their normal growth medium (PosCtr), serum-free medium (NegCtr) or serum-free medium supplemented with infant CDC-EV (Figure 23I). Surprisingly, infant CDC-EV significantly increased proliferation of CF compared to NegCtr (Figure 23J). (Kogan *et al*., submitted manuscript 2020, (148))

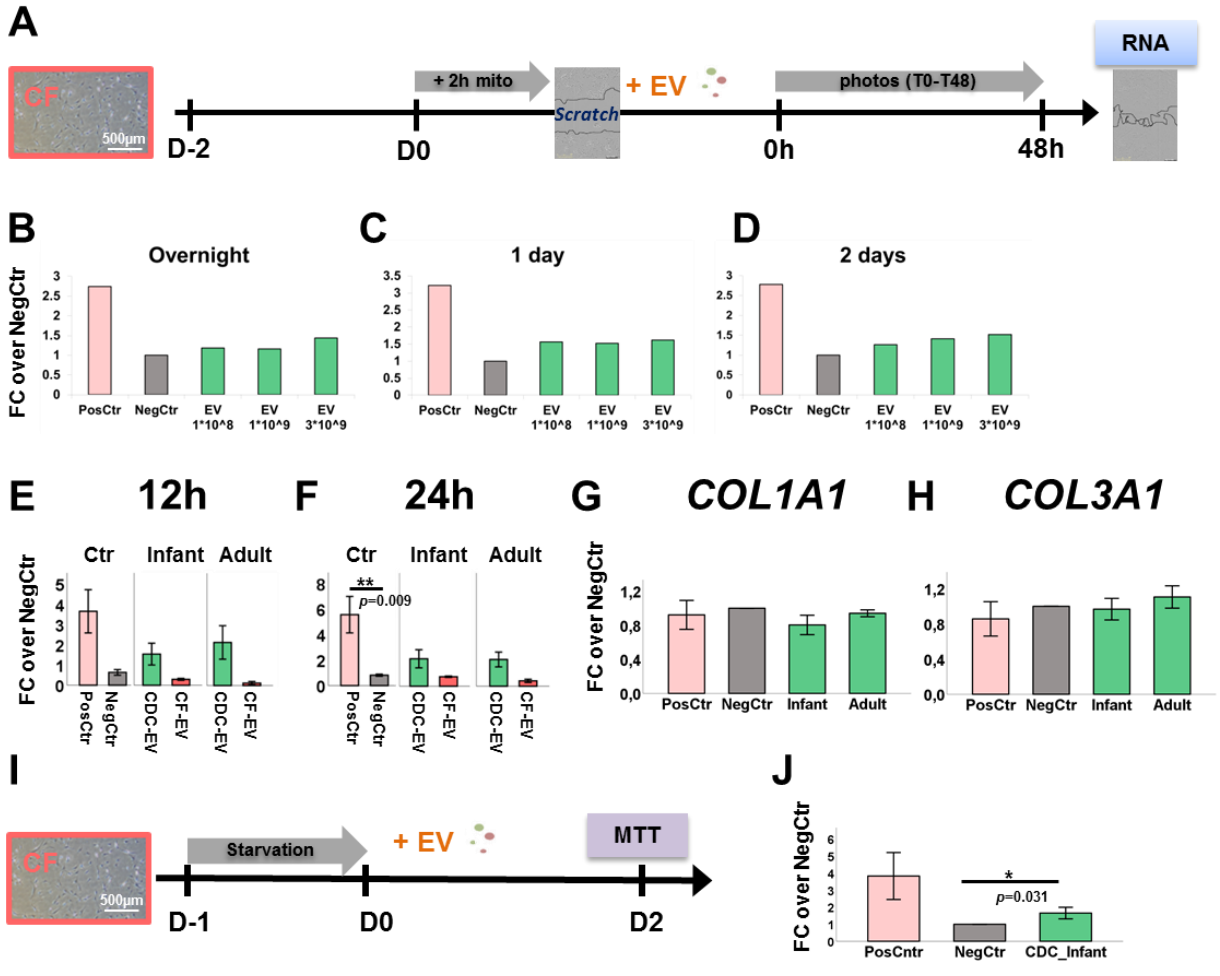

Figure 23: Effects of CDC-/CF-EV on CF - CF migration and proliferation assays.
Abbreviations: CDC: cardiosphere-derived cells; CF: cardiac fibroblasts, EV: extracellular vesicles. A) Experimental outline for migration assays. B-D) Concentration (particles per 96 well) series for CF scratch assay was analyzed with neonatal CDC-EV overnight (B), 1 day (C) or 2 days (D) after performing the

scratch. E-F) Comparison of difference of cell-free area between 12h (E)/24h (F) and 0h after the scratch normalized to the according negative control (fold change to negative control, "FC over NegCtr"), (n ≥ 2) G-H) Gene expression analysis by qRT-PCR of COL1A1 (G) and COL3A1 (H) in CF at the end of the migration test. Relative expression was normalized to β-ACTIN and to the according NegCtr (fold change to NegCtr, "FC over NegCtr"), n ≥ 5). I-J) ***Proliferation assay of CF (MTT assay)*** *I) Experimental outline. J) Absorbance of CF lysates after MTT assay normalized to the according NegCtr (fold change to NegCtr, "FC over NegCtr"), n ≥ 3.*
*Data are represented as mean ± SEM, exact numbers of samples are indicated in Table 38, post-hoc tests: Tukey-HSD/Bonferroni for homogeneous variances or Games-Howell-test/Dunnett-T3-test for inhomogeneous variances, significance is shown as *: p < 0.05, **: p < 0.01, exact significances and statistical tests are indicated in Table 39. Adapted from Suppl. Figure S9 from (148)*

To conclude, infant but not adult CDC-EV promoted angiogenesis and proliferation of CF. CF-EV of the infant group did not replicate the effects of age-matched CDC-EV. However, CDC-EV did not reduce CF migration, CF proliferation or NRCM apoptosis.

5.2.3 Comparison of CDC and CF derived from two infant age groups

As an age-dependent effect of CDC has previously been described for pediatric patients (67), the CDC/CF gene expression profile and *in vitro* EV effects of two infant age-groups (termed HLH1 and HLH2/3, see age groups 1 and 2 in Table 15) were compared. Even though not only HLHS patients were included due to the rarity of this disease (92, 93), the patients analyzed were chosen according to the age of HLHS patients when undergoing the first surgical procedure (Norwood I, termed HLH1, age: 5-21 days) and the second or third surgical palliation procedures (termed: HLH2/3, age: 1 month-6 years), see experimental scheme in Figure 24A.

Figure 24B-D shows the gene expression analysis (qRT-PCR) of both infant age groups. Significant difference between CDC and CF was observed in both age groups for the cardiac TFs *GATA4*, *TBX5* (Figure 24B), fibrobast marker *THY1* (*CD90*) (Figure 24C) and the CDC-typical miR-146a-5p (Figure 24D), as already observed in the analysis of the whole infant patient group (Figure 16). However, the markers *DDR2* and *ALDH1A2* were significantly differently regulated between CDC and CF in the HLH1 age group only (Figure 24C). None of the markers analyzed was significantly differentialy regulated between HLH1- and HLH2/3-CDC. Nevertheless, age-related differences were observed in the expression of *TBX5* (Figure 24B) and *THY1* (*CD90*) (Figure 24C) in CF. The expression patterns of *NKX2-5* (Figure 24B), miR-21 (Figure 24C) and miR-132-3p (Figure 24D) showed neither age- nor celltype-related differences between HLH1- and HLH2/3 patients.

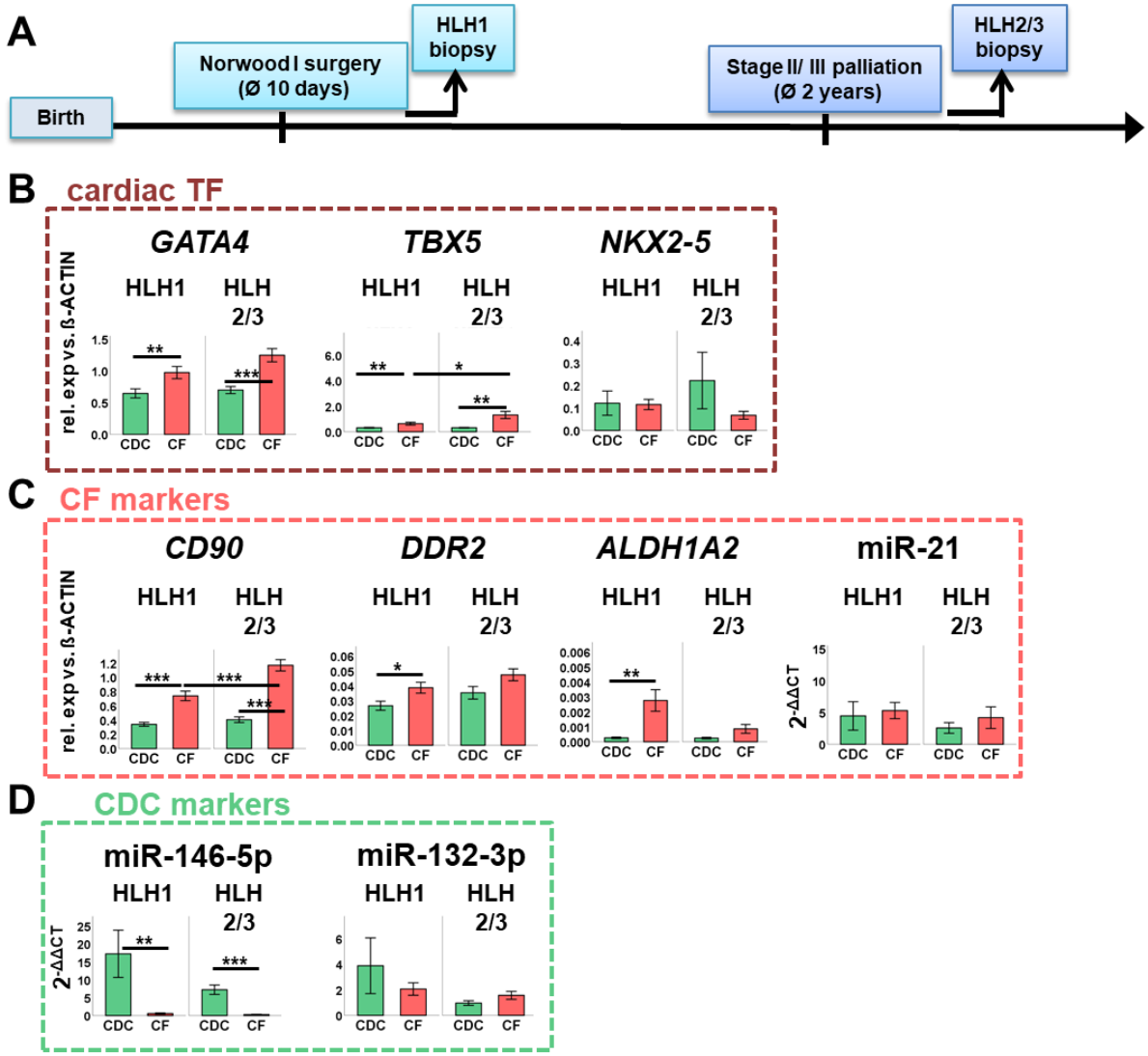

Figure 24: Gene expression analysis of two infant age groups and the adult group.

Analyzed cell types are abbreviated as follows: CDC: cardiosphere-derived cells; CF: cardiac fibroblasts. A) Experimental outline of acquisition of biopsy samples of HLH1- (5-21 days, see age group 1 in Table 15) and HLH2/3-patients (1 month-6 years, see age group 2 in Table 15). B-D) qRT-PCR analysis of CDC- and CF samples derived from HLH1- and HLH2/3- patients for B) cardiac transcription factors (TFs), C) CF markers and D) CDC typical microRNAs (miRs).

*Data are represented as mean ± SEM, n ≥ 6, post-hoc tests: Tukey-HSD/Bonferroni for homogeneous variances or Games-Howell-test/Dunnett-T3-test for inhomogeneous variances, significance is shown as *: p < 0.05, **: p < 0.01, ***: p < 0.001, exact significances and statistical tests are indicated in Table 39.*

Figure 25 illustrates the results of tube formation assay when comparing both infant age groups. As documented by photographs at the end of the assay, EC incubated with HLH2/3-CF-EV samples hardly built any tube-like structures compared to HLH1-CF-EV or NegCtr (Figure 25A).

Therefore, no values could be retrieved for those samples by ImageJ angiogenesis analyzer tool (102), so parameters had to be set to 0. Figure 25B-E shows the statistical evaluation of selected parameters for the comparison of both infant age groups. Unlike the whole infant CDC-EV group (Figure 20G-J), either HLH1-CDC-EV or HLH2/3-CDC-EV significantly promoted tube formation compared to the NegCtr as measured by the parameters shown (Figure 25B-E). However, for the parameter Number of pieces, significance was reached when comparing NegCtr to HLH2/3-CF-EV, since the latter group contained samples preventing tube formation (Figure 25D).

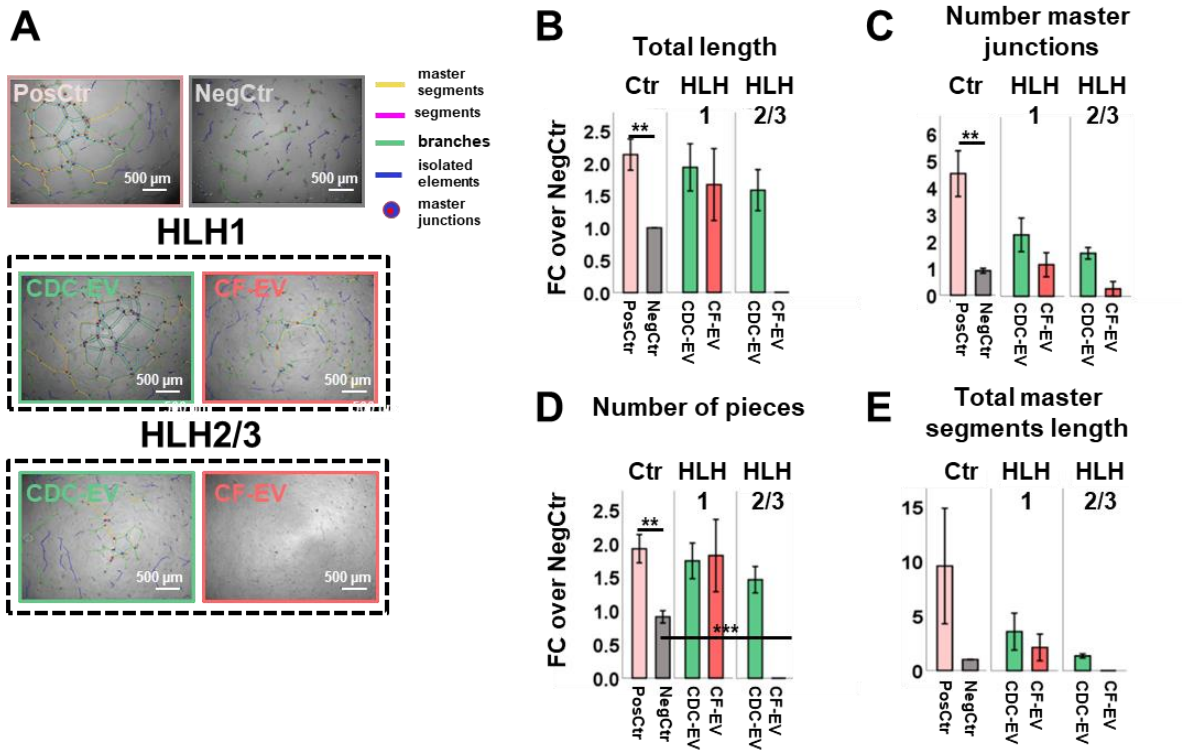

Figure 25: Comparison of two infant age groups and the adult group in the tube formation assay.
*Abbreviations: CDC: cardiosphere-derived cells; CF: cardiac fibroblasts; EV: extracellular vesicles. A) Exemplary pictures of PosCtr, NegCtr and serum-free medium supplemented with HLH1- (patients group at the age of 5-21 days, see age group 1 in Table 15) or HLH2/3- (patients group at the age of 1 month-6 years, see age group 2 in Table 15) CDC-/CF-extracellular vesicles (EV) at the end of the matrigel assay. B-C) Quantitative analysis of selected parameters normalized to the respective negative control (NegCtr, fold change over NegCtr, "FC over NegCtr"), so that samples across different assays could be compared; $n \geq 3$, exact numbers of samples per group are indicated in Table 38, data are represented as mean ± SEM, post-hoc tests: Tukey-HSD/Bonferroni for homogeneous variances or Games-Howell-test/Dunnett-T3-test for inhomogeneous variances, significance is shown as *: $p < 0.05$, **: $p < 0.01$, ***: $p < 0.001$, exact significances and statistical tests are indicated in Table 39.*

HLH1-CDC-EV significantly induced EC migration at all evaluated timepoints, namely 12h, 24h and 48h after the scratch (Figure 26A-C). This was not observed for HLH2/3-CDC-EV. Differences between CDC-EV and CF-EV were not evident.

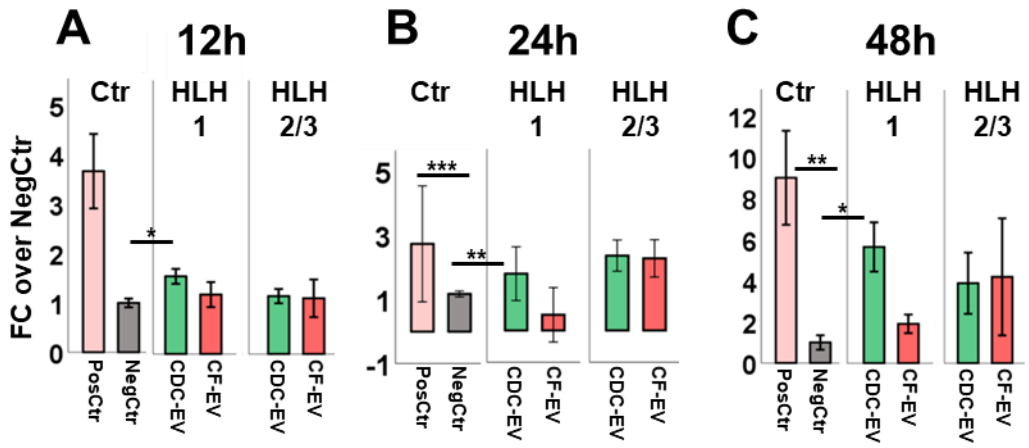

Figure 26: Comparison of two infant age groups in the EC scratch assay.

*Analyzed cell types are abbreviated as follows: CDC: cardiosphere-derived cells; CF: cardiac fibroblasts. A-C) Quantitative analysis of endothelial cell (EC) scratch assay results. EC wells incubated with either PosCtr, NegCtr or and serum-free medium supplemented with HLH1- (5-21 days, see age group 1 in Table 15) and HLH2/3- (1 month-6 years, see age group 2 in Table 15) CDC-/CF-extracellular vesicles (EV) were analyzed for the difference of cell-free area betweeb timepoint 0h and the timepoints 12h (A), 24h (B) and 48h (C) after the scratch. Data are represented as mean ± SEM, n ≥ 5, exact numbers of samples per group are indicated in Table 38, post-hoc tests: Tukey-HSD/Bonferroni for homogeneous variances or Games-Howell-test/Dunnett-T3-test for inhomogeneous variances, significance is shown as *: p < 0.05, **: p < 0.01, ***: p < 0.001, exact significances are indicated in Table 39.*

The results of the NRCM apoptosis assay further emphasized age-dependent differences between HLH1- and HLH2/3-derived primary cells. Whereas no significances were measured between whole infant CF and NegCtr (Figure 22F), splitting the samples into two age groups revealed that HLH2/3-derived CF-EV significantly reduced NRCM apoptosis. Neither HLH1-CDC-EV nor -CF-EV had influence on NRCM apoptosis (Figure 27). An overview of statistical parameters of the age group comparisons can be viewed in Table 38 and Table 39.

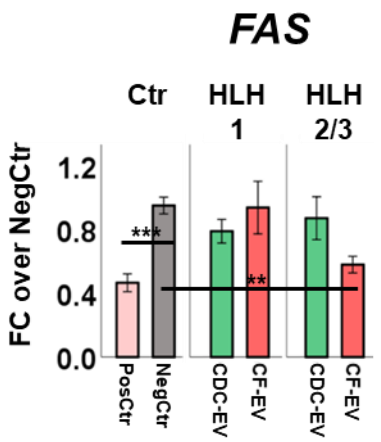

Figure 27: Comparison of two infant age groups in the NRCM assay.
*Analyzed cell types are abbreviated as follows: CDC: cardiosphere-derived cells; CF: cardiac fibroblasts. Expression of FAS was measured in NRCM incubated with either PosCtr, NegCtr or and serum-free medium supplemented with HLH1-, HLH2/3- and adult CDC-/CF-EV, n ≥ 8. Data are represented as mean ± SEM, exact numbers of samples per group are indicated in Table 38, post-hoc tests: Tukey-HSD/Bonferroni for homogeneous variances or Games-Howell-test/Dunnett-T3-test for inhomogeneous variances, significance is shown as *: p < 0.05, **: p < 0.01, ***: p < 0.001, exact significances are indicated in Table 39.*

Table 38: Number of samples (*in vitro* assays with age groups)

Experiment	Cell type	Number of samples per group (n)		
Matrigel assay	CDC	Infant n = 17		Adult n = 7
		HLH1 n = 9	HLH2/3 n = 8	
	CF	Infant n = 8		Adult n = 4
		HLH1 n = 5	HLH2/3 n = 3	
	CFSPh	HLH1 n = 4	-	-
EC Scratch assay	CDC	Infant n = 16		Adult n = 7
		HLH1 n = 11	HLH2/3 n = 5	
	CF	Infant n = 11		Adult n = 4
		HLH1 n = 5	HLH2/3 n = 6	
	CFSPh	HLH1 n = 4		
CF Scratch Assay	CDC	Infant n = 19		Adult n = 10
		HLH1 n = 11	HLH2/3 n = 8	
	CF	Infant n = 9		Adult n = 2
		HLH1 n = 5	HLH2/3 n = 4	
	CFSPh	HLH1 n = 4		
CF Scratch Assay (Gene expression of *COL1A1* and *COL3A1*)	CDC-EV	Infant = 11		Adult = 5
MTT assay	CDC-EV	Infant n = 6		No adult samples
NRCM-Assay	CDC	Infant n = 16		Adult n = 11
		HLH1 n = 8	HLH2/3 n = 8	Adult n = 11

	CF	Infant n = 11		Adult n = 6
		HLH1 n = 8	HLH2/3 n = 3	
	CFSPh	HLH1 n = 5		

Abbreviations: CDC: cardiosphere-derived cells; CF: cardiac fibroblasts, CFSPh: cardiac-fibroblast-sphere-derived cells, HLH1: neonatal patients aged ≤ 21 days (see Table 15), HLH2/3: pediatric patients aged 1 month - 5 years (see Table 15), Matrigel assay: Tube formation assay on matrigel, EC Scratch: EC migration assay, CF Scratch: CF migration assay, NRCM assay: apoptosis test with neonatal rat cardiomyocytes, MTT assay: Proliferation assay of cardiac fibroblasts.

Table 39: Significant differences between age groups and cell types (Figures 16, 20-27)

Marker/ Experiment parameter	Group	Subgroup 1	Subgroup 2	Significance Test	*p*-value
GATA4	Infant	CDC	CF	ANOVA	0.000
	CDC	Infant	Adult	ANOVA	0.012
	HLH1	CDC	CF	Welch-Test	0.007
	HLH2/3	CDC	CF	ANOVA	0.000
NKX2-5	CDC	Infant	Adult	Welch-Test	0.012
	CF	Infant	Adult	Welch-Test	0.000
TBX5	CDC	Infant	Adult	ANOVA	0.001
	Infant	CDC	CF	Welch-Test	0.000
	HLH1	CDC	CF	Welch-Test	0.009
	HLH2/3	CDC	CF	Welch-Test	0.002
	CF	HLH1	HLH2/3	ANOVA	0.027
CD90	Infant	CDC	CF	Welch-Test	0.000
	Adult	CDC	CF	Welch-Test	0.009
	CDC	Infant	Adult	Welch-Test	0.000
	CF	Infant	Adult	Welch-Test	0.000
	HLH1	CDC	CF	Welch-Test	0.000
	HLH2/3	CDC	CF	Welch-Test	0.000
	CF	HLH1	HLH2/3	ANOVA	0.000
DDR2	Infant	CDC	CF	ANOVA	0.005
	HLH1	CDC	CF	ANOVA	0.020
ALDH1A2	Infant	CDC	CF	Welch-Test	0.001
	Adult	CDC	CF	Welch-Test	0.000
	CDC	Infant	Adult	Welch-Test	0.009
	CF	Infant	Adult	ANOVA	0.012
	HLH1	CDC	CF	Welch-Test	0.002
miR-146a-5p	Infant	CDC	CF	Welch-Test	0.001
	HLH1	CDC	CF	Welch-Test	0.017
	HLH2/3	CDC	CF	Welch-Test	0.000
Total length (Matrigel assay)		PosCtr	NegCtr	Games-Howell	0.003
		NegCtr	Infant-CDC-EV	Games-Howell	0.039
Number of master junctions		PosCtr	NegCtr	Dunnett-T3	0.008
Number of pieces (Matrigel assay)		PosCtr	NegCtr	Dunnett-T3	0.003
		NegCtr	Infant	Dunnett-T3	0.011
		NegCtr	HLH2/3-CF-EV	Dunnett-T3	0.000
FAS (NRCM assay)		PosCtr	NegCtr	Dunnett-T3	0.000
	Adult	CDC-EV	CF-EV	Bonferroni	0.004
		NegCtr	Adult-CF-EV	Bonferroni	0.001
		NegCtr	HLH2/3-CF-EV	Dunnett-T3	0.005

12h (EC Scratch)		NegCtr	Infant-CDC-EV	Dunnett-T3	0.039
		NegCtr	HLH1-CDC-EV	Dunnett-T3	0.044
24h (EC Scratch)	Ctr	PosCtr	NegCtr	Bonferonni	0.000
		NegCtr	Infant-CDC-EV	Dunnett-T3	0.000
		NegCtr	HLH1-CDC-EV	Dunnett-T3	0.005
48h (EC Scratch)	Ctr	PosCtr	NegCtr	Tukey-HSD	0.006
	-	NegCtr	HLH1-CDC-EV	Dunnett-T3	0.027
24h (CF Scratch)	Ctr	PosCtr	NegCtr	Tukey-HSD	0.001
MTT assay		NegCtr	Infant-CDC-EV	Dunnett-T3	0.031

Abbreviations: CDC: cardiosphere-derived cells; CF: cardiac fibroblasts, HLH1: neonatal patients aged ≤ 21 days (see Table 15), HLH2/3: pediatric patients aged 1 month- 5 years (see Table 15),Matrigel assay: Tube formation assay on matrigel, NRCM assay: apoptosis test with neonatal rat cardiomyocytes, EC Scratch: EC migration assay, CF Scratch: CF migration assay.

To conclude, HLH1- and HLH2/3-derived CDC did not significantly differ in any of the parameters analyzed. Both HLH1- and HLH2/3-CDC differed from their aged-matched CF in the expression of developmental and CF markers. Nevertheless, HLH1-CDC-EV, but not HLH2/3-CDC-EV promoted EC migration to a significantly higher extent than the NegCtr.

5.2.4 Assessment of sphere-formation as a prerequisite for regenerative characteristics

To examine the hypothesis that CDC develop their properties mainly by the exposure to several growth factors and a three-dimensional formation of spheres, the possibility to achieve a similar cell type when treating CF in the same manner was assessed. Therefore, a protocol in which CF were replated at passage one to poly-D-lysine coated plates and cultivated with the same growth factor mixture as CDC was developed (Figure 28A). In 86% of experiments, this procedure resulted in the formation of spheres which had a similar appearance to CDC-cardiospheres (Figure 28B). Cell layers grown out of replated CF- derived spheres were termed CF-sphere-derived cells (CFSPh, Figure 28A-B). (Kogan *et al*., submitted manuscript 2020, (148))

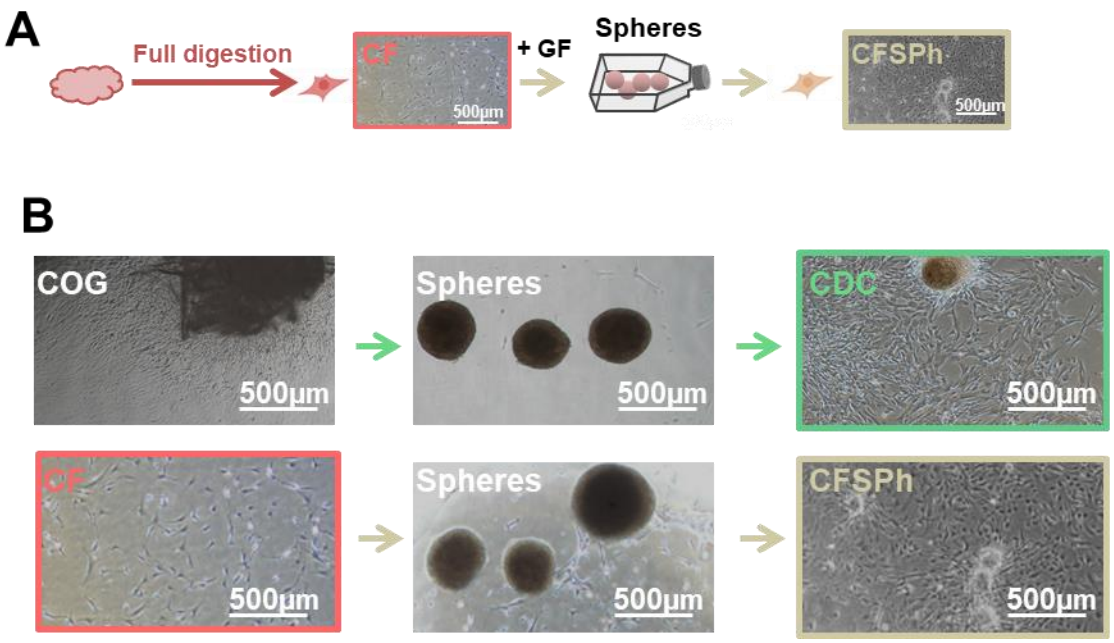

Figure 28: CFSPh cell culture

Abbreviations: CF: cardiac fibroblasts; GF: growth factors; CFSPh: cardiac-fibroblast-sphere-derived cells; COG: cardiac outgrowth; CDC: cardiosphere-derived cells. A) Isolation protocol of CFSPh out of cardiac tissue samples of neonatal patients (age ≤ 21 days, see age group 1, Table 15), B) Exemplary pictures of the three cultivation stages of CDC (top) and CFSPh (bottom). Adapted from Figure 6 and Suppl. Figure S10 from (148)

First, molecular characterization of CFSPh derived from neonatal patients (≤ 21 days) compared to other primary cells of the same age group was performed (Figure 29 and Figure 30).

Similar to CDC, cardiac TF *GATA4* was significantly downregulated in CFSPh compared to CF (Figure 29A, left panel). CFSPh expressed *TBX5* at a level between CDC and CF, but they were not significantly different from one of these cell types (Figure 29A, middle panel). In contrast, *NKX2-5* was expressed in CFSPh even at a significant lower level than in CF (Figure 29A, right panel). The expression of the mesenchymal marker *ENG* (*CD105*) did not significantly differ across the cell types (Figure 29B). CF markers *ALDH1A2* and *THY1* (*CD90)* were upregulated in CF compared to both CDC and CFSPh, however *DDR2* expression of CFSPh, other than that of CDC, did not significantly differ to CF. MiR-21 expression was not significantly different in any of the analyzed cell types derived from neonatal patients (Figure 29C). Similarly, although increased, miR-146a-5p expression of CFSPh did not reach significant difference to CF in contrast to CDC. MiR-132-3p expression showed high deviation between different CDC samples and thus did not reach a significant level to either CFSPh or CF which both expressed miR-132-3p to a similar extent (Figure 29D). (Kogan *et al.*, submitted manuscript 2020, (148))

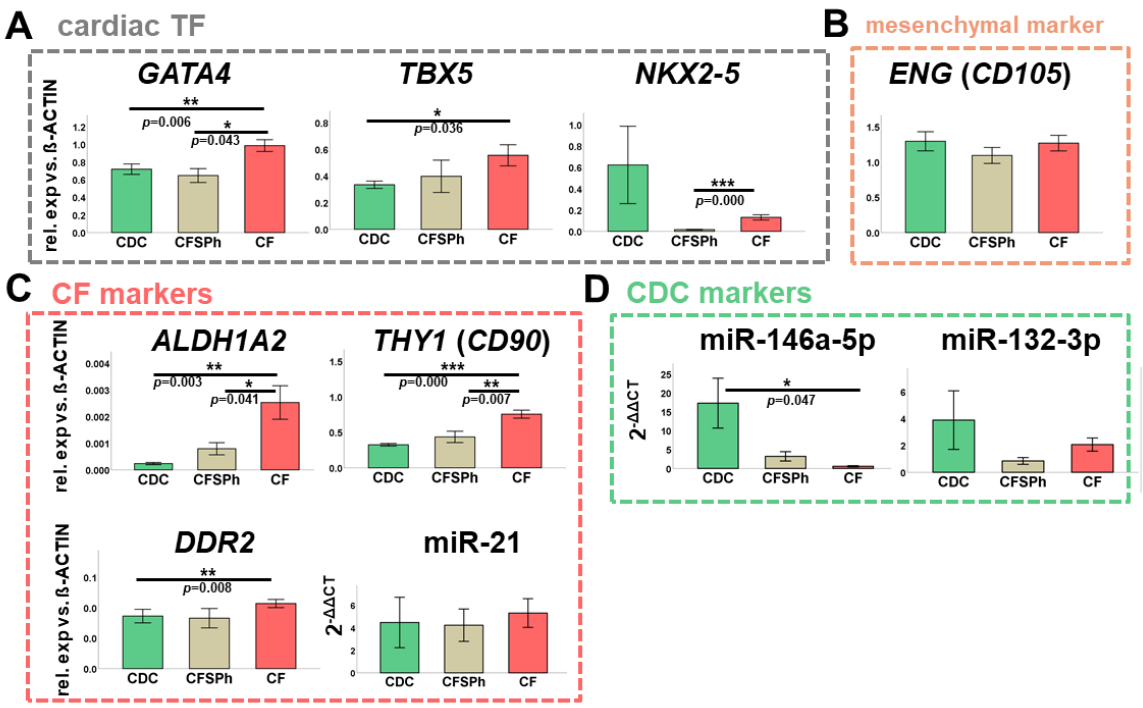

Figure 29: Characterization of CFSPh by gene expression analysis.

*Analyzed cell types are abbreviated as follows: CDC: cardiosphere-derived cells; CFSPh: cardiac-fibroblast-sphere-derived cells; CF: cardiac fibroblasts. Relative gene expression levels versus β-ACTIN (gene symbol: ACTB) by qRT-PCR are illustrated for A) cardiac transcription factors (TFs), B) mesenchymal-, C) CF- and D) CDC markers. Data are represented as mean ± SEM, n ≥ 6, significance is shown as *: p < 0.05, **: p < 0.01, ***: p < 0.001, post-hoc tests: Tukey-HSD/Bonferroni for homogeneous variances or Games-Howell-test/Dunnett-T3-test for inhomogeneous variances, complete overview of significance tests is shown in Table 40. Adapted from Figure 6 and Suppl. Figure S10 from (148)*

Analysis of protein expression by FC showed no significant cell type differences with respect to the frequency of CD105- and CD90- positive cells (Figure 30A-B). ICC showed clear expression of mesenchymal VIM or fibroblast markers, DDR2 and CD90 with no considerable difference between CFSPh and the other analyzed primary cell types (Figure 30C). (Kogan *et al*., submitted manuscript 2020, (148))

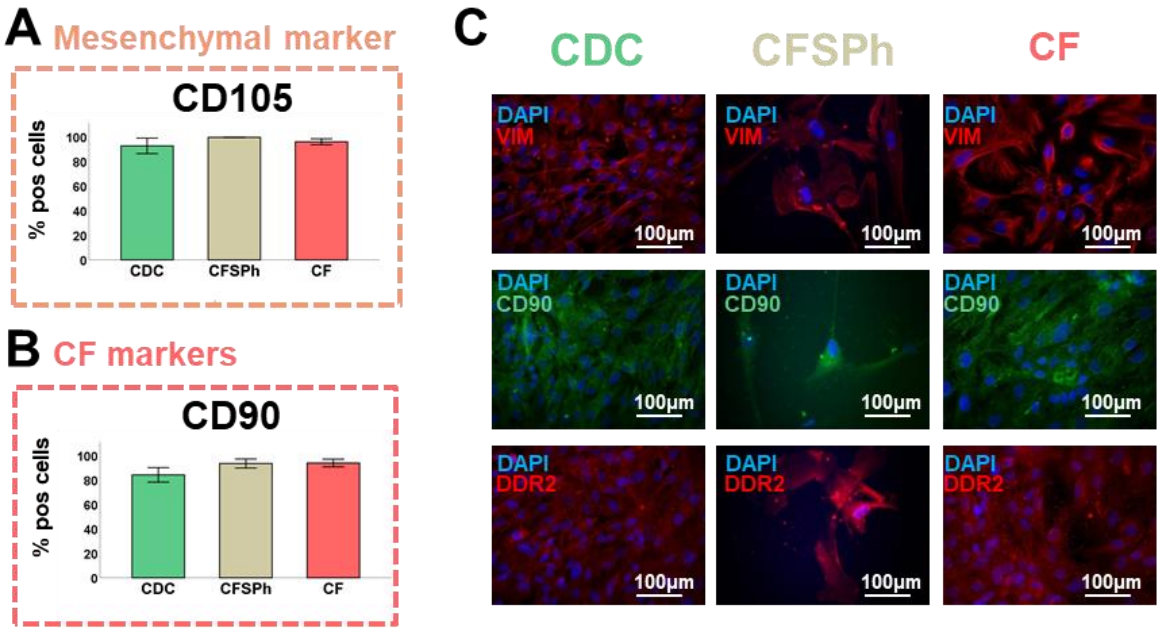

Figure 30: Characterization of CFSPh by FC ICC.

Abbreviation: CF: cardiac fibroblasts.; CDC: cardiosphere-derived cells; CFSPh: cardiac-fibroblast-sphere-derived cells; FC: flow cytometry; ICC: immunocytochemistry.

FC analysis of (A) mesenchymal and (B) CF-markers in CDC, CFSPh and CF. FC data are represented as mean of positive cells of the according marker (n ≥ 2). Data are represented as mean ± SEM, post-hoc tests: Tukey-HSD/Bonferroni for homogeneous variances or Games-Howell-test/Dunnett-T3-test for inhomogeneous variances. C) ICC analysis of DDR2, VIMENTIN (VIM) and CD90 in CDC, CFSPh and CF (n = 1). Adapted from Suppl. Figure S10 from (148)

The same protocol as for isolation of CDC- and CF-EV was used to isolate CFSPh-EV (Figure 19A, paragraph 4.7.1). The percentage of of dead cells and the cell number of CFSPh per T75 flask after conditioning with serum-free medium for seven days did not significantly differ from that of CDC or CF (Figure 31A-B). CFSPh-EV yield (particle number per T75 flask) and their size range was comparable to CDC-EV (Figure 31C-E). By contrast to the whole infant group, miR-146a-5p expression, did not reach significances between CDC- and CF- or CFSPh-EV in the neonatal patient group only (Figure 31F). MiR-132-3p and miR-21 expression analyzed in CFSPh-EV compared to CDC-EV or CF-EV did not show significant differences, respectively (Figure 31G-H). (Kogan *et al*., submitted manuscript 2020, (148))

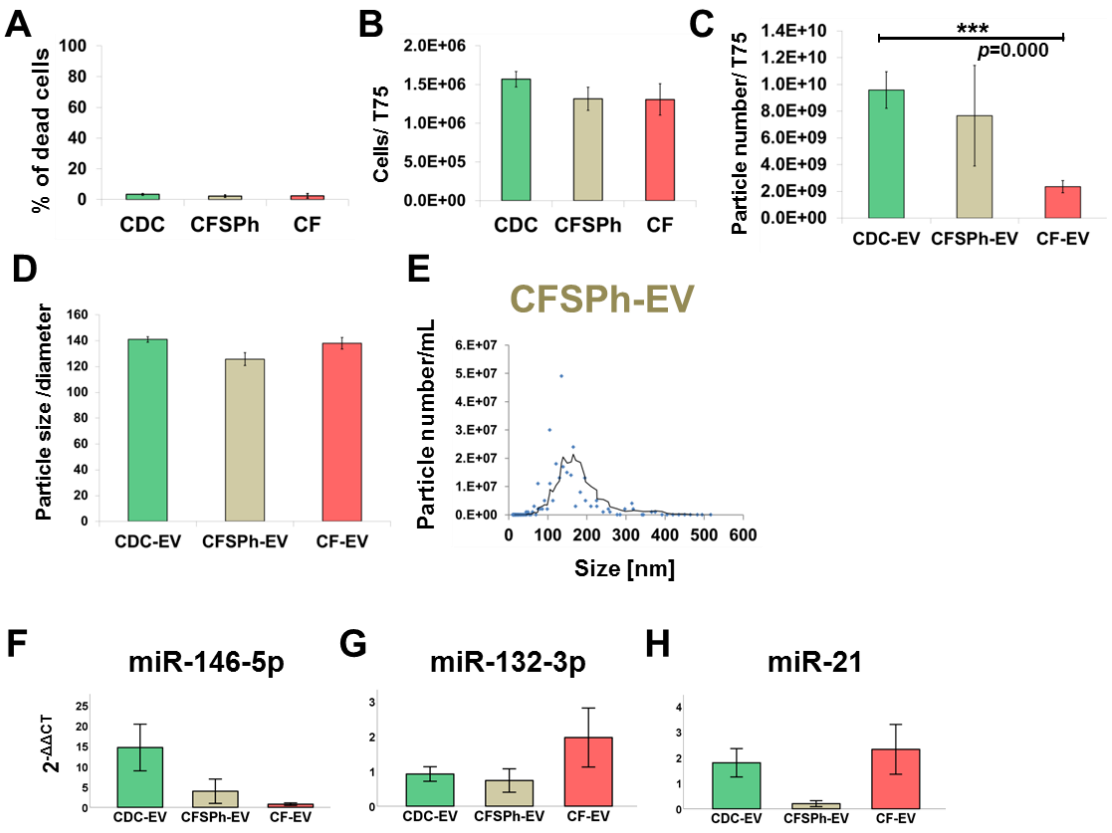

Figure 31: EV Characterization of CFSPh-EV.

*Analyzed cell types are abbreviated as follows: CDC: cardiosphere-derived cells; CFSPh: cardiac-fibroblast-sphere-derived cells; CF: cardiac fibroblasts. A-B) Percentage of dead cells (n ≥ 3) (A) and cell number per T75 cell culture flask (n ≥ 10) (B) of CDC, CFSPh and CF after conditioning with serum-free medium for seven days. C) Extracellular vesicles (EV) yield measured in particle number per T75 flask (n ≥ 7, statistical test: Dunnett-T3, ***: p < 0.001). D) Statistical analysis of particle size of CDC-EV, CFSPh-EV and CF-EV. E) Exemplary size distribution of particles in a CFSPh-EV preparation. F-H) MicroRNA (miR) expression analysis in CDC-/CFSPh-/CF-EV (n ≥ 3).*

Bar diagrams show mean ± SEM, post-hoc tests: Tukey-HSD/Bonferroni for homogeneous variances or Games-Howell-test/Dunnett-T3-test for inhomogeneous variances. Adapted from Suppl. Figure S10 from (148)

Finally, CDC-, CF- and CFSPh-EV derived from neonatal patients (≤ 21 days) were compared to evaluate their paracrine functional effects assessed by the same *in vitro* assays as described in paragraph 5.2.2 (matrigel assays, EC/CF-scratch assays and NRCM assays). CFSPh-EV did not have a significantly higher potential than the NegCtr to augment angiogenesis in the matrigel assay (Figure 32A-E) or in the EC scratch assay (Figure 32F-J, see Figure 21F for pictures of EC medium with supplements used as PosCtr). In contrast, CDC-EV of the corresponding age group increased EC migration at 8h, 24h and 48h after the scratch compared to NegCtr (Figure 32G-J). (Kogan *et al.*, submitted manuscript 2020, (148))

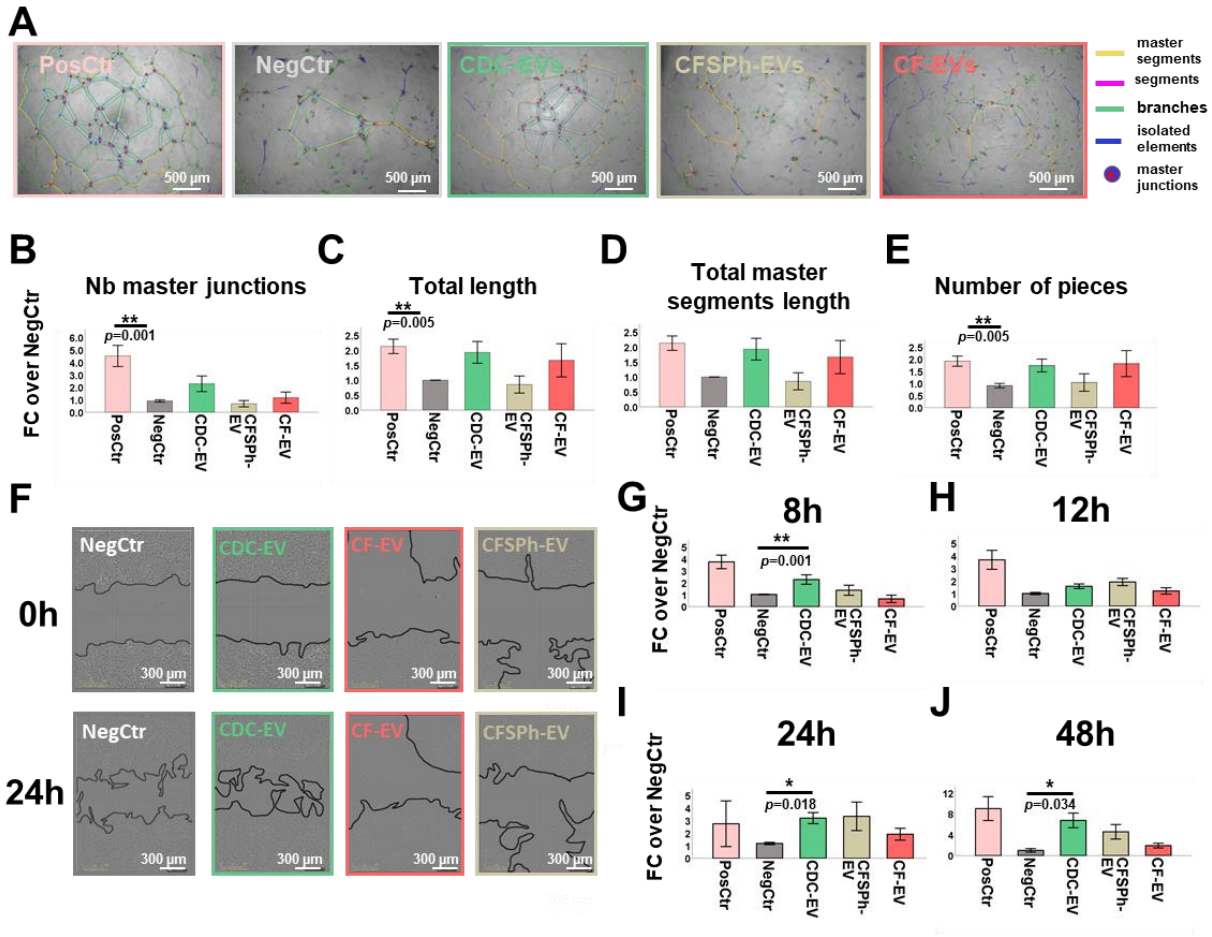

Figure 32: Angiogenesis assays with CFSPh-EV.

Analyzed cell types are abbreviated as follows: CDC: cardiosphere-derived cells; CFSPh: cardiac-fibroblast-sphere-derived cells; CF: cardiac fibroblasts. ***Matrigel assay:*** *A) Exemplary pictures of the positive control (PosCtr, EC medium with supplements), the negative control (NegCtr, serum-free medium) or CDC-, CFSPh- and CF-EV at the end of the matrigel assay. B-E) Quantitative analysis of selected parameters which were normalized to the respective NegCtr (fold change to NegCtr, "FC over NegCtr"), so that different assays could be compared, n ≥ 4.* ***EC-scratch assay:*** *F) Exemplary pictures of incubated with the negative control (NegCtr, serum-free medium), and CDC-, CFSPh- and CF-EV preparations at 0h and 24h after the scratch. G-J) Comparison of difference of cell-free area between 8h (G), 12h (H), 24h (I) and 48h (J) and 0h after the scratch normalized to the according NegCtr (fold change to NegCtr, "FC over NegCtr"), n ≥ 4. Exact numbers of samples per group are indicated in Table 38. Data are represented as mean ± SEM, significance is shown as *: p < 0.05, **: p < 0.01, post-hoc tests: Tukey-HSD/Bonferroni for homogeneous variances or Games-Howell-test/Dunnett-T3-test for inhomogeneous variances, complete overview of significance tests is shown in Table 40. Adapted from Figure 6 from (148)*

Further, no significant alteration of CF migration (Figure 33A-C) or reduction of NRCM apoptosis was observed by CFSPh-EV (Figure 33D) which is in line with the results for CDC- and CF-EV. (Kogan *et al*., submitted manuscript 2020, (148))

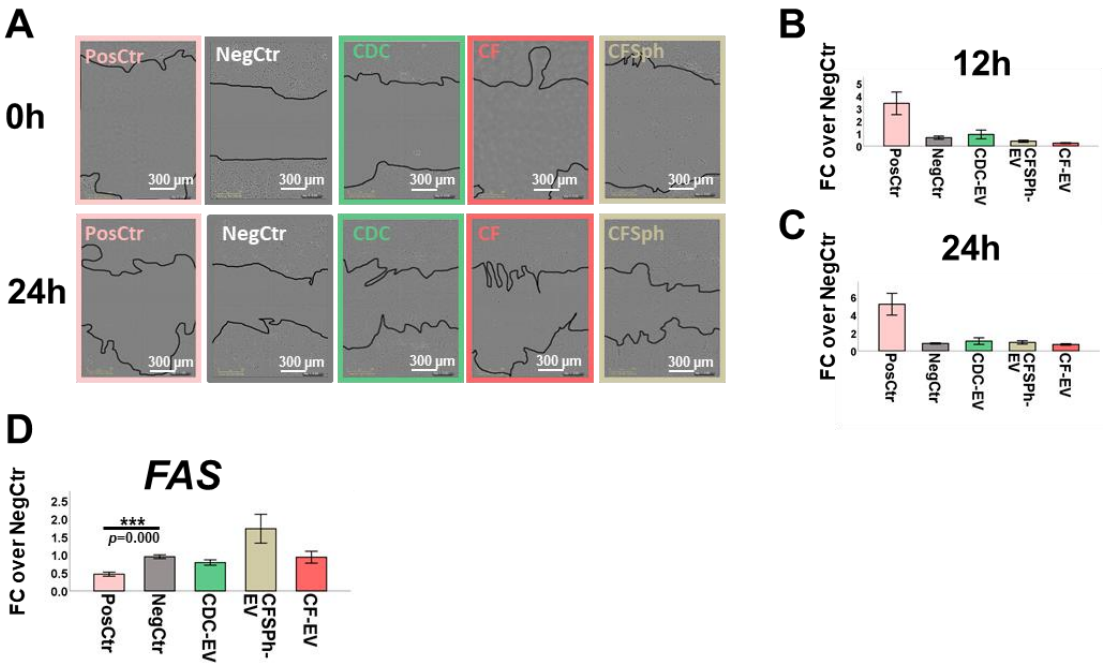

Figure 33: CF migration assay and neonatal rat cardiomyocytes (NRCM) assay with CFSPh.

*Analyzed cell types are abbreviated as follows: CDC: cardiosphere-derived cells; CFSPh: cardiac-fibroblast-sphere-derived cells; CF: cardiac fibroblasts. A) Exemplary pictures of CF incubated with MEF medium (PosCtr), serum-free medium (NegCtr,), CDC-, CFSPh- and CF-extracellular vesicles (EV) in serum-free medium at 0h and 24h after the scratch. B-C) Comparison of difference of cell-free area between 12h (B)/24h (C) and 0h after the scratch normalized to the according NegCtr (fold change to NegCtr, "FC over NegCtr"), n ≥ 4. D) Apoptosis test on NRCM. Gene expression analysis (by qRT-PCR) of the apoptosis marker FAS in NRCM at the end of the test. Relative expression to β-Actin was normalized to the according NegCtr (fold change to NegCtr, "FC over NegCtr"), n ≥ 5, significance is shown as ***: p < 0.001, statistical test: Tukey-HSD.*

Exact numbers of samples per group are indicated in Table 38, post-hoc tests: Tukey-HSD/Bonferroni for homogeneous variances or Games-Howell-test/Dunnett-T3-test for inhomogeneous variances, complete overview of significance tests is shown in Table 40, data are represented as mean ± SEM. Adapted from Suppl. Figure S10 from (148)

Table 40: Significant differences between neonatal cell types (Figures 29, 32, 33)

Marker/ Experiment parameter	Cell group 1	Cell group 2	Significance Test	*p*-value
GATA4	CDC	CF	Tukey-HSD	0.006
	CFSPh	CF	Tukey-HSD	0.043
TBX5	CDC	CF	Dunnett-T3	0.036
NKX2-5	CFSPh	CF	Dunnett-T3	0.000
ALDH1A2	CDC	CF	Dunnett-T3	0.003
	CFSPh	CF	Dunnett-T3	0.041
***THY1* (*CD90*)**	CDC	CF	Dunnett-T3	0.000
	CFSPh	CF	Dunnett-T3	0.007
DDR2	CDC	CF	Tukey-HSD	0.008

miR-146a-5p	CDC	CF	Dunnett-T3	0.047
Number of master junctions (Matrigel assay)	PosCtr	NegCtr	Dunnett-T3	0.001
Total length (Matrigel assay)	PosCtr	NegCtr	Games-Howell	0.005
Number of pieces (Matrigel assay)	PosCtr	NegCtr	Dunnett-T3	0.005
8h (EC Scratch)	NegCtr	CDC-EV	Tukey-HSD	0.001
24h (EC Scratch)	NegCtr	CDC-EV	Dunnett-T3	0.018
48h (EC Scratch)	NegCtr	CDC-EV	Dunnett-T3	0.034
***Fas* (NRCM assay)**	PosCtr	NegCtr	Dunnett-T3	0.000

Abbreviations: CDC: cardiosphere-derived cells; CF: cardiac fibroblasts; CFSPh: cardiac-fibroblast-sphere-derived cells; Matrigel assay: Tube formation assay on matrigel; EC Scratch: EC migration assay; CF Scratch: CF migration assay; NRCM assay: apoptosis test with neonatal rat cardiomyocytes.

In summary, incubation of CF with growth factors and their cultivation in three-dimensional culture conditions, rendered them more similar to CDC with respect to their gene expression, but did not augment their EV-mediated angiogenesis potential to the level of CDC-EV.

5.3 Non-myocyte cells directly derived from a fresh cardiac biopsy

It has been reported that prolonged exposure of primary cells to cell culture conditions alters their gene expression profiles (170). In order to overcome this bias, sc-RNAseq of freshly isolated NMC of a cardiac biopsy was performed. The biopsy was obtained from the left atrial appendage of a patient suffering from biatrial tumor and mitral valve insufficiency (for detailed patient data see patient 22 in Table 14).

5.3.1 Characterization of cardiac biopsy derived non-myocyte cells (NMC)

To enable efficient cDNA library preparation of biopsy derived NMC by the 10x Chromium platform, first an isolation procedure had to be established which excluded erythrocytes (Ery), cardiomyocytes (CM) and debris (see paragraph 4.5.4.1.2 and Figure 34A). The quality of single cell isolation was controlled by blue-fluorescent staining of all cells and by this distinguishing them from debris particels. Besides, dead cells were stained by green fluorescence (see paragraph 4.5.4.1 for staining procedure). Cells were then counted by an automated cell counter. This analysis revealed that 99% of particles were cells, 7% of which were dead (Figure 34B). The average size of the biopsy derived cells was 8.45 µm (Figure 34C).

After sc-RNA sequencing, the data underwent raw data analysis by the 10x Chromium platform followed by subsequent analysis with Seurat (134-136) (see paragraph 4.5.4.3). Filtration parameters to remove low quality cells, doublets and cells with high percentage of mitochondrial genes from the biopsy sample are listed in Table 29. Notably, threshold for filtration of cells containing mitochondrial genes was set higher (75%) than for cultured cells (20%), as a considerable part of biopsy derived cells contained high percentages of mitochondrial genes (Figure 34B, right panel). Table 41 summarize the sequencing quality parameters, reads per cell, cell counts before and after filtering, and medians/distribution of the

Seurat parameters genes/cell, UMI count/cell and % MT Genes after filtering, also shown in Figure 34D-F.

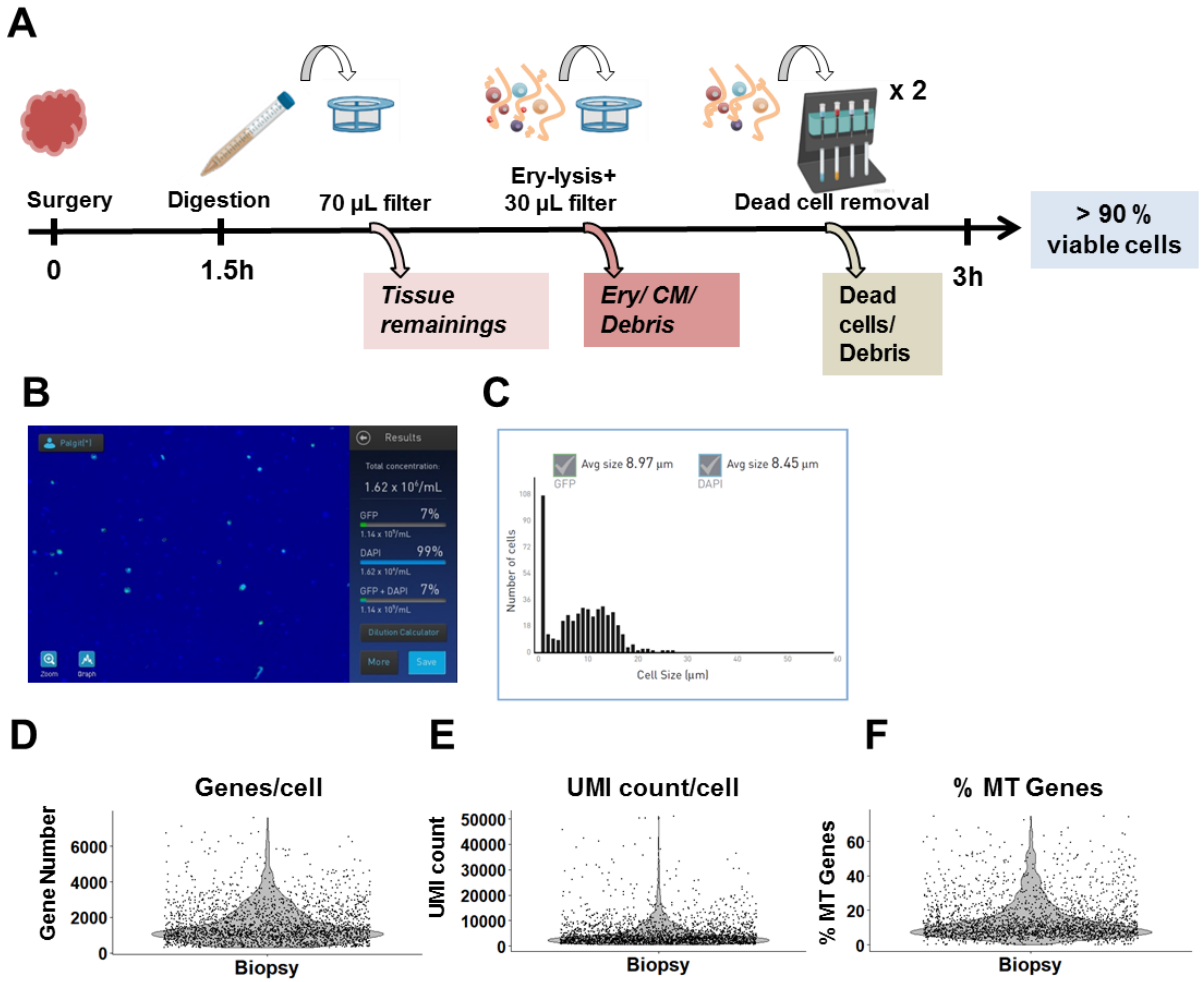

Figure 34: Isolation and quality control of biopsy derived cells

A) Isolation procedure of non-myocyte cells from a fresh cardiac biopsy, abbreviations: Ery: erythrocytes; CM: cardiomyocytes. B-C) Analysis of B) cell concentration and C) cell size distributrion on Countess II FL (Life Technologies™, Thermo Fisher Scientific, see paragraph 4.5.4.1.1.). D-F) Violin plots of D) detected gene number per cell (Genes/cell), E) unique molecular identifier (UMI) counts per cell (UMI count/cell) and F) percentage of mitochondrial genes per cell (% MT genes), illustrated for the biopsy sample after filtering procedure.

Table 41: Quality control parameters of the biopsy sc-RNAseq sample

	bef. filtering		after filtering			
Sample	Reads per cell (mean)	Cell number	Cell number	Genes/cell (median)	UMI count/cell (median)	% MT Genes (median)
Biopsy	47,512	2,407	2,388	1,258	3,242	10.4

Abbreviations: Genes/cell: gene number per cell, UMI count/cell: unique molecular identifier (UMI) read count per cell and % MT genes: percentage of mitochondrial genes per cell.

Nearest neighbor unsupervised clustering followed by UMAP dimensionality reduction revealed thirteen clusters (Figure 35A). To elucidate which cell types are represented by each cluster, GSEA analysis of uDEG of each cluster was performed (see Table 42) and marker genes were analyzed (see Figure 35B-H).

The cluster group (39% of total cell number) comprising clusters 2, 4, 5, 7, 11 and 12 were associated with GO-terms such as “immune system process”. Clusters 2, 4 and 7 (27.6% of total cell number) built a separate cluster group and expressed the T-cell receptor subunits *CD3D*, *CD3E* and *CD3G* (171) (see Figure 35B for *CD3E* expression). Typical B-cell markers such as *MS4A1* (16, 172), *CD79A* and *CD79B* (173) were highly upregulated in cluster 11 (1.9% of total cell number, see Figure 35C for *MS4A1* and *CD79A* expression). Granulocyte markers (*CCR1, CSF3R, S100A9*) as well as macrophage markers (*MRC1*, *DAB2*, *FCGR1*, *CD163*, *CCL4*, *CXCL8*) (16, 21) were found to be upregulated in cluster 5 (8.4% of total cell number, see Figure 35D for *MRC1* expression). The fact that cells included in cluster 5 derived from the myeloid lineage was confirmed by GO analysis of its uDEG which revealed the term “myeloid leukocyte activation” (Table 42).

Since this work is focused on the non-immune NMC of the heart, clusters 0, 1, 3, 6, 8, 9, 10 and 13 were analyzed in more detail. uDEG in cluster 0 (13.6% of total cell number) were attributed to mitochondrial processes, therefore this cluster was classified as low quality cells which were left after filtration procedure. To better understand which cell types were included in clusters 1, 3, 6, 8, 9, 10 and 13, uDEG for each cluster compared to all other biopsy clusters were examined. Dotplot illustrating the top nine or ten uDEG in these clusters clearly shows a common expression profile of clusters 1, 3, 6 and 9 compared to clusters 8, 10 and 13 (Figure 35E).

In cluster 8 typical EC genes, such as *VWF*, *IF27*, (Figure 35E) *PECAM1* (5, 21) (Figure 35F) and *CDH5* (174) were highly expressed and GO analysis of its uDEG elucidated terms such as “cardiovascular system development” and “tube morphogenesis” approving them being cardiac EC. *IF27* was one of the top ten upregulated genes in cultured EC (Figure 8B). Cluster 10 (2.3% of total cell number) showed high expression of cardiomyocyte markers such as *TNNT2* and *MYH6*, indicating that a small amount of cardiomyocytes remained in the sample despite the 30 µm filtration step during the cell preparation procedure (Figure 35E). Cluster 13 which comprised only 1.1% of total cell number showed high overexpression (avg_logFC > 1.5) of typical SMC markers such as *ACTA2* (156), *MYH11* (175)**,** *MYLK* (176) and *TAGLN* (16) (Figure 35E, G). Besides, *ADIRF* was found to be in the top ten upregulated genes in cluster 13. This marker had been also found in the top ten uDEG for cultured SMC, respectively (Figure 35E and Figure 8B). However, *NR4A1,* which was identified as the only gene specific to cultured SMC compared to all other primary cells analyzed (Figure 8B), was not upregulated in cluster 13, but in clusters 9, 3, 8 and 6 of the biopsy. Nevertheless, involvement of cluster 13 biological features in muscular processes (GO-term “muscle system process”) as well as vascular processes (GO-term “tube development”) confirmed its SMC identity.

The largest cluster group which constituted 50% of the detected cells contained clusters 0, 1, 3, 6 and 9. These clusters showed enrichment for GO-terms related to ECM processes, such as “collagen containing extracellular matrix”, “biological adhesion” and “locomotion”, indicating that these are subtypes of fibroblast-like cells. However, in cluster 0 processes such as “oxidative phosphorylation” and “mitochondrial membrane part” predominated. Genes previously described as fibroblast markers such as *COL1A1*, *PDGFRA* (9) (see expression Figure 35H), *COL1A2*, *DCN, LUM* and *FBLN1* (16, 21) were upregulated in clusters 1, 3, 6, 9 compared to the other clusters. Nevertheless, *IGFBP2* which was found to be the only gene specifically upregulated in cultured CF (Figure 8B), was not upregulated in clusters 0, 1, 3, 6 and 9 of the biopsy, but was highly enriched in cluster 10 (avg_logFC = 1.4).

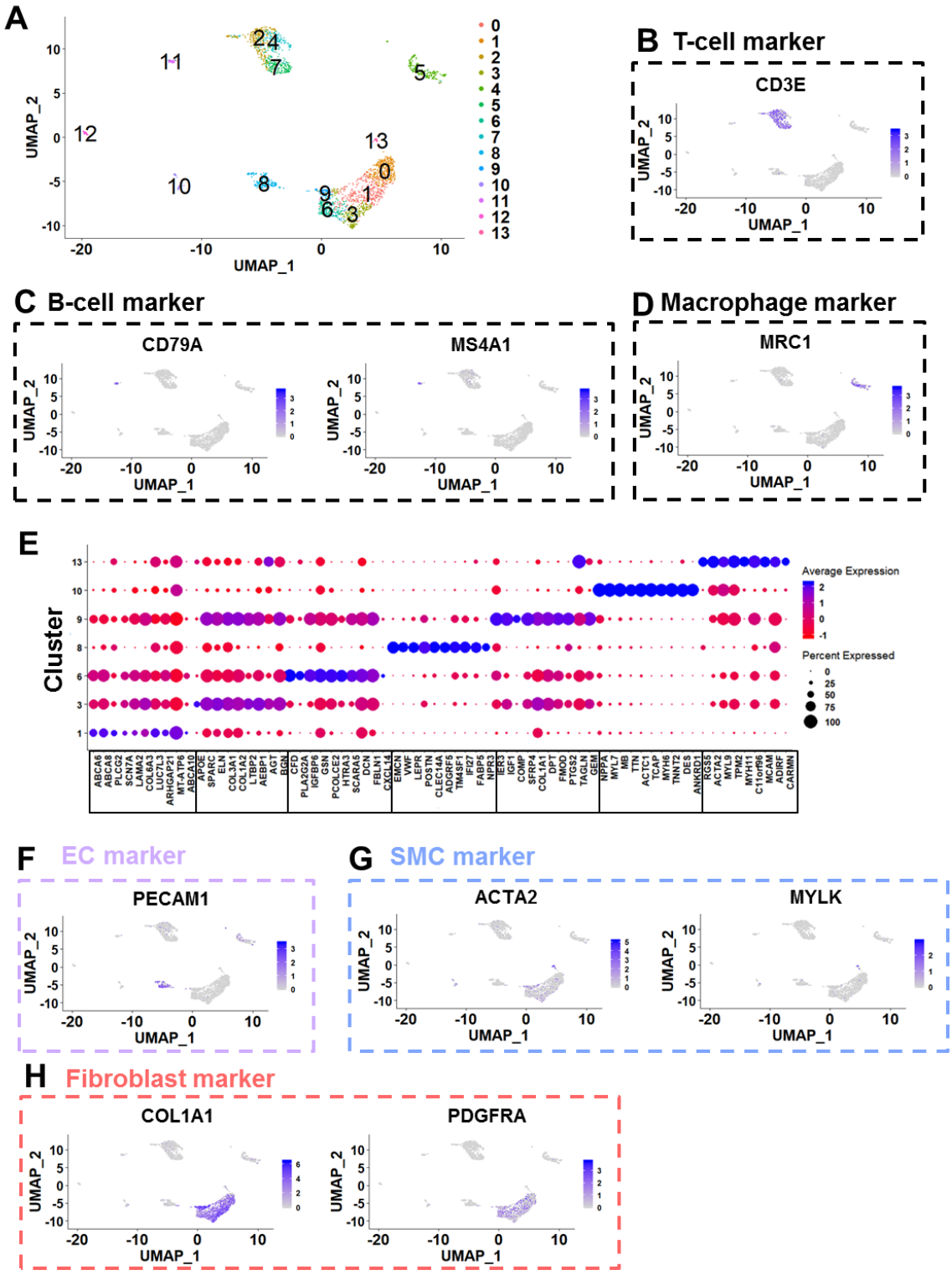

Figure 35: scRNA-seq characterization of cardiac biopsy derived cell types

A) Uniform manifold approximation and projection (UMAP) plot of the filtered biopsy sample colored by clusters, see Table 42 for cluster specific GO-terms. B-D) Feature plots of selected (B) T-cell marker, (C) B-cell markers and (D) macrophage marker. E) Top nine or ten overexpressed genes in non-immune cell

biopsy clusters (Wilcoxon rank sum test performed for illustrated clusters only, p < 0.05, genes were sorted by avg_logFC for each cluster). F-H) Feature plots of selected (F) endothelial cell (EC) marker, (G) smooth muscle cell (SMC) marker and (H) fibroblast marker.

Table 42: GO-Analysis of biopsy clusters

Cluster	% of total cell number	Enriched GO-terms (*p*-value)
0	**13.6**	GO_OXIDATIVE_PHOSPHORYLATION (17) GO_COLLAGEN_CONTAINING_EXTRACELLULAR_MATRIX (13) GO_MITOCHONDRIAL_MEMBRANE_PART (11)
1	**16.5**	GO_COLLAGEN_CONTAINING_EXTRACELLULAR_MATRIX (98) GO_BIOLOGICAL_ADHESION (48) GO_LOCOMOTION (37) GO_CIRCULATORY_SYSTEM_DEVELOPMENT (32) GO_NEURON_DIFFERENTIATION (19)
2	**12.4**	GO_CYTOSOLIC_RIBOSOME (85) GO_REGULATION_OF_IMMUNE_SYSTEM_PROCESS (79) GO_T_CELL_ACTIVATION (57) GO_DEFENSE_RESPONSE (49)
3	**9.2**	GO_COLLAGEN_CONTAINING_EXTRACELLULAR_MATRIX (115) GO_BIOLOGICAL_ADHESION (56) GO_LOCOMOTION (49) GO_NEUROGENESIS (36)
4	**7.5**	GO_CYTOSOLIC_RIBOSOME (68) GO_REGULATION_OF_IMMUNE_SYSTEM_PROCESS (59) GO_LYMPHOCYTE_ACTIVATION (56)
5	**8.4**	GO_CELL_ACTIVATION (116) GO_REGULATION_OF_IMMUNE_SYSTEM_PROCESS (78) GO_MYELOID_LEUKOCYTE_ACTIVATION (94)
6	**7.6**	GO_COLLAGEN_CONTAINING_EXTRACELLULAR_MATRIX (72) GO_SECRETION (45) GO_BIOLOGICAL_ADHESION (42) GO_REGULATION_OF_CELL_POPULATION_PROLIFERATION (36)
7	**7.7**	GO_COTRANSLATIONAL_PROTEIN_TARGETING_TO_MEMBRANE (129) GO_PROTEIN_LOCALIZATION_TO_ENDOPLASMIC_RETICULUM (110) GO_VIRAL_GENE_EXPRESSION (105)
8	**7.2**	GO_CIRCULATORY_SYSTEM_DEVELOPMENT (88) GO_CARDIOVASCULAR_SYSTEM_DEVELOPMENT (86) GO_TUBE_MORPHOGENESIS (81) GO_BLOOD_VESSEL_MORPHOGENESIS (77)
9	**3.1**	GO_COLLAGEN_CONTAINING_EXTRACELLULAR_MATRIX (96) GO_RESPONSE_TO_ENDOGENOUS_STIMULUS (62) GO_BIOLOGICAL_ADHESION (61) GO_REGULATION_OF_CELL_DIFFERENTIATION (58) GO_REGULATION_OF_CELL_DEATH (56) GO_NEUROGENESIS (39)
10	**2.3**	GO_MITOCHONDRION (148) GO_GENERATION_OF_PRECURSOR_METABOLITES_AND_ENERGY (111) GO_CELLULAR_RESPIRATION (89)
11	**1.9**	GO_COTRANSLATIONAL_PROTEIN_TARGETING_TO_MEMBRANE (142) GO_TRANSLATIONAL_INITIATION (116) GO_VIRAL_GENE_EXPRESSION (114)

		GO_POSITIVE_REGULATION_OF_IMMUNE_SYSTEM_PROCESS (34)
12	**1.5**	GO_CYTOSOLIC_RIBOSOME (49) GO_CELL_ACTIVATION_INVOLVED_IN_IMMUNE_RESPONSE (30) GO_MYELOID_LEUKOCYTE_ACTIVATION (30)
13	**1.1**	GO_MUSCLE_SYSTEM_PROCESS (35) GO_CIRCULATORY_SYSTEM_DEVELOPMENT (29) GO_ACTIN_FILAMENT_BASED_PROCESS (24) GO_TUBE_DEVELOPMENT (20)

Abbreviation: GO: gene ontology

To shed light on the differences between the fibroblast subtypes, a separate gene expression comparison of the clusters 1, 3, 6 and 9 was performed. Genes upregulated in cluster 1 in this analysis, were enriched for terms related to “oxidative phosphorylation”, “cellular respiration”, “mitochondrial membrane part”, and ”generation of precursor metabolites and energy”. Upregulated genes in clusters 3, 6 and 9 respectively, showed enrichment for 36 common GO-terms related to translation and protein processing processes (for example: “protein localization to organelle”, “ribosome” and “amide biosynthetic process”). Among the GO-terms which exclusively popped up in cluster 3 were “collagen containing extracellular matrix” and “ribosome biogenesis”. In cluster 6 processes such as “exocytosis”, “immune effector process” and “positive regulation of signaling” were unique, whereas in cluster 9 “cellular response to oxygen containing compound”, “regulation of cell population proliferation” and “response to cytokine” predominated. Although the Schwann cell marker *PLP1* (177) was significantly upregulated in cluster 9, the Schwann cell markers *S100B* (178) and *CNP* (179) were found to be expressed in other clusters as well, though without upregulation in any of them (see Table 43 and Figure 36A). The GO-term “neurogenesis” was significantly enriched in clusters 1, 3 and 9. Additionally, cluster 1 and 3 showed enrichment for the term “neuron differentiation”, whereas GO enrichment analysis for cluster 6 did not reveal any neuro-related terms. Similarly, pericyte marker were found to be upregulated in several clusters, including clusters 1 and 3, but also cluster 13 and cluster 8 (see Table 43).

To comprehend whether these fibroblast subtypes derive from different embryonic lineages, the expression of several developmental markers was examined. The epicardial markers *TBX18* (180) and *WT1* (181), as well as *SOX9* (182) were found to be expressed in clusters 1, 3, 6 and 9 to a similar extent, whereas *TCF21* (42) and *MYH10* (183) was downregulated in cluster 9 compared to clusters 1, 3 and 6. On the other hand, *TBX20*, which is expressed at different stages and in different lineages of cardiac development (184), was upregulated in cluster 1 compared to the other fibroblast clusters (see Table 43 and Figure 36B).

In the next step, fibroblast clusters were examined for typical myofibroblast markers. *ACTA2* (185), *POSTN* (186), and *TCN* (187) were upregulated in clusters 3 and 9 compared to cluster 1 and 6. Notably, myofibroblast associated collagens, *COL1A1* (45) and *COL3A1* (188), were higher regulated in clusters 1, 3 and 9 as well. However, other typical myofibroblast markers such as *VCL* (189) and *DDR2* (39, 190) were upregulated in clusters 3 and 6 (see Table 43).

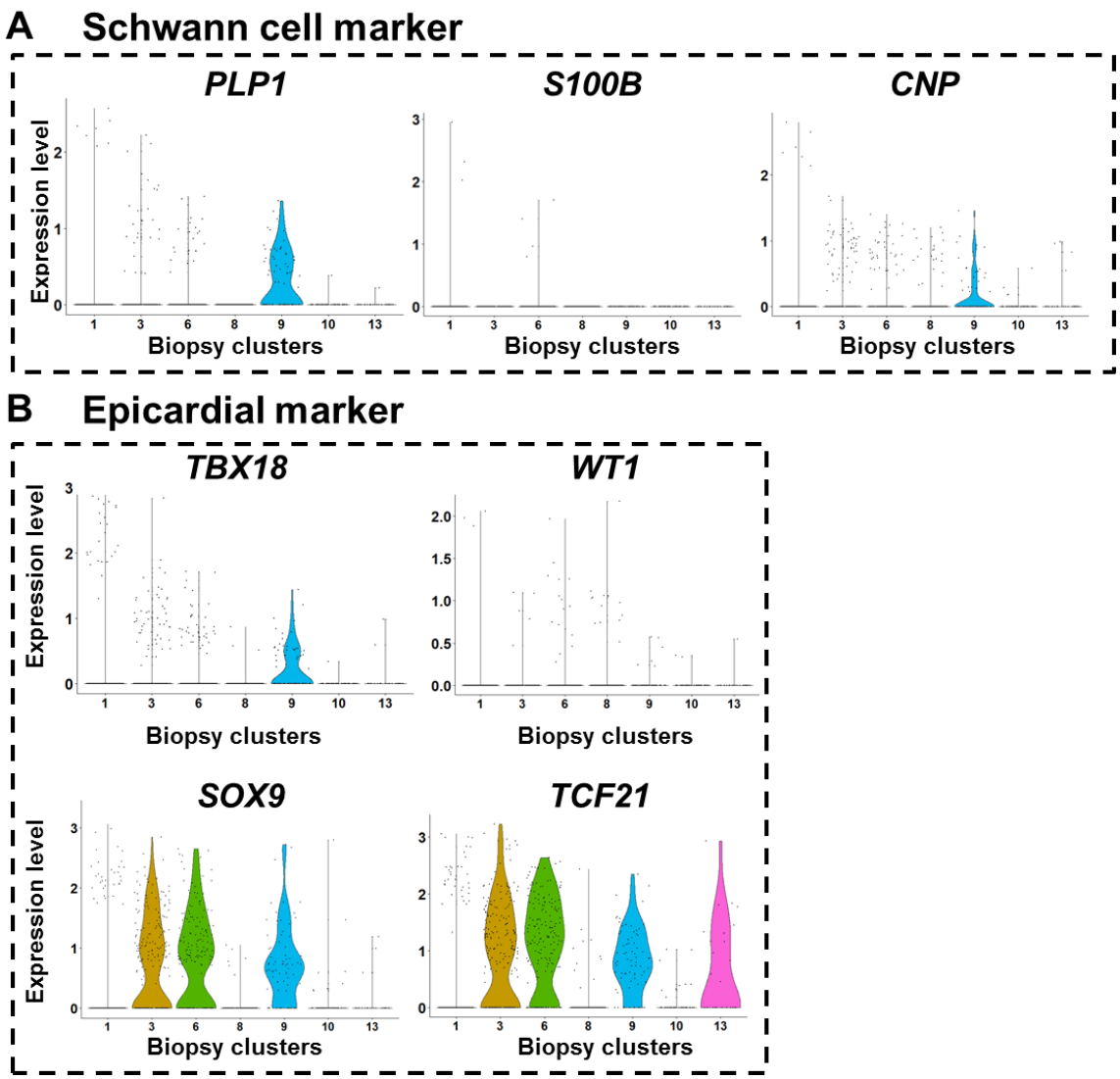

Figure 36: Marker analysis of additional cell types

A) Expression of Schwann cell markers in in non-immune cell biopsy clusters shown by violin plots. Only PLP1 is significantly upregulated in cluster 9 ($p = 3.53*10^{-64}$, avg_logFC = 0.27), B) Expression levels of epicardial markers in biopsy clusters shown by violin plots. SOX9 and TCF2 were significantly upregulated ($p < 6* 10^{-11}$) in several clusters see Table 43.

Table 43: Marker expression in biopsy clusters

Gene name	Upregulated in which cluster(s) compared to all Biopsy clusters (avg_logFC)	Marker for which cell type (Reference)
TBX20	1 (0.45)	Cardiac developmental Marker (184)
TCF21	6 (0.76), 1 (0.70), 3 (0.64)	Epicardial Marker (42)
SOX9	1 (0.55), 6 (0.54), 3 (0.51), 9 (0.39)	Epicardial Marker (182)
MYH10	3 (0.92), 1 (0.88), 9 (0.53)	Myofibroblast (183)
ACTA2	13 (3.20), 10 (1.10), 3 (0.37), 9 (0.30)	Myofibroblast (185)/ Pericyte (191, 192)
POSTN	8 (2.57), 9 (1.07), 3 (0.52)	Myofibroblast (186)

TNC	9 (0.57), 3 (0.46)	Myofibroblast (187)
VCL	3 (0.25), 9 (0.25)	Myofibroblast (189)
DDR2	6 (0.70), 1 (0.53), 3 (0.45)	Myofibroblast (39, 190)
COL3A1	3 (1.53), 9 (1.36), 1 (0.88)	Myofibroblast (188)
COL1A1	3 (1.64), 9 (1.52),1 (0.85)	Myofibroblast (45)
FN1	3 (1.05), 9 (1.04), 1 (0.85), 6 (0.48)	Myofibroblast (40)
ITGB1	9 (0.53), 3 (0.41), 1 (0.36)	Myofibroblast (193)
S100A4	2 (0.72), 12 (0.65), 9 (0.57), 5 (0.39)	CF/Myofibroblast (194)
THY1	9 (0.33)	CF Marker(40, 41)/Pericyte Marker (180, 192)
PLP1	9 (0.27)	Schwann Cell (177)
MYH11	13 (2.15)	Pericyte (192) and SMC (195)
PDGFRB	13 (1.32), 1 (0.61)	Pericyte (191, 192)
STEAP4	1 (0.61), 3 (0.33)	Pericyte (16)
KCNJ8	13 (0.56)	Pericyte (16)
MCAM	13 (2.06), 8 (0.50)	Pericyte (191), Schwann cells and SMC (16)
TIMP3	6 (1.37), 1 (0.82), 9 (0.51), 0(0.41)	SMC-, CF-Marker, See paragraph 5.1

Abbreviations: avg_logFC: average natural logarithm of the gene's fold change, CF: cardiac fibroblast, SMC: smooth muscle cell.

In summary, marker and GO analysis revealed the presence of main cardiac cell types in the analyzed biopsy. However, high percentage of immune cells and cells upregulating mitochondrial genes demonstrated some drawbacks in the enrichment procedure of viable non-myocytes out of cardiac tissue.

5.3.2 Comparison of biopsy derived non-myocytes and primary cultures of non-myocyte cells (NMC)

After biopsy derived cells were characterized, the next aim was to elucidate to which extent biopsy derived NMC differed from primary cultured NMC.

Sc-RNAseq data of the biopsy sample and the adult cultured cells (CDC, CF, SMC, EC) were merged and subsequently comparatively analyzed. Figure 37A shows by UMAP dimensionality reduction plot that the clusters of the biopsy sample were completely separated from the samples of the cultured cells. As illustrated in Figure 37B, joint unsupervised clustering of these five samples partitioned the biopsy sample in five main clusters (0, 1, 2, 10 and 11). Clusters 0 and 10 included immune cells (GO-terms enriched "regulation of immune system process"), whereby cluster 10 represented the myeloid cells expressing the granulocyte and macrophage markers mentioned in paragraph 5.3.1. Cluster 11 included the biopsy derived EC (GO-terms enriched "circulatory system development" and "tube morphogenesis") and was located in proximity to the clusters of cultured EC (clusters 6 and 9). As seen in Figure 37A, some dots of the biopsy were distributed across clusters 6 and 9, pointing out the similarity of some of the biopsy derived cells to cultured EC. The other NMC types of the biopsy were found in clusters 1 and 2 (NMC_1_2), however, it was not possible to distinguish between different cell (sub-) types based on the GO enrichment analysis of uDEG in NMC_1_2. Histograms illustrating the

parameters genes/cell and UMI count/cell for the merged Seurat object of the cultured cell samples and the biopsy sample (Figure 37C-D) show that these quality parameters were less evenly distributed when comparing them to the merged Seurat object without the biopsy sample (Figure 7H-I). Decreased median values of the biopsy (see Table 41) compared to the cultured cells (see Table 35) pulled down the median values of the merged Seurat object to 2,254 detected genes/cells (Figure 37C) and 7,681 UMI count/cell only (Figure 37D), reflecting the lower quality of sc-RNAseq for the biopsy sample.

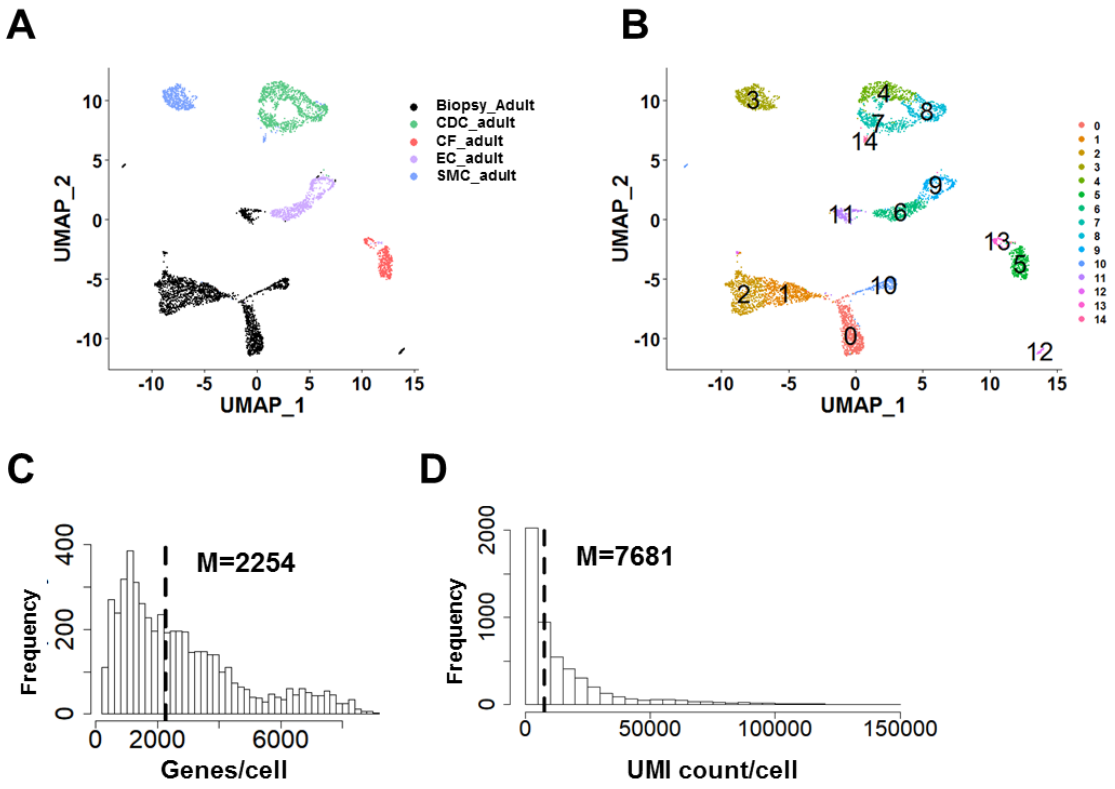

Figure 37: Comparative analysis of biopsy and cultured cells.
A-B) Uniform manifold approximation and projection (UMAP) plots of the global analysis of the biopsy and primary cultured cells, colored by (A) sample identifier and (B) clusters. C-D) Histograms illustrating C) genes/cell or D) unique molecular identifier (UMI) count/cell of the filtered merged Seurat object containing CDC, cardiac fibroblasts (CF), endothelial cells (EC), smooth muscle cells (SMC) and the biopsy sample.

Figure 38A-C illustrates comparisons of the cultured EC, CF and SMC to the corresponding clusters found in the biopsy (see Figure 37B for cluster numbering). A common observation for all three comparisons was that genes uniquely expressed in the cultured cell types were assigned to GO-terms related to protein biogenesis and translational processes.
Figure 38A illustrates the comparison of uDEG in cluster 11 (biopsy derived EC) and clusters 6/9 (cultured EC). Only 9.5% of the genes overexpressed in cultured EC were also found in the

biopsy derived EC population. These common genes were attributed to typical EC terms such as “blood vessel morphogenesis” and “cardiovascular system development”. When analyzing the genes which are solely upregulated in the cluster of biopsy derived EC, terms related to vessel/tube formation were found as well.

Analogously, cultured CF (cluster 5) were compared to the NMC_1_2 from the biopsy. Genes both upregulated in cluster 5 and NMC_1_2 (cluster 1, 2) represented 12% of the total gene number of cluster 5 and were attributed to processes related to ECM. Genes exclusively upregulated in NMC_1_2 were additionally assigned to biological processes such as “regulation of cell differentiation”, “tube development” and “neurogenesis” (Figure 38B).

Comparison of cultured SMC (cluster 3) to NMC_1_2 (cluster 1, 2) revealed that the common genes represented 9.5% of the genes upregulated in cultured SMC (Figure 38C). Even though many significantly enriched GO-terms in the common gene group were related to ECM processes, GO-terms such as “circulatory system development” and “epithelial cell proliferation” indicated that both cluster groups expressed SMC-typical genes. Besides, GO-terms related to development such as “regulation of cell differentiation” and “animal organ morphogenesis” were enriched in the common gene group. *ADIRF* and *TIMP3* which already arose in the comparison of cultured cells as SMC specific (Figure 8B) were present among the common genes. However, genes uniquely expressed in NMC_1_2 were associated with “extracellular matrix”, ”regulation of cell differentiation” and “circulatory system development”, reassuring the fact that either cultured SMC or NMC_1_2 represent pure SMC populations.

As in the joint analysis biopsy derived SMC could not be distinguished from the other NMC, the SMC cluster in the separate biopsy analysis (cluster 13, Figure 35A) was compared with cultured SMC (cluster 3, Figure 37B). A total number of sixteen common genes were identified in those clusters (3% of the total gene number of the cultured SMC sample only). Among these genes were *ADAMTS1* and *IGFBP5* which had the GO annotation “positive regulation of vascular associated smooth muscle cell migration”. Besides, *ID3*, *MYLK* and *NR2F2* which were annotated to the process of “muscle structure development” were upregulated in both cultured and biopsy derived SMC. In contrast to upregulated genes in the biopsy derived SMC (236 genes) which were significantly assigned to GO-terms such as “muscle contraction” and “circulatory system process”, genes exclusively upregulated in cultured SMC (509 genes) were involved in protein biosynthesis processes, similarly, to cultured EC and CF.

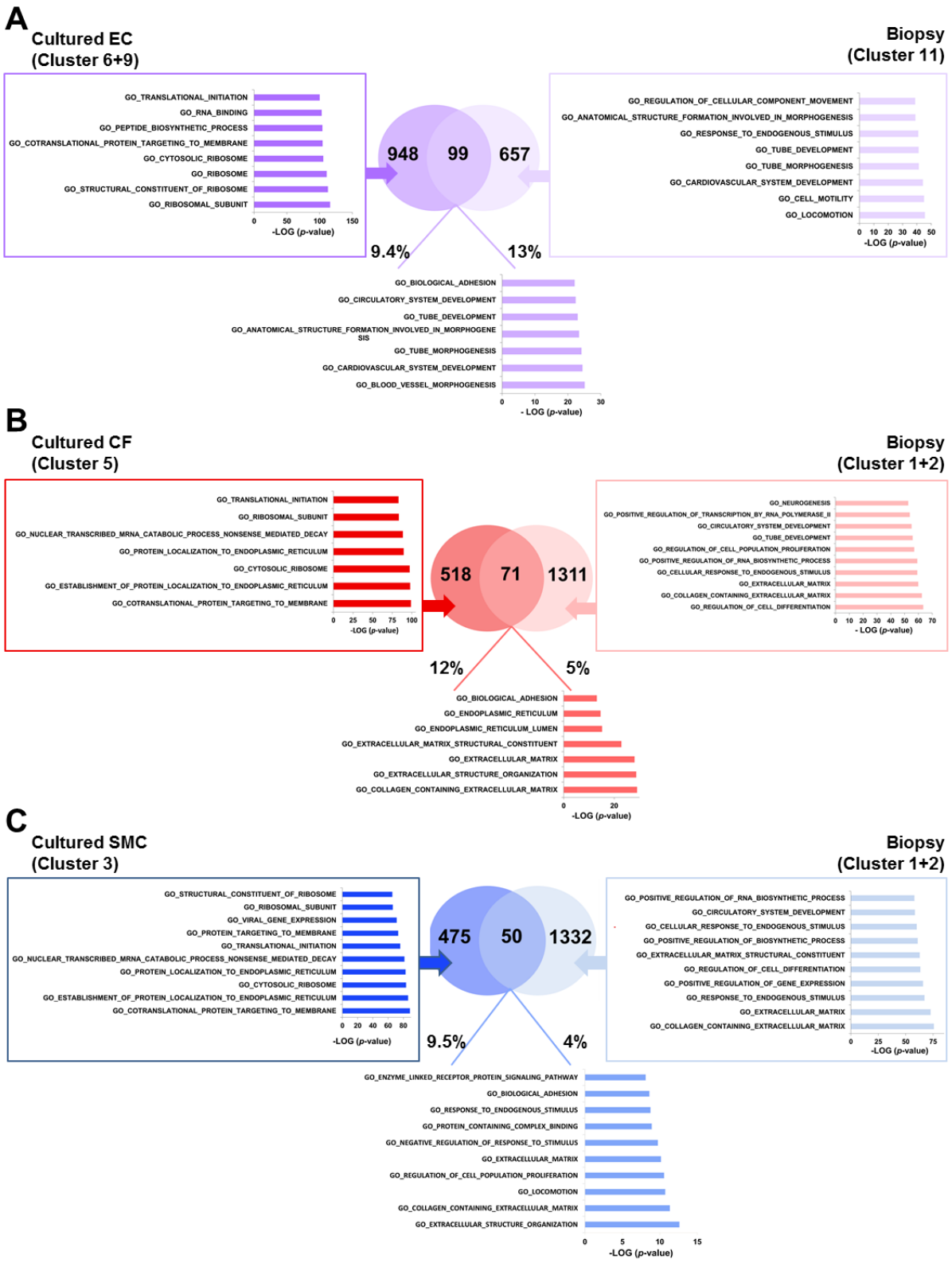

Figure 38: Comparative GO analysis of biopsy derived NMC and cultured NMC.

Analyzed cell types are abbreviated as follows: NMC: non-myocyte cells, EC: endothelial cells, CF: cardiac fibroblasts; SMC: smooth muscle cells. Clusters shown in Figure 37B were compared concerning their

uDEG (upregulated differentially expressed genes, defined by p< 0.05 and avg_logFC ≥ 0.25). Thereby cultured cells were compared with the according biopsy clusters associated with similar biological processes. A) Venn diagrams show the overlap of uDEG of A) clusters 6 and 9 (cultured EC) with cluster 11 (biopsy derived EC), B) cluster 5 (cultured CF) with cluster 1 and 2 (biopsy derived NMC_1_2), C) cluster 3 (cultured SMC) with cluster 1 and 2 (biopsy derived NMC_1_2). Percentages of common uDEG are indicated for cultured cells (left side) and biopsy derived cells (right side) for each comparison. Significantly enriched ($p< 10^{-6}$) gene ontology (GO)-terms associated with the overlapping (middle diagram) a non-overlapping uDEG groups (left and right diagrams) are illustrated for each comparison, respectively.

To elucidate whether there are characteristics which are in common between CDC and biopsy derived NMC, joint analysis clusters 4, 7 and 8 (CDC) were also compared to NMC_1_2 for shared upregulated genes (see Figure 39). The analysis revealed 61 common genes constituting 4% of the total gene number of the CDC clusters, which is less than the according percentages for EC, CF and SMC (Figure 38). The commonly expressed genes in CDC and the NMC_1_2 were mainly enriched for processes related to ECM and secretion. In contrast to cultured EC, CF and SMC, genes exclusively upregulated in the CDC clusters (1535 genes) were mainly assigned to GO-terms related to mitochondrial processes and cell cycle. Genes solely upregulated NMC_1_2 had a comparable functional profile to the corresponding gene group of the comparison with CF (see Figure 38B), revealing GO-terms such as “collagen containing extracellular matrix”, “response to endogenous stimulus”, “regulation of cell differentiation” and “tube development”.

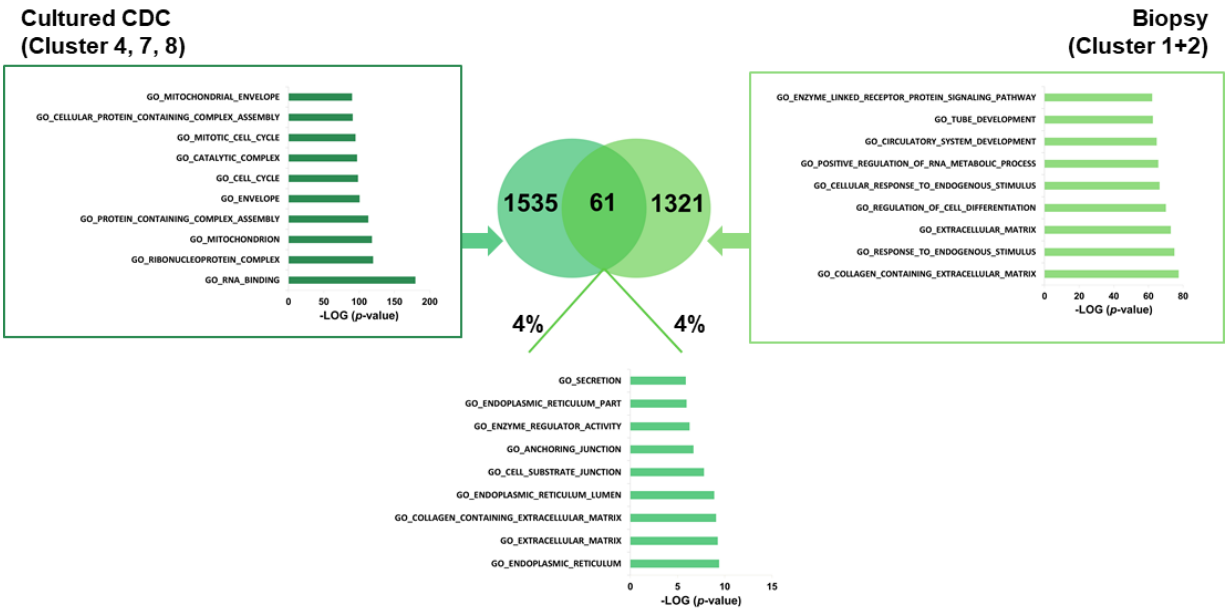

Figure 39: Comparison of CDC and biopsy derived NMC

Analyzed cell types are abbreviated as follows: NMC: non-myocyte cells, CDC: cardiosphere-derived cells. Clusters shown in Figure 37B were compared concerning their uDEG (upregulated differentially expressed genes, defined by p< 0.05 and avg_logFC ≥ 0.25). Thereby clusters 4, 7, 8 (CDC) were compared with cluster 1 and 2 (biopsy derived NMC). Percentages of common uDEG are indicated for CDC (left side) and biopsy derived cells (right side).

In conclusion, cultured EC, CF and SMC shared a subset of upregulated genes with their counterpart biopsy clusters which was associated with cell type typical biological processes. Whereas uDEG uniquely expressed in biopsy derived clusters were associated with biological processes typical for NMC, in cultured cells a substantial part of uDEG, which was not observed in the biopsy derived cells, was related to protein synthesis processes.

6. Discussion

Although cardiac research and drug development were progressing for decades, cardiac abnormalities and disorders still represent a severe threat for the society. This fact motivates scientists to investigate molecular mechanisms associated with physiological and pathological dysregulations of the heart. However, until recently, cardiac research has mostly focused on cardiomyocytes and less attention was payed to the non-myocyte cell types (196). Nowadays, state-of-the-art techniques such as sc-RNAseq enable a detailed view on the diversity of molecular processes at the cellular level. In general, there are two approaches to use this technique. The first one is to create a cellular *in vitro* model for a specific cell type or a pathological state to examine specific molecular changes (197, 198). The second approach is to globally investigate the cellular composition of cardiac tissue in order to gain an insight, as unbiased as possible, on the cardiac cellular state *in vivo* (16, 21).
In this work, *in vitro* cultivated primary cell types were investigated first as a model for the three main non-myocyte cardiac cell types: CF, SMC and EC. In addition, heart-derived CDC were compared to the non-myocyte cell types. Subseqeuntly, cellular analysis of a cardiac tissue biopsy was performed, and its data was compared to the *in vitro* cultivated cell types.

6.1 Characterization of primary non-myocyte cultured cells

6.1.1 Primary cardiac non myocyte cell types

The main non-myocyte cell types of the heart, namely CF, SMC and EC, are an important research topic considering their potential role in cardiac homeostasis and disease. However, until now, only few comparative studies of these cell types have been performed at the single-cell level (16, 21, 199).

The data presented in this work clearly showed the outstanding transcription profile of EC and on the other hand the similarity between CF and SMC. Both in qRT-PCR (Figure 5) and sc-RNAseq (paragraph 5.1.2), typical EC markers were selectively upregulated in the cultured EC, whereas CF and SMC often expressed the same marker genes at similar levels. Similar observations were made by Li *et al.* who reported several shared expressed genes in CF and SMC which were differentiated from murine embryonic stem cells (sc-RNAseq data) (199). Wang *et al*. identified in sc-RNAseq data from non-failing human adult hearts CF and SMC clusters which were both linked to ECM organization (21). Single nucleus RNA sequencing (sn-RNAseq) of postnatal mouse hearts showed also a transcriptional overlap between CF clusters and pericytes/SMC (200). The similarity between CF and SMC was also confirmed on the protein level by FC- and ICC-data in this work (Figure 6). Doll *et al.* analyzed human cultured EC, CF and SMC on the proteomic level. Pearson correlation of SMC and CF revealed a coefficient of 0.88, whereas CF and SMC were slightly less related to EC (CF-EC: 0.83; SMC-EC: 0.81), which was also confirmed by PCA (5). Considering the fact that CF and coronary SMC both derive from the

epicardium during heart development, their phenotypic and transcriptomic similarities as well as their functional overlap are not surprising (25, 180). In contrast, vascular and cardiac endothelial cells are known to derive from different embryonic lineages than CF and SMC (33) (see paragraph 1.1.2).

Comparison of proteomic data by Doll *et al*. (5) and sc-RNAseq data from this work shown in Suppl. Figure S 4 revealed that in both, CF and SMC, about 24% of upregulated genes (uDEG), had previously been detected upregulated in the same cell type at the proteomic level. However, in EC this overlap comprised 47% of genes. The proteomic study was technically more sensitive than the sc-RNAseq study, since a much higher number of proteins (7,965, AF included) was detected compared to the total gene number of cultured cells in sc-RNAseq (1,706). Thus, this result should be interpreted carefully. Nevertheless, the overlap of genes upregulated in EC was almost twice as high compared to CF or SMC, suggesting that this cell type retains a robust molecular phenotype during *in vitro* culture. In addition, its transcriptome and proteome are clearly distinguishable from CF and SMC.

In the literature a number of marker specific for either CF or SMC have been reported (CD90 (201), DDR2 (14), S100A4 (202), FBLN2 (203), PDGFRA (204), TAGLN (205), PDGFRB (206), TIMP3 (207, 208)). However, none of these markers could be confirmed as specific for a single cell type in this work (paragraphs 5.1.1 and 5.1.2). Nevertheless, some exclusive markers for CF, such as ALDH1A2 (5) (Figure 5C), *CPA4 and IGFBP2* (Figure 8B) were detected. CPA4 was previously described as a regulator of cardiomyocyte hypertrophy (209) and *IGFBP2* encodes for a protein which was found to be a biomarker for cardiovascular disease (210). This might suggest that cultured CF upregulated pathological pathways. *NR4A1* was reported to play an important role in SMC homeostasis (211, 212).

The heterogeneity of samples was reflected by the number of clusters, revealing EC as the most heterogeneous and SMC as the most homogeneous type among the NMC. However, the subdivision in several clusters in EC and CF was caused by enhanced proliferative capacity of one cluster, respectively (EC: Cluster 6, CF: Cluster 9, Figure 12A). EC sense changes in their microenvironment, such as biomechanical forces and biochemical settings, and respond to them by modulating their mRNA expression (36, 213). Culture conditions such as the cultivation medium clearly influence the expression profile of EC and the results presented here must be seen as model with pivotal biases in comparison to *in-vivo* cardiac cells (see paragraph 6.3). Since the endothelial cell cultivation medium contains a variety of growth factors (see paragraph 3.12), the mechanism underlying the EC heterogeneity could be explained by a different response of EC subtypes upon exposure to these chemical compounds, resulting in three clusters. CF are cultured in cultivation medium containing 10 % FBS which is known to promote proliferation in stromal cells to a certain extent (214). Wang *et al.* reported that human cardiac biopsy derived CF were separated in three clusters, one of them was associated with

proliferation (21), suggesting that a subset of CF is prone to activate this transcriptional pattern. On the contrary, SMC in the tunica media were reported to undergo clonal expansion which is associated with enhanced proliferation when building atherosclerotic plaques (215). Similarly, in the SMC cluster analyzed in this work the GO-term "regulation of cell population proliferation" was enriched. Despite being a topic of debate (29), this hypothesis would support the transcriptional homogeneity of a proliferative SMC subset which is promoted by cell culture.

Yet, each of the analyzed non-myocyte cell types had clusters in which typical functional processes for the corresponding cell type exist, encouraging the usage of primary cultured cell as a simple model for *in vivo* cardiac cells when analyzing gene expression.

6.1.2 Defining the identity and heterogeneity of CDC

CDC have originally been postulated to display characteristics of cardiac progenitor cells, which are partially differentiated on their way to cardiomyocytes (70). This study, however, clearly showed the similarity of CDC with non-myocyte cell types and seperates them from veritable cardiac progenitor cells derived from human iPSC.

Morphologically, CDC had a fibroblast-like appearance (see ICC Figure 6) and beating of CDC or cardiospheres was not observed, unlike described by Messina *et al*. (70). The marginal expression of the progenitor markers *GATA4*, *TBX5* and *NKX2-5* compared to iPSC-derived cardiac progenitors (Figure 5A) and the absent expression of typical cardiomyocyte markers such as *TNNT2* and *MYH6* (sc-RNAseq data), confirmed that there is no relation to the cardiomyocyte lineage. In contrast to the findings by Ishigami *et al*. (87), CF had a higher expression of *GATA4* and *TBX5* compared to CDC of infant patients in this work (Figure 16A). Most of the markers described to be specific for fibroblasts and SMC previously, and analyzed by qRT-PCR and FACS in this work, were expressed to a similar extent by CDC (Figure 5C). Only *CD90* and *ALDH1A2* were significantly downregulated in CDC compared to CF. This corresponds to several publications which reported a variable expression profile of CD90 in CDC (61, 73, 87). DDR2 expression measured by qRT-PCR and ICC did not differ between CDC and CF (Figure 5C and Figure 6A), other than reported by Ishigami *et al.* (87). Malliaras *et al.* (216) analyzed α-SMA and PDGFRB expression in CDC by FC, which matched qRT-PCR and ICC results obtained in this work. In many clinical trials, the criteria for usage of CDC were the uniform expression of the mesenchymal marker CD105 and the absence of CD45 (hematopoietic marker) as well as CD31 (endothelial marker) (61, 62, 87). These criteria were also met by the CDC established and analyzed here (Figure 5 and Figure 6). However, the same holds true for CF, SMC and also AF. Thus, these do not seem to be reliable or specific criteria for the cell type of CDC.

Cellular miR-146a-5p, unlike miR-132, appeared to be a specific marker to distinguish CDC from CF, yet only in cells derived from pediatric patients (Figure 16C). However, miR-146a-5p was significantly upregulated in CDC-EV vs. CF-EV both in the infant and the adult group (Figure 19H-

J), confirming results by Ibrahim *et al.* and Tseliou *et al.* who analyzed the miR profile of CDC exosomes compared to those of normal human dermal fibroblasts (78, 80).

Sc-RNAseq analysis finally revealed a more detailed picture of CDC. For the first time, light was shed on the heterogeneity of this cell type. Cluster analysis reflected the effects of the exposure of CDC to growth factors and other medium supplements during the stage of 3D sphere formation in cell culture. Cell proliferation of fibroblasts and SMC is known to be induced by bFGF (217, 218) and by EGF (219). B-27 supplement contains a variety of fatty acids, hormones, vitamins and proteins such as insulin which also promote cell growth (220, 221). For this reason, it is not surprising that a major part of CDC upregulated processes related to mitotic cell cycle and mitochondrion (see CDC cluster 4 and 8, Figure 12A-B). In addition, this exposure to extensive growth factor concentrations most probably activates responding pathways resulting in augmented chemokine and cytokine transcription in CDC, as seen by the expression of *IL1B* and *CXCL6* (Figure 8B and Figure 10B) and GO-terms such as “cytokine activation” in cluster 3 or “cell activation involved in immune response” in cluster 5 (Figure 12A-B). Indeed, the interplay between the proinflammatory cytokine IL1B and the growth factor bFGF was previously described in different pathological situations, particularly in infectious and inflammatory diseases (222-224). In the context of myocardial infarction, CF alter their production of ECM compounds and by this activate the innate immune response leading to an inflammatory reaction (225). In addition, as a reaction to endothelial barrier damage, EC acquire an inflammatory phenotype and also release inflammatory cytokines (225). Therefore, one could suppose that the growth factors activate expression patterns characteristic for an inflammatory cell type in cardiosphere-forming cells and thus in CDC, as observed in non-myocyte cell types such as myofibroblasts during myocardial infarction.

Another feature of CDC which was observed both in sc-RNAseq data (Figure 12A-B, cluster 3) and during further *in vitro* assays, is that CDC exhibited high secretory activity, producing a significantly higher amount of EV than CF (Figure 19D). Interestingly, the GO-terms related to secretion were enriched in the same clusters where immune activation processes were observed (see cluster 3 and 5, Figure 12A-B). As a method of cell-cell communication, cytokines are exchanged between cells and it has recently been reported, that this process is mediated by EV, at least in part (226). CDC release several cytokines such as angiopoetin-2, bFGF, HGF, IGF-1, SDF-1 and VEGF (227). A positive influence of growth factors on CDC was reported for EGF, which increased their migration activity (228), and for bFGF which promoted engraftment of CDC *in vivo* (229). This suggests that cytokines might induce the secretion of vesicles containing other cytokines, which then in turn mediate positive paracrine effects.

Marker expression and sc-RNAseq analysis clearly revealed that CDC resembled NMC of non-hematopoietic origin, as previously described (230, 231). The heterogeneity analysis of CDC also revealed clusters which were attributed to similar processes as some of the SMC and CF

clusters, respectively (Figure 14). It must be mentioned that the comparison of uDEG of the analyzed CDC clusters with corresponding CF or SMC clusters provided a small number of common genes. However, when analyzing the respective uDEG by GSEA, the number of enriched GO-terms shared by these clusters was relatively high. This suggests that CDC do not consist of SMC and CF, but represent a unique heterogenic cell type which is involved in a variety of similar processes.

Since CDC and CF both derived from heart tissue biopsies, one could assume that CDC mostly resembled CF. However, a definite similarity was only seen in processes related to ECM production. Although a detailed transcriptomic comparison of CDC and CF was not published previously, the miR expression profiles of CDC and dermal fibroblast were investigated several times, revealing appreciable differences (78, 80). Besides, CDC and CF were reported to influence each other by their secreted products (80, 232), suggesting a higher similarity when co-cultured. The protocol of CDC generation does not ensure that only the sphere-forming cells are harvested, so there is a certain probability that some CF are also present in the cardiac outgrowth layer which are used to build the spheres. This hypothesis is supported by the findings of Davis *et al.* that the surface of spheres is enriched with mesenchymal markers like CD90 and procollagen I (231), which also represent fibroblast markers (40, 41, 233). Taken together, the CDC cluster enriched for ECM related processes could represent a subpopulation of CDC which highly resembles CF.

Many studies have analyzed the angiogenic potential of CDC (77, 78, 80, 83, 85, 86, 234). As shown in Figure 20 and Figure 21, pro-angiogenic properties assessed by *in vitro* assays such as matrigel assays (77, 84-86) and migration assays (84) with CDC-EV could be reproduced for, the infant group only. The fact that cluster 1 representing infant-CDC only (Table 36) was associated with many GO-terms typical for EC, confirms these observations.

Interestingly, CDC resembled SMC in three main processes: ECM production, angiogenesis and response to cytokines (Figure 14D). SMC are known to produce ECM in atherosclerotic plaques and this process is influenced by cytokines such as TGFB1 (235), a component of the medium supplement FBS (236). Being additionally activated by bFGF and EGF from the medium, at least a part of cultured SMC most likely acquired the phenotype of atherosclerotic SMC which have increased proliferation, migration and synthetic capacity (28). These properties were also observed for CDC (Table 36) which were partly exposed to the same medium supplements (FBS, bFGF, EGF). The angiogenic capacity of SMC has been shown to be modulated by bFGF and VEGF production which influenced EC in their close proximity (237), another common characteristic shared with CDC (227).

The overlap of CDC with biopsy derived NMC clusters excluding EC, as shown in Figure 39, revealed that commonly upregulated genes in these clusters were attributed to ECM production

(paragraph 5.3.2), suggesting this characteristic to be the main similarity with NMC *in vivo*. This finding corresponds to the comparison of cultured CF and SMC to CDC (Figure 14C and D). The fact that the percentage of commonly expressed genes in CDC and the biopsy clusters analyzed (Figure 39) was smaller than the according percentage of EC, CF and SMC (Figure 38) emphasizes that CDC represent a cell type which is more influenced by its cell culture conditions and therefore stronger differs from heart-tissue cells.

Taken together, CDC can be defined as a heterogenic non-myocyte and non-cardiac progenitor cell type influenced by cell culture conditions to have proliferative, secretory, ECM producing and to some extent angiogenic properties.

6.2 Age-dependent comparison of non-myocyte primary cells (CDC, CF)

The TICAP trial with CDC derived from SV patients clearly revealed that the clinical significance of autologous CDC transplantation in children is superior to the same procedure in adults in the CADUCEUS trial (62, 67). Although only seven treated patients were included in the TICAP trial, the authors illustrate a correlation between age of the patient and the positive change in ejection fraction (67).

In this work 22 adult patients and 49 infant patients, 32 of which were neonates aged ≤ 21 days, were analyzed (see Table 14 and Table 15). It is beyond the capability of most hospitals to obtain this number of pediatric patients with the required diagnosis. For this reason, there are only few studies which have investigated the biological properties of CDC derived from patients of different ages in such an extensive manner.

Comparison of the transcriptome (Figure 18) and the regenerative potential during *in vitro* assays (Figure 20 and Figure 21) of infant and adult derived CDC, emphasized the increased angiogenic potential of CDC derived from infant patients when compared to those derived from adults. Sc-RNAseq data revealed a cluster in the infant sample which was not present in adult CDC in which genes associated with angiogenesis related processes were upregulated. *In vitro* effects of CDC-EV on EC showed that infant CDC-EV, unlike adult CDC-EV, augmented EC tube formation and migration. These data correspond to the finding by Simpson *et al.* reporting an enhanced expression profile of angiogenic factors (e.g. ANG, VEGFA, IGF) in CDC derived from neonates (exact age not indicated) compared to adult derived CDC. In addition, augmented vessel formation was observed in neonatal derived CDC treated infarcted rat hearts assessed by histological staining (88).
In contrast, Walravens *et al.* published the only available analysis in which the transcriptomes of CDC derived from infants (1 day – 14 years) and adults (47 – 84 years) were compared. Interestingly, their results suggested that the angiogenic potential of CDC derived from adult patient is superior to that of CDC derived from infants (90). Nakamura *et al*. also assessed the angiogenic potential of CDC derived from donors of different age and did not find any significant

differences in tube formation on matrigel between younger (2-64 years) and older patients (65-83 years) (89). This discrepancy could evolve from different age of donor patients, different diagnosis or culture conditions, as described by Agarwal *et al*. and Sharma *et al.* who reported that the angiogenic potential of infant derived primary progenitor cells and CDC is dependent on whether hypoxic or normoxic culture conditions were used (238) and whether donor patients had an end-stage heart failure diagnosis (83). In both cases the angiogenic potential was assessed by immunohistochemistry. Walravens *et al.* included two neonates only (13 %) within their infant patient group containing 15 patients (90). Nakamura *et al.* divided the patients' groups in age groups younger and older than 65 years. Therfore, their "younger" patients group included only three children, so the majority of patients in this group were nevertheless adults (89). Taken together, these findings suggest that the angiogenic potential is higher the younger the donor patient and thus could be detected more often in neonate samples.

Analysis of the angiogenesis effects of neonate (HLH1) CDC-EV samples compared to older children (HLH2/3) CDC-EV revealed that only HLH1 CDC-EV significantly promoted EC migration (Figure 26). This finding confirms again that the angiogenic potential of CDC is age-dependent. However, in the tube formation assay no significant differences either from HLH1- or from HLH2/3-CDC-EV to NegCtr were observed (Figure 25). This discrepancy might indicate that different angiogenesis processes are influenced differently by neonatal CDC-EV. Similar findings was reported by Agarwal *et al.* who described no difference in the angiogenesis potential of human primary cardiac progenitor cells isolated from neonate (1 day to 1 month), infant (1 month to 1 year), and child (1 to 5 years) patients, assessed by isolection staining of right ventricular tissue of athymic rats 28 days after cardiac progenitor cell transplantation. However, they observed that conditioned medium from neonatal cardiac progenitor cells only induced migration of mesenchymal cells (238).

Age dependent differences of the regenerative potential of CDC have been additionally investigated by NRCM apoptosis assays (Figure 22) and CF migration as well as CF proliferation assays (Figure 23). Rather unexpected, benefical effects in the NRCM apoptosis assay were only evident with adult patient derived CF-EV. Lang *et al.* performed a co-culture experiment of murine primary neonatal cardiomyocytes with CDC and detected significantly decreased apoptosis compared to the medium control by a TUNEL assay (85). Tseliou *et al.* performed annexin-V-staining of NRCM conditioned with cardiosphere-EV and then stressed with H_2O_2, measuring an anti-apoptotic effect compared to dermal fibroblast derived EV (measured by FC) (80). Although the method used in this work was based on the method of Tseliou *et al*., there were several differences. The most substantial differences were that the timepoint of hypoxia induction was set before the incubation with EV and that CF- EV instead of dermal fibroblast EV were used as a comparative group. Previously investigated *in vitro* effects of CF conditioned

medium on NRCM measured by TUNEL assay revealed no significant change in apoptosis, though at least a trend for a decrease was observed (239). Migration of CF, an *in vitro* assay for scar formation, was not affected by CDC-EV or CF-EV treatment (Figure 23A-F). Proliferation of CF was upregulated by infant CDC-EV (Figure 23J). However, as no age-dependent comparison was performed, no conclusions with respect to the advantage using CDC-EV derived from patients of specific age can be drawn. Tseliou *et al.* reported that CDC-EV altered fibroblasts in a way to acquire characteristics of CDC such as CDC-specific miR expression patterns, pro-angiogenic, anti-fibrotic properties and the ability to promote cardiomyocyte proliferation (80). Even though fibroblast proliferation was not investigated in Tseliou's study, a logical conclusion would be that the used infant CDC-EV transferred their proliferative characteristics to the fibroblasts, as shown in Figure 23J. However, Lang *et al.* reported a reduction of fibroblast proliferation induced by CDC-EV derived from adults (85).

Another aspect of the data presented here is that more significant differences in marker expression were detected between CDC and CF in the infant patients group compared to the adult group (Figure 16). This is in agreement with the finding that genes associated with ECM were upregulated in the adult CDC sample in the sc-RNAseq dataset (Figure 18D, F), suggesting that CDC from adult donors were more similar to CF than CDC derived from infants. This hypothesis was confirmed by the differential gene expression analysis by Walravens *et al*. in which the biological process of "extracellular matrix organization" was upregulated in adult CDC (90). For miR-146a-5p no direct age-dependent differences of expression were detected in CDC. However, comparing cell types, a differentential expression of CDC compared to CF was only measured in the infant group (Figure 16C). Fuentas *et al.* reported the differential miR expression profile of CDC derived from neonatal patients compared to adult patients, revealing an upregulation of migration promoting miRs in neonatal patients (240). Agarwal *et al*. analyzed the differential expression profile of exosomal miR in neonate- (age: 0-1 months), infant- (age: 1-12 months), and child- (2-5 years) derived c-KIT positive cardiac progenitor cells and found age-dependent differences (234). The fact that miR-146a was not found among the miRs shown in these publications suggests that its expression does not significantly differ depending on the age of the donor patient. However, in contrast to the results presented here, Fuentas *et al.* reported that miR-132 was upregulated in adult clones compared to neonates (240).

Significant age-dependent changes in the gene expression of primary cells were measured for *GATA4* and *TBX5* (CDC: decrease with younger age), *ALDH1A2* (CDC/CF: decrease with younger age) and *NKX2-5* and *CD90* (CDC/CF: increase with younger age) (Figure 16). As the expression of *GATA4* and *TBX5* as well as high protein levels of ALDH1A2 were reported to be typical for CF (5, 196), the hypothesis that adult CDC were more similar to CF than infant CDC was once more confirmed. The cardiac developmental TF *NKX2-5* was previously reported to be strongly upregulated in infant CDC compared to infant CF (87) and to be strongly upregulated in

neonatal cells compared to adult cardiac fibroblasts (241). Although CD90 is often used as a fibroblast marker, it is also a common marker of a subset of mesenchymal cells reported to decrease in number during aging (242), which could be one reason for the reduced *CD90* expression level in adult CDC and CF.

To conclude, although age-related differences between CDC and CF were not extensively investigated previously, the observations made in this work, such as a differential gene expression profile as well as an enhanced angiogenic potential of infant- compared to adult-CDC and CF-EV, could be related to results of preceding studies.

6.3 Cardiac biopsy derived non-myocytes

In this work a protocol for digestion of adult human heart biopsies to generate single cell suspensions for subsequent sc-RNAseq analysis was established. At the time of the experiments digestion protocols for cardiac tissue were only published for murine cardiac tissue (16-18, 20) or human embryonic tissue (22). Therefore, the digestion procedure had to be adjusted to digest more fibrous and/or fatty tissue. For this reason, the utilized digestion procedure lasted longer (1.5h) than the procedures of murine tissue (15-60 min) (16, 17, 20) and a higher concentration of the digestion enzymes (trypsin/collagenase II) had to be used. However, this may have caused apoptosis of numerous cells, possibly reflected by the high percentage of cells expressing mitochondrial genes in this sample (Figure 34F). In clustering analysis (Figure 35A) these apoptotic cells were mainly represented by clusters 0 and 1, in which genes were assigned to the GO-term “collagen containing extracellular matrix”, suggesting their belonging to the non-myocyte cell group. This fact could indicate that NMC are more affected by higher enzyme (trypsin/collagenase II) concentrations and longer digestion times than immune cells which did not show signs of apoptosis and were generally overrepresented in the sample compared to no hematopoietic NMC (9). For a more efficient and reliable analysis of NMC, it is, therefore, desirable to further optimize the digestion protocol.

Nevertheless, in this experiment all major cardiac non-myocyte cell types were detected. Despite differences in analyzed heart region, species and digestion technique, data shown in this work correspond to results reported by Skelly *et al.* (16). They showed that non hematopoietic NMC represented the largest cell group, while immune cells ranked second. However, data presented here, show that T-cells constituted the largest cluster of immune cells, whereas in the analysis of Skelly *et al.* the macrophages represented the largest immune cell cluster. Wang *et al.* (21) and Gladka *et al*. (17) only identified macrophages, but no T- or B-cells in their samples. This discrepancy could possibly be due to remaining blood in the tissue sample analyzed, also a candidate for optimization in the digestion protocol. Skelly *et al.* discriminated between macrophages, dendritic-like cells and granulocytes (16). Since this work is focused on non hematopoietic cell types, no subclustering of cluster 5 was performed. However, as granulocyte and macrophage markers were upregulated in cluster 5 (see paragraph 5.3.1), it is

tempting to speculate that analysis of transcriptional gradients would reveal several myeloid populations.

As illustrated in Table 1, the percentage of EC in the heart is a topic of continuous debate (6, 10, 11). In this analysis cluster 8, which showed enrichment for typical EC terms and expression of typical EC markers, represented only 7.2% of the total cell number of the biopsy (Table 42). However, it cannot be excluded that some EC are dispersed in clusters 1, 3, 6, 9 or 13, as the GO-term "tube development" was significantly enriched in these clusters as well. Wang *et al.* reported an EC cluster with enriched GO-terms such as "cell-matrix adhesion" and "cell-junction assembly" (21). This suggested that there are certain EC groups which may exhibit similarities to CF or SMC, and common clusters of such EC with CF and/or SMC could evolve.

Fibroblast transcriptional heterogeneity has been reported numerous times (16, 17, 21, 243). In this analysis of a human cardiac biopsy four different fibroblast subtypes were identified (clusters 1, 3, 6, 9 of Figure 35A). To reveal which features separated the fibroblasts into four clusters, the aspects of their developmental origin, differentiation to myofibroblasts and incorporation of different cell types within the clusters were reviewed.

Regarding the expression of developmental markers (see Table 43 and Figure 36), no clear separation of clusters according to the fibroblasts developmental origin, such as epicardial, endocardial or neural crest derived CF could be determined. Sc-RNAseq studies with embryonic (18) and fetal hearts (22) did not address the transcriptional differences related to the developmental origin of fibroblast clusters. Suryawanshi *et al*. differentiated between two fibroblast clusters according to their proliferative capacity, however, it was not correlated with their developmental stage (22). In this data, all clusters showed enrichment for the GO-term "regulation of cell population proliferation". However, cluster 1 and 6 upregulated the developmental markers *TCF21* and *SOX9*, suggesting their epicardial origin. *TBX20* was exclusively upregulated in cluster 1 which could indicate that this cluster also involved CF from endocardial developmental origins (244, 245).

In the context of cardiac fibrosis, there is much evidence that CF undergo a transcriptional change allowing them to differentiate to the phenotype of myofibroblasts (40, 246). Myofibroblasts differ from quiescent CF by higher proliferation, enhanced production of ECM and cytokines and expression of SMC related features (247). Myofibroblast are considered to evolve only in diseased tissue, but not in healthy tissue (247). The tissue analyzed derived from left atrial appendage of a patient suffering from biatrial tumor and mitral valve insufficiency (see patient 22, Table 14). According to the surgeons, the tumor did not affect the analyzed tissue. However, atrial fibrosis is correlated with mitral valve insuffiency and the appendage tissue is also affected (248). This would explain why in the analyzed biopsy different myofibroblast markers were upregulated in several different clusters (see Table 43). Nevertheless, all

myofibroblast markers examined were found to be upregulated in cluster 3 and/or 9 (see Table 43), suggesting that a transcriptional shift to this type of "activated" fibroblast has occurred in these cells. Wang *et al.* addressed the change in NMC subclusters in heart failure and reported a certain CF cluster which increased in failing compared to normal hearts and which showed enrichment of GO-terms such as "ECM organization" and "fibroblast proliferation" (21). Similarly, in this study cluster 3 and 9 showed enrichment for GO-terms related to ECM production and differentiation, indicating a possible phenotypic shift in these clusters.

Clearly outstanding from the other fibroblast-like clusters was cluster 6, as it showed association with secretion and immune processes, upregulation of developmental markers and no relation to neurogenesis. A characteristic of fibroblasts in injured environment is secretion of chemokines (249, 250) resulting in the recruitment of immune cells to the inflammation site (251). Shook *et al.* reported different subsets of skin myofibroblasts, which could be distinguished on the transcriptional level by different ECM components and cytokines (193). In uninjured skin, mesenchymal subsets positive for CD29 (ITGB1) correlated with high *Acta2* and *Col1* expression, similarly to characteristics of cluster 9 and 3 in the data presented here (Table 43). Cluster 6 corresponded to a mesenchymal subset of CD29 low expressing cells, since *ITGB1* was not upregulated in this cluster in contrast to cluster 3, 9 and 1 (Table 43). Thus, cluster 6 might represent a subtype of activated fibroblasts which is focused on secretion of cytokines mediating immune response rather than on extensive production of ECM.

In contrast to the data by Skelly *et al.* (16), small cell groups such as pericytes or Schwann cells which showed similarities to fibroblasts, were not identified as separate clusters in the dataset shown. Other than Skelly *et al*., who observed association with neuro-regulatory terms in the Schwann cell cluster, in the dataset presented here, GO-terms such as "neurogenesis" and "neuron differentiation" arose in three of the four fibroblast-subtypes (cluster 1, 3 and 9, see Table 42). This might indicate that potential Schwann cells did not build their own cluster but were dispersed among several clusters. Wang *et al.* (21), Gladka *et al.* (17), DeLaughter *et al.* (20), Suryawanshi *et al.* (22) and Soysa *et al.* (18) did also not report Schwann cells as a separate cluster/cell group in their analysis, possibly due to limited sensitivity of the methods used or the low number of cells analyzed.

In this analysis only a small cluster (cluster 13, 1.1%) has been identified as SMC. Nevertheless, it is likely that a considerable amount of SMC was included in clusters 0, 1, 3, 6 or 9 as well. It has often been reported that the discrimination between CF and SMC is difficult and not always possible. For example, Bergmann *et al*. termed cells which did not express CM or EC marker (non PCM-1, non UEA-1) as mesenchymal cells (6). DeLaughter *et al.* reported of a group of "fibroblast-enriched cells" which could be distinguished from CM and EC by sc-RNAseq (20). Although Wang *et al.* distinguished between two approximately equal cell clusters as fibroblasts and SMC, they reported of a functionally similar cluster present in each of these cell groups (FB1

and SMC1), which was linked to ECM organization. For this reason they concluded that in the adult heart CF and SMC overlap in their functions (21). Phenotypic similarity between SMC and CF related to ECM gene expression was also reported by Li *et al.* (199) and Cui *et al.* (243). The fact that *NR4A1*, which was identified as specific SMC marker in the cultured model (Figure 8B), was upregulated in the biopsy fibroblast clusters 9, 3 and 6 as well as in biopsy EC cluster 8, but not in cluster 13, again emphasizes the fluent transcriptional transitions between non-myocyte cell types. However, the assumption that cluster 13 represented SMC was assured by upregulation of *ENTPD1* and *MCAM* in this cluster, a strategy presented by Skelly *et al*. to discriminate SMC from pericytes and Schwann cells (16).

Pericytes, which were reported to have a density of about 3.6×10^7 pericytes/cm^3 in left ventricular tissue (252), could not be identified as a separate cell cluster in this atrial biopsy. This mural cell type is considered to be a mesenchymal cell type which regulates vasculature by building connections with EC (253). Pericytes are mainly defined by their periendothelial location, their function as regulators of vessel growth and permeability and their rounded morphology with finger-like projections, but they cannot be clearly distinguished from CF and SMC by their transcriptional patterns (253, 254). As pericytes, CF and SMC derive from the epicardial lineage (180), their immunologic phenotype and marker expression is similar, making it hard to find a reliable marker specific for pericytes (253). However, Skelly *et al.* identified a separate pericyte cluster based on the expression of *P2ry14*, a marker not upregulated in any cluster in the data presented here, and *Pdgfrb* (see Table 43 for upregulation in this work). Besides, Skelly *et al*. presented a flow cytometric isolation technique of pericytes based on the expression of MCAM and the absence of ENTPD1 and CD59a (16). A cluster with such characteristics was not present in the data of this work. Four out of five pericyte markers listed in Table 43 were significantly upregulated in cluster 13, revealing the functional relation of pericytes and SMC. The marker *STEAP4* was upregulated in the fibroblast subclusters 1 and 3 and *MCAM* was also upregulated in the EC cluster 8. Thus, similarly to Schwann cells and SMC, pericytes were likely to be dispersed among several clusters, the majority of which was probably included in cluster 13.

In summary, sc-RNAseq data of a human cardiac tissue biopsy revealed that non hematopoietic NMC could be separated into the major groups of EC and CF/SMC. However, their transcriptomic patterns frequently showed overlapping genes, particularly the different CF subsets and SMC.

Comparison of cultured cells to biopsy derived cell types revealed that culture conditions clearly altered gene expression. It is has been previously shown that cell culture changed gene and protein expression of CF, making them more similar to myofibroblasts (185). Generally, the effect of cell culture is dependent on the culture medium used, which usually contains different supplements and growth factors promoting cell growth (255). Therefore, the observation that

cultured cells upregulated protein biosynthesis and proliferation processes compared to biopsy derived cells is not surprising.

A direct comparison of biopsy derived and cultured NMC has not been published yet. An issue raised by the comparison presented in Figure 38 is that the biopsy derived cells do not represent pure cell populations, but rather mixtures of different cell types, making cell clusters from the biopsy sample not an ideal comparison for one purified single cell type. This mostly affected the comparison between cultured SMC and biopsy derived SMC, which were not distinguishable from other mesenchymal cells in global clustering. Besides, cultured SMC and EC were obtained from vessels and not directly from cardiac tissue, so in those cases cells from two different anatomical regions were compared.

Nevertheless, the results presented in this work emphasized that the analyzed cultured cells do have common features with their counterparts in the biopsy. Although commonly upregulated genes constituted less than 13% of the total number of genes upregulated in cultured cells, GO-analysis revealed association with terms typical for the according cell type. EC most closely resembled the biopsy derived EC cluster, as shown by the UMAP plot (Figure 37B). The reason for this might be that EC culture medium contains VEGF which is known to promote cell differentiation into an endothelial phenotype and enhances endothelial angiogenic ability (256, 257). SMC medium is supplemented with EGF which has been reported to promote a pathological phenotype of SMC (258, 259). This was confirmed by common upregulation of *ADAMTS1* in both cultured and biopsy derived SMC, a gene associated with atherosclerosis (260). In contrast, MEF medium, the usual CF culture medium, is only supplemented with FBS, which has been criticized because of its lot-to-lot variability (261, 262). This may explain why markers found to be specific in cultured CF such as *CPA4* and *IGFBP2* were not expressed in any of the biopsy clusters identified as fibroblast-like cells.

Altogether, main cellular subpopulations known to be present in cardiac tissue were identified in this analysis. However, smaller cell populations could not be distinguished by subclustering analysis. The comparison of cultured and biopsy derived NMC demonstrated that cultured cells represented a reliable but not ideal model for *in vivo* NMC. Therefore, sc-RNAseq of biopsy derived cells would be the method of choice to explore *in vivo* cell characteristics.

7. Conclusion and outlook

Historically, studies of cardiac function in healthy and diseased states concentrated on the muscular component of the heart and thus on molecular properties of cardiomyocytes. However, since recent years, more attention is beeing payed to non-myocyte cell populations. With the growing availability of modern techniques such as sc-RNAseq, scientists are starting to understand that CF, EC and SMC comprise a considerable part of cardiac cell types and play crucial roles in the proper function of the heart as well as in repair mechanisms during disease.

The focus of this work was the investigation of the main cardiac NMC types CF, SMC and EC and the cardiac-derived CDC. The analysis of cultured CF, SMC, and EC revealed a distinct phenotype of EC, both on gene and protein level. On the contrary, CF and SMC showed more similarities, particularly in pathways related to ECM production. Characterization of the clinically used cell type CDC demonstrated its heterogeneity and partial similarity to NMC types, particularly CF and SMC, which is most likely driven by its special culture conditions (3D spheres) including the exposure to high concentrations of growth factors. Thus, CDC were identified as a highly proliferative, secretory, and ECM producing cell type reflecting the features of inflammatory cells such as myofibroblasts. Besides, the previously common hypothesis that CDC have properties of cardiac progenitor cells could be excluded by direct comparison to iPSC-derived cardiac progenitors.
The angiogenic potential of CDC was higher in CDC derived from pediatric patients compared to adult patients. Despite the low sample number included in the comparison of two pediatric age groups, CDC-EV-mediated effects on EC migration were increased in the neonate patient (HLH1) group compared to the group of older infant patients (HLH2/3). The positive CDC-EV-mediated effects could not be reproduced with CF-EV derived from age-matched patients. CF exposed to the same culture conditions as CDC (CFSPh) showed gene expression profiles approaching that of CDC, but did not recapitulate their secretory effects. Beneficial effects in clinical trials observed with infant CDC might therefore be explained by their enhanced paracrine angiogenic potential and reduced similarity to CF compared to adult CDC.

Although gene expression of cultured CF, SMC and EC could be associated with corresponding GO-terms typical of each cell type, a clear influence of cell culture conditions was detected by upregulation of protein biosynthetic processes in cultured cells, which were not observed in cells derived from the cardiac biopsy. Sc-RNAseq of biopsy derived cells comprised a more detailed pictured of NMC, allowing to discriminate between several CF subtypes and showing the fluid transitions of the transcriptome between SMC and CF. However, less abundant cell types such as Schwann cells or pericytes could not be identified in this analysis, possibly due to the low cell number in the sample. A drawback of the biopsy sc-RNAseq data presented here is

the relative high percentage of apoptotic cells and blood-derived immune cells. However, this can be improved by further optimization of the protocol.

For a more reliable and representative analysis of the *in vivo* NMC gene expression patterns and of the distribution of various NMC populations in different locations of the human heart, the digestion protocol of cardiac biopsies should be further optimized. Finally, the ideal protocol would allow the analysis of biopsy samples small enough to analyze individual cardiac regions in pediatric or adult patients. Such a fine-mapping of the human heart would enable a better comprehension of gene regulation patterns throughout homeostasis and disease development and possibly identify novel therapeutic targets or pathways.

8. Acknowledgments

First and foremost, I would like to express my appreciation and thanks to my first advisor Prof. Dr. Markus Krane for supporting my thesis and enabling related research. I would also like to thank PD Dr. Harald Lahm and Prof. Dr. Alessandra Moretti for being my mentors and for their insightful comments. I specially thank Dr. Stefanie Doppler who continuously mentored me during all my PhD studies and shared with me her research experience. Besides, I'd like to express my gratitude to the whole team of the department of experimental surgery for their assistance in the laboratory work and to the surgeons who provided me with numerous cardiac biopsy samples. Moreover, I thank the clinic director Prof. Dr. Rüdiger Lange for enabling the establishment of a basic research facility in the German Heart Center and for taking care of its financial support.

This work would not have been possible without the collaborators whom I'd also like to express my thanks. Particularly the research group of Dr. Raffaele Teperino (Institute of Experimental Genetics, Helmholtz Zentrum München, German Research center for Environmental Health - Neuherberg, Germany; German Center for Diabetes Research (DZD) - Neuherberg, Germany) provided immense help with sc-RNAseq library preparation (Dr. Jonathan Darr) and data analysis (Archana Tomar). Dr. Kathrin Gärtner and Dr. Corinna Hüls from the group of Prof. Reinhard Zeidler (Research Unit Gene Vectors, Helmholtz Center Munich German Research Center for Environmental Health, Munich, Germany) enabled the measurement of the EV preparations on their ZetaView PMX110 instrument. Dr. Deepak Ramanujam from the group of Prof. Dr. Engelhardt (Institute of Pharmacology and Toxicology, Technische Universität München, Biedersteiner Str. 29, Munich 80802, Germany) organized the NRCM preparation and their transport to DHM. Dr. Catharina Wenk from the group of Prof. Dr. Dr. Lesca M. Holdt (Institute of Laboratory Medicine, Ludwig-Maximilians-University Munich, Munich, Germany) provided me the IncuCyte ZOOM® 96-Well Migration Assay system instrument for the migration assays. Dr. Helmut Blum (Gene Center - Laboratory for Functional Genome Analysis, Ludwig-Maximilians-Universität München, Feodor-Lynen-Straße 25, 81377 Munich) and Prof. Dr. Meitinger (Institute of Human Genetics, Helmholtz Center Munich German Research Center for Environmental Health, Munich, Germany) organized the sequencing.

I sincerely thank the organizers of the MLST program for providing the PhD students such an interesting course program and continuous organizational support. Particularly, I'd like to thank the MLST committee for chosing me to receive a PhD scholarship for my first semester. Finally, I thank my family for their continuous care during my PhD studies.

9. List of Figures

10. List of Supplemental Figures

11. List of Tables

12. Abbreviations

% MT Genes	percentage of mitochondrial genes per cell
AF	adipose-tissue-derived fibroblasts
ASD secundum	atrial septal defect type 2
AVC	atrioventricular canal
AVR	aortic valve Replacement
avg_logFC	average natural logarithm of the gene's fold change
BSA	albumin from Bovine Serum
bFGF	basic fibroblast growth factor
CABG	coronary artery bypass graft
CAVSD	Complete atrioventricular septum defect
CCA	canonical correlation analysis
CDC	cardiosphere-derived cells
CDC/CF-EV	CDC/CF derived extracellular vesicles
cDNA	complementary DNA
CEM	complete explant medium
CF	cardiac fibroblasts
CF Scratch (assay)	cardiac fibroblast migration assay
CFSPh	cardiac-fibroblast-sphere-derived cells
CGM	cardiosphere-growing medium
CM	cardiomyocytes
COG	cardiac outgrowth
DAPI	4',6-Diamidino-2-Phenylindole
DMEM	Dulbecco´s MEM Medium
DIFF D8	Human induced pluripotent cells on day 8 of cardiac differentiation protocol
DILV	Double inlet left ventricle
dims	Which dimensions to use as input features by RunUMAP function
DMSO	dimethylsulfoxid
DNA	desoxyribonucleic acid
DORV	Double-outlet right ventricle
D-PBS	dulbecco's phosphate-buffered saline
dsDNA	double-stranded DNA
EC	endothelial cells
EC Scratch (assay)	endothelial cell migration assay
ECM	extracellular matrix
EGF	epidermal growth factor
EMT	epithelial-to-mesenchymal transition
EPDC	epicardial-derived cells
EV	extracellular vesicles
FBS	fetal bovine serum
FC	flow cytometry
FGF	fibroblast growth factor

FSC	forward scatter
GEMs	Gel Bead-In-EMulsions
Genes/cell	number of genes detected per cell
GF	growth factors
GFP	green fluorescent protein
GO	gene ontology
GSEA	gene set enrichment analysis
HBSS	hank's balanced salt solution
HLH1	neonatal patients aged ≤ 21 days (see Table 15)
HLH2/3	pediatric patients aged 1 month- 6 years (see Table 15)
HLHS	hypoplastic left heart syndrome
ICC	immunocytochemistry
IHC	immunehistochemistry
IMDM	Iscove's Modified Dulbecco's Medium
iPSC	induced pluripotent stem cells
IVS	intact ventricular septum
LNA	locked nucleic acid
LV	left ventricle
Matrigel	tube formation assay on matrigel (matrigel assay)
MAZE	MAZE procedure for Atrial Fibrillation
mCF	murine cardiac fibroblasts
MI	myocardial infarction
miR	microRNA
MVR	mitral valve replacement
mRNA	messenger RNA
MTT	3-(4,5-dimethylthiazol-2-yl)-2,5-diphenyltetrazolium bromide
MTT assay	Proliferation assay of cardiac fibroblasts
n.d.	not determined
NegCtr	negative control
NMC	non-myocyte cells
NMC_1_2	clusters 1 and 2 of global analysis of biopsy and cultured cells (Figure 37B)
Norwood	norwood I procedure for single-ventricle patients
npcs	total number of PCs to computed and stored by RunPCA function
NRCM	neonatal rat cardiomyocytes
NRCM assay	apoptosis test with neonatal rat cardiomyocytes
p_val_adj	adjusted *p*-value
PBS-T	phosphate-buffered saline-Triton X mixture
PCA	principle component analysis
qRT-PCR	semiquantitative real-time polymerase chain reaction
Ref.	reference
RT	reverse transcription
sc-RNAseq	single cell RNA sequencing
SEM	standard error of the mean

SMC	smooth muscle cells
SSC	side scatter
STS-code	diagnostic code of the Society of Thoracic Surgeons
SV	single ventricle
TBE Buffer	tris borate EDTA Buffer
TEM	transmission electron microscopy
TF	transcription factor
TGA	transposition of great arteries
TIMP	tissue inhibitor of metalloproteinases
TVR	tricuspid valve replacement
uDEG	upregulated differentially expressed genes
UMAP	uniform manifold approximation and projection
UMI	unique molecular identifier
UMI count/cell	number of UMIs per cell
VEGF	vascular endothelial growth factor
VSD	ventricular septum defect

13. References

1. Xin M, Olson EN, Bassel-Duby R. Mending broken hearts: cardiac development as a basis for adult heart regeneration and repair. Nat Rev Mol Cell Biol. 2013;14(8):529-41.
2. Zak R. Development and proliferative capacity of cardiac muscle cells. Circulation research. 1974;35(2):suppl II:17-26.
3. Souders CA, Bowers SL, Baudino TA. Cardiac fibroblast: the renaissance cell. Circulation research. 2009;105(12):1164-76.
4. Nag AC. Study of non-muscle cells of the adult mammalian heart: a fine structural analysis and distribution. Cytobios. 1980;28(109):41-61.
5. Doll S, Dressen M, Geyer PE, Itzhak DN, Braun C, Doppler SA, et al. Region and cell-type resolved quantitative proteomic map of the human heart. Nat Commun. 2017;8(1):1469.
6. Bergmann O, Zdunek S, Felker A, Salehpour M, Alkass K, Bernard S, et al. Dynamics of Cell Generation and Turnover in the Human Heart. Cell. 2015;161(7):1566-75.
7. Zhou P, Pu WT. Recounting Cardiac Cellular Composition. Circulation research. 2016;118(3):368-70.
8. Vliegen HW, van der Laarse A, Cornelisse CJ, Eulderink F. Myocardial changes in pressure overload-induced left ventricular hypertrophy. A study on tissue composition, polyploidization and multinucleation. Eur Heart J. 1991;12(4):488-94.
9. Doppler SA, Carvalho C, Lahm H, Deutsch MA, Dressen M, Puluca N, et al. Cardiac fibroblasts: more than mechanical support. Journal of thoracic disease. 2017;9(Suppl 1):S36-S51.
10. Banerjee I, Fuseler JW, Price RL, Borg TK, Baudino TA. Determination of cell types and numbers during cardiac development in the neonatal and adult rat and mouse. Am J Physiol Heart Circ Physiol. 2007;293(3):H1883-91.
11. Pinto AR, Ilinykh A, Ivey MJ, Kuwabara JT, D'Antoni ML, Debuque R, et al. Revisiting Cardiac Cellular Composition. Circulation research. 2016;118(3):400-9.
12. Wong AK, Osborn TG, Miller JG, Wickline SA. Quantification of ventricular remodeling in the tight-skin mouse cardiomyopathy with acoustic microscopy. Ultrasound Med Biol. 1993;19(5):365-74.
13. Bregagnollo EA, Zornoff LA, Okoshi K, Sugizaki M, Mestrinel MA, Padovani CR, et al. Myocardial contractile dysfunction contributes to the development of heart failure in rats with aortic stenosis. International journal of cardiology. 2007;117(1):109-14.
14. Camelliti P, Borg TK, Kohl P. Structural and functional characterisation of cardiac fibroblasts. Cardiovascular research. 2005;65(1):40-51.
15. Wagner A, Regev A, Yosef N. Revealing the vectors of cellular identity with single-cell genomics. Nat Biotechnol. 2016;34(11):1145-60.
16. Skelly DA, Squiers GT, McLellan MA, Bolisetty MT, Robson P, Rosenthal NA, et al. Single-Cell Transcriptional Profiling Reveals Cellular Diversity and Intercommunication in the Mouse Heart. Cell Rep. 2018;22(3):600-10.
17. Gladka MM, Molenaar B, de Ruiter H, van der Elst S, Tsui H, Versteeg D, et al. Single-Cell Sequencing of the Healthy and Diseased Heart Reveals Cytoskeleton-Associated Protein 4 as a New Modulator of Fibroblasts Activation. Circulation. 2018;138(2):166-80.
18. de Soysa TY, Ranade SS, Okawa S, Ravichandran S, Huang Y, Salunga HT, et al. Single-cell analysis of cardiogenesis reveals basis for organ-level developmental defects. Nature. 2019;572(7767):120-4.
19. Liu X, Chen W, Li W, Li Y, Priest JR, Zhou B, et al. Single-Cell RNA-Seq of the Developing Cardiac Outflow Tract Reveals Convergent Development of the Vascular Smooth Muscle Cells. Cell Rep. 2019;28(5):1346-61 e4.

20. DeLaughter DM, Bick AG, Wakimoto H, McKean D, Gorham JM, Kathiriya IS, et al. Single-Cell Resolution of Temporal Gene Expression during Heart Development. Developmental cell. 2016;39(4):480-90.
21. Wang L, Yu P, Zhou B, Song J, Li Z, Zhang M, et al. Single-cell reconstruction of the adult human heart during heart failure and recovery reveals the cellular landscape underlying cardiac function. Nat Cell Biol. 2020;22(1):108-19.
22. Suryawanshi H, Clancy R, Morozov P, Halushka MK, Buyon JP, Tuschl T. Cell atlas of the fetal human heart and implications for autoimmune-mediated congenital heart block. Cardiovascular research. 2019.
23. Olivey HE, Svensson EC. Epicardial-myocardial signaling directing coronary vasculogenesis. Circulation research. 2010;106(5):818-32.
24. Mikawa T, Gourdie RG. Pericardial mesoderm generates a population of coronary smooth muscle cells migrating into the heart along with ingrowth of the epicardial organ. Developmental biology. 1996;174(2):221-32.
25. Zhou B, Ma Q, Rajagopal S, Wu SM, Domian I, Rivera-Feliciano J, et al. Epicardial progenitors contribute to the cardiomyocyte lineage in the developing heart. Nature. 2008;454(7200):109-13.
26. Wang G, Jacquet L, Karamariti E, Xu Q. Origin and differentiation of vascular smooth muscle cells. The Journal of physiology. 2015;593(14):3013-30.
27. Tian X, Hu T, Zhang H, He L, Huang X, Liu Q, et al. Vessel formation. De novo formation of a distinct coronary vascular population in neonatal heart. Science. 2014;345(6192):90-4.
28. Owens GK, Kumar MS, Wamhoff BR. Molecular regulation of vascular smooth muscle cell differentiation in development and disease. Physiological reviews. 2004;84(3):767-801.
29. Liu M, Gomez D. Smooth Muscle Cell Phenotypic Diversity. Arteriosclerosis, thrombosis, and vascular biology. 2019;39(9):1715-23.
30. Regan CP, Adam PJ, Madsen CS, Owens GK. Molecular mechanisms of decreased smooth muscle differentiation marker expression after vascular injury. J Clin Invest. 2000;106(9):1139-47.
31. Dobnikar L, Taylor AL, Chappell J, Oldach P, Harman JL, Oerton E, et al. Disease-relevant transcriptional signatures identified in individual smooth muscle cells from healthy mouse vessels. Nat Commun. 2018;9(1):4567.
32. Humphrey JD, Dufresne ER, Schwartz MA. Mechanotransduction and extracellular matrix homeostasis. Nat Rev Mol Cell Biol. 2014;15(12):802-12.
33. Ishii Y, Langberg J, Rosborough K, Mikawa T. Endothelial cell lineages of the heart. Cell and tissue research. 2009;335(1):67-73.
34. Linask KK, Lash JW. Early heart development: dynamics of endocardial cell sorting suggests a common origin with cardiomyocytes. Dev Dyn. 1993;196(1):62-9.
35. Haack T, Abdelilah-Seyfried S. The force within: endocardial development, mechanotransduction and signalling during cardiac morphogenesis. Development. 2016;143(3):373-86.
36. Aird WC. Phenotypic heterogeneity of the endothelium: I. Structure, function, and mechanisms. Circulation research. 2007;100(2):158-73.
37. Aird WC. Endothelial cell heterogeneity. Cold Spring Harbor perspectives in medicine. 2012;2(1):a006429.
38. Kanekar S, Hirozanne T, Terracio L, Borg TK. Cardiac fibroblasts form and function. Cardiovascular pathology : the official journal of the Society for Cardiovascular Pathology. 1998;7(3):127-33.
39. Tarbit E, Singh I, Peart JN, Rose'Meyer RB. Biomarkers for the identification of cardiac fibroblast and myofibroblast cells. Heart Fail Rev. 2019;24(1):1-15.
40. Moore-Morris T, Guimaraes-Camboa N, Yutzey KE, Puceat M, Evans SM. Cardiac fibroblasts: from development to heart failure. Journal of molecular medicine. 2015;93(8):823-30.

41. Lajiness JD, Conway SJ. Origin, development, and differentiation of cardiac fibroblasts. Journal of molecular and cellular cardiology. 2014;70:2-8.
42. Acharya A, Baek ST, Huang G, Eskiocak B, Goetsch S, Sung CY, et al. The bHLH transcription factor Tcf21 is required for lineage-specific EMT of cardiac fibroblast progenitors. Development. 2012;139(12):2139-49.
43. Milgrom-Hoffman M, Harrelson Z, Ferrara N, Zelzer E, Evans SM, Tzahor E. The heart endocardium is derived from vascular endothelial progenitors. Development. 2011;138(21):4777-87.
44. Combs MD, Yutzey KE. Heart valve development: regulatory networks in development and disease. Circulation research. 2009;105(5):408-21.
45. Moore-Morris T, Guimaraes-Camboa N, Banerjee I, Zambon AC, Kisseleva T, Velayoudon A, et al. Resident fibroblast lineages mediate pressure overload-induced cardiac fibrosis. J Clin Invest. 2014;124(7):2921-34.
46. Gourdie RG, Dimmeler S, Kohl P. Novel therapeutic strategies targeting fibroblasts and fibrosis in heart disease. Nat Rev Drug Discov. 2016;15(9):620-38.
47. Chilton L, Ohya S, Freed D, George E, Drobic V, Shibukawa Y, et al. K+ currents regulate the resting membrane potential, proliferation, and contractile responses in ventricular fibroblasts and myofibroblasts. Am J Physiol Heart Circ Physiol. 2005;288(6):H2931-9.
48. Murakami M, Simons M. Fibroblast growth factor regulation of neovascularization. Curr Opin Hematol. 2008;15(3):215-20.
49. Villaschi S, Nicosia RF. Paracrine interactions between fibroblasts and endothelial cells in a serum-free coculture model. Modulation of angiogenesis and collagen gel contraction. Laboratory investigation; a journal of technical methods and pathology. 1994;71(2):291-9.
50. Rychli K, Kaun C, Hohensinner PJ, Dorfner AJ, Pfaffenberger S, Niessner A, et al. The anti-angiogenic factor PEDF is present in the human heart and is regulated by anoxia in cardiac myocytes and fibroblasts. Journal of cellular and molecular medicine. 2010;14(1-2):198-205.
51. Chirco R, Liu XW, Jung KK, Kim HR. Novel functions of TIMPs in cell signaling. Cancer Metastasis Rev. 2006;25(1):99-113.
52. Hamano Y, Zeisberg M, Sugimoto H, Lively JC, Maeshima Y, Yang C, et al. Physiological levels of tumstatin, a fragment of collagen IV alpha3 chain, are generated by MMP-9 proteolysis and suppress angiogenesis via alphaV beta3 integrin. Cancer Cell. 2003;3(6):589-601.
53. Liu H, Chen B, Lilly B. Fibroblasts potentiate blood vessel formation partially through secreted factor TIMP-1. Angiogenesis. 2008;11(3):223-34.
54. Gabbiani G, Ryan GB, Majne G. Presence of modified fibroblasts in granulation tissue and their possible role in wound contraction. Experientia. 1971;27(5):549-50.
55. Gabbiani G. The cellular derivation and the life span of the myofibroblast. Pathol Res Pract. 1996;192(7):708-11.
56. Sun Y, Weber KT. RAS and connective tissue in the heart. Int J Biochem Cell Biol. 2003;35(6):919-31.
57. Calderone A, Bel-Hadj S, Drapeau J, El-Helou V, Gosselin H, Clement R, et al. Scar myofibroblasts of the infarcted rat heart express natriuretic peptides. J Cell Physiol. 2006;207(1):165-73.
58. Brown RD, Ambler SK, Mitchell MD, Long CS. The cardiac fibroblast: therapeutic target in myocardial remodeling and failure. Annu Rev Pharmacol Toxicol. 2005;45:657-87.
59. Lighthouse JK, Small EM. Transcriptional control of cardiac fibroblast plasticity. Journal of molecular and cellular cardiology. 2016;91:52-60.
60. Masur SK, Dewal HS, Dinh TT, Erenburg I, Petridou S. Myofibroblasts differentiate from fibroblasts when plated at low density. Proc Natl Acad Sci U S A. 1996;93(9):4219-23.
61. Malliaras K, Makkar RR, Smith RR, Cheng K, Wu E, Bonow RO, et al. Intracoronary cardiosphere-derived cells after myocardial infarction: evidence of therapeutic regeneration in the final 1-year results

of the CADUCEUS trial (CArdiosphere-Derived aUtologous stem CElls to reverse ventricULar dySfunction). J Am Coll Cardiol. 2014;63(2):110-22.
62. Makkar RR, Smith RR, Cheng K, Malliaras K, Thomson LE, Berman D, et al. Intracoronary cardiosphere-derived cells for heart regeneration after myocardial infarction (CADUCEUS): a prospective, randomised phase 1 trial. Lancet. 2012;379(9819):895-904.
63. Chakravarty T, Makkar RR, Ascheim DD, Traverse JH, Schatz R, DeMaria A, et al. ALLogeneic Heart STem Cells to Achieve Myocardial Regeneration (ALLSTAR) Trial: Rationale and Design. Cell transplantation. 2017;26(2):205-14.
64. Timothy DH. Intracoronary ALLogeneic Heart STem Cells to Achieve Myocardial Regeneration - ALLSTAR. American Heart Association Annual Scientific Sessions (AHA 2017), Anaheim, CA.
65. Taylor M, Jefferies J, Byrne B, Lima J, Ambale-Venkatesh B, Ostovaneh MR, et al. Cardiac and skeletal muscle effects in the randomized HOPE-Duchenne trial. Neurology. 2019;92(8):e866-e78.
66. Shirokova N, Niggli E. Cardiac phenotype of Duchenne Muscular Dystrophy: insights from cellular studies. Journal of molecular and cellular cardiology. 2013;58:217-24.
67. Tarui S, Ishigami S, Ousaka D, Kasahara S, Ohtsuki S, Sano S, et al. Transcoronary infusion of cardiac progenitor cells in hypoplastic left heart syndrome: Three-year follow-up of the Transcoronary Infusion of Cardiac Progenitor Cells in Patients With Single-Ventricle Physiology (TICAP) trial. J Thorac Cardiovasc Surg. 2015;150(5):1198-207, 208 e1-2.
68. Ishigami S, Ohtsuki S, Eitoku T, Ousaka D, Kondo M, Kurita Y, et al. Intracoronary Cardiac Progenitor Cells in Single Ventricle Physiology: The PERSEUS (Cardiac Progenitor Cell Infusion to Treat Univentricular Heart Disease) Randomized Phase 2 Trial. Circulation research. 2017;120(7):1162-73.
69. Sano T, Ousaka D, Goto T, Ishigami S, Hirai K, Kasahara S, et al. Impact of Cardiac Progenitor Cells on Heart Failure and Survival in Single Ventricle Congenital Heart Disease. Circulation research. 2018;122(7):994-1005.
70. Messina E, De Angelis L, Frati G, Morrone S, Chimenti S, Fiordaliso F, et al. Isolation and expansion of adult cardiac stem cells from human and murine heart. Circulation research. 2004;95(9):911-21.
71. Armstrong MT, Lee DY, Armstrong PB. Regulation of proliferation of the fetal myocardium. Dev Dyn. 2000;219(2):226-36.
72. Reynolds BA, Weiss S. Generation of neurons and astrocytes from isolated cells of the adult mammalian central nervous system. Science. 1992;255(5052):1707-10.
73. Smith RR, Barile L, Cho HC, Leppo MK, Hare JM, Messina E, et al. Regenerative potential of cardiosphere-derived cells expanded from percutaneous endomyocardial biopsy specimens. Circulation. 2007;115(7):896-908.
74. Chien KR, Frisen J, Fritsche-Danielson R, Melton DA, Murry CE, Weissman IL. Regenerating the field of cardiovascular cell therapy. Nat Biotechnol. 2019;37(3):232-7.
75. van Berlo JH, Kanisicak O, Maillet M, Vagnozzi RJ, Karch J, Lin SC, et al. c-kit+ cells minimally contribute cardiomyocytes to the heart. Nature. 2014;509(7500):337-41.
76. Bergmann O, Bhardwaj RD, Bernard S, Zdunek S, Barnabe-Heider F, Walsh S, et al. Evidence for cardiomyocyte renewal in humans. Science. 2009;324(5923):98-102.
77. Chimenti I, Smith RR, Li TS, Gerstenblith G, Messina E, Giacomello A, et al. Relative roles of direct regeneration versus paracrine effects of human cardiosphere-derived cells transplanted into infarcted mice. Circulation research. 2010;106(5):971-80.
78. Ibrahim AG, Cheng K, Marban E. Exosomes as critical agents of cardiac regeneration triggered by cell therapy. Stem Cell Reports. 2014;2(5):606-19.
79. Gallet R, Dawkins J, Valle J, Simsolo E, de Couto G, Middleton R, et al. Exosomes secreted by cardiosphere-derived cells reduce scarring, attenuate adverse remodelling, and improve function in acute and chronic porcine myocardial infarction. Eur Heart J. 2017;38(3):201-11.

80. Tseliou E, Fouad J, Reich H, Slipczuk L, de Couto G, Aminzadeh M, et al. Fibroblasts Rendered Antifibrotic, Antiapoptotic, and Angiogenic by Priming With Cardiosphere-Derived Extracellular Membrane Vesicles. J Am Coll Cardiol. 2015;66(6):599-611.
81. Thery C. Exosomes: secreted vesicles and intercellular communications. F1000 Biol Rep. 2011;3:15.
82. Barile L, Moccetti T, Marbán E, Vassalli G. Roles of exosomes in cardioprotection. Eur Heart J. 2017;38(18):1372-9.
83. Sharma S, Mishra R, Simpson D, Wehman B, Colletti EJ, Deshmukh S, et al. Cardiosphere-derived cells from pediatric end-stage heart failure patients have enhanced functional activity due to the heat shock response regulating the secretome. Stem Cells. 2015;33(4):1213-29.
84. Redgrave RE, Tual-Chalot S, Davison BJ, Singh E, Hall D, Amirrasouli MM, et al. Cardiosphere-Derived Cells Require Endoglin for Paracrine-Mediated Angiogenesis. Stem Cell Reports. 2017;8(5):1287-98.
85. Lang JK, Young RF, Ashraf H, Canty JM, Jr. Inhibiting Extracellular Vesicle Release from Human Cardiosphere Derived Cells with Lentiviral Knockdown of nSMase2 Differentially Effects Proliferation and Apoptosis in Cardiomyocytes, Fibroblasts and Endothelial Cells In Vitro. PLoS One. 2016;11(11):e0165926.
86. Barile L, Lionetti V, Cervio E, Matteucci M, Gherghiceanu M, Popescu LM, et al. Extracellular vesicles from human cardiac progenitor cells inhibit cardiomyocyte apoptosis and improve cardiac function after myocardial infarction. Cardiovascular research. 2014;103(4):530-41.
87. Ishigami S, Ohtsuki S, Tarui S, Ousaka D, Eitoku T, Kondo M, et al. Intracoronary autologous cardiac progenitor cell transfer in patients with hypoplastic left heart syndrome: the TICAP prospective phase 1 controlled trial. Circulation research. 2015;116(4):653-64.
88. Simpson DL, Mishra R, Sharma S, Goh SK, Deshmukh S, Kaushal S. A strong regenerative ability of cardiac stem cells derived from neonatal hearts. Circulation. 2012;126(11 Suppl 1):S46-53.
89. Nakamura T, Hosoyama T, Kawamura D, Takeuchi Y, Tanaka Y, Samura M, et al. Influence of aging on the quantity and quality of human cardiac stem cells. Sci Rep. 2016;6:22781.
90. Walravens AS, Vanhaverbeke M, Ottaviani L, Gillijns H, Trenson S, Driessche NV, et al. Molecular signature of progenitor cells isolated from young and adult human hearts. Sci Rep. 2018;8(1):9266.
91. Yabrodi M, Mastropietro CW. Hypoplastic left heart syndrome: from comfort care to long-term survival. Pediatric research. 2017;81(1-2):142-9.
92. Lahm H, Schon P, Doppler S, Dressen M, Cleuziou J, Deutsch MA, et al. Tetralogy of Fallot and Hypoplastic Left Heart Syndrome - Complex Clinical Phenotypes Meet Complex Genetic Networks. Current genomics. 2015;16(3):141-58.
93. Lindinger A, Schwedler G, Hense HW. Prevalence of congenital heart defects in newborns in Germany: Results of the first registration year of the PAN Study (July 2006 to June 2007). Klinische Padiatrie. 2010;222(5):321-6.
94. Zaidi S, Choi M, Wakimoto H, Ma L, Jiang J, Overton JD, et al. De novo mutations in histone-modifying genes in congenital heart disease. Nature. 2013;498(7453):220-3.
95. Feinstein JA, Benson DW, Dubin AM, Cohen MS, Maxey DM, Mahle WT, et al. Hypoplastic left heart syndrome: current considerations and expectations. J Am Coll Cardiol. 2012;59(1 Suppl):S1-42.
96. W. Mastropietro C, A. Clark J, M. Grimaldi L, S. Killinger J, Richmond M. The Patient with a Single Cardiac Ventricle. Current Pediatric Reviews. 2012;8(3):253-76.
97. Abramoff MD. Image Processing with ImageJ. Biophotonics Intl. 2004;11(7):36-42.
98. Schneider CA, Rasband WS, Eliceiri KW. NIH Image to ImageJ: 25 years of image analysis. Nature Methods. 2012;9(7):671-5.
99. Schindelin J, Arganda-Carreras I, Frise E, Kaynig V, Longair M, Pietzsch T, et al. Fiji: an open-source platform for biological-image analysis. Nature methods. 2012;9(7):676-82.

100. Team RC. R: A language and environment for statistical computing. 2013.
101. Altschul SF, Gish W, Miller W, Myers EW, Lipman DJ. Basic local alignment search tool. Journal of molecular biology. 1990;215(3):403-10.
102. Carpentier G MM, Courty J and Cascone I. Angiogenesis Analyzer for ImageJ. Mondorf-les-Bains, Luxembourg: 4th ImageJ User and Developer Conference proceedings; 2012. p. 198-201.
103. Burridge PW, Holmstrom A, Wu JC. Chemically Defined Culture and Cardiomyocyte Differentiation of Human Pluripotent Stem Cells. Curr Protoc Hum Genet. 2015;87:21 3 1-15.
104. Wu SM, Fujiwara Y, Cibulsky SM, Clapham DE, Lien CL, Schultheiss TM, et al. Developmental origin of a bipotential myocardial and smooth muscle cell precursor in the mammalian heart. Cell. 2006;127(6):1137-50.
105. Strober W. Trypan blue exclusion test of cell viability. Curr Protoc Immunol. 2001;Appendix 3:Appendix 3B.
106. McGuire PG, Seeds NW. The interaction of plasminogen activator with a reconstituted basement membrane matrix and extracellular macromolecules produced by cultured epithelial cells. Journal of cellular biochemistry. 1989;40(2):215-27.
107. Vukicevic S, Kleinman HK, Luyten FP, Roberts AB, Roche NS, Reddi AH. Identification of multiple active growth factors in basement membrane Matrigel suggests caution in interpretation of cellular activity related to extracellular matrix components. Exp Cell Res. 1992;202(1):1-8.
108. Kleinman HK, McGarvey ML, Liotta LA, Robey PG, Tryggvason K, Martin GR. Isolation and characterization of type IV procollagen, laminin, and heparan sulfate proteoglycan from the EHS sarcoma. Biochemistry. 1982;21(24):6188-93.
109. Bissell DM, Arenson DM, Maher JJ, Roll FJ. Support of cultured hepatocytes by a laminin-rich gel. Evidence for a functionally significant subendothelial matrix in normal rat liver. J Clin Invest. 1987;79(3):801-12.
110. Lian X, Hsiao C, Wilson G, Zhu K, Hazeltine LB, Azarin SM, et al. Robust cardiomyocyte differentiation from human pluripotent stem cells via temporal modulation of canonical Wnt signaling. Proc Natl Acad Sci U S A. 2012;109(27):E1848-57.
111. Burridge PW, Matsa E, Shukla P, Lin ZC, Churko JM, Ebert AD, et al. Chemically defined generation of human cardiomyocytes. Nat Methods. 2014;11(8):855-60.
112. Sun N, Yazawa M, Liu J, Han L, Sanchez-Freire V, Abilez OJ, et al. Patient-specific induced pluripotent stem cells as a model for familial dilated cardiomyopathy. Sci Transl Med. 2012;4(130):130ra47.
113. Chen KG, Hamilton RS, Robey PG, Mallon BS. Alternative cultures for human pluripotent stem cell production, maintenance, and genetic analysis. J Vis Exp. 2014(89).
114. Davies SP, Reddy H, Caivano M, Cohen P. Specificity and mechanism of action of some commonly used protein kinase inhibitors. The Biochemical journal. 2000;351(Pt 1):95-105.
115. Ishizaki T, Uehata M, Tamechika I, Keel J, Nonomura K, Maekawa M, et al. Pharmacological properties of Y-27632, a specific inhibitor of rho-associated kinases. Molecular pharmacology. 2000;57(5):976-83.
116. Li X, Krawetz R, Liu S, Meng G, Rancourt DE. ROCK inhibitor improves survival of cryopreserved serum/feeder-free single human embryonic stem cells. Human reproduction. 2009;24(3):580-9.
117. Koyanagi M, Takahashi J, Arakawa Y, Doi D, Fukuda H, Hayashi H, et al. Inhibition of the Rho/ROCK pathway reduces apoptosis during transplantation of embryonic stem cell-derived neural precursors. Journal of neuroscience research. 2008;86(2):270-80.
118. Ungrin MD, Joshi C, Nica A, Bauwens C, Zandstra PW. Reproducible, ultra high-throughput formation of multicellular organization from single cell suspension-derived human embryonic stem cell aggregates. PLoS One. 2008;3(2):e1565.

119. Watanabe G, Saito Y, Madaule P, Ishizaki T, Fujisawa K, Morii N, et al. Protein kinase N (PKN) and PKN-related protein rhophilin as targets of small GTPase Rho. Science. 1996;271(5249):645-8.
120. Mehta A, Ramachandra CJ, Sequiera GL, Sudibyo Y, Nandihalli M, Yong PJ, et al. Phasic modulation of Wnt signaling enhances cardiac differentiation in human pluripotent stem cells by recapitulating developmental ontogeny. Biochimica et biophysica acta. 2014;1843(11):2394-402.
121. Bennett CN, Ross SE, Longo KA, Bajnok L, Hemati N, Johnson KW, et al. Regulation of Wnt signaling during adipogenesis. J Biol Chem. 2002;277(34):30998-1004.
122. Sassi Y, Avramopoulos P, Ramanujam D, Gruter L, Werfel S, Giosele S, et al. Cardiac myocyte miR-29 promotes pathological remodeling of the heart by activating Wnt signaling. Nat Commun. 2017;8(1):1614.
123. Dragan AI, Pavlovic R, McGivney JB, Casas-Finet JR, Bishop ES, Strouse RJ, et al. SYBR Green I: fluorescence properties and interaction with DNA. J Fluoresc. 2012;22(4):1189-99.
124. Rychlik W. Selection of primers for polymerase chain reaction. Mol Biotechnol. 1995;3(2):129-34.
125. Lee PY, Costumbrado J, Hsu CY, Kim YH. Agarose gel electrophoresis for the separation of DNA fragments. J Vis Exp. 2012(62).
126. Bartel DP. MicroRNAs: genomics, biogenesis, mechanism, and function. Cell. 2004;116(2):281-97.
127. Jensen SG, Lamy P, Rasmussen MH, Ostenfeld MS, Dyrskjot L, Orntoft TF, et al. Evaluation of two commercial global miRNA expression profiling platforms for detection of less abundant miRNAs. BMC Genomics. 2011;12:435.
128. Vester B, Wengel J. LNA (locked nucleic acid): high-affinity targeting of complementary RNA and DNA. Biochemistry. 2004;43(42):13233-41.
129. Burry RW. Controls for immunocytochemistry: an update. J Histochem Cytochem. 2011;59(1):6-12.
130. Krishnamurthy H, Scott Cram L. Basics of flow cytometry. In: Awtar Krishan HKaST, editor. Applications of Flow Cytometry in Stem Cell Research and Tissue Regeneration: Wiley-Blackwell; 2010.
131. Chazotte B. Labeling nuclear DNA using DAPI. Cold Spring Harbor protocols. 2011;2011(1):pdb prot5556.
132. Kivioja T, Vaharautio A, Karlsson K, Bonke M, Enge M, Linnarsson S, et al. Counting absolute numbers of molecules using unique molecular identifiers. Nature methods. 2011;9(1):72-4.
133. Rozenberg A, Leese F, Weiss LC, Tollrian R. Digital gene expression analysis with sample multiplexing and PCR duplicate detection: A straightforward protocol. BioTechniques. 2016;61(1):26-32.
134. Butler A, Hoffman P, Smibert P, Papalexi E, Satija R. Integrating single-cell transcriptomic data across different conditions, technologies, and species. Nature Biotechnology. 2018;36(5):411-20.
135. Macosko EZ, Basu A, Satija R, Nemesh J, Shekhar K, Goldman M, et al. Highly Parallel Genome-wide Expression Profiling of Individual Cells Using Nanoliter Droplets. Cell. 2015;161(5):1202-14.
136. Satija R, Farrell JA, Gennert D, Schier AF, Regev A. Spatial reconstruction of single-cell gene expression data. Nature Biotechnology. 2015;33(5):495-502.
137. Becht E, McInnes L, Healy J, Dutertre C-A, Kwok IWH, Ng LG, et al. Dimensionality reduction for visualizing single-cell data using UMAP. Nature Biotechnology. 2019;37(1):38-44.
138. Subramanian A, Tamayo P, Mootha VK, Mukherjee S, Ebert BL, Gillette MA, et al. Gene set enrichment analysis: A knowledge-based approach for interpreting genome-wide expression profiles. Proceedings of the National Academy of Sciences. 2005;102(43):15545-50.
139. Ashburner M, Ball CA, Blake JA, Botstein D, Butler H, Cherry JM, et al. Gene ontology: tool for the unification of biology. The Gene Ontology Consortium. Nat Genet. 2000;25(1):25-9.
140. Gene Ontology C. Gene Ontology Consortium: going forward. Nucleic acids research. 2015;43(Database issue):D1049-56.
141. Bosch S, de Beaurepaire L, Allard M, Mosser M, Heichette C, Chretien D, et al. Trehalose prevents aggregation of exosomes and cryodamage. Sci Rep. 2016;6:36162.

142. Bachurski D, Schuldner M, Nguyen PH, Malz A, Reiners KS, Grenzi PC, et al. Extracellular vesicle measurements with nanoparticle tracking analysis - An accuracy and repeatability comparison between NanoSight NS300 and ZetaView. J Extracell Vesicles. 2019;8(1):1596016.
143. Gartner K, Battke C, Dunzkofer J, Huls C, von Neubeck B, Kellner MK, et al. Tumor-derived extracellular vesicles activate primary monocytes. Cancer Med. 2018;7(5):2013-20.
144. Liang CC, Park AY, Guan JL. In vitro scratch assay: a convenient and inexpensive method for analysis of cell migration in vitro. Nat Protoc. 2007;2(2):329-33.
145. Tomasz M. Mitomycin C: small, fast and deadly (but very selective). Chemistry & biology. 1995;2(9):575-9.
146. Mosmann T. Rapid colorimetric assay for cellular growth and survival: application to proliferation and cytotoxicity assays. Journal of immunological methods. 1983;65(1-2):55-63.
147. Schmider E, Ziegler M, Danay E, Beyer L, Bühner M. Is it really robust? Methodology. 2010.
148. Kogan P-S, Tomar A, Darr J, Teperino R, Lahm H, Dreßen M, et al. Single Cell RNA Sequencing of Cardiosphere Derived Cells (CDCs) Revealed Their Heterogeneity and Similarities to Cardiac Non-Myocyte Cell Types. Manuscript submitted for publication 2020.
149. Furtado MB, Nim HT, Boyd SE, Rosenthal NA. View from the heart: cardiac fibroblasts in development, scarring and regeneration. Development. 2016;143(3):387-97.
150. Greulich F, Rudat C, Kispert A. Mechanisms of T-box gene function in the developing heart. Cardiovascular research. 2011;91(2):212-22.
151. Harvey RP, Lai D, Elliott D, Biben C, Solloway M, Prall O, et al. Homeodomain factor Nkx2-5 in heart development and disease. Cold Spring Harbor symposia on quantitative biology. 2002;67:107-14.
152. Thum T, Gross C, Fiedler J, Fischer T, Kissler S, Bussen M, et al. MicroRNA-21 contributes to myocardial disease by stimulating MAP kinase signalling in fibroblasts. Nature. 2008;456(7224):980-4.
153. Ramanujam D, Sassi Y, Laggerbauer B, Engelhardt S. Viral Vector-Based Targeting of miR-21 in Cardiac Nonmyocyte Cells Reduces Pathologic Remodeling of the Heart. Mol Ther. 2016;24(11):1939-48.
154. Assinder SJ, Stanton JA, Prasad PD. Transgelin: an actin-binding protein and tumour suppressor. Int J Biochem Cell Biol. 2009;41(3):482-6.
155. Mellgren AM, Smith CL, Olsen GS, Eskiocak B, Zhou B, Kazi MN, et al. Platelet-derived growth factor receptor beta signaling is required for efficient epicardial cell migration and development of two distinct coronary vascular smooth muscle cell populations. Circulation research. 2008;103(12):1393-401.
156. Yuan SM. alpha-Smooth Muscle Actin and ACTA2 Gene Expressions in Vasculopathies. Brazilian journal of cardiovascular surgery. 2015;30(6):644-9.
157. Lane EB, Hogan BL, Kurkinen M, Garrels JI. Co-expression of vimentin and cytokeratins in parietal endoderm cells of early mouse embryo. Nature. 1983;303(5919):701-4.
158. Luecken MD, Theis FJ. Current best practices in single-cell RNA-seq analysis: a tutorial. Mol Syst Biol. 2019;15(6):e8746.
159. Casula M, Montecucco F, Bonaventura A, Liberale L, Vecchie A, Dallegri F, et al. Update on the role of Pentraxin 3 in atherosclerosis and cardiovascular diseases. Vascular pharmacology. 2017;99:1-12.
160. Khan SA, Dong H, Joyce J, Sasaki T, Chu ML, Tsuda T. Fibulin-2 is essential for angiotensin II-induced myocardial fibrosis mediated by transforming growth factor (TGF)-beta. Laboratory investigation; a journal of technical methods and pathology. 2016;96(7):773-83.
161. Li X, Zhao D, Guo Z, Li T, Qili M, Xu B, et al. Overexpression of SerpinE2/protease nexin-1 Contribute to Pathological Cardiac Fibrosis via increasing Collagen Deposition. Sci Rep. 2016;6:37635.
162. Hsu DR, Economides AN, Wang X, Eimon PM, Harland RM. The Xenopus dorsalizing factor Gremlin identifies a novel family of secreted proteins that antagonize BMP activities. Molecular cell. 1998;1(5):673-83.
163. Peng J, Zhao S, Li Y, Niu G, Chen C, Ye T, et al. DLL4 and Jagged1 are angiogenic targets of orphan nuclear receptor TR3/Nur77. Microvascular research. 2019;124:67-75.

164. Raposo G, Stoorvogel W. Extracellular vesicles: exosomes, microvesicles, and friends. J Cell Biol. 2013;200(4):373-83.
165. Gyorgy B, Szabo TG, Pasztoi M, Pal Z, Misjak P, Aradi B, et al. Membrane vesicles, current state-of-the-art: emerging role of extracellular vesicles. Cellular and molecular life sciences : CMLS. 2011;68(16):2667-88.
166. Thery C, Zitvogel L, Amigorena S. Exosomes: composition, biogenesis and function. Nature reviews Immunology. 2002;2(8):569-79.
167. Ponce ML. Tube formation: an in vitro matrigel angiogenesis assay. Methods Mol Biol. 2009;467:183-8.
168. Davis GE, Stratman AN, Sacharidou A, Koh W. Molecular basis for endothelial lumen formation and tubulogenesis during vasculogenesis and angiogenic sprouting. Int Rev Cell Mol Biol. 2011;288:101-65.
169. Waring P, Mullbacher A. Cell death induced by the Fas/Fas ligand pathway and its role in pathology. Immunol Cell Biol. 1999;77(4):312-7.
170. Januszyk M, Rennert RC, Sorkin M, Maan ZN, Wong LK, Whittam AJ, et al. Evaluating the Effect of Cell Culture on Gene Expression in Primary Tissue Samples Using Microfluidic-Based Single Cell Transcriptional Analysis. Microarrays (Basel). 2015;4(4):540-50.
171. Wucherpfennig KW, Gagnon E, Call MJ, Huseby ES, Call ME. Structural biology of the T-cell receptor: insights into receptor assembly, ligand recognition, and initiation of signaling. Cold Spring Harb Perspect Biol. 2010;2(4):a005140.
172. Kawabata KC, Ehata S, Komuro A, Takeuchi K, Miyazono K. TGF-beta-induced apoptosis of B-cell lymphoma Ramos cells through reduction of MS4A1/CD20. Oncogene. 2013;32(16):2096-106.
173. Liu X, Li YS, Shinton SA, Rhodes J, Tang L, Feng H, et al. Zebrafish B Cell Development without a Pre-B Cell Stage, Revealed by CD79 Fluorescence Reporter Transgenes. J Immunol. 2017;199(5):1706-15.
174. Dejana E, Orsenigo F. Endothelial adherens junctions at a glance. Journal of cell science. 2013;126(Pt 12):2545-9.
175. Guo DC, Pannu H, Tran-Fadulu V, Papke CL, Yu RK, Avidan N, et al. Mutations in smooth muscle alpha-actin (ACTA2) lead to thoracic aortic aneurysms and dissections. Nat Genet. 2007;39(12):1488-93.
176. Milewicz DM, Trybus KM, Guo DC, Sweeney HL, Regalado E, Kamm K, et al. Altered Smooth Muscle Cell Force Generation as a Driver of Thoracic Aortic Aneurysms and Dissections. Arteriosclerosis, thrombosis, and vascular biology. 2017;37(1):26-34.
177. Doerflinger NH, Macklin WB, Popko B. Inducible site-specific recombination in myelinating cells. Genesis. 2003;35(1):63-72.
178. Fregoso SP, Hoover DB. Development of cardiac parasympathetic neurons, glial cells, and regional cholinergic innervation of the mouse heart. Neuroscience. 2012;221:28-36.
179. Deng Y, Kim B, He X, Kim S, Lu C, Wang H, et al. Direct visualization of membrane architecture of myelinating cells in transgenic mice expressing membrane-anchored EGFP. Genesis. 2014;52(4):341-9.
180. Cai CL, Martin JC, Sun Y, Cui L, Wang L, Ouyang K, et al. A myocardial lineage derives from Tbx18 epicardial cells. Nature. 2008;454(7200):104-8.
181. Ali SR, Ranjbarvaziri S, Talkhabi M, Zhao P, Subat A, Hojjat A, et al. Developmental heterogeneity of cardiac fibroblasts does not predict pathological proliferation and activation. Circulation research. 2014;115(7):625-35.
182. Hofsteen P, Plavicki J, Johnson SD, Peterson RE, Heideman W. Sox9b is required for epicardium formation and plays a role in TCDD-induced heart malformation in zebrafish. Molecular pharmacology. 2013;84(3):353-60.
183. Tan K, Markby G, Muirhead R, Blake R, Bergeron L, Fici G, et al. Evaluation of canine 2D cell cultures as models of myxomatous mitral valve degeneration. PLoS One. 2019;14(8):e0221126.

184. Boogerd CJ, Zhu X, Aneas I, Sakabe N, Zhang L, Sobreira DR, et al. Tbx20 Is Required in Mid-Gestation Cardiomyocytes and Plays a Central Role in Atrial Development. Circulation research. 2018;123(4):428-42.
185. Santiago JJ, Dangerfield AL, Rattan SG, Bathe KL, Cunnington RH, Raizman JE, et al. Cardiac fibroblast to myofibroblast differentiation in vivo and in vitro: expression of focal adhesion components in neonatal and adult rat ventricular myofibroblasts. Dev Dyn. 2010;239(6):1573-84.
186. Zhao S, Wu H, Xia W, Chen X, Zhu S, Zhang S, et al. Periostin expression is upregulated and associated with myocardial fibrosis in human failing hearts. J Cardiol. 2014;63(5):373-8.
187. Turner NA, Porter KE. Function and fate of myofibroblasts after myocardial infarction. Fibrogenesis Tissue Repair. 2013;6(1):5.
188. Liguori TTA, Liguori GR, Moreira LFP, Harmsen MC. Fibroblast growth factor-2, but not the adipose tissue-derived stromal cells secretome, inhibits TGF-beta1-induced differentiation of human cardiac fibroblasts into myofibroblasts. Sci Rep. 2018;8(1):16633.
189. Kattan WM, Alarfaj SF, Alnooh BM, Alsaif HF, Alabdul Karim HS, Al-Qattan NM, et al. Myofibroblast-Mediated Contraction. J Coll Physicians Surg Pak. 2017;27(1):38-43.
190. Ivey MJ, Tallquist MD. Defining the Cardiac Fibroblast. Circ J. 2016;80(11):2269-76.
191. Crisan M, Yap S, Casteilla L, Chen CW, Corselli M, Park TS, et al. A perivascular origin for mesenchymal stem cells in multiple human organs. Cell Stem Cell. 2008;3(3):301-13.
192. Chen WC, Baily JE, Corselli M, Diaz ME, Sun B, Xiang G, et al. Human myocardial pericytes: multipotent mesodermal precursors exhibiting cardiac specificity. Stem Cells. 2015;33(2):557-73.
193. Shook BA, Wasko RR, Rivera-Gonzalez GC, Salazar-Gatzimas E, Lopez-Giraldez F, Dash BC, et al. Myofibroblast proliferation and heterogeneity are supported by macrophages during skin repair. Science. 2018;362(6417).
194. Bursac N. Cardiac fibroblasts in pressure overload hypertrophy: the enemy within? J Clin Invest. 2014;124(7):2850-3.
195. Kwartler CS, Chen J, Thakur D, Li S, Baskin K, Wang S, et al. Overexpression of smooth muscle myosin heavy chain leads to activation of the unfolded protein response and autophagic turnover of thick filament-associated proteins in vascular smooth muscle cells. J Biol Chem. 2014;289(20):14075-88.
196. Furtado MB, Costa MW, Pranoto EA, Salimova E, Pinto AR, Lam NT, et al. Cardiogenic genes expressed in cardiac fibroblasts contribute to heart development and repair. Circulation research. 2014;114(9):1422-34.
197. Churko JM, Garg P, Treutlein B, Venkatasubramanian M, Wu H, Lee J, et al. Defining human cardiac transcription factor hierarchies using integrated single-cell heterogeneity analysis. Nat Commun. 2018;9(1):4906.
198. Paik DT, Tian L, Lee J, Sayed N, Chen IY, Rhee S, et al. Large-Scale Single-Cell RNA-Seq Reveals Molecular Signatures of Heterogeneous Populations of Human Induced Pluripotent Stem Cell-Derived Endothelial Cells. Circulation research. 2018;123(4):443-50.
199. Li G, Plonowska K, Kuppusamy R, Sturzu A, Wu SM. Identification of cardiovascular lineage descendants at single-cell resolution. Development. 2015;142(5):846-57.
200. Hu P, Liu J, Zhao J, Wilkins BJ, Lupino K, Wu H, et al. Single-nucleus transcriptomic survey of cell diversity and functional maturation in postnatal mammalian hearts. Genes & development. 2018;32(19-20):1344-57.
201. Kisselbach L, Merges M, Bossie A, Boyd A. CD90 Expression on human primary cells and elimination of contaminating fibroblasts from cell cultures. Cytotechnology. 2009;59(1):31-44.
202. Kong P, Christia P, Saxena A, Su Y, Frangogiannis NG. Lack of specificity of fibroblast-specific protein 1 in cardiac remodeling and fibrosis. Am J Physiol Heart Circ Physiol. 2013;305(9):H1363-72.
203. Strom A, Olin AI, Aspberg A, Hultgardh-Nilsson A. Fibulin-2 is present in murine vascular lesions and is important for smooth muscle cell migration. Cardiovascular research. 2006;69(3):755-63.

204. Chong JJ, Reinecke H, Iwata M, Torok-Storb B, Stempien-Otero A, Murry CE. Progenitor cells identified by PDGFR-alpha expression in the developing and diseased human heart. Stem Cells Dev. 2013;22(13):1932-43.
205. Liu R, Hossain MM, Chen X, Jin JP. Mechanoregulation of SM22alpha/Transgelin. Biochemistry. 2017;56(41):5526-38.
206. Hosaka K, Yang Y, Seki T, Fischer C, Dubey O, Fredlund E, et al. Pericyte-fibroblast transition promotes tumor growth and metastasis. Proc Natl Acad Sci U S A. 2016;113(38):E5618-27.
207. Fan D, Takawale A, Basu R, Patel V, Lee J, Kandalam V, et al. Differential role of TIMP2 and TIMP3 in cardiac hypertrophy, fibrosis, and diastolic dysfunction. Cardiovascular research. 2014;103(2):268-80.
208. Lovelock JD, Baker AH, Gao F, Dong JF, Bergeron AL, McPheat W, et al. Heterogeneous effects of tissue inhibitors of matrix metalloproteinases on cardiac fibroblasts. Am J Physiol Heart Circ Physiol. 2005;288(2):H461-8.
209. Gao W, Guo N, Zhao S, Chen Z, Zhang W, Yan F, et al. Carboxypeptidase A4 promotes cardiomyocyte hypertrophy through activating PI3K-AKT-mTOR signaling. Bioscience reports. 2020;40(5).
210. Ho JE, Lyass A, Courchesne P, Chen G, Liu C, Yin X, et al. Protein Biomarkers of Cardiovascular Disease and Mortality in the Community. Journal of the American Heart Association. 2018;7(14).
211. Liu K, Zhou W, Chen H, Pan H, Sun X, You Q. Autologous vein graft stenosis inhibited by orphan nuclear receptor Nur77-targeted siRNA. Vascular pharmacology. 2015;73:64-70.
212. Evans PC. Nur77: Orphaned at Birth but Adopted by the Nuclear Factor κB Signaling Pathway. Am Heart Assoc; 2009.
213. Aird W. Spatial and temporal dynamics of the endothelium. Journal of Thrombosis and Haemostasis. 2005;3(7):1392-406.
214. Sondergaard RH, Follin B, Lund LD, Juhl M, Ekblond A, Kastrup J, et al. Senescence and quiescence in adipose-derived stromal cells: Effects of human platelet lysate, fetal bovine serum and hypoxia. Cytotherapy. 2017;19(1):95-106.
215. Chappell J, Harman JL, Narasimhan VM, Yu H, Foote K, Simons BD, et al. Extensive proliferation of a subset of differentiated, yet plastic, medial vascular smooth muscle cells contributes to neointimal formation in mouse injury and atherosclerosis models. Circulation research. 2016;119(12):1313-23.
216. Malliaras K, Li TS, Luthringer D, Terrovitis J, Cheng K, Chakravarty T, et al. Safety and efficacy of allogeneic cell therapy in infarcted rats transplanted with mismatched cardiosphere-derived cells. Circulation. 2012;125(1):100-12.
217. Ettelt V, Belitsky A, Lehnert M, Loidl-Stahlhofen A, Epple M, Veith M. Enhanced selective cellular proliferation by multi-biofunctionalization of medical implant surfaces with heterodimeric BMP-2/6, fibronectin, and FGF-2. J Biomed Mater Res A. 2018;106(11):2910-22.
218. Li D, Zhang C, Song F, Lubenec I, Tian Y, Song QH. VEGF regulates FGF-2 and TGF-beta1 expression in injury endothelial cells and mediates smooth muscle cells proliferation and migration. Microvascular research. 2009;77(2):134-42.
219. Jia YY, Zhou JY, Chang Y, An F, Li XW, Xu XY, et al. Effect of Optimized Concentrations of Basic Fibroblast Growth Factor and Epidermal Growth Factor on Proliferation of Fibroblasts and Expression of Collagen: Related to Pelvic Floor Tissue Regeneration. Chin Med J (Engl). 2018;131(17):2089-96.
220. Hill D, Milner R. Insulin as a growth factor. Pediatric research. 1985;19(9):879-86.
221. Wicha MS, Liotta LA, Kidwell WR. Effects of free fatty acids on the growth of normal and neoplastic rat mammary epithelial cells. Cancer research. 1979;39(2 Part 1):426-35.
222. Jiang L, Dai Y, Cui F, Pan Y, Zhang H, Xiao J, et al. Expression of cytokines, growth factors and apoptosis-related signal molecules in chronic pressure ulcer wounds healing. Spinal Cord. 2014;52(2):145-51.

223. Tamai M, Kobayashi N, Shimada K, Oka N, Takahashi M, Tanuma A, et al. Increased interleukin-1beta and basic fibroblast growth factor levels in the cerebrospinal fluid during human herpesvirus-6B (HHV-6B) encephalitis. Biochem Biophys Res Commun. 2017;486(3):706-11.
224. Alzahrani FA. Melatonin improves therapeutic potential of mesenchymal stem cells-derived exosomes against renal ischemia-reperfusion injury in rats. Am J Transl Res. 2019;11(5):2887-907.
225. Timmers L, Pasterkamp G, de Hoog VC, Arslan F, Appelman Y, de Kleijn DPV. The innate immune response in reperfused myocardium. Cardiovascular research. 2012;94(2):276-83.
226. Fitzgerald W, Freeman ML, Lederman MM, Vasilieva E, Romero R, Margolis L. A system of cytokines encapsulated in extracellular vesicles. Scientific reports. 2018;8(1):1-11.
227. Li T-S, Cheng K, Malliaras K, Smith RR, Zhang Y, Sun B, et al. Direct comparison of different stem cell types and subpopulations reveals superior paracrine potency and myocardial repair efficacy with cardiosphere-derived cells. Journal of the American College of Cardiology. 2012;59(10):942-53.
228. Aghila Rani KG, Kartha CC. Effects of epidermal growth factor on proliferation and migration of cardiosphere-derived cells expanded from adult human heart. Growth Factors. 2010;28(3):157-65.
229. Takehara N, Tsutsumi Y, Tateishi K, Ogata T, Tanaka H, Ueyama T, et al. Controlled delivery of basic fibroblast growth factor promotes human cardiosphere-derived cell engraftment to enhance cardiac repair for chronic myocardial infarction. Journal of the American College of Cardiology. 2008;52(23):1858-65.
230. Ye J, Boyle AJ, Shih H, Sievers RE, Wang ZE, Gormley M, et al. CD45-positive cells are not an essential component in cardiosphere formation. Cell and tissue research. 2013;351(1):201-5.
231. Davis DR, Zhang Y, Smith RR, Cheng K, Terrovitis J, Malliaras K, et al. Validation of the cardiosphere method to culture cardiac progenitor cells from myocardial tissue. PLoS One. 2009;4(9):e7195.
232. Pagano F, Angelini F, Castaldo C, Picchio V, Messina E, Sciarretta S, et al. Normal versus Pathological Cardiac Fibroblast-Derived Extracellular Matrix Differentially Modulates Cardiosphere-Derived Cell Paracrine Properties and Commitment. Stem Cells Int. 2017;2017:7396462.
233. Fu L, Wei CC, Powell PC, Bradley WE, Collawn JF, Dell'Italia LJ. Volume overload induces autophagic degradation of procollagen in cardiac fibroblasts. Journal of molecular and cellular cardiology. 2015;89(Pt B):241-50.
234. Agarwal U, George A, Bhutani S, Ghosh-Choudhary S, Maxwell JT, Brown ME, et al. Experimental, Systems, and Computational Approaches to Understanding the MicroRNA-Mediated Reparative Potential of Cardiac Progenitor Cell-Derived Exosomes From Pediatric Patients. Circulation research. 2017;120(4):701-12.
235. Amento EP, Ehsani N, Palmer H, Libby P. Cytokines and growth factors positively and negatively regulate interstitial collagen gene expression in human vascular smooth muscle cells. Arteriosclerosis and thrombosis: a journal of vascular biology. 1991;11(5):1223-30.
236. Zheng X, Baker H, Hancock WS, Fawaz F, McCaman M, Pungor E, Jr. Proteomic analysis for the assessment of different lots of fetal bovine serum as a raw material for cell culture. Part IV. Application of proteomics to the manufacture of biological drugs. Biotechnol Prog. 2006;22(5):1294-300.
237. Brogi E, Wu T, Namiki A, Isner JM. Indirect angiogenic cytokines upregulate VEGF and bFGF gene expression in vascular smooth muscle cells, whereas hypoxia upregulates VEGF expression only. Circulation. 1994;90(2):649-52.
238. Agarwal U, Smith AW, French KM, Boopathy AV, George A, Trac D, et al. Age-Dependent Effect of Pediatric Cardiac Progenitor Cells After Juvenile Heart Failure. Stem Cells Transl Med. 2016;5(7):883-92.
239. Pedrotty DM, Klinger RY, Kirkton RD, Bursac N. Cardiac fibroblast paracrine factors alter impulse conduction and ion channel expression of neonatal rat cardiomyocytes. Cardiovascular research. 2009;83(4):688-97.

240. Fuentes TI, Appleby N, Tsay E, Martinez JJ, Bailey L, Hasaniya N, et al. Human neonatal cardiovascular progenitors: unlocking the secret to regenerative ability. PLoS One. 2013;8(10):e77464.
241. Serpooshan V, Liu YH, Buikema JW, Galdos FX, Chirikian O, Paige S, et al. Nkx2.5+ Cardiomyoblasts Contribute to Cardiomyogenesis in the Neonatal Heart. Sci Rep. 2017;7(1):12590.
242. An Z, Sabalic M, Bloomquist RF, Fowler TE, Streelman T, Sharpe PT. A quiescent cell population replenishes mesenchymal stem cells to drive accelerated growth in mouse incisors. Nat Commun. 2018;9(1):378.
243. Cui Y, Zheng Y, Liu X, Yan L, Fan X, Yong J, et al. Single-Cell Transcriptome Analysis Maps the Developmental Track of the Human Heart. Cell Rep. 2019;26(7):1934-50 e5.
244. Cai X, Zhang W, Hu J, Zhang L, Sultana N, Wu B, et al. Tbx20 acts upstream of Wnt signaling to regulate endocardial cushion formation and valve remodeling during mouse cardiogenesis. Development. 2013;140(15):3176-87.
245. Boogerd CJ, Aneas I, Sakabe N, Dirschinger RJ, Cheng QJ, Zhou B, et al. Probing chromatin landscape reveals roles of endocardial TBX20 in septation. J Clin Invest. 2016;126(8):3023-35.
246. Kanisicak O, Khalil H, Ivey MJ, Karch J, Maliken BD, Correll RN, et al. Genetic lineage tracing defines myofibroblast origin and function in the injured heart. Nat Commun. 2016;7:12260.
247. Baum J, Duffy HS. Fibroblasts and myofibroblasts: what are we talking about? J Cardiovasc Pharmacol. 2011;57(4):376-9.
248. Yang PS, Lee SH, Park J, Kim TH, Uhm JS, Joung B, et al. Atrial tissue expression of receptor for advanced glycation end-products (RAGE) and atrial fibrosis in patients with mitral valve disease. International journal of cardiology. 2016;220:1-6.
249. Brouty-Boye D, Pottin-Clemenceau C, Doucet C, Jasmin C, Azzarone B. Chemokines and CD40 expression in human fibroblasts. Eur J Immunol. 2000;30(3):914-9.
250. Lukacs NW, Kunkel SL, Allen R, Evanoff HL, Shaklee CL, Sherman JS, et al. Stimulus and cell-specific expression of C-X-C and C-C chemokines by pulmonary stromal cell populations. Am J Physiol. 1995;268(5 Pt 1):L856-61.
251. Van Linthout S, Miteva K, Tschope C. Crosstalk between fibroblasts and inflammatory cells. Cardiovascular research. 2014;102(2):258-69.
252. Nees S, Weiss DR, Senftl A, Knott M, Forch S, Schnurr M, et al. Isolation, bulk cultivation, and characterization of coronary microvascular pericytes: the second most frequent myocardial cell type in vitro. Am J Physiol Heart Circ Physiol. 2012;302(1):H69-84.
253. Murray IR, Baily JE, Chen WCW, Dar A, Gonzalez ZN, Jensen AR, et al. Skeletal and cardiac muscle pericytes: Functions and therapeutic potential. Pharmacol Ther. 2017;171:65-74.
254. Cappellari O, Cossu G. Pericytes in development and pathology of skeletal muscle. Circulation research. 2013;113(3):341-7.
255. Arora M. Cell culture media: a review. Mater Methods. 2013;3(175):24.
256. Ge Q, Zhang H, Hou J, Wan L, Cheng W, Wang X, et al. VEGF secreted by mesenchymal stem cells mediates the differentiation of endothelial progenitor cells into endothelial cells via paracrine mechanisms. Molecular medicine reports. 2018;17(1):1667-75.
257. Mayer H, Bertram H, Lindenmaier W, Korff T, Weber H, Weich H. Vascular endothelial growth factor (VEGF-A) expression in human mesenchymal stem cells: autocrine and paracrine role on osteoblastic and endothelial differentiation. Journal of cellular biochemistry. 2005;95(4):827-39.
258. Savikko J, Rintala JM, Rintala S, Koskinen P. Epidermal growth factor receptor inhibition by erlotinib prevents vascular smooth muscle cell and monocyte-macrophage function in vitro. Transpl Immunol. 2015;32(3):175-8.
259. Schreier B, Hunerberg M, Mildenberger S, Rabe S, Bethmann D, Wickenhauser C, et al. Deletion of the EGF receptor in vascular smooth muscle cells prevents chronic angiotensin II-induced arterial wall stiffening and media thickening. Acta Physiol (Oxf). 2018;222(3).

260. Li M, Liu Q, Lei J, Wang X, Chen X, Ding Y. MiR-362-3p inhibits the proliferation and migration of vascular smooth muscle cells in atherosclerosis by targeting ADAMTS1. Biochem Biophys Res Commun. 2017;493(1):270-6.
261. Bieback K. Platelet lysate as replacement for fetal bovine serum in mesenchymal stromal cell cultures. Transfus Med Hemother. 2013;40(5):326-35.
262. Jochems CE, van der Valk JB, Stafleu FR, Baumans V. The use of fetal bovine serum: ethical or scientific problem? Altern Lab Anim. 2002;30(2):219-27.

14. Publications/Talks

14.1 Oral Presentations

- *German Society of Cardiology, 85th Annual Meeting, Mannheim, 27.04.2019:* Characterization of heart tissue-derived cells from HLHS patients and functional analysis of their extracellular vesicles
- *Science Day, Technical University of Munich, Munich, 18.10.2019:* Characterization of heart-tissue derived cells from HLHS patients and functional analysis of their extracellular vesicles
- *8th European & Swiss MD-PhD Conference, Geneva, 23.10.2019:* Characterization of heart tissue derived cells from Single Ventricle patients and functional analysis of their extracellular vesicles

14.2 Poster Presentations

- *Munich Heart Alliance Winter Meeting, Munich, 13.02.2017:* Cardiosphere-derived cells: resident stem cells or cardiac fibroblasts?
- *Poster Symposium, TUM Medical Faculty Day, 19.07.2017.:* Cardiosphere-derived cells: resident stem cells or cardiac fibroblasts?
- *Munich Heart Alliance Summer Meeting, Bernried, 19.07.2018*. Characterization of heart derived cells from HLHS patients and functional analysis of their extracellular vesicles

14.3 Publications

Palgit-S. **Kogan**, Archana Tomar, Jonathan Darr, Raffaele Teperino, Harald Lahm, Martina Dreßen, Nazan Puluca, Zhong Zhang, Kathrin Gärtner, Corinna Hüls, Reinhard Zeidler, Deepak Ramanujam, Stefan Engelhardt, Catharina Wenk, Lesca M. Holdt, Rüdiger Lange, Markus Krane, Stefanie A. Doppler. *Single Cell RNA Sequencing of Cardiosphere Derived Cells (CDCs) Reveals Their Heterogeneity and similarity Compared to Cardiac Non-Myocyte Cell Types.* Manuscript submitted for publication (2020).

15. Supplementary Figures

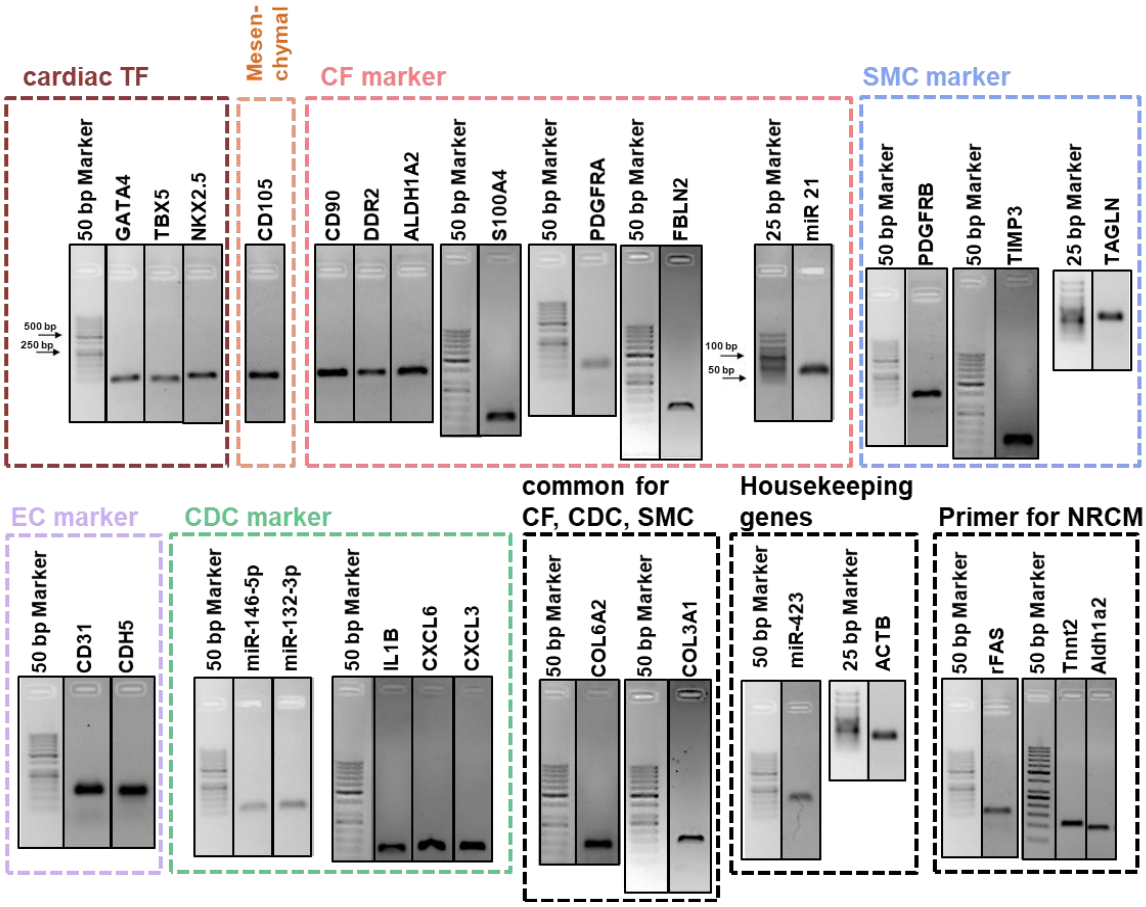

Suppl. Figure S 1 Quality control of qRT-PCR primers by gel electrophoresis.
Abbreviations: TF: transcription factors; CF: cardiac fibroblasts; SMC: smooth muscle cells; EC: endothelial cells; CDC: cardiosphere-derived cells; NRCM: neonatal rat cardiomyocytes.
Gel electrophoresis of qRT-PCR products was performed as described in paragraph 4.5.1.3.4. Exemplary agarose gel electrophoresis photographs of the primer sets used in this work (Figures: 5, 7, 11, 15- 17, 19, 22-24, 27, 29, 31, 33). 50 bp (#SM0371, Thermo Scientific™, Thermo Fisher Scientific) and 25 bp (#250216, Biozym Scientific GmbH) markers were electrophorized simultaneously with the analyzed PCR products and are illustrated to the left side of the product's electrophoresis results, respectfully.

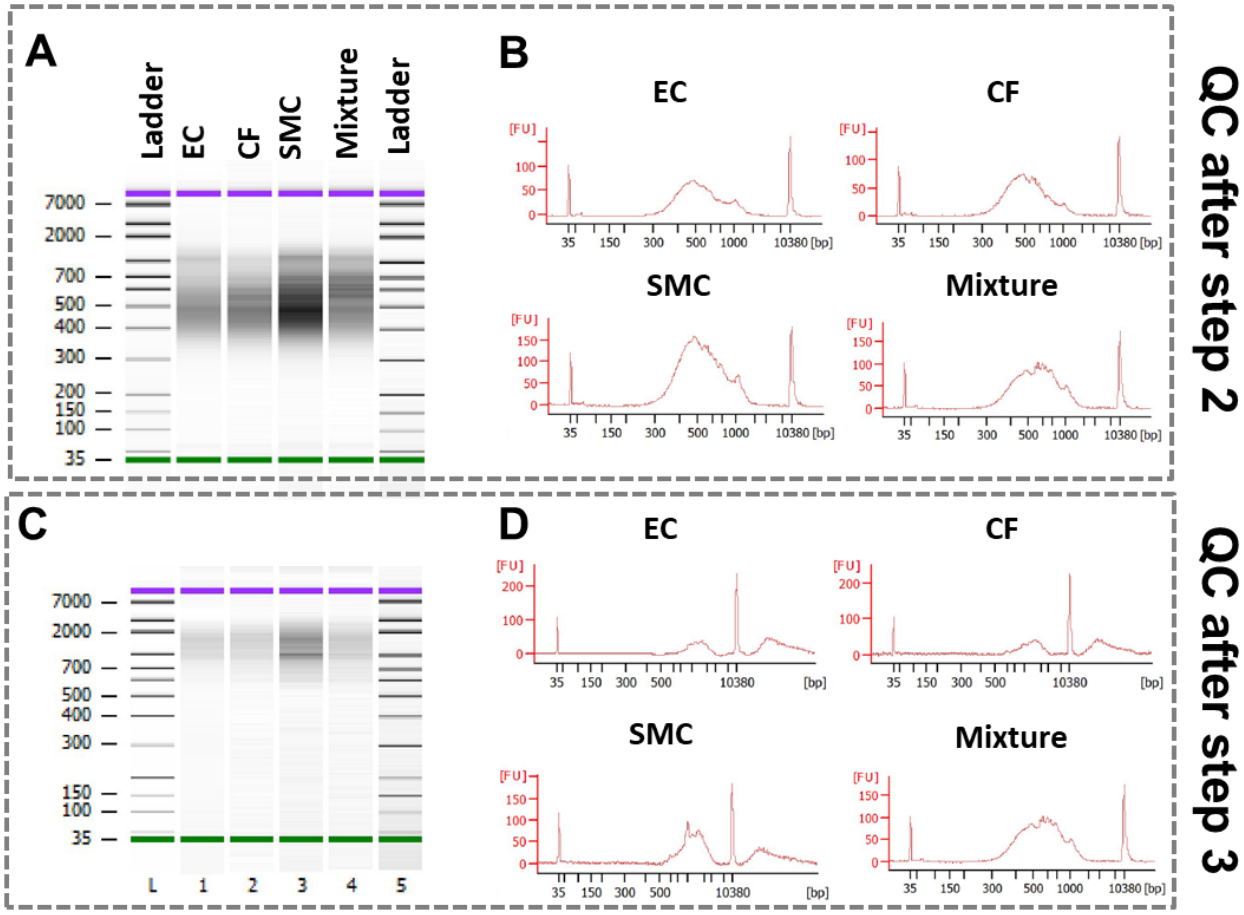

Suppl. Figure S 2: Quality control by bioanalyzer for sc-RNAseq samples 1-4

Abbreviations: EC: endothelial cells; CF: cardiac fibroblasts; SMC: smooth muscle cells; QC: quality control; sc-RNAseq: single-cell RNA sequencing. A-B) Bioanalyzer results of cDNA after step 2 of sc-RNAseq library preparation (see paragraph 4.5.4.2). A) Gel-like image of the ladder provided in the kit, sample 1 (EC), sample 2 (CF), sample 3 (SMC), sample 4 (mixture of 20% EC, 30%SMC, 50% CF) and again the ladder (from left to right). B) Electropherograms of samples 1-4. C-D) Bioanalyzer results of cDNA after step 3 of sc-RNAseq library preparation which includes fragmentation and size-selection. Gel-like image C) and electropherograms (D) of the according samples are shown

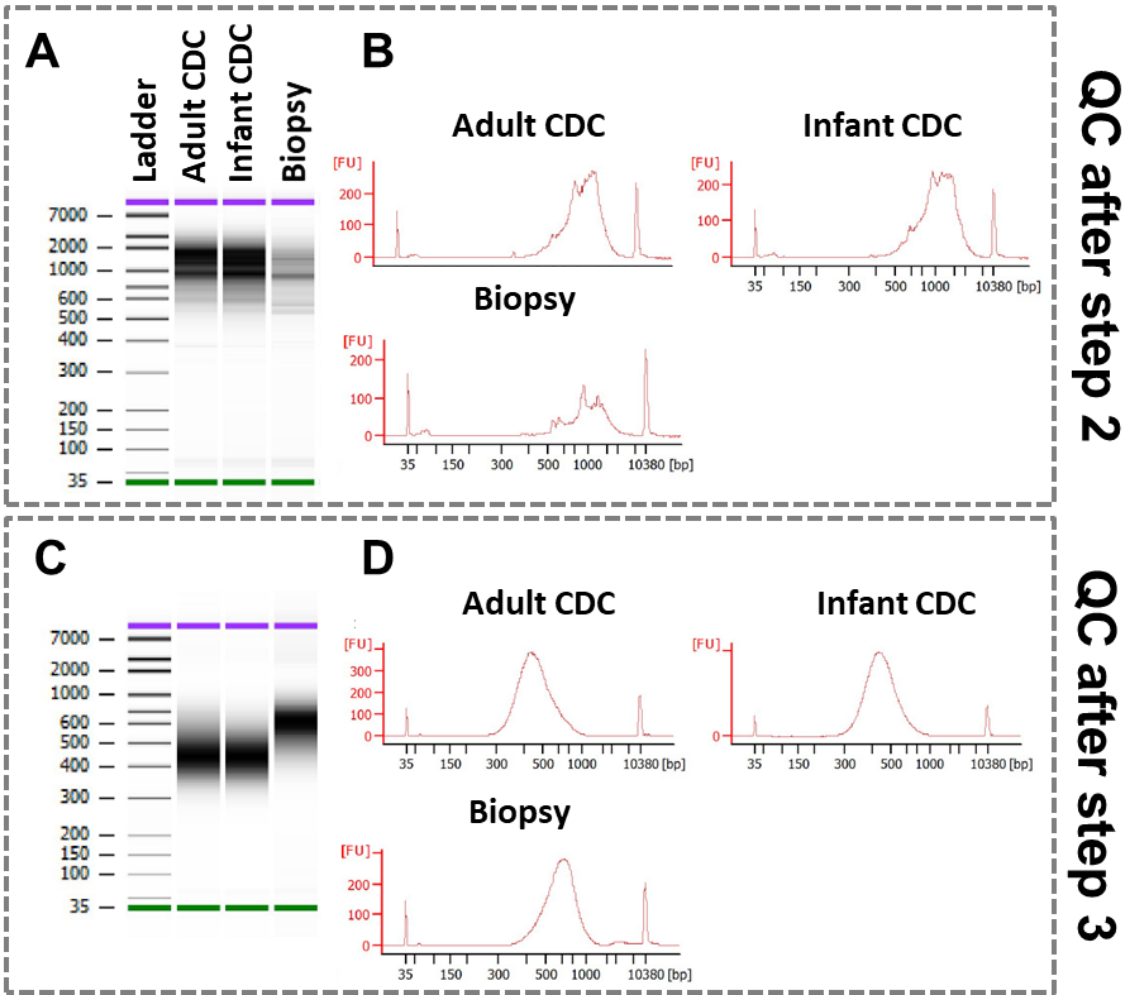

Suppl. Figure S 3: Quality control by bioanalyzer for sc-RNAseq samples 5-6 and the biopsy sample

Abbreviations: CDC: cardiosphere-derived cells; QC: quality control; sc-RNAseq: single-cell RNA sequencing. A-B) Bioanalyzer results of cDNA after step 2 of sc-RNAseq library preparation (see paragraph 4.5.4.2). A) Gel-like image of the ladder provided in the kit, sample 5 (Adult CDC), sample 6 (Infant CDC) and the biopsy sample (from left to right). B) Electropherograms of samples 5, 6 and biopsy. C-D) Bioanalyzer results of cDNA after step 3 of sc-RNAseq library preparation which includes fragmentation and size-selection. Gel-like image C) and electropherograms (D) of the according samples are shown.

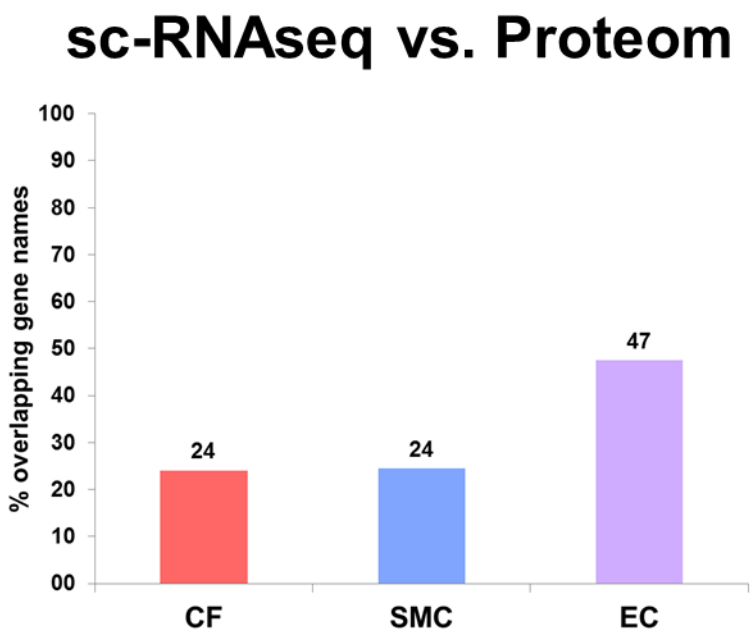

Suppl. Figure S 4: Comparison of sc-RNAseq data to proteome data base

Abbreviations: sc-RNAseq: single-cell RNA sequencing; CF: cardiac fibroblasts; SMC: smooth muscle cells; EC: endothelial cells. Overlapping upregulated genes in sc-RNAseq data and proteomic data base by Doll et al. (5) in CF, SMC and EC. Percentage refers to the total number of upregulated differentially expressed genes (uDEG) in sc-RNAseq data.